

Vibrational Band Contours Analysis of Symmetric Top Molecules

by Ian Robert Hill, B.Sc.

A Thesis presented to the
Faculty of Science of the University
of London in Candidature for the Degree
of Doctor of Philosophy.

Department of Chemistry,
Royal Holloway College,
(University of London),
Egham Hill,
Egham,
Surrey.
TW20 OEX

| | |
|------------------|---------|
| R. H. G. LIBRARY | |
| CLASS | CDC |
| No. | Hil |
| ADG. No. | 126,721 |
| DATE ACQ | 29.9.75 |

December 1974

ProQuest Number: 10097394

All rights reserved

INFORMATION TO ALL USERS

The quality of this reproduction is dependent upon the quality of the copy submitted.

In the unlikely event that the author did not send a complete manuscript and there are missing pages, these will be noted. Also, if material had to be removed, a note will indicate the deletion.



ProQuest 10097394

Published by ProQuest LLC(2016). Copyright of the Dissertation is held by the Author.

All rights reserved.

This work is protected against unauthorized copying under Title 17, United States Code.
Microform Edition © ProQuest LLC.

ProQuest LLC
789 East Eisenhower Parkway
P.O. Box 1346
Ann Arbor, MI 48106-1346

ACKNOWLEDGMENTS

My sincere gratitude to Dr. Derek Steele for his advice and guidance during the course of this work.

Thanks are also due to Donald G. Owen for his help and useful discussions.

My grateful thanks to the Science Research Council for the receipt of a Studentship.

My sincere gratitude to Evelyn Evans for typing this thesis and also to David Evans, Valerie and Thomas Fordick, Evelyn Taylor and my parents for help and financial assistance in getting this thesis printed. To Don, Frank,

and Robert

ACKNOWLEDGMENTS

My sincere gratitude to Dr. Derek Steele for his advice and guidance during the course of this work.

Thanks are also due to Donald G. Owens for his help and useful discussions.

My grateful thanks to the Science Research Council for the receipt of a Studentship.

My sincere gratitude to Evelyn Evans for typing this thesis and also to David Evans, Valerie and Thomas Forsdick, Evelyn Taylor and my parents for help and financial assistance in getting this thesis printed.

| | <u>CONTENTS</u> | <u>Page No.</u> |
|----------------------|--|-----------------|
| <u>CHAPTER ONE</u> | Introduction and General Theory | 8 |
| Section 1.1 | Abstract | 8 |
| Section 1.2 | Measurement of Spectra and the Observables used | 9 |
| Section 1.3 | Measurement of the Path Length of a Liquid Cell and also the Refractive Index | 13 |
| Section 1.4 | Symmetric Top Molecules and Rotation-Vibration Spectra | 15 |
| Section 1.5 | Computer Simulation of the Rotation-Vibration Spectra of Symmetric Top Molecules | 30 |
| <u>CHAPTER THREE</u> | | |
| Section 1.6 | Collision Broadening | 35 |
| Section 1.7 | The Fourier Transform | 39 |
| Section 1.8 | Computer Programming | 43 |
| Section 1.9 | Purification of Compounds | 44 |
| <u>CHAPTER TWO</u> | Correction of Spectra for Instrumental and Physical Distortions | 45 |
| Section 2.1 | General Instrumental Conditions when Running a Spectrum | 45 |
| Section 2.2 | Distortion of the Transmittance Curve due to the Finite Width of the Slit | 46 |
| Section 2.3 | Correction of the Slit Distortion using Fourier Transformation | 47 |
| Section 2.4 | Correction of the Slit Distortion using the Derivatives of the Transmitted Intensity Curve | 63 |
| Section 2.5 | Correction of the Distortion of Infra-red Absorption Bands due to Refractive Index Effects | 74 |
| Section 2.6 | The Dispersion Relations | 75 |

| | | |
|----------------------|---|-----|
| Section 2.7 | The Lorentz Model of Absorption and Dispersion | 78 |
| Section 2.8 | The Kramers - Kronig Transform | 81 |
| Section 2.9 | The Reflection Loss Correction | 83 |
| Section 2.10 | The Theory of the Local Field Correction | 88 |
| Section 2.11 | Application of the Local Field Correction | 93 |
| Section 2.12 | Hot Bands | 97 |
| Section 2.13 | Isotopic Shifts | 102 |
| CHAPTER SIX | | |
| <u>CHAPTER THREE</u> | Infra-red Band Moment Theory | 108 |
| Section 3.1 | Introduction | 108 |
| Section 3.2 | Band Moment Theory and the Odd Order moments | 111 |
| Section 3.3 | The Second Moment - Gordon's Formulation | 114 |
| Section 3.4 | The Second Moment - A Gas Phase Approach for Symmetric Top Molecules | 121 |
| Section 3.5 | The Fourth Moment | 139 |
| CHAPTER FOUR | | |
| | Experimental Vapour and Condensed Phase Second Moments and Condensed Phase Band Shapes | 142 |
| Section 4.1 | The Determination of the Coriolis Constant of an "e" Band of a Symmetric Top Molecule from the Vapour Phase Second Moment | 142 |
| Section 4.2 | Experimental Second Moments and Band Shapes in the Condensed Phase | 147 |
| Section 4.3 | Statistical Analysis of the Condensed Phase Contours of Infra-red Bands - I | 161 |
| CHAPTER FIVE | | |
| | Fourier Transformation on Infra-red Band Contours | 182 |

| | | |
|--------------------|---|-----|
| Section 5.1 | Derivation of the Relationship between the Transition Dipole Moment Correlation Function and the Frequency Spectrum | 182 |
| Section 5.2 | The Short and Long Time Behavior of the Autocorrelation Function | 194 |
| Section 5.3 | Autocorrelation Functions - Experimental Results | 198 |
| Section 5.4 | Statistical Analysis of the Condensed Phase Contours of Infra-red Bands - <u>II</u> | 207 |
| <u>CHAPTER SIX</u> | Broadening of Infra-red Band Shapes and Weak Molecular Complexes in Benzene Systems | 212 |
| Section 6.1 | Initial Survey | 212 |
| Section 6.2 | Proton Magnetic Resonance Evidence for Interaction between Benzene and Various Solvents | 217 |
| Section 6.3 | Correlation of Experimental Bandwidths and Frequency Shifts with Macroscopic Physical Properties of the Solvent | 223 |
| Section 6.4 | Measurement of the Second and Fourth Moments of the ν_{11} Band of Benzene in Different Solvents | 238 |
| Section 6.5 | Broadening and the ν_{11} Band | 243 |
| Section 6.6 | Broadening and the Combination Bands | 252 |
| Section 6.7 | Three Component Solutions | 254 |
| Section 6.8 | Conclusions | 257 |
| Section 6.9 | Evidence for the Formation of Weak Complexes between:- a) Benzene / Chloroform, and, b) Benzene / Hexafluorobenzene | 263 |
| Section 6.10 | Infra-red Proof of the Existence of the Benzene / Chloroform and Benzene / Hexafluorobenzene Complexes | 267 |

| | | |
|----------------------|--|-----|
| <u>CHAPTER SEVEN</u> | <u>Additional Work</u> | 272 |
| Section 7.1 | Vibrational Relaxation | 272 |
| Section 7.2 | Use of Carbon Tetrachloride as a Solvent | 279 |

| | | |
|-------------------|-------------|-----|
| APPENDIX <u>I</u> | Mathematics | 282 |
|-------------------|-------------|-----|

| | | |
|--------------------|---------------------|-----|
| APPENDIX <u>II</u> | Computer Programmes | 287 |
|--------------------|---------------------|-----|

| | | |
|------------|--|-----|
| REFERENCES | | 318 |
|------------|--|-----|

PUBLISHED MATERIAL

| | | |
|--------|--------------------------|--|
| FOLDER | Diagrams for Chapter Six | |
|--------|--------------------------|--|

CHAPTER ONEIntroduction and General TheorySection 1.1

Abstract

Vibrational spectroscopy is increasingly being used as a tool for research into the condensed phase, on a molecular scale. R.G. Gordon has interpreted the intensity moments of infra-red bands, taken about the band centre, in terms of the rotational kinetic energy of the molecules and intermolecular potential energies between the molecules. Gordon has also suggested that interpretation of a frequency spectrum can be aided by transforming the spectrum into a time domain function, which is related to molecular motion on a picosecond time scale. The aim of this work is to investigate the practical aspects of Gordon's moment theory and to utilise the theory to extract information about molecular interactions in the condensed phase, with the help of the time domain function. Specific interactions between benzene and various solvents will be analysed.

R.H.C.
LIBRARY

Section 1.2

Measurement of Spectra and the Observables used.

All spectra were measured in the infra-red region using a Perkin Elmer model 325 Spectrograph equipped with an air drier and carbon dioxide absorber. Spectra were recorded in the transmittance mode. Accurate spectra of a single band were obtained using scale expansions of up to 1 cm^{-1} per cm.

A knowledge of infra-red spectroscopy is assumed and the nomenclature used here is set out below. S.I. units have been used where it is convenient to do so but "spectroscopist" units, consistent with the wavenumber measured in reciprocal centimetres (c.g.s. units), are used when dealing with spectra. Thus, S.I. units have been used in dispersion theory but c.g.s. units in band moment theory.

A typical condensed phase spectrum is shown in Fig. 1.1a. In this figure, $I(\bar{\nu})$ is the intensity of radiation transmitted through a sample. This gives rise to a spectrum which will be called the transmitted intensity curve. $I_0(\bar{\nu})$ is the intensity of... radiation transmitted through a reference and gives rise to a base line for the transmitted intensity curve. In the case of a pure liquid sample, the reference was a non-absorbing liquid and in the case of a sample in solution, the reference was the pure solvent. For solutions two cells were used, one of which was a variable path length cell. Any absorption due to the solvent (provided the solvent did not absorb all the radiation) was cancelled out by adjusting the variable path length

Fig. 1.1b The diagram shows how interference of radiation arises in a thin cell. t is of the order of 10^{-2} cm or less.

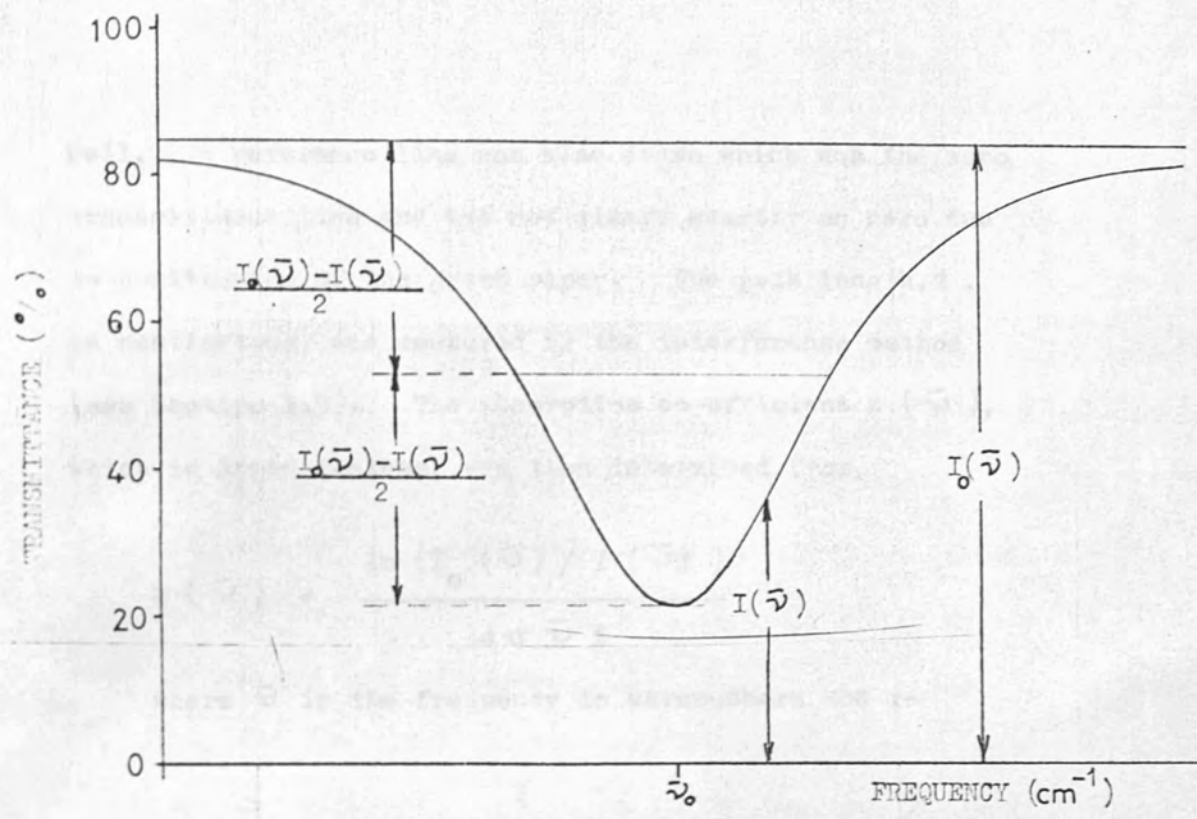


Fig.1.1a The diagram shows how the transmittance curve half height bandwidth is defined.

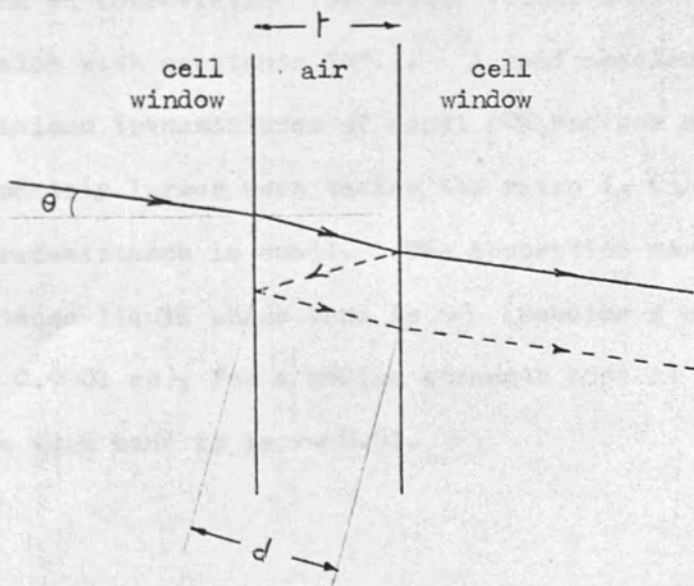


Fig.1.1b The diagram shows how interference of radiation arises in a thin cell. t is of the order of 10^{-2} cm or less.

cell. A reference line was also drawn which was the zero transmittance line and was not always exactly on zero due to positioning of the graph paper. The path length, t , in centimetres, was measured by the interference method (see Section 1.3). The absorption co-efficient $k(\bar{\nu})$, which is dimensionless, was then determined from

$$k(\bar{\nu}) = \frac{\ln(I_0(\bar{\nu})/I(\bar{\nu}))}{4\pi\bar{\nu}t}$$

where $\bar{\nu}$ is the frequency in wavenumbers and :-

$$\bar{\nu} \text{ cm}^{-1} = \frac{1}{\lambda \text{ cm (wavelength)}}$$

$$= \frac{\nu \text{ Hz (frequency)}}{c \text{ cm sec}^{-1} \text{ (velocity of light in vacuo)}}$$

(Using S.I. units, λ and t would be measured in metres, sec is used as an abbreviation for second rather than "s" in case of confusion with constants "s".). A good spectrum should have a minimum transmittance of about 20%, because errors are proportionately larger when taking the ratio $I_0(\bar{\nu})/I(\bar{\nu})$, if the transmittance is small. The absorption co-efficient of an intense liquid phase band is ~ 1 (needing a path length of about 0.0001 cm), for a medium strength band it is ~ 0.1 and for a weak band it is ~ 0.01 .

Alternatively, the molar absorption co-efficient of a species a, $\epsilon_a(\bar{\nu})$, is defined as :-

$$\epsilon_a = \frac{\ln(I_0(\bar{\nu}) / I(\bar{\nu}))}{C_a t}$$

where C_a is the concentration of the absorbing species measured in mol dm^{-3} . Absorbance is assumed to be constant with path length and concentration for the conditions used. The shape of the absorption band will be referred to as the band contour or band profile.

For the transmittance spectrum of Fig. 1.1a the curve width at half height will be called the transmittance curve half height width. For the absorbance profile, the width at $k(\bar{\nu}_0)/2$ will be called the half height bandwidth and given the symbol $\Delta\bar{\nu}_{\frac{1}{2}}$ (cm^{-1}).

The integrated intensity of an absorbance profile, Γ , is defined as :-

$$\Gamma = \frac{1}{C_a t} \int_{\text{band}} \frac{\ln(I_0(\bar{\nu})/I(\bar{\nu}))}{\bar{\nu}} d\bar{\nu}$$

and is called the band intensity.

Section 1.3 Measurement of the Path Length of a Liquid Cell and also the Refractive Index.

In the course of this work it was found that interference

The path length of an infra-red liquid cell was measured by placing the empty cell in the sample beam of the spectrometer and recording a spectrum. This consisted of a sine wave oscillation which was caused by interference of radiation in the sample space between the cell windows.

An expanded section through a cell is shown in Fig. 1.1b.

The condition for interference to occur is $2d \cos \theta = n\lambda$, where n is a positive integer. Now, from the diagram, $d \cos \theta = t$, but for near-normal incidence we may assume $\theta = 0$ and $d = t$. So for a constructive interference fringe :-

$2t = n\lambda_1 = n / \bar{\nu}_1$,
and the next constructive interference fringe will be at

$2t = (n+1)\lambda_2 = (n+1) / \bar{\nu}_2$

Thus, $\bar{\nu}_1 - \bar{\nu}_2 = 1 / 2t$

and $t = 1 / (2(\bar{\nu}_1 - \bar{\nu}_2))$

It is more accurate to measure the distance between N fringes, separated by a distance $\Delta\bar{\nu}$, in which case

$$t = N / (2 \Delta\bar{\nu}) \text{ cm} \quad (1.1)$$

have used this method of determining refractive indices.

This method of measuring path lengths is very accurate with an error of about 0.5% in the path length. In the course of this work it was found that interference fringes could be obtained, superimposed on a spectrum, when using a liquid of refractive index appreciably lower than that of the cell window, i.e. 0.3 different. This occurred with path lengths of the order of 0.001 cm and was visible in the wings of a band, away from absorption. For radiation entering a liquid medium of mean refractive index \bar{n} , the wavelength of the radiation, λ , is reduced to λ/\bar{n} . This means that equation (1.1) is modified to

$$t = N / (2 \Delta \bar{v} \bar{n}) \quad (1.2)$$

for the path length of a cell filled with the liquid. As will be discussed in a later chapter, the refractive index of a liquid (or solution) varies with absorption and frequency, so this equation may only be used away from absorption. This is obviously a good quick method for measuring the mean refractive index. The path length is first measured using the empty cell and then the fringes are measured when the cell is filled with the appropriate liquid. Cell windows of different refractive indices are available and so the ones which give the best fringes should be used. It was found that Young and Jones (11) have used this method of determining refractive indices.

Section 1.4Symmetric Top Molecules and Rotation -
Vibration Spectra.

Symmetric top molecules are molecules which have two equal moments of inertia about two of the three axes of rotation. The third axis is the main axis of rotation and is called the "z" axis and the other two axes are the "x" and "y" axes. The symmetric top molecules fall into two categories :-

- a) The prolate symmetric top, in which the moment of inertia about the z axis, I_z , is less than moment of inertia about the x and y axes. An example is methyl iodide which is shown in Fig. 1.2a.
- b) The oblate symmetric top, in which $I_x = I_y < I_z$. An example is benzene which is shown in Fig. 1.2b.

The rotational constant about the i axis, $B(i)$, is defined by :-

$$B(i) = \frac{h}{8\pi^2} \frac{1}{I_i} c \quad \text{cm}^{-1} \quad (1.3)$$

and it is usual to label the rotational constant for the z axis A and the rotational constant for the x and y axes B.

• It is quite straight forward to calculate the rotational constants from molecular geometry. Methyl iodide will be used as an example so, referring to Fig. 1.2a, the distance along the z axis from the carbon atom to the x y plane containing the three hydrogen atoms is :-

Fig. 1.2b The geometry of a molecule of benzene is shown. The data is taken from reference (10).

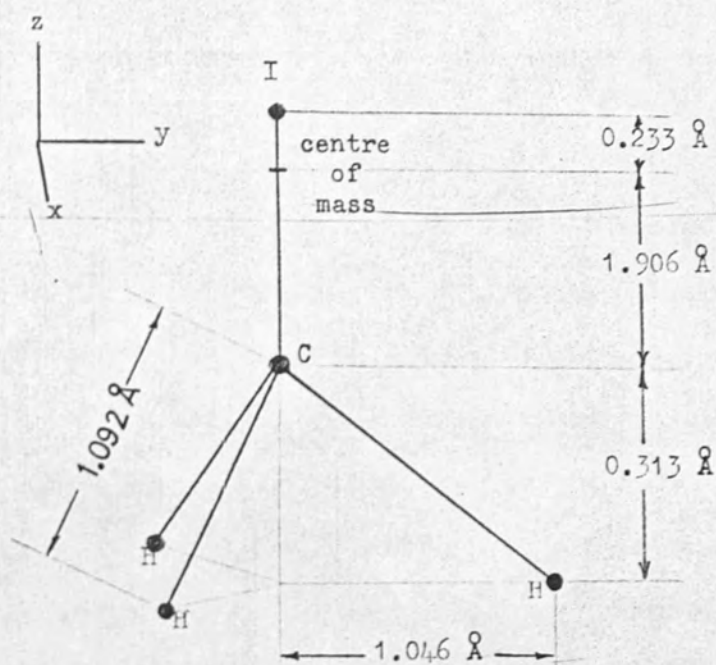


Fig.1.2a The geometry of a molecule of methyl iodide is shown. The data is taken from reference (87). The bond angles are $\angle\text{ICH} = 106^{\circ}40'$ and $\angle\text{HCH} = 112^{\circ}71'$.

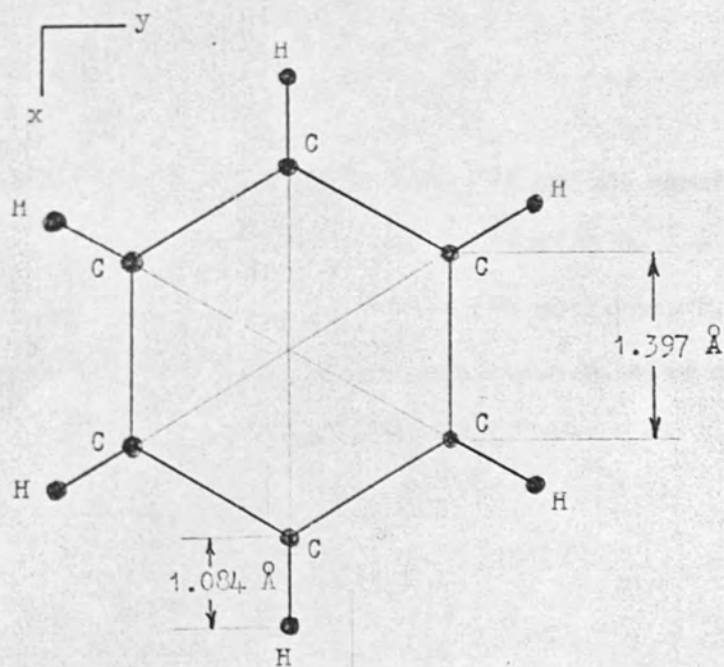


Fig.1.2b The geometry of a molecule of benzene is shown. The data is taken from reference (10).

$$1.092 \cos 73^\circ 20' = 0.3132 \text{ \AA}$$

The centre of mass of the molecule may be calculated from the first order moments, where x is the distance of the centre of mass from the centre of the iodine atom.

$$127x = 12(2.139 - x) + 3(2.139 + 0.313 - x)$$

$$x = 0.233 \text{ \AA}$$

The moment of inertia about the z axis is determined simply by the hydrogens. Using $I_i = m_j r_{ij}^2$, where m is the mass of an atom j and r is its distance from the i axis in centimetres

$$\begin{aligned} I_z &= 3 \times 1.046^2 \times 10^{-16} / (6.0225 \times 10^{23}) \\ &= 5.45 \times 10^{-40} \text{ g cm}^2 \end{aligned}$$

Use of equation (1.3) gives us $A = 5.136 \text{ cm}^{-1}$.

$$\begin{aligned} I_x = I_y &= (127 \times 0.233^2 + 12 \times 1.906^2 + 3 \times 2.219^2) \\ &\quad \times 10^{-16} / (6.02253 \times 10^{23}) \\ &= 108.36 \times 10^{-40} \text{ g cm}^2. \end{aligned}$$

$$B = 0.2583 \text{ cm}^{-1}$$

The same calculations carried out on the benzene molecule yielded $B = 0.1894 \text{ cm}^{-1}$ and $A = 0.0947 \text{ cm}^{-1} = B/2$.

* The total energy of vibration and rotation, T , of a symmetric top molecule in a particular degenerate or non-degenerate vibrational state is given by (5) :-

$$T_{v, J, K} = G(v) + F_v(J, K)$$

where $G(v)$ is the vibrational term value, given to a first approximation by

$$G(v) = \left(v + \frac{1}{2}\right) \left(\frac{k}{\mu}\right)^{\frac{1}{2}} / (2\pi c) \quad \text{cm}^{-1}$$

where v is the vibrational quantum number ($v = 0, 1, 2, 3 \dots$), k is the effective force constant for the vibrational and μ is the effective mass for the vibration.

$F_v(J, K)$ is the rotational term value which has

two forms depending on whether the vibration is degenerate or non-degenerate. For symmetric top molecules, a

non-degenerate vibration (an A mode vibration) has a transition

dipole directed along the z axis and the resulting band is

called a parallel band, whereas a doubly degenerate vibration

(an E mode vibration) has a transition dipole directed along the

x axis or the y axis and the resulting band is called a

perpendicular band. J is the quantum number determining the

total angular momentum of the system and K is the quantum number

determining the component of this angular momentum about the

unique axis of the molecule. J takes integer values of

0, 1, 2 ... and K takes integer values of 0, $\pm 1, \pm 2 \dots \pm J$.

Consider firstly a parallel band. The rotational term value is given by :-

$$F_v(J, K) = B_v J(J+1) + (A_v - B_v) K^2$$

The selection rules for a parallel transition of a symmetric top molecule are :-

$$K = 0 \quad \Delta J = \pm 1 \quad \Delta K = 0$$

$$K \neq 0 \quad \Delta J = 0, \pm 1 \quad \Delta K = 0$$

For a particular K level (except when K = 0) we may have $\Delta J = -1, 0$ and $+1$ and these lead to P, Q and R branches respectively. For a transition from a lower state (v'', J'') to an upper state (v', J'), the frequencies are given by :- $\bar{\nu}_0$ is the fundamental vibrational frequency. Rotational

P branch $\bar{\nu}_{J'', K}^{J''-1, K} = \bar{\nu}_0^{\text{sub}} + B_{v'} J'' (J'' - 1) - B_{v''} J'' (J'' + 1)$

The term $(B_{v'} - B_{v''}) J'' (J'' + 1)$ leads to convergence of the rotational lines in the P branch towards low

$$= \bar{\nu}_0^{\text{sub}} + (B_{v'} - B_{v''}) J'' (J'' + 1) - 2 B_{v''} J''$$

Q branch $\bar{\nu}_{J'', K}^{J'', K} = \bar{\nu}_0^{\text{sub}} + (B_{v'} - B_{v''}) J'' (J'' + 1)$

R branch $\bar{\nu}_{J'', K}^{J''+1, K} = \bar{\nu}_0^{\text{sub}} + B_{v'} (J'' + 1) (J'' + 2) - B_{v''} J'' (J'' + 1)$

$$= \bar{\nu}_0^{\text{sub}} + (B_{v'} - B_{v''}) J'' (J'' + 1) + 2 B_{v'} (J'' + 1)$$

The complete parallel band is obtained from superposition of a number of such sub-bands corresponding to various values of K . Due to differences in the rotational constants of different vibrational levels, the origins of the sub-bands do not coincide but vary according to the relation :-

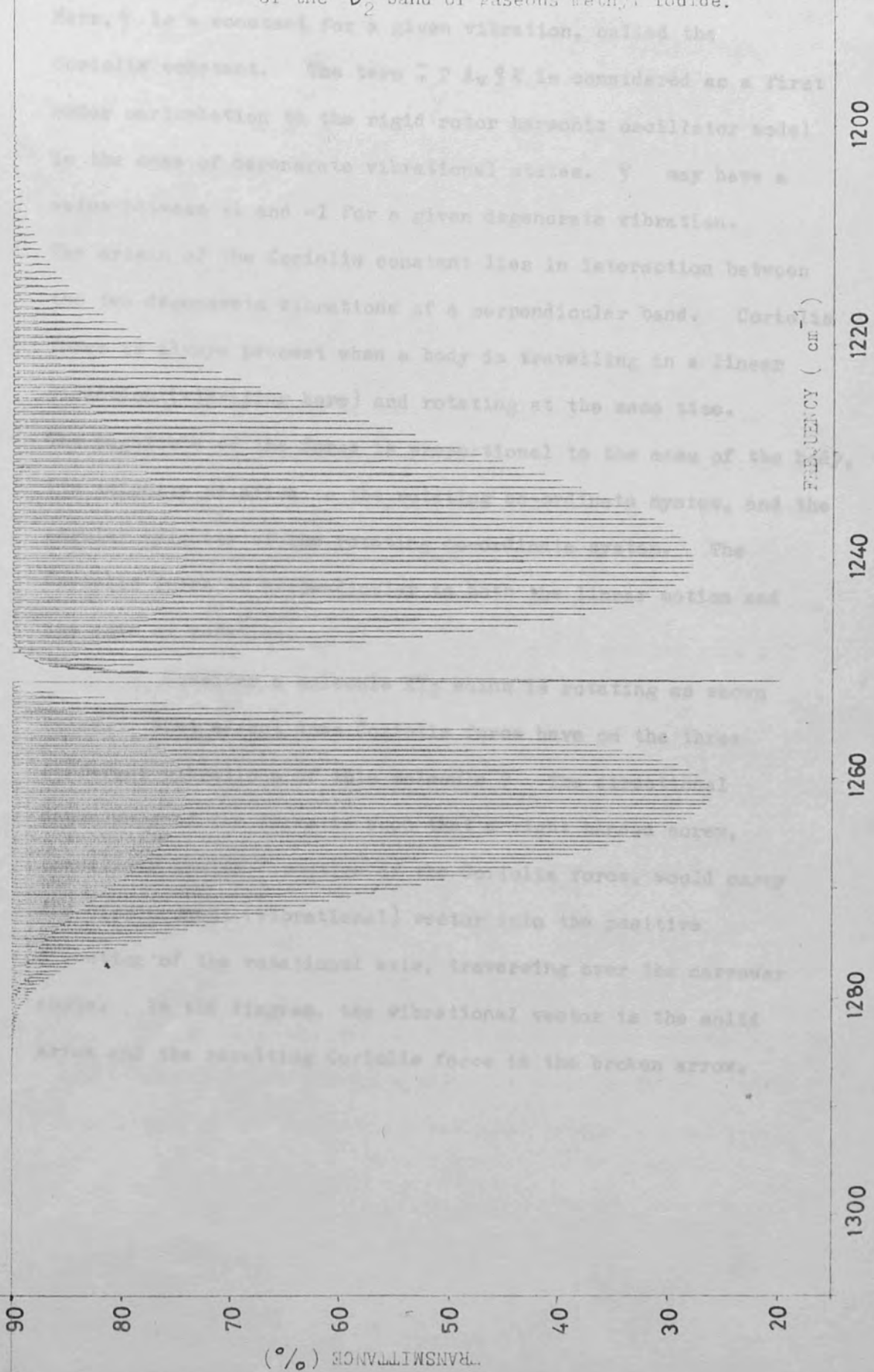
$$\bar{\nu}_0^{\text{sub}} = \bar{\nu}_0 + \left[(A_V' - A_V'') - (B_V' - B_V'') \right] K^2$$

where $\bar{\nu}_0$ is the fundamental vibrational frequency. Rotational constants change by about 1% when going from one vibrational energy level to the next, so this term leads to a slight broadening of the individual lines of the P, Q and R branches. The term $(B_V' - B_V'') J'' (J'' + 1)$ leads to convergence of the rotational lines in the R branch towards high frequency and a divergence of rotational lines in the P branch towards low frequency. This effect can be seen in Fig. 1.3 which is a computer simulated parallel band of methyl iodide. It may also be noticed in this figure that the R branch minimum is slightly lower than the P branch minimum. This is also due to $B_V'' \neq B_V'$.

The rotational term value for a perpendicular band of a symmetric top molecule is given by :-

$$F_V(J, K) = B_V J(J+1) + (A_V - B_V) K^2 + 2A_V \zeta K$$

Fig.1.3 A computer simulated spectrum of the ν_2 band of gaseous methyl iodide.




Here, ζ is a constant for a given vibration, called the Coriolis constant. The term $\mp 2 A_v \zeta K$ is considered as a first order perturbation to the rigid rotor harmonic oscillator model in the case of degenerate vibrational states. ζ may have a value between +1 and -1 for a given degenerate vibration.

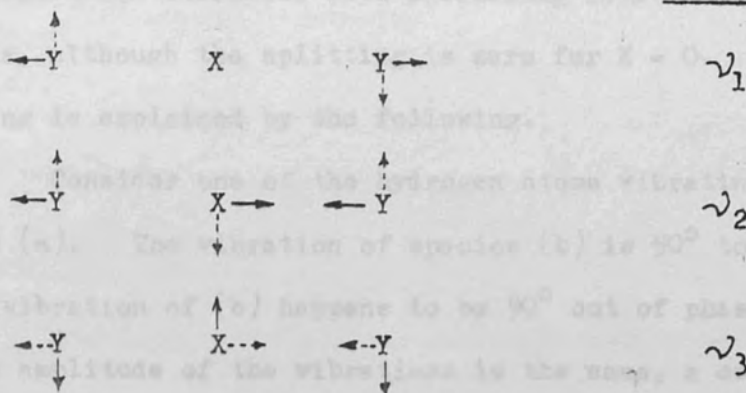
The origin of the Coriolis constant lies in interaction between the two degenerate vibrations of a perpendicular band. Coriolis force is always present when a body is travelling in a linear direction (vibrating here) and rotating at the same time.

The magnitude of the force is proportional to the mass of the body, its velocity relative to the rotating co-ordinate system, and the angular velocity of the rotating co-ordinate system. The Coriolis force is perpendicular to both the linear motion and the axis of rotation.

Consider a molecule XY_2 which is rotating as shown below. What effect does Coriolis force have on the three different vibrations of this molecule? The directional dependence of the force is such that a right handed screw, travelling in the direction of the Coriolis force, would carry the displacement (vibrational) vector into the positive direction of the rotational axis, traversing over the narrower angle. In the diagram, the vibrational vector is the solid arrow and the resulting Coriolis force is the broken arrow,

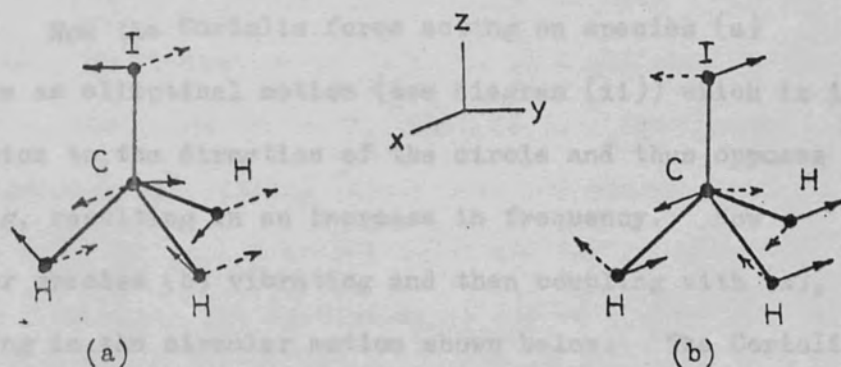

 Direction of Rotation

Vibration



For the case of the ν_1 band, the Coriolis force produces oscillatory rotation with the phase of the vibration. For the ν_2 band, the Coriolis force excites the ν_3 band, and vice versa. The two modes are thus coupled.

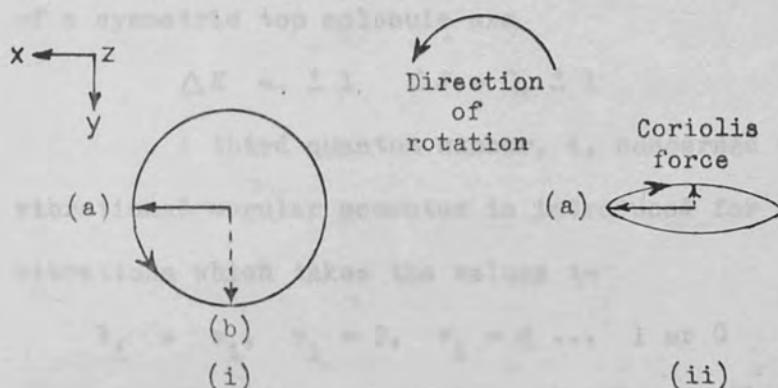
Now consider the ν_6 band of methyl iodide (degenerate vibration) which is the in-plane bending and rocking mode as shown below :-



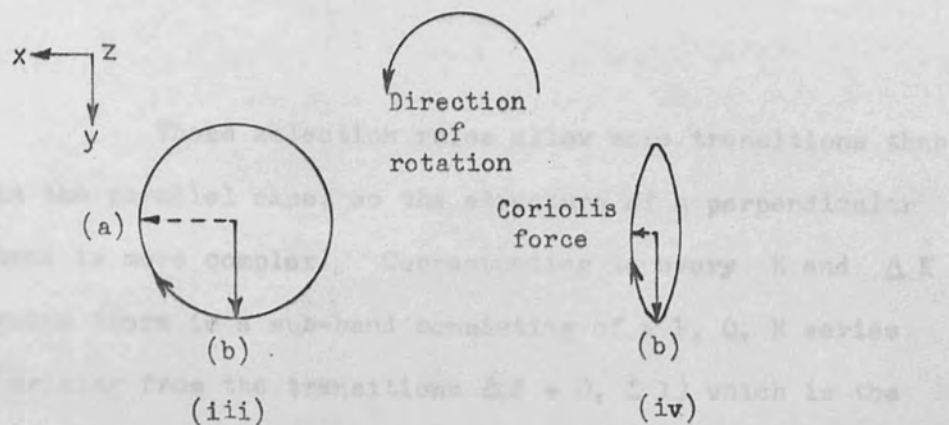
Consider species (a) to be coupled with species (b) and to be rotating about the z axis. The Coriolis force produces a splitting of the degenerate vibrational levels into two levels

whose separation increases with increasing rotation (K) about the z axis, although the splitting is zero for $K = 0$. The splitting is explained by the following.

Consider one of the hydrogen atoms vibrating as per species (a). The vibration of species (b) is 90° to this. If the vibration of (b) happens to be 90° out of phase with (a) and the amplitude of the vibrations is the same, a coupling of the vibrations can result in a circular motion of a hydrogen atom as shown below (i).



Now the Coriolis force acting on species (a) produces an elliptical motion (see diagram (ii)) which is in opposition to the direction of the circle and thus opposes coupling, resulting in an increase in frequency. Now consider species (b) vibrating and then coupling with (a), resulting in the circular motion shown below. The Coriolis force acting on species (b) produces an elliptical motion which enhances coupling, resulting in a decrease in frequency.



The degenerate species are thus seen to move apart from each other.

The selection rules for a perpendicular transition of a symmetric top molecule are

$$\Delta K = \pm 1, \quad \Delta J = 0, \pm 1$$

A third quantum number, \pm , concerned with vibrational angular momentum is introduced for degenerate vibrations which takes the values :-

$$\pm_1 = v_1, v_1 - 2, v_1 - 4 \dots 1 \text{ or } 0$$

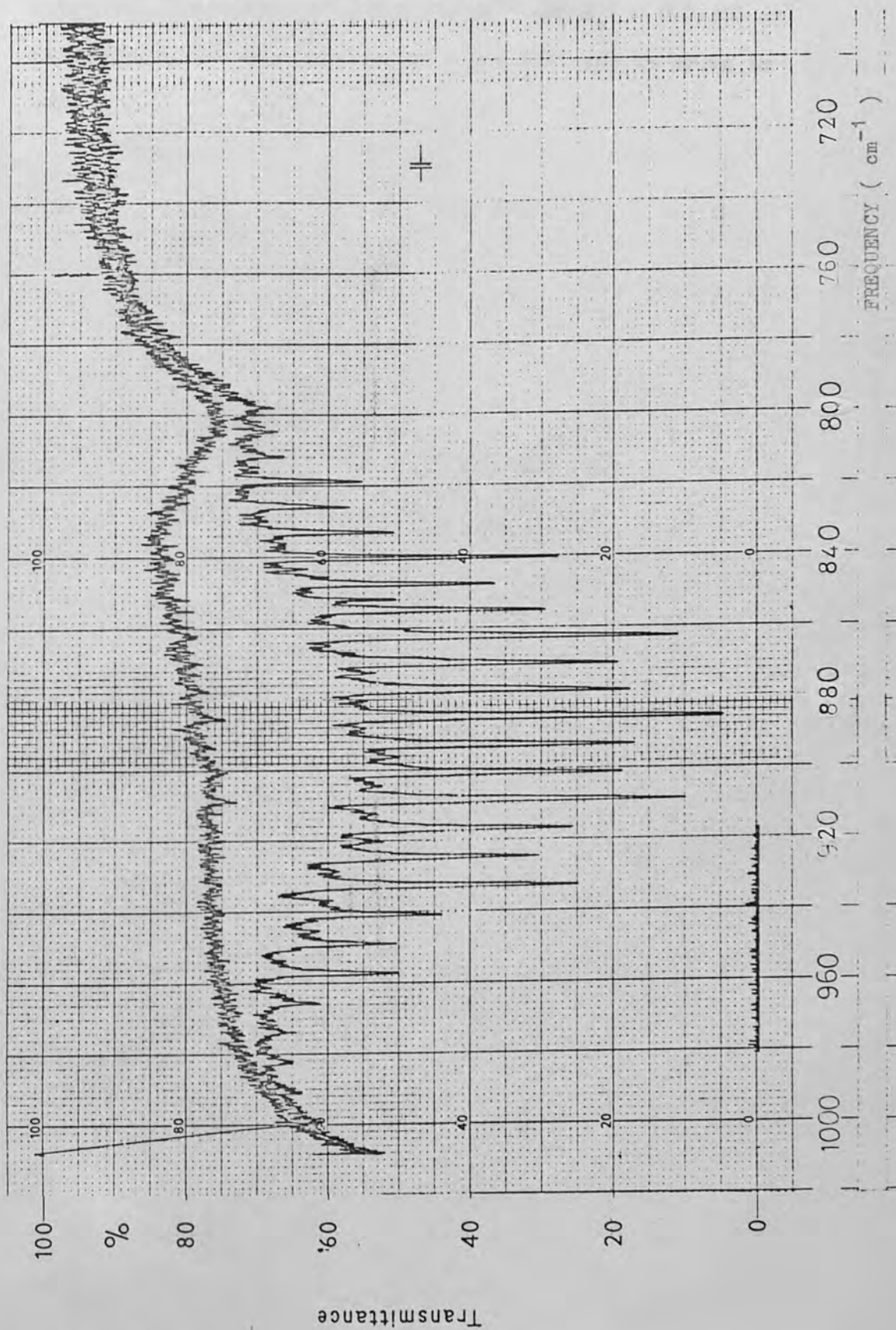
where i refers to a particular vibration. When v_i is an even number the lowest value \pm_1 takes is 0 and when v_i is an odd number the lowest value \pm_1 takes is 1. This work is only concerned with transitions from the $v_i = 0$ energy level to $v_i = 1$ and $\pm = 1$ in the higher energy level and has a degeneracy of 2. The two components are denoted by $+\pm$ and $-\pm$ (5) so the vibrational angular momentum may be the same or opposite in sign to the rotational angular momentum.

These selection rules allow more transitions than in the parallel case, so the structure of a perpendicular band is more complex. Corresponding to every K and ΔK value there is a sub-band consisting of a P, Q, R series (arising from the transitions $\Delta J = 0, \pm 1$) which is the same as for the parallel case. The frequencies for these sub-band centres are given by :-

$$\begin{aligned} \bar{\nu}_0^{\text{sub}} &= \bar{\nu}_0 + [A_{\mathbf{V}'} (1 - 2\xi) - B_{\mathbf{V}'}] \pm \\ &2 [A_{\mathbf{V}'} (1 - \xi) - B_{\mathbf{V}'}] K'' \\ &+ [(A_{\mathbf{V}'} - B_{\mathbf{V}'}) - (A_{\mathbf{V}''} - B_{\mathbf{V}''})] K''^2 \end{aligned}$$

The third term on the right hand side of this equation has a + sign for the R branch ($\Delta K = +1$) and a - sign for the P branch ($\Delta K = -1$), to take into account the selection rule for $+i$ and $-i$ levels. The separation of the sub-bands is thus $2 (A_{\mathbf{V}'} (1 - \xi) - B_{\mathbf{V}'})$. This means that a perpendicular band may not only have a range of shapes depending on the difference between the two rotational constants, but also depending on ξ . For methyl iodide $A_{\mathbf{V}'} = 5.069 \text{ cm}^{-1}$ and $B_{\mathbf{V}'} = 0.2484 \text{ cm}^{-1}$ (26), so the sub-bands are widely spaced. Fig. 1.4 shows the ν_6 band of methyl iodide at 882 cm^{-1} which has a Coriolis constant of 0.21 (33). The shape of this band contrasts greatly with the e_{1u} band of hexafluorobenzene at 315 cm^{-1} which has

Fig.1.4 The ν_6 band of methyl iodide.
Pressure is 1.97×10^4 Pa.



rotational constants $A_V' = 0.01734 \text{ cm}^{-1}$ and $B_V' = 0.03468 \text{ cm}^{-1}$ (36) with a Coriolis constant of -0.6 (36) and is shown in Fig. 1.5.

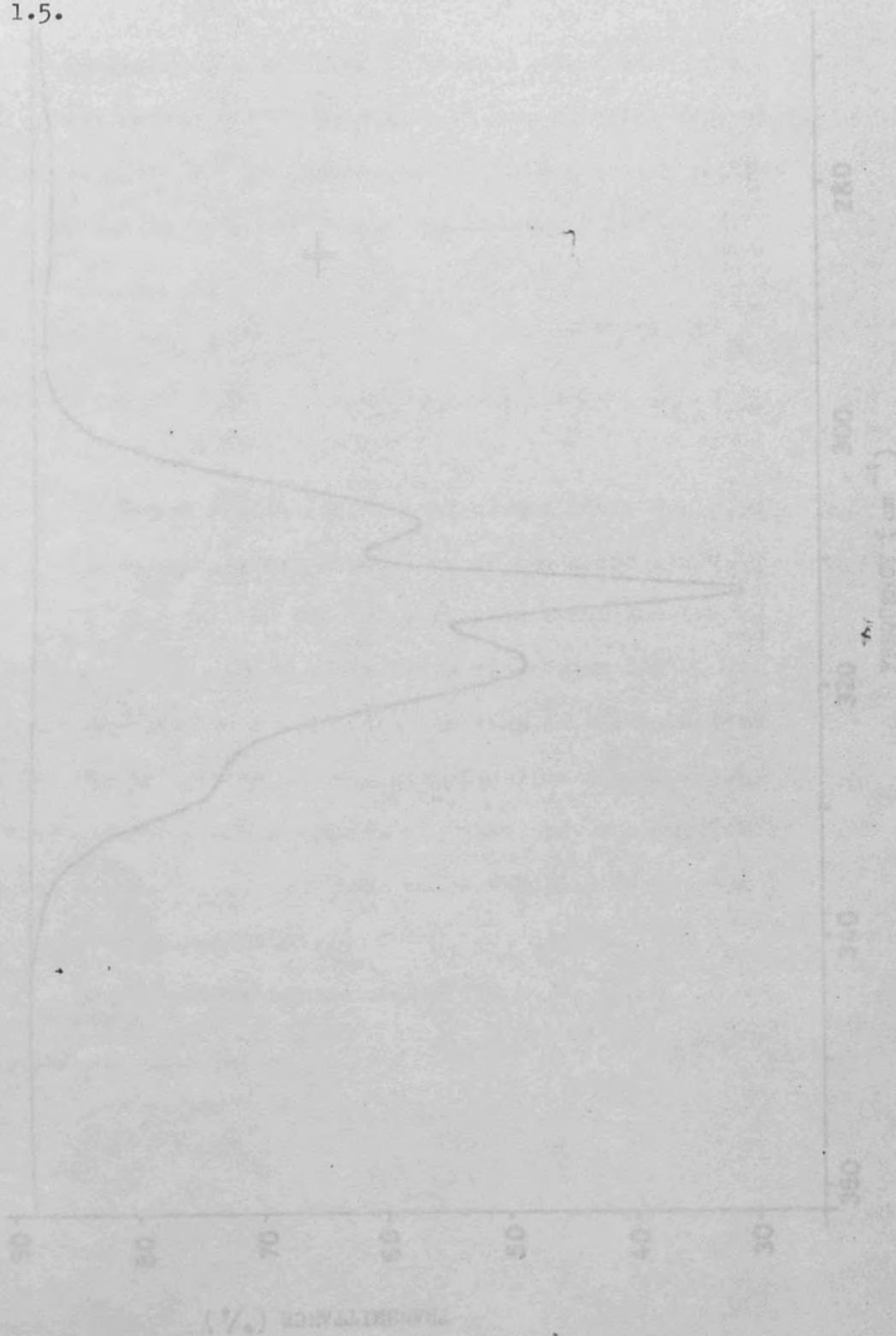
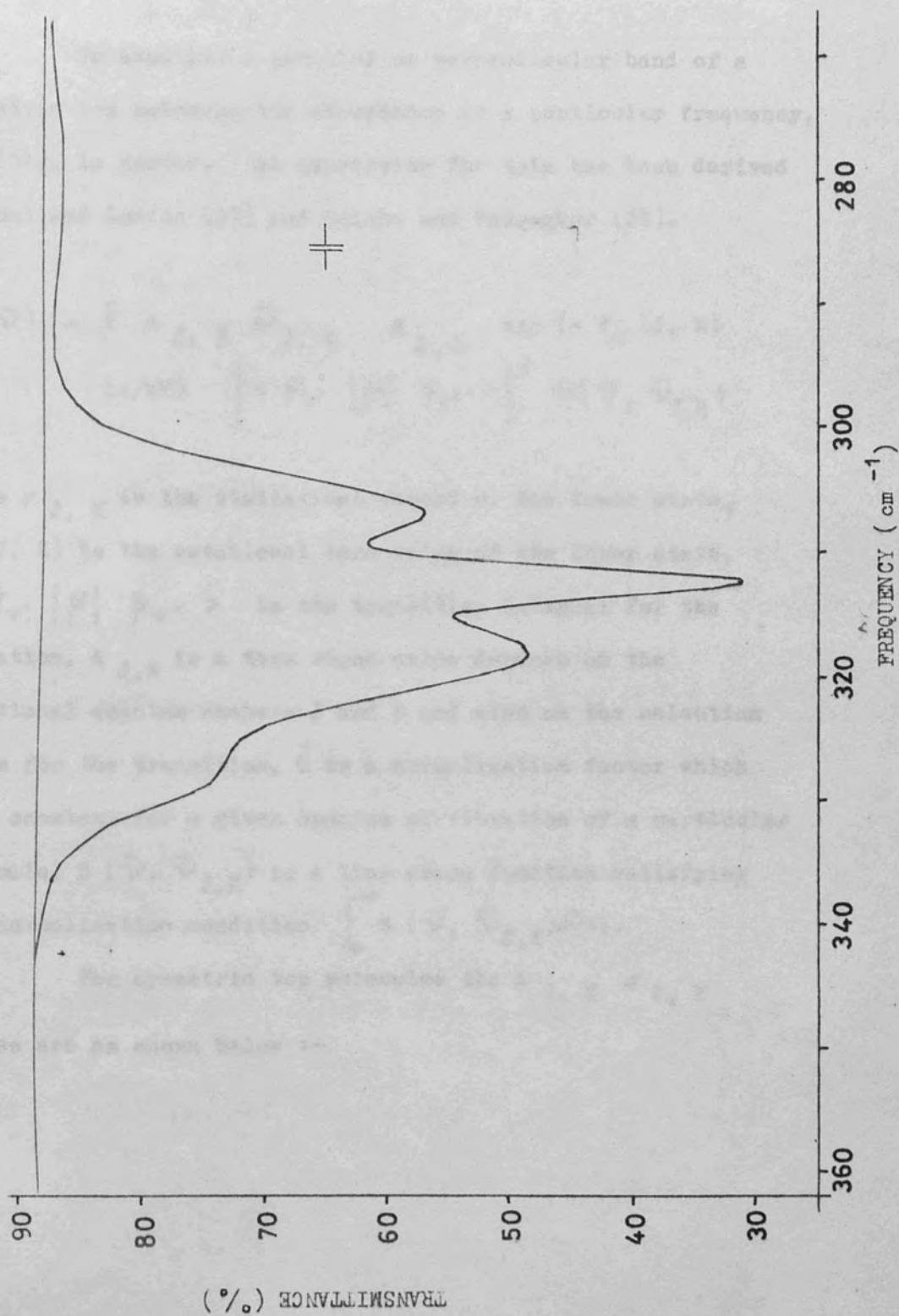


Fig. 1.5 The 315 cm^{-1} band of hexafluorobenzene, measured in a 10 cm gas cell, at a pressure of 1.05×10^4 Pa.



Section 1.5

Computer Simulation of the Rotation -
Vibration Spectra of Symmetric Top
Molecules.

To simulate a parallel or perpendicular band of a symmetric top molecule the absorbance at a particular frequency, $\alpha(\bar{\nu})$, is needed. An expression for this has been derived by Honl and London (27) and Reiche and Rademaker (28).

$$\alpha(\bar{\nu}) = \bar{C} A_{J,K} \bar{\nu}_{J,K} g_{J,K} \exp(-F_V(J,K) / hc/kT) \left| \langle \psi_{v'} | \mu | \psi_{v''} \rangle \right|^2 S(\bar{\nu}, \bar{\nu}_{J,K})$$

where $g_{J,K}$ is the statistical weight of the lower state, $F_V(J,K)$ is the rotational term value of the lower state, $\langle \psi_{v'} | \mu | \psi_{v''} \rangle$ is the transition integral for the vibration, $A_{J,K}$ is a term whose value depends on the rotational quantum numbers J and K and also on the selection rules for the transition, \bar{C} is a normalisation factor which is a constant for a given species of vibration of a particular molecule, $S(\bar{\nu}, \bar{\nu}_{J,K})$ is a line shape function satisfying the normalisation condition $\int_0^{\infty} S(\bar{\nu}, \bar{\nu}_{J,K}) d\bar{\nu} = 1$.

For symmetric top molecules the $A_{J,K} g_{J,K}$ values are as shown below :-

Parallel transitions :-

$$J, |K| \rightarrow J+1, |K| \quad (2 - \delta_{K,0}) \frac{(J+K+1)(J-K+1)}{J+1}$$

$$J, |K| \rightarrow J, |K| \quad (2 - \delta_{K,0}) \frac{(2J+1)K^2}{J(J+1)}$$

$$J, |K| \rightarrow J-1, |K| \quad (2 - \delta_{K,0}) \frac{(J+K)(J-K)}{J}$$

Perpendicular transitions :-

$$J, |K| \rightarrow J+1, |K| \pm 1 \quad \frac{(J \pm K + 1)(J \pm K + 2)}{J+1}$$

$$J, |K| \rightarrow J, |K| \pm 1 \quad \frac{(2J+1)(J \mp K)(J \pm K + 1)}{J(J+1)}$$

$$J, |K| \rightarrow J-1, |K| \pm 1 \quad \frac{(J \mp K)(J \mp K - 1)}{J}$$

In the above J and K refer to the lower state and $\delta_{K,0}$ is the Kronecker delta function which is equal to 1 when $K = 0$ and is equal to 0 when $K \neq 0$.

For the purposes of simulating the band shape the equation may be simplified to

$$\alpha(\bar{\nu})/\bar{\nu}_{J,K} = A_{J,K} \epsilon_{J,K} \exp(-F_V(J,K) hc/kT)$$

Two programmes were written, one for a parallel band (which was called PLSPEC) and one for a perpendicular band (PLESPC). The programmes were written using Fortran IV language and using the above equations for the line positions and intensities. The outputs from the computer were plotted out using a graph plotting facility. The listings of the programmes are to be found in Appendix II.

Programme PLESPC was used to simulate the ν_6 band of methyl iodide using a Coriolis constant of 0.21. The result is to be seen in Fig. 1.6 and is very similar to the experimental band contour of Fig. 1.4. To see the effect that Coriolis coupling may have on this spectrum the programme was re-run using a Coriolis constant of 1.0. The result is shown in Fig. 1.7 and the P, Q, R branches are seen to have bunched up together, whereas before the P and R branches merged into a continuous background with only the Q branches standing out.

Fig.1.6 A computer simulation of the ν_6 band of gaseous methyl iodide using $\xi=0.21$

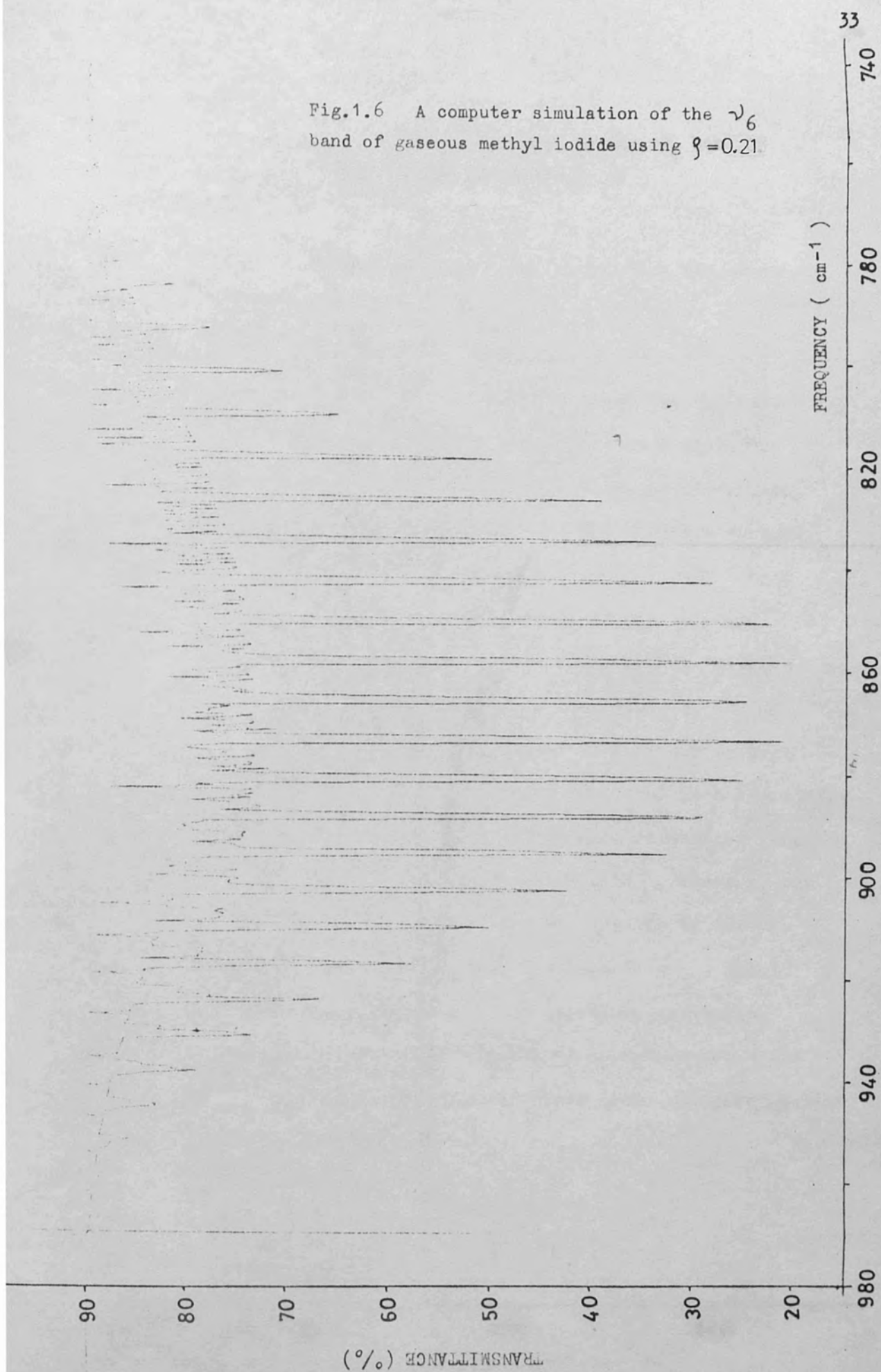
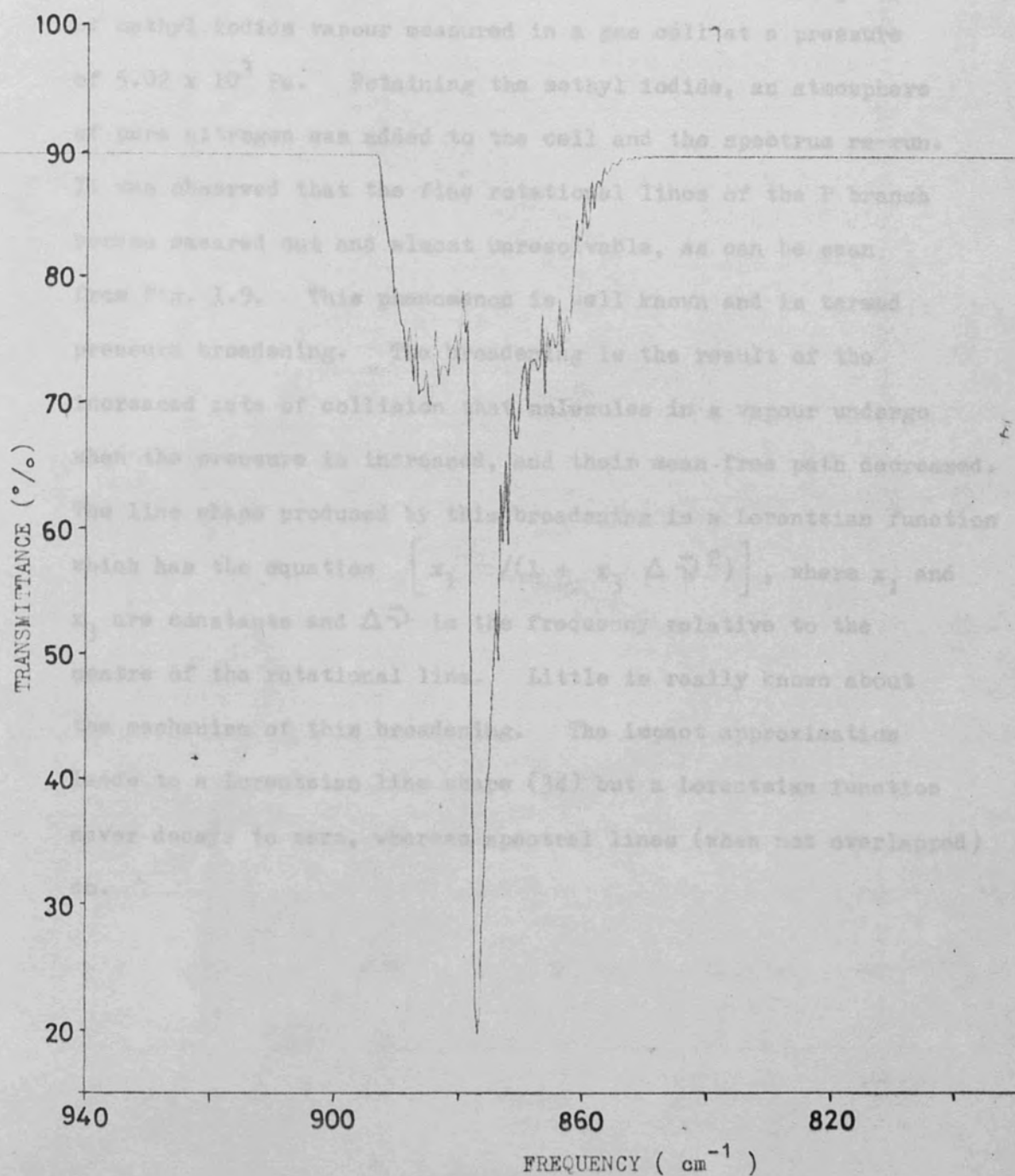


Fig.1.7 A computer simulation of the ν_6 band of gaseous methyl iodide using $\xi=1.0$.



The natural line width of rotational fine structure in a gas phase spectrum is expected to be of the order of 10^{-6} cm^{-1} (35), but the observed lines are several orders of magnitude wider ($\sim 10^{-1}$ cm^{-1}). Fig. 1.8 shows the ν_2 band of methyl iodide vapour measured in a gas cell at a pressure of 5.02×10^3 Pa. Retaining the methyl iodide, an atmosphere of pure nitrogen was added to the cell and the spectrum re-run. It was observed that the fine rotational lines of the P branch became smeared out and almost unresolvable, as can be seen from Fig. 1.9. This phenomenon is well known and is termed pressure broadening. The broadening is the result of the increased rate of collision that molecules in a vapour undergo when the pressure is increased, and their mean free path decreased. The line shape produced by this broadening is a Lorentzian function which has the equation $\left[\frac{x_1}{1 + x_3 \Delta \bar{\nu}^2} \right]$, where x_1 and x_3 are constants and $\Delta \bar{\nu}$ is the frequency relative to the centre of the rotational line. Little is really known about the mechanism of this broadening. The impact approximation leads to a Lorentzian line shape (34) but a Lorentzian function never decays to zero, whereas spectral lines (when not overlapped) do.

Fig.1.8

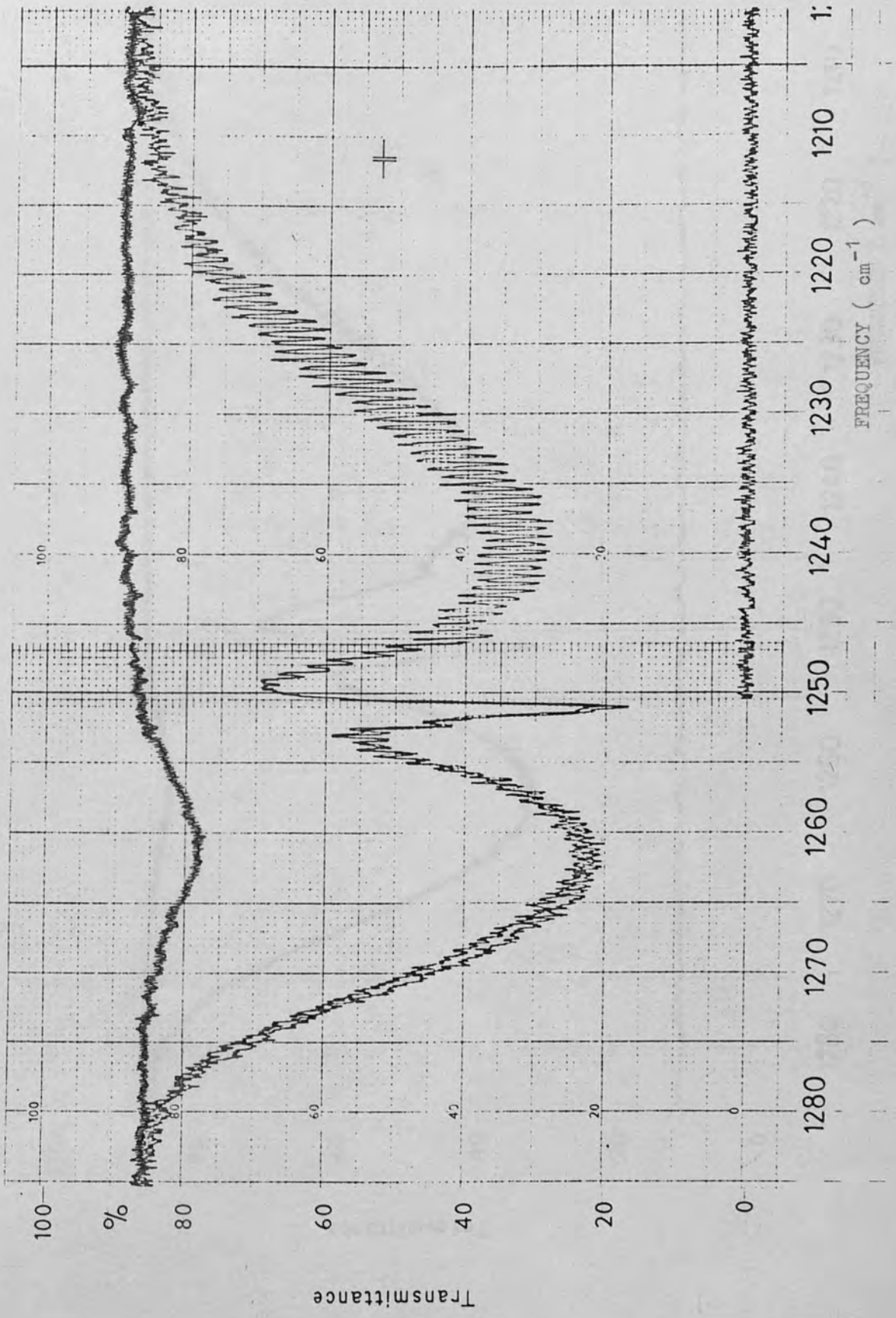
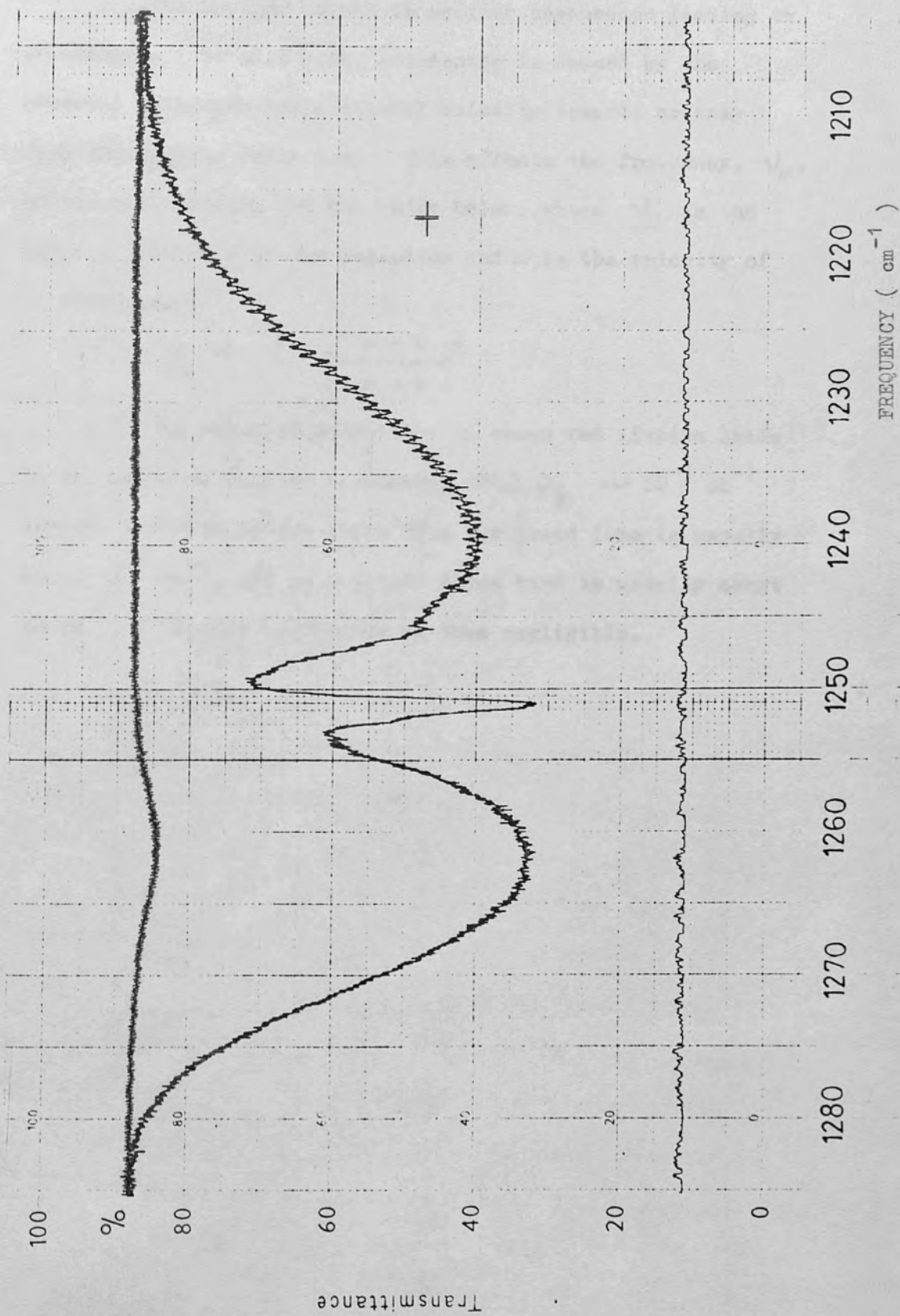


Fig.1.9



The Doppler effect is another phenomenon leading to broadening. In this case, broadening is caused by the observed molecules translational velocity towards or away from the probing radiation. This affects the frequency, ν_p , of the radiation in the way shown below, where ν_D is the Doppler frequency of the radiation and u is the velocity of of molecule.

$$\nu_D = \nu_P \left(\frac{c - u}{c + u} \right)^{\frac{1}{2}}$$

The range of velocities in gases and liquids leads to an expected Doppler broadening of $\Delta \bar{\nu}_{\frac{1}{2}} \sim 10^{-3} \text{ cm}^{-1}$ whereas the half height width of a gas phase line is usually about 10^{-1} cm^{-1} , and of a liquid phase band is usually about 10 cm^{-1} . Doppler broadening is thus negligible.

Section 1.7

The Fourier Transform

Electromagnetic radiation is sinusoidal in nature and is expressed by, for example, (amplitude) = $A \sin(2\pi \nu t)$. An absorption spectrum is a measure of the intensity of a given waveform, which is proportional to the amplitude squared, and is plotted against frequency. The Fourier transform may be used to convert this frequency spectrum into a time spectrum.

The conditions for a Fourier transform of a function of angular frequency $\omega = 2\pi \nu$, $f(\omega)$, to exist are

- a) that the integral of $f(\omega)$ from $-\infty$ to $+\infty$ exists, and,
- b) any discontinuities in $f(\omega)$ are finite.

The Fourier transform has the reciprocal property that when a function is transformed and then re-transformed, we finish up with the original function.

Fig. 1.10a shows a finite wave train and the corresponding power spectrum in the frequency domain. If the wave train is extended, the frequency spectrum becomes narrower, as is to be seen in Fig. 1.10b. In this way one can see that the bandwidth is related to the history of the wave in the time domain. A real electromagnetic wave has a finite length and is damped, or truncated, in a specific fashion.

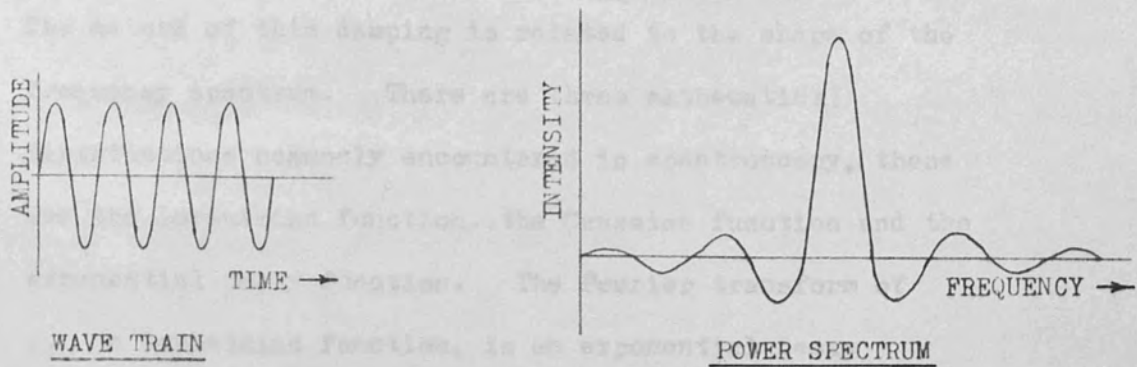


Fig. 1.10a

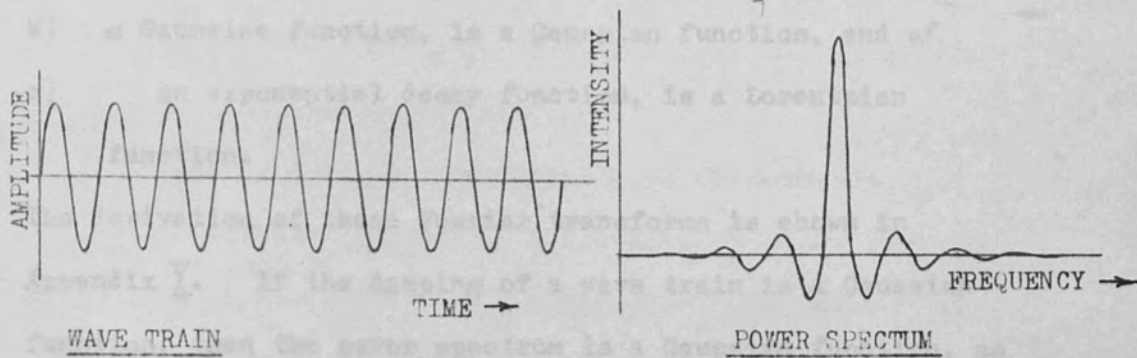


Fig. 1.10b

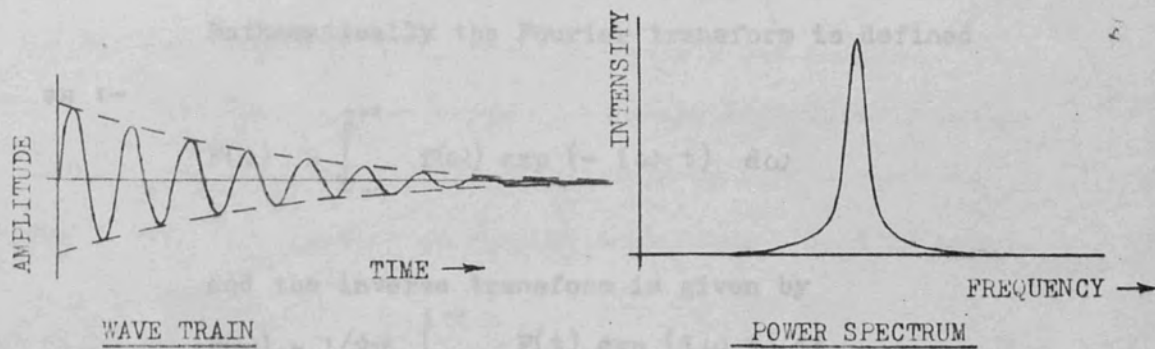


Fig. 1.10c

Fig. 1.10 shows the way in which the Fourier transform of a wave train leads to the contour of the power spectrum.

The nature of this damping is related to the shape of the frequency spectrum. There are three mathematical distributions commonly encountered in spectroscopy, these are the Lorentzian function, the Gaussian function and the exponential decay function. The Fourier transform of

- a) a Lorentzian function, is an exponential decay function, of,
- b) a Gaussian function, is a Gaussian function, and of
- c) an exponential decay function, is a Lorentzian function.

The derivation of these Fourier transforms is shown in Appendix I. If the damping of a wave train is a Gaussian function, then the power spectrum is a Gaussian function, as shown in Fig. 1.10c.

Mathematically the Fourier transform is defined

as :-

$$F(\omega) = \int_{-\infty}^{+\infty} f(t) \exp(-i\omega t) dt$$

and the inverse transform is given by

$$f(t) = 1/2\pi \int_{-\infty}^{+\infty} F(\omega) \exp(i\omega t) d\omega$$

$F(\omega)$ is said to be the Fourier transform of $f(t)$ and $f(t)$ is said to be the inverse transform of $F(\omega)$. In the equation $i = (-1)^{1/2}$. The argument of the exponential must be a dimensionless quantity, which is seen to be true for the

product of frequency and time. The exponential of the integral may be written as

$$\exp(-i\omega t) = \cos(\omega t) - i \sin(\omega t)$$

and consequently the Fourier transform for an even function may be re-written as :-

$$F(t) = 2 \int_0^{\infty} f(\omega) \cos(\omega t) d\omega$$

In this work, the Fourier transform of a frequency spectrum will be termed the time decay curve.

The concept of convolution also involves the Fourier transform. Physically a convolution is the smearing out of a physical quantity by a mathematical function. An example is a photograph which has been taken out of focus. All the information is on the photograph but it is smeared out by the lens function. In fact, scientists use computers to deconvolute (the opposite process) television pictures from the moon. The convolution will be encountered in Chapter Two. For further information on Fourier transforms a good reference book is (1).

Section 1.8

Computer Programming

The computer programmes used in this work were all written by myself in Fortran IV and punched onto cards. Listings of various programmes are to be found in alphabetical order in Appendix II. The programme names are printed in capital letters in the text. The programmes were run on the CDC 6600 computer of the University of London, using a terminus at Royal Holloway College.

Section 1.9Purification of Compounds
Instrumental
and Physical Disturbances

The main compounds used in this work were liquids which were obtained as spectroscopic grade purity. These were distilled and stored over molecular sieve, and then re-distilled in a vacuum line immediately before use. Methyl iodide was also stored over copper, which absorbs any iodine liberated in dissociation caused by light.

adjusted so that there was a slight drift of the pen towards high transmittance.

The linearity of the pen recorder was then checked by setting the transmittance to, for example, 100% without anything in the two beams. A high speed rotating motor was then placed in the sample beam and the sample beam chopped according to the calibration of the rotating motor. The accuracy of the pen recorder was always within the noise level of $\pm 0.2\%$ transmittance.

When running a spectrum the concentration and path length were such that the minimum transmittance was about 20% so that when using the ratio $(I(\nu)/I(\bar{\nu}))$ the accuracy was acceptable. For example, for $I_0(\bar{\nu}) = 50\%$ transmittance and an inaccuracy of $\pm 0.1\%$ transmittance at 20% transmittance, the percentage inaccuracy in $(I_0(\bar{\nu})/I(\bar{\nu}))$ is $(4.500 - 4.473)/4.500 \times 100 = 0.60\%$ whereas for an inaccuracy of $\pm 0.1\%$ transmittance at 5% transmittance the percentage inaccuracy in $(I_0(\bar{\nu})/I(\bar{\nu}))$ is $(18.000 - 17.647)/18.000 \times 100 = 1.96\%$.

CHAPTER TWOCorrection of Spectra for Instrumental
and Physical DistortionsSection 2.1General Instrument Conditions when
Running a Spectrum

Before running a spectrum on the model 325, electronic balance of the pen recorder was checked by closing off both the sample and reference beams to observe the drift of the pen when set at 50% transmittance. The balance was adjusted so that there was a slight drift of the pen towards high transmittance.

The linearity of the pen recorder was then checked by setting the transmittance to, for example, 100% without anything in the two beams. A high speed rotating sector was then placed in the sample beam and the sample beam chopped according to the calibration of the rotating sector. The accuracy of the pen recorder was always within the noise level of $\pm 0.25\%$ transmittance.

When running a spectrum the concentration and path length used were such that the minimum transmittance was about 20% so that, when taking the ratio $(I_0(\bar{\nu})/I(\bar{\nu}))$ the accuracy was acceptable. For example, for $I_0(\bar{\nu}) = 90\%$ transmittance and an inaccuracy in $I(\bar{\nu})$ of $+0.1\%$ transmittance at 20% transmittance, the percentage inaccuracy in $(I_0(\bar{\nu})/I(\bar{\nu}))$ is $(4.500 - 4.478)/4.500 \times 100 = 0.497$ whereas for an inaccuracy in $I(\bar{\nu})$ of 0.1% transmittance at 5% transmittance the percentage inaccuracy in $(I_0(\bar{\nu})/I(\bar{\nu}))$ is $[(18.000 - 17.647)/18.000] \times 100 = 1.961$.

Section 2.2Distortion of the Transmittance Curve
due to the Finite Width of the Slit

In order to record a sensible spectrum with a spectrometer the variable slits, through which the radiation passes to the detector, need to be of a finite width or there will be insufficient energy available to give a stable signal. This produces an error in the recorded spectrum due to radiation of different frequencies being allowed through these "wide" slits at the same time. Any given frequency becomes smeared out, or convoluted.

The model 325 was equipped with a fore monochromator in the form of a KBr prism and a main monochromator consisting of two echelette gratings. A resolution of 0.2 cm^{-1} can be obtained from this system in the region 2000 cm^{-1} to 500 cm^{-1} . The mechanical slit widths generally employed give a spectral slit width of about 1.0 cm^{-1} . The spectral slit width is obtained directly from the instrument display panels as the product of the reciprocal linear dispersion and the mechanical slit width. For example, at 670 cm^{-1} the reciprocal linear dispersion is 17 cm^{-1} per cm and the mechanical slit width is 0.052 cm , thus the spectral slit width is 0.88 cm^{-1} . Also of note is that the wavelength at 670 cm^{-1} is 0.00149 cm which means that the mechanical slit width is 35 times the wavelength of the radiation and so diffraction at the slits is not a problem. From the above it is seen that the overall resolution is slit width limited and so a means of correcting for the finite slit widths was sought.

Section 2.3Correction of the Slit Distortion using
Fourier Transformation

Rautian (2) has done a comprehensive study of the distortion of infra-red transmitted intensity curves due to the so called apparatus function. The apparatus function is a composite function of all the physical and electronic distortions due to the non-ideality of the spectrometer. The apparatus function convolutes the recorded signal in the instrument. This convolution is expressed mathematically as :-

$$f(\omega) = \int_{-\infty}^{+\infty} a(\omega - \omega') \phi(\omega') d\omega' \quad (2.1)$$

where $f(\omega)$ is the apparent intensity, $\phi(\omega')$ the true intensity and $a(\omega - \omega')$ is the apparatus function which defines the fraction of energy of frequency ω' which is transmitted through the system to the recorder when the instrument is set to record at a frequency ω .

For the model 325 the predominant distortion is due to the slit and for this work "slit function" can be substituted for "apparatus function". Equation (2.1) can be solved by first taking the Fourier transform of the entire equation :-

$$F(t) = \int_{-\infty}^{+\infty} \int_{-\infty}^{+\infty} a(\omega - \omega') \phi(\omega') \exp(-i\omega t) d\omega' d\omega$$

substituting $\omega - \omega' = x$ and separating the new variables ω' and x then

$$F(t) = \int \phi(\omega') \exp(-i\omega' t) d\omega' \int a(x) \exp(-ixt) dx$$

$$\rightarrow F(t) = \Phi(t) A(t) \quad (2.2)$$

The Fourier transform of the true intensity is thus obtained from the Fourier transforms of the apparent intensity and the slit function. The true intensity is hence obtained from the inverse Fourier transform of $\Phi(t)$.

The model 325 has two slits of identical width with mirror symmetry about the dispersive grating and so, during scanning, any infinitely narrow band of radiation will be convoluted into a rectangular band by the first slit, of length s , where s is the spectral slit width. Then this rectangular band is convoluted by the second slit into a triangle of base length $2s$. The equation of the triangle is :-

$$\left. \begin{aligned} a(\omega - \omega') &= 1/s \left(1 - \frac{|\omega - \omega'|}{s}\right) & \text{for } |\omega - \omega'| \leq s \\ a(\omega - \omega') &= 0 & \text{for } |\omega - \omega'| > s \end{aligned} \right\} \quad (2.3)$$

The $(1/s)$ in equation(2.3) is to normalise the equation so that

$$\int a(\omega - \omega') d\omega' = 1$$

and the total intensity is not affected by the convolution.

The Fourier transform of the triangular slit function is derived in Appendix I to be :-

$$A(t) = \left[\frac{\sin(st/2)}{\frac{st}{2}} \right]^2 = \text{sinc}^2(st/2)$$

The above theory was first tested using computer simulation. A Fortran IV programme was written to simulate a Gaussian function which has the form :-

$$g(\bar{\nu}) = x_1 \exp(-x_4(\bar{\nu} - \bar{\nu}_0)^2)$$

where x_1 is the peak height and $x_4 = \ln(2)/(0.5 \Delta \bar{\nu}_{1/2})^2$. A Fourier transform routine first needed to be tested and this was done by performing a Fourier transform and then an inverse Fourier transform on the Gaussian function to see if this yielded the original curve.

The integration was carried out using the trapezium rule, i.e.

$$\int_1^n f(x) dx = (1/2 f(1) + f(2) + \dots + f(n-1) + 1/2 f(n)) \Delta x$$

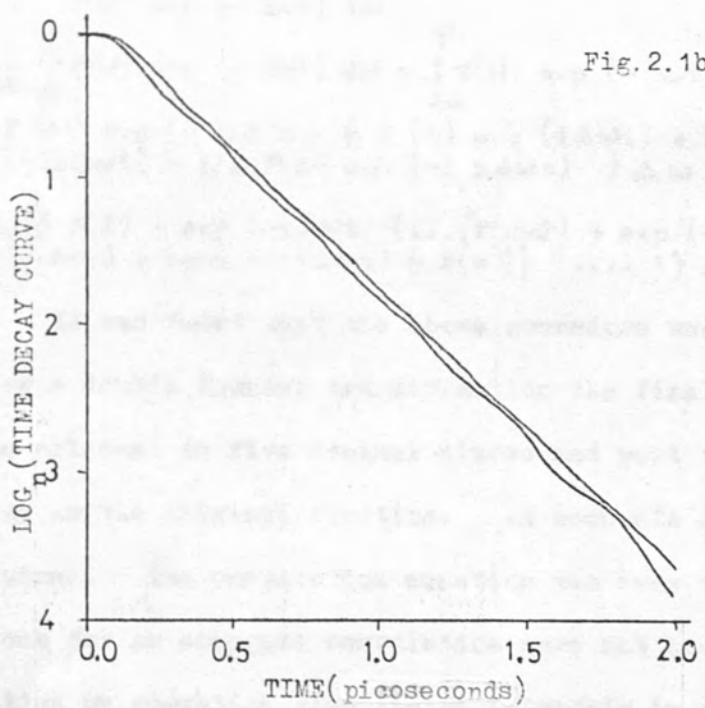
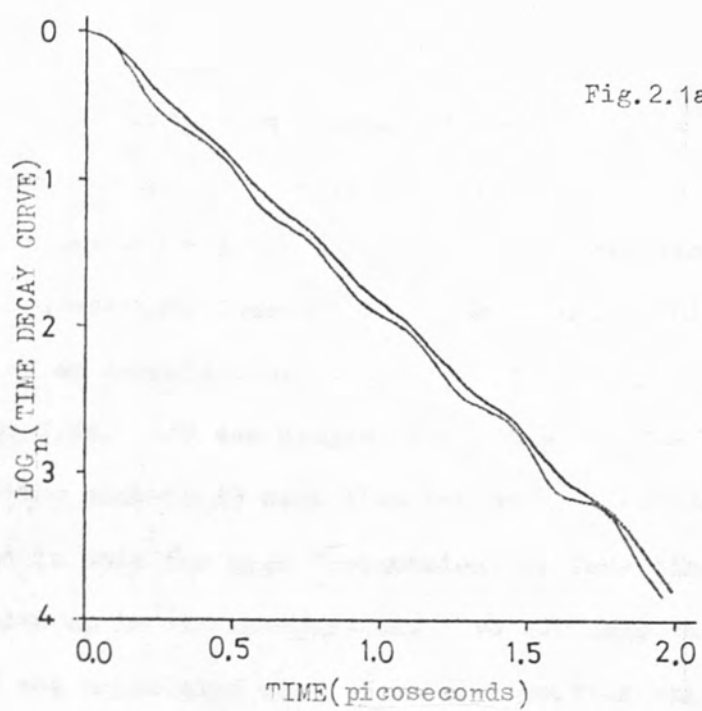
So, if we write ω in place of $(\omega - \omega_0)$ for simplicity, we have

$$\left[\sum_{j=1}^{j=n-1} f(\omega_j) \exp(-i\omega_j t) \right] \Delta \omega + \left[\begin{array}{l} 1/2 f(\omega_1) \exp(-i\omega_1 t) + 1/2 f(\omega_n) \\ \exp(-i\omega_n t) \end{array} \right] \Delta \omega$$

Because a Gaussian function is symmetric, $\exp(-i\omega t)$ was replaced by $\cos(\omega t)$ in the programme. Also, for an accurate transform, because $\nu = 1/t$ a rule must be followed (1) that the number of points used for the transform (N) is greater than the maximum time to be observed in the transform multiplied by the frequency width ($\nu_{max} - \nu_{min}$) across the spectrum. Also $N > 1/(\Delta t \Delta \nu)$.

Oscillations were superimposed on the Fourier transform decay when the limits of the integration were not taken far enough out into the wings. This was because the Fourier transform saw the truncated Gaussian function as the sum of a curve and a rectangle, and the Fourier transform of a rectangle is a $\text{sinc}(at)$ function (where a is a constant).

The effect on the Fourier transform of a band contour from raising or lowering the baseline was calculated. A Lorentzian function of half height bandwidth equal to 20cm^{-1} was simulated and the Fourier transform calculated out to 100cm^{-1} from the band centre. As mentioned in Chapter One, the Fourier transform of a Lorentzian function is an exponential function, which is a straight line when plotted on a logarithmic scale. The logarithm of the time decay curve is plotted against time in Fig. 2.1a and is the higher of the two lines. Small oscillations are seen to be superimposed along the line due to truncation of the limits of the integration (the Lorentzian contour still has an appreciable intensity 100cm^{-1} away from the band centre). The Lorentzian function was then turned into a transmittance curve plotted between 20% and 90% transmittance. The baseline was then raised from 90% to 91% transmittance and the Fourier transform of the band contour obtained using this baseline was then calculated. This second time decay curve is the lower line in Fig. 2.1a and it is seen that the previous small oscillations are very much increased in amplitude. The baseline was next lowered to 89.12% so that the intensity was zero 100cm^{-1} from the band centre. The Fourier transform of the band contour obtained using this baseline was calculated and plotted on a logarithmic scale. Fig. 2.1b shows this time decay curve, along with the original time decay curve for comparison, and it is seen to be a much smoother line with a marked curvature at very short time. An accurate baseline is thus necessary in this work. The overall gradient of the time decay curve is seen to have increased when the baseline was raised. This is due to the bandwidth being effectively increased.



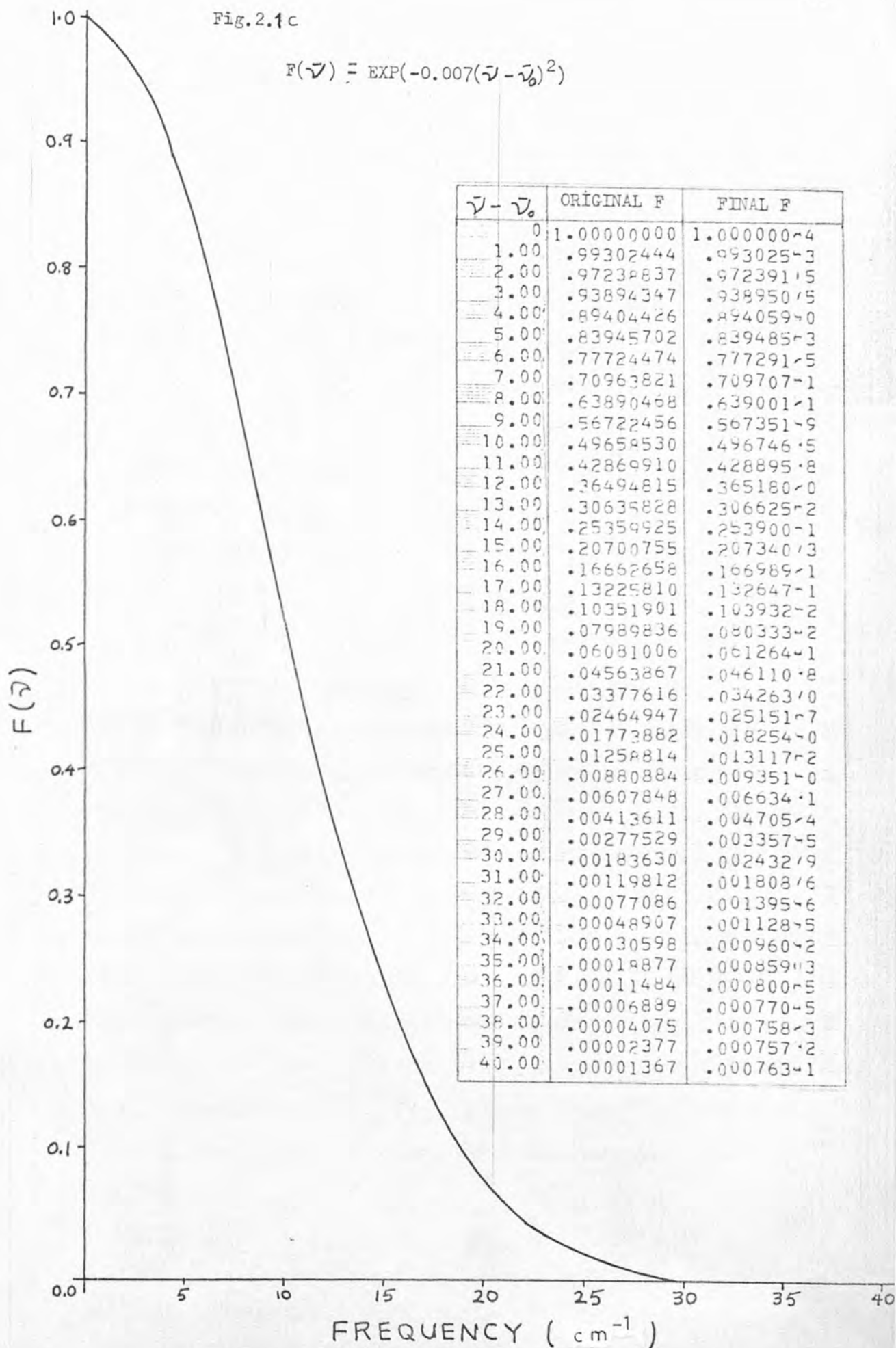
The Fourier transform of a Gaussian spectrum is a Gaussian decay (see Appendix I) and so the accuracy of the first transform was checked. It was found that the time decay became increasingly inaccurate at long time. This inaccuracy increased on transforming back to the frequency domain. See Fig. 2.1c. It was decided that this was due to calculating $\exp(-i\omega_j t)$ each time and small inaccuracies were produced in this for high frequencies and long time which were added up in the integration. To overcome this $\exp(-i\Delta\omega t)$ was calculated once for each time, then raised to the power n .

$$\begin{aligned}
 F(t) &= \int_{-\infty}^{+\infty} f(\omega) \exp(-i\omega t) d\omega \\
 &= \int_{-\infty}^{+\infty} f(\omega) \exp(-i\omega t) d\omega + \int_{-\infty}^{-1} f(\omega) \exp(-i\omega t) d\omega + 2 f(0) \\
 &= \int_{-\infty}^{+\infty} f(\omega) \exp(-i\omega t) d\omega = \left(\frac{1}{2} f(1) \exp(-i\Delta\omega t) + f(2) \exp(-i2\Delta\omega t) + \dots + \frac{1}{2} f(n) \exp(-in\Delta\omega t) \right) \Delta\omega \\
 &= \left\{ \exp(-i\Delta\omega t) \left(\frac{1}{2} f(1) + \exp(-i\Delta\omega t) \left(\dots \left(f(n-2) + \exp(-i\Delta\omega t) \left(f(n-1) + \exp(-i\Delta\omega t) \frac{1}{2} f(n) \right) \right) \right) \right) \right\} \Delta\omega
 \end{aligned}$$

It was found that the above procedure was really accurate and after a double Fourier transformation the final function agreed with the original to five decimal places and went to zero at the same frequency as the original function. An accurate convolution was now required. The convolution equation was easy to use but the conditions for an accurate convolution were not known because integration by summation with finite intervals is not as accurate as algebraic integration. The accuracy depends on the number of points inside the slit function equation, $a(\omega - \omega')$.

Fig. 2.1c

$$F(\nu) = \text{EXP}(-0.007(\nu - \bar{\nu}_0)^2)$$



Programme CORSLT was written to simulate a typical liquid phase infra-red transmitted intensity curve. Liquid band profiles are generally Lorentzian near the band centre and so a Lorentzian function was calculated and then converted into a transmitted intensity curve between 20% and 90%. This intensity curve $I(\bar{\nu})$ was convoluted to $I'(\bar{\nu})$ using equation (2.3). The convolution was performed four times using different frequency intervals ($\Delta\bar{\nu}$) to see how $I'(\bar{\nu})$ was affected. The results are set out in Table 2.1. As can be seen, the intensity for $(2s/\Delta\bar{\nu})+1 = 33$ is only 0.092% different from the $(2s/\Delta\bar{\nu})+1 = 17$ case at the band centre and so is inside experimental error. Hence I used $(2s/\Delta\bar{\nu}) + 1 \geq 33$ as a criterion for an accurate convolution by a triangle.

The Fourier transform routine and the convolution routine were combined in programme FTSLIT and the convoluted intensity was deconvoluted by dividing the Fourier transform of the convoluted intensity by the Fourier transform of the slit function. The result was transformed back to the frequency domain and compared with the original intensity. The programme was run for a spectral slit width of 5 cm^{-1} and a half height band width of 10 cm^{-1} (transmitted intensity curve half height width $> 10 \text{ cm}^{-1}$). The result was a really good fit within experimental accuracy. See Fig. 2.2a where the Fourier transform of $I'(\bar{\nu})$ is compared with $\text{sinc}^2(st/2)$, and Fig. 2.2b, in which $I_{\text{cor}}(\bar{\nu})$ is the corrected intensity and a table compares this with $I(\bar{\nu})$.

| $(2s/\Delta\nu)+1$ | I'_1 (%) - DIFFERENCES | I'_2 (%) - DIFFERENCES |
|--------------------|--------------------------|--------------------------|
| 9 | 31.016 1.355 | 42.686 0.517 |
| 12 | 32.623 0.374 | 43.303 0.137 |
| 17 | 32.997 0.092 | 43.340 0.034 |
| 33 | 33.089 | 43.374 |

Table 2.1 A comparison of the accuracy of the numerical convolution of a typical infrared transmitted intensity curve of a liquid, by a triangle, using an increasing number of points for the integration. The number of points inside the triangle for integration was $(2s/\Delta\nu)+1$. The half height bandwidth of the Lorentzian function used was 10 cm^{-1} and the slit width, s , used was 10 cm^{-1} . I'_1 was the intensity at the band centre and I'_2 was the intensity 5 cm^{-1} away from the band centre. The differences refer to the $I'_{1,2}$'s of adjacent rows.

Fig. 2.2a

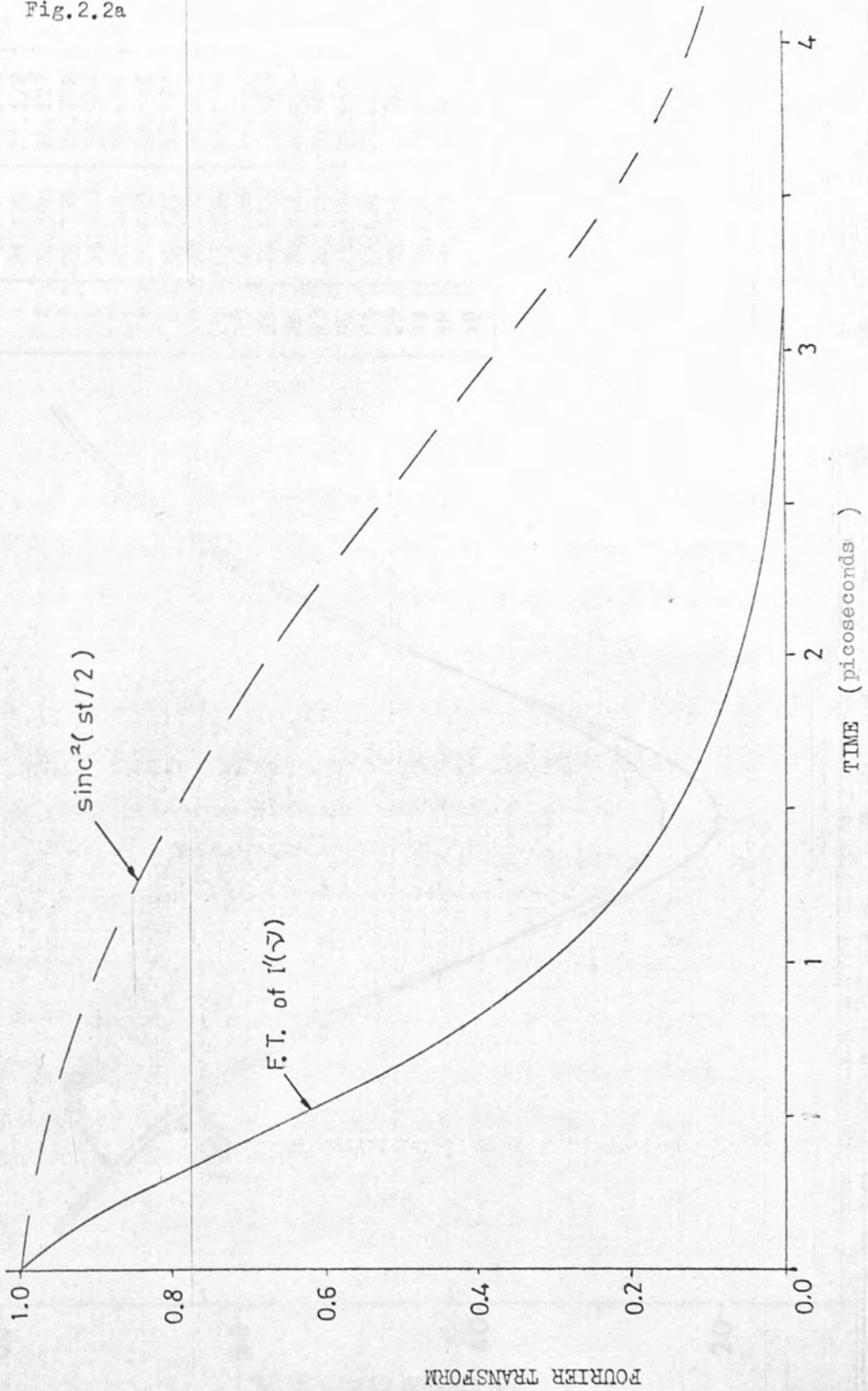
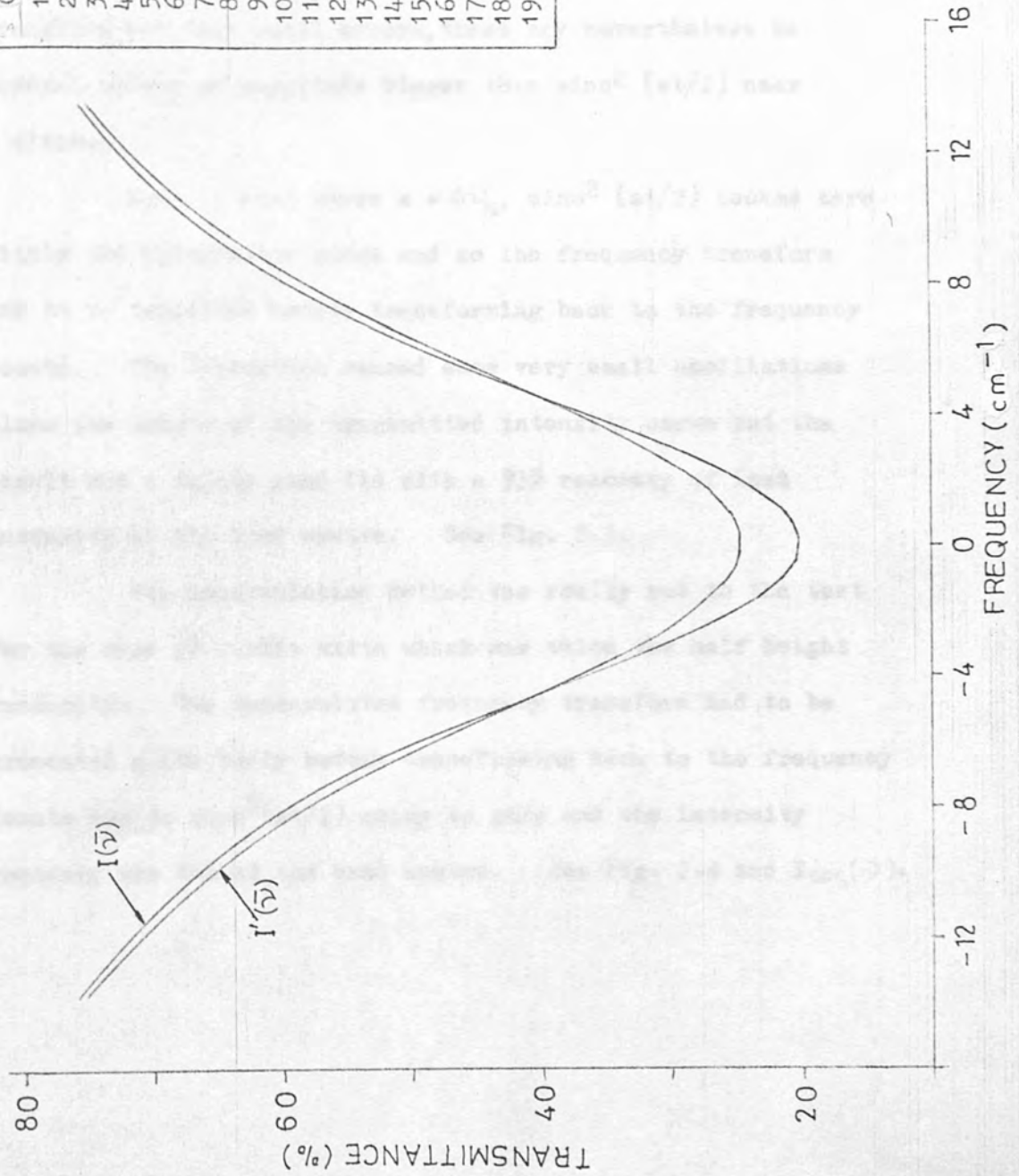


Fig. 2.2b

| $ \bar{\nu} - \bar{\nu}_0 $ | $I(\bar{\nu})$ | $I_{cor}(\bar{\nu})$ |
|-----------------------------|----------------|----------------------|
| 0 | 19.980 | 19.995 |
| 1 | 21.171 | 21.172 |
| 2 | 24.590 | 24.627 |
| 3 | 29.759 | 29.792 |
| 4 | 35.948 | 35.956 |
| 5 | 42.405 | 42.410 |
| 6 | 48.569 | 48.593 |
| 7 | 54.127 | 54.170 |
| 8 | 58.970 | 59.013 |
| 9 | 63.108 | 63.130 |
| 10 | 66.606 | 66.632 |
| 11 | 69.553 | 69.586 |
| 12 | 72.036 | 72.079 |
| 13 | 74.133 | 74.181 |
| 14 | 75.910 | 75.955 |
| 15 | 77.424 | 77.461 |
| 16 | 78.721 | 78.755 |
| 17 | 79.836 | 79.876 |
| 18 | 80.802 | 80.849 |
| 19 | 81.461 | 81.693 |



The limits of this method were investigated for larger spectral slit widths compared with transmitted intensity curve half height width. For wider slits $\text{sinc}^2(st/2)$ has a shorter period of oscillation with minima of zero. Hence, the period can become short enough to interfere with the deconvolution, because dividing by zero or a really small number is useless. Even though the Fourier transform has only small errors, these may nevertheless be several orders of magnitude bigger than $\text{sinc}^2(st/2)$ near a minimum.

For the case where $s = \Delta\bar{\nu}_h$, $\text{sinc}^2(st/2)$ became zero within the integration range and so the frequency transform had to be truncated before transforming back to the frequency domain. The truncation caused some very small oscillations along the length of the transmitted intensity curve but the result was a fairly good fit with a 93% recovery of lost intensity at the band centre. See Fig. 2.3.

The deconvolution method was really put to the test for the case of a slit width which was twice the half height bandwidth. The deconvoluted frequency transform had to be truncated quite badly before transforming back to the frequency domain due to $\text{sinc}^2(st/2)$ going to zero and the intensity recovery was 66% at the band centre. See Fig. 2.4 and $I_{\text{cor}_1}(\bar{\nu})$.

Fig.2.3

| $\bar{\nu}$ | $I(\bar{\nu})$ | $I_{cor}(\bar{\nu})$ |
|-------------|----------------|----------------------|
| 0 | 19.979 | 20.871 |
| 1 | 21.171 | 21.896 |
| 2 | 24.589 | 24.858 |
| 3 | 29.758 | 29.444 |
| 4 | 35.947 | 35.185 |
| 5 | 42.404 | 41.537 |
| 6 | 48.568 | 47.958 |
| 7 | 54.126 | 53.988 |
| 8 | 58.970 | 59.301 |
| 9 | 63.107 | 63.731 |
| 10 | 66.605 | 67.268 |
| 11 | 69.553 | 70.021 |
| 12 | 72.035 | 72.177 |
| 13 | 74.132 | 73.937 |
| 14 | 75.910 | 75.479 |
| 15 | 77.424 | 76.921 |
| 16 | 78.720 | 78.311 |
| 17 | 79.836 | 79.640 |
| 18 | 80.801 | 80.859 |
| 19 | 81.641 | 81.911 |

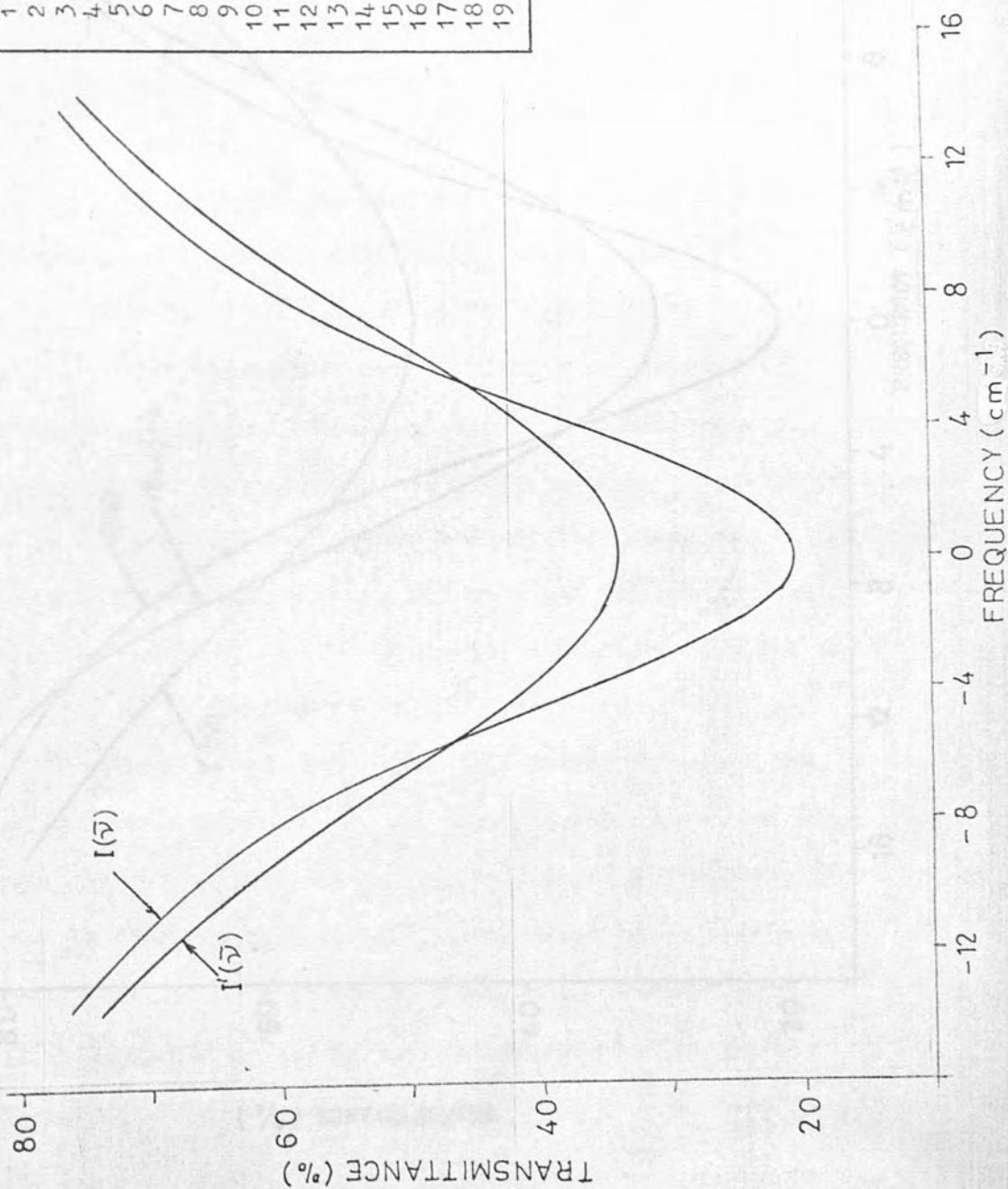
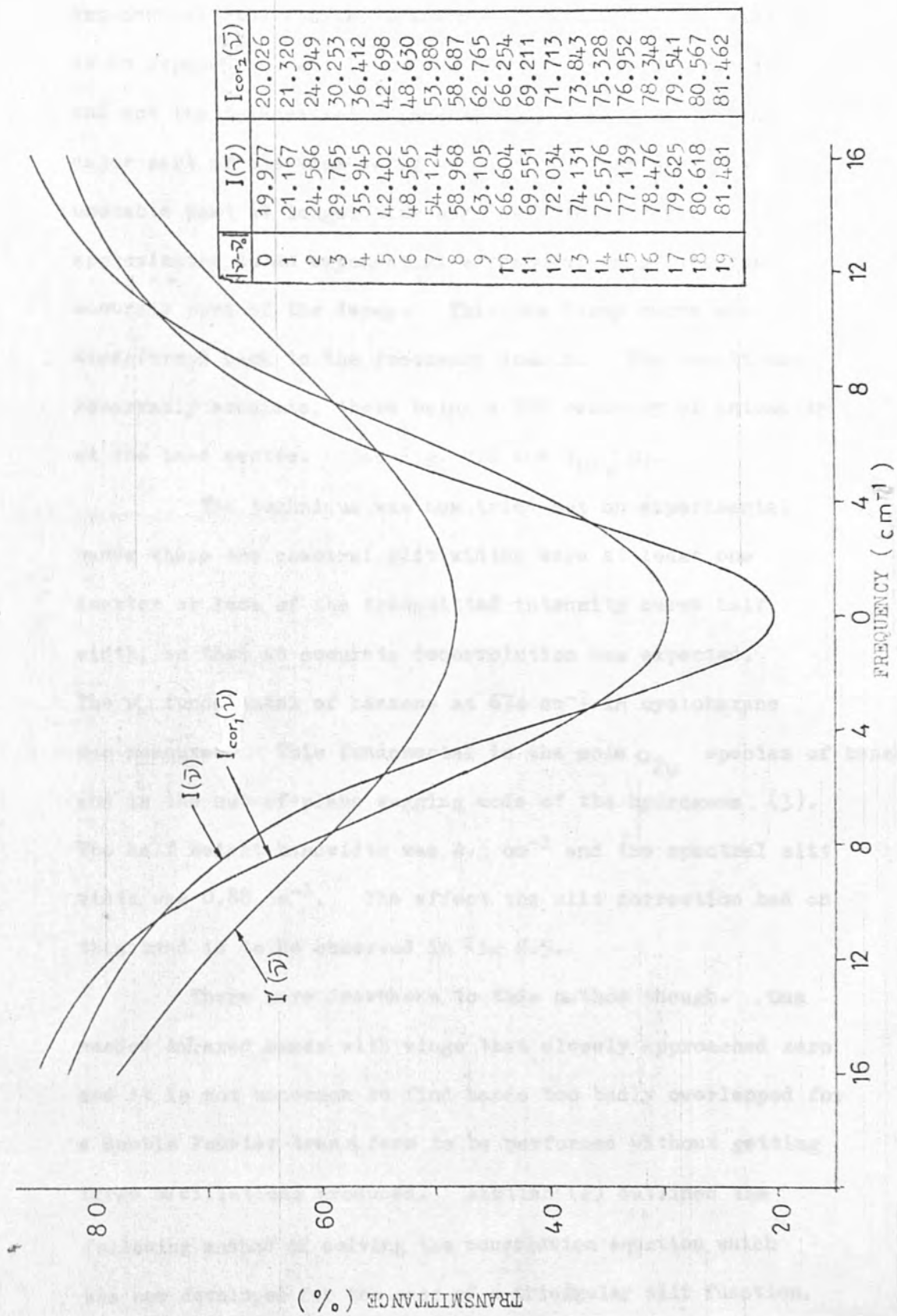


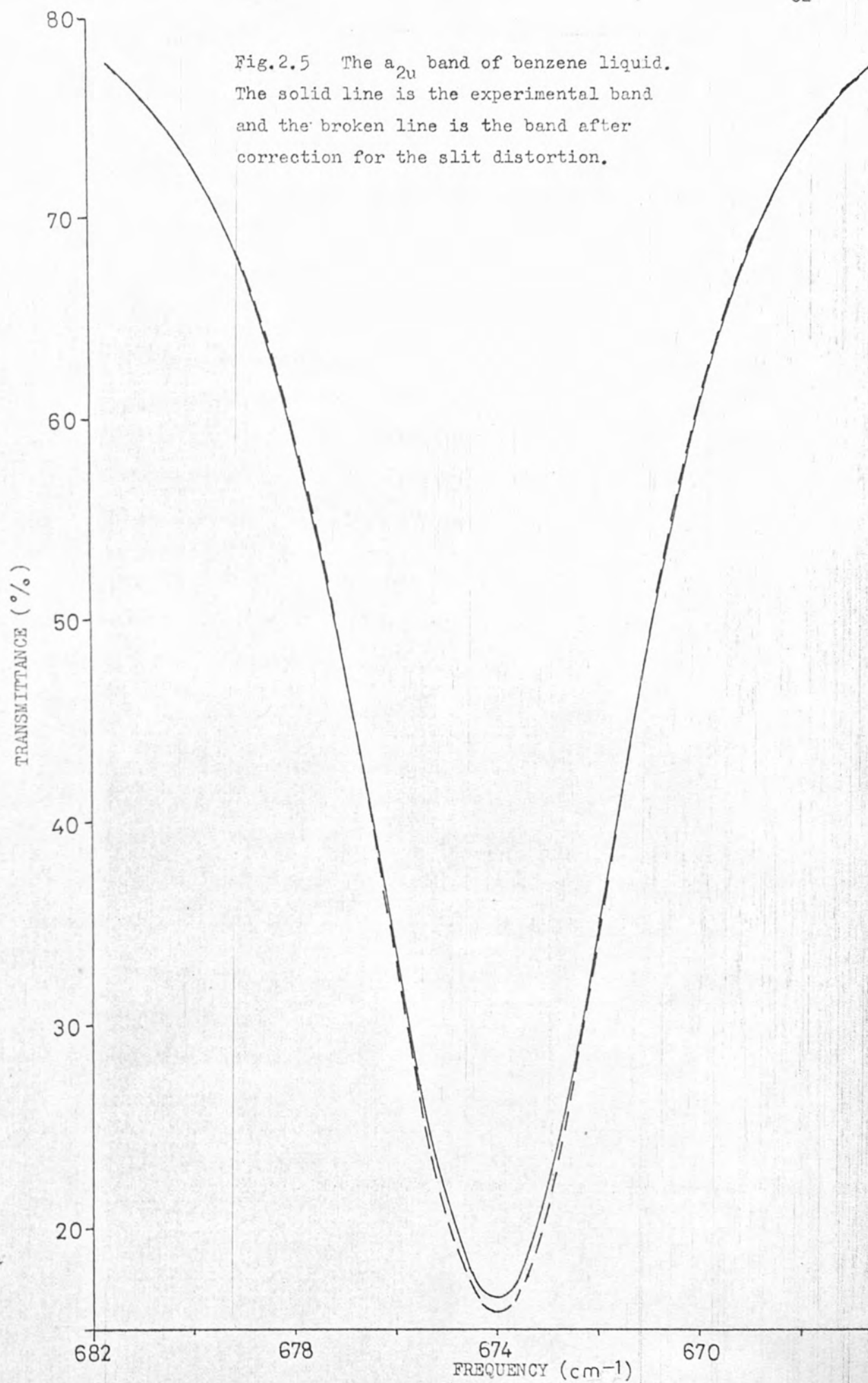
Fig.2.4



It was noticed that the time decay was approximately an exponential (the Fourier transform of a Lorentzian function is an exponential but it is the profile that is Lorentzian and not the transmitted intensity curve) so, because the major part of the time decay was known accurately, the unstable part at longer time and low intensity was approximated to an exponential extrapolation of the last accurate part of the decay. This new decay curve was transformed back to the frequency domain. The result was remarkably accurate, there being a 99% recovery of intensity at the band centre. See Fig. 2.4 and $I_{cor_2}(\nu)$.

The technique was now tried out on experimental bands where the spectral slit widths were at least one quarter or less of the transmitted intensity curve half width, so that an accurate deconvolution was expected. The ν_{11} fundamental of benzene at 674 cm^{-1} in cyclohexane was measured. This fundamental is the sole a_{2u} species of benzene and is the out-of-plane wagging mode of the hydrogens (3). The half height bandwidth was 4.3 cm^{-1} and the spectral slit width was 0.88 cm^{-1} . The effect the slit correction had on this band is to be observed in Fig 2.5.

There were drawbacks to this method though. One needed infrared bands with wings that closely approached zero and it is not uncommon to find bands too badly overlapped for a double Fourier transform to be performed without getting large oscillations produced. Rautian (2) outlined the following method of solving the convolution equation which was now developed for the case of a triangular slit function.



Section 2.4

Correction of the Slit Distortion using
the Derivatives of the Transmitted
Intensity Curve.

The true intensity curve is related to its Fourier
transform by

$$\vartheta(\omega) = \frac{1}{2\pi} \int_{-\infty}^{+\infty} \Phi(t) \exp(i\omega t) dt$$

From equation (2.2)

$$\begin{aligned} \vartheta(\omega) &= \frac{1}{2\pi} \int F(t) A^{-1}(t) \exp(i\omega t) dt \\ &= \frac{1}{2\pi} \int F(t) [A^{-1}(t) - 1] \exp(i\omega t) dt + \frac{1}{2\pi} \int F(t) \exp(i\omega t) dt \\ \therefore \vartheta(\omega) &= f(\omega) + \frac{1}{2\pi} \int F(t) [A^{-1}(t) - 1] \exp(i\omega t) dt \end{aligned}$$

This equation expresses the correction to the
intensity at any frequency as a function involving the Fourier
transforms of the observed spectra and of the slit function.

If $[A^{-1}(t) - 1]$ can be expressed as a power series $\sum_{n=0}^{\infty} b_n t^n$ then

$$\vartheta(\omega) = f(\omega) + \sum_n b_n \frac{1}{2\pi} \int F(t) t^n \exp(i\omega t) dt$$

but $\frac{d^n f(\omega)}{d\omega^n} = \frac{i^n}{2\pi} \int F(t) t^n \exp(i\omega t) dt$

and hence $\vartheta(\omega) = f(\omega) + \sum_n \frac{b_n}{i^n} \times \frac{d^n f(\omega)}{d\omega^n}$ (2.4)

The derivatives $\frac{d^n f(\omega)}{d\omega^n}$ can be measured directly from
the intensity curve and so all that was needed to be found was
a series expansion for the Fourier transform of the slit function.

Now for small x

$$\begin{aligned} \sin x &= x - \frac{x^3}{3!} + \frac{x^5}{5!} - \frac{x^7}{7!} + \dots \\ \Rightarrow \left[\sin\left(\frac{st}{2}\right) / \left(\frac{st}{2}\right) \right]^2 &= \left(1 - \frac{(st)^2}{24} + \frac{(st)^4}{1920} - \dots \right)^2 \\ A(t) &= 1 - \frac{(st)^2}{12} + \frac{(st)^4}{360} - \dots \end{aligned}$$

Also for small x , by binomial expansion

$$(1 - x)^{-1} = 1 + x + x^2 + x^3 + \dots$$

$$\begin{aligned} \Rightarrow A^{-1}(t) &= 1 + \left\{ \frac{(st)^2}{12} - \frac{(st)^4}{360} + \dots \right\} + \left\{ \frac{(st)^2}{12} - \frac{(st)^4}{360} + \dots \right\}^2 \\ &= 1 + \frac{(st)^2}{12} + \frac{(st)^4}{240} + \frac{(st)^6}{6048} \end{aligned}$$

Substituting in equation (2.4)

$$\delta(\omega) = f(\omega) - \frac{s^2}{12} \frac{d^2 f(\omega)}{d\omega^2} + \frac{s^4}{240} \frac{d^4 f(\omega)}{d\omega^4} - \frac{s^6}{6048} \frac{d^6 f(\omega)}{d\omega^6} \quad (2.5)$$

Equation (2.5) seemed a very simple equation which must have been discovered before by previous workers and so a good search through the non-chemical literature was made. This yielded that in 1871 Strutt (6) first considered correcting a curve for convolution through a single slit and derived the equation

$$\delta(\omega) = f(\omega) - \frac{s^2}{24} \frac{d^2 f(\omega)}{d\omega^2}$$

A little later in 1897 Runge (7) considered the error in an observation due to a triangular convolution and derived the following equation

$$\begin{aligned} \delta(\omega) &= f(\omega) - \frac{s^2}{12} \frac{d^2 f(\omega)}{d\omega^2} + \frac{s^4}{90} \frac{d^4 f(\omega)}{d\omega^4} - \dots \\ \dots &\frac{(-1)^{n/2} 2 [(n/2)!]^2}{(n+2)!} \frac{d^n f(\omega)}{d\omega^n} \end{aligned}$$

This equation differs from equation (2.5) in all but the leading term. Hardy and Young (4) made the first rigorous analysis of slit width errors in 1949 giving a general method of correcting for different slit functions. Their method was a

Fourier transform approach and following through their equations for a triangular slit function yielded equation (2.5).

We now want to calculate the second derivative

$$\left[\frac{d^2 f(\omega)}{d\omega^2} \equiv f''(\omega) \right] \quad \text{and a very good geometric approximation}$$

to this is

$$f''(\omega) = \frac{f(\omega+h) - 2f(\omega) + f(\omega-h)}{h^2}$$

where h is a small increment.

This equation is readily derived if the transmitted intensity curve across a small frequency interval is considered to be a quadratic with the equation

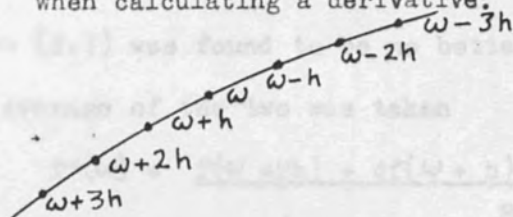
$$f(\omega) = a\omega^2 + b\omega + c$$

The first and second derivatives of this quadratic are given by

$$f'(\omega) = 2a\omega + b$$

$$\text{and } f''(\omega) = 2a$$

Fig.2.6 This diagram shows how the points are numbered when calculating a derivative.



(i) From Fig. 2.6

$$\begin{aligned}
 f(\omega + h) - f(\omega - h) &= 4 a\omega h + 2bh \\
 f(\omega + h) - f(\omega) &= 2 a\omega h + bh + ah^2 \\
 f(\omega + h) - 2 f(\omega) + f(\omega - h) &= 2 ah^2 \\
 \Rightarrow f''(\omega) &= \frac{f(\omega + h) - 2 f(\omega) + f(\omega - h)}{h^2} \quad (2.6)
 \end{aligned}$$

Equation (2.6) was applied to the measured intensities of the ν_3 band of methyl iodide at 527.2 cm^{-1} in carbon tetrachloride solution. This band has a half height bandwidth of 8.8 cm^{-1} and the points were not measured with the greatest accuracy. The second derivative was plotted out and was a wildly oscillating curve. See Fig 2.7. The oscillations were due to amplification of noise on the measured (by eye) data. Different methods for measuring the second derivative were thus sought, which involved more points to average out the noise

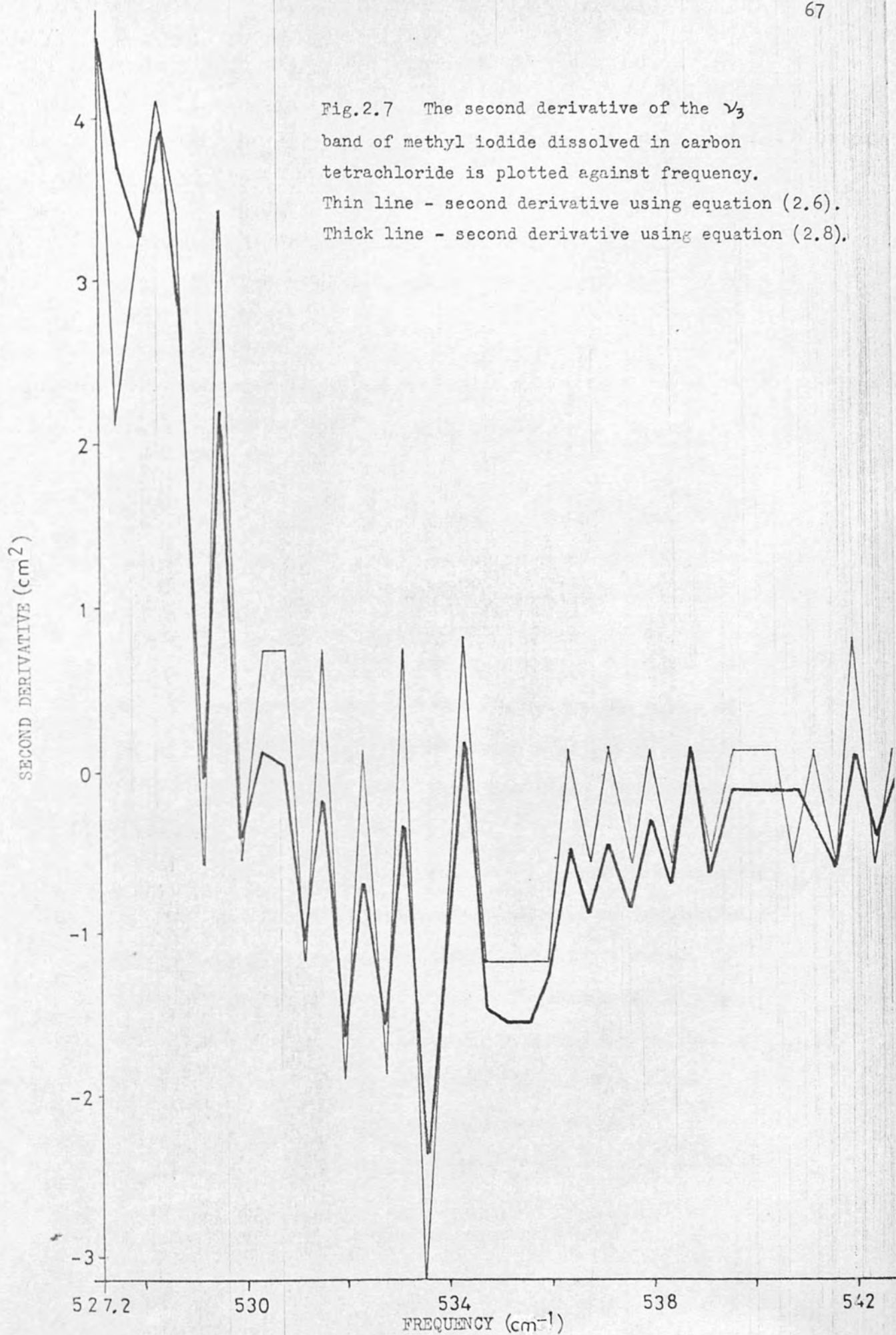
(ii) Referring again to Fig. 2.6

$$\begin{aligned}
 f(\omega + 2h) - f(\omega - 2h) &= 8a\omega h + 4bh \\
 f(\omega + 2h) - f(\omega) &= 4a\omega h + 2bh + 4ah^2 \\
 f''(\omega) &= \frac{f(\omega + 2h) - 2 f(\omega) + f(\omega - 2h)}{4h^2} \quad (2.7)
 \end{aligned}$$

Equation (2.7) was found to be no better than equation (2.6) and an average of the two was taken

$$f''(\omega) = \frac{f(\omega + 2h) + 4f(\omega + h) - 10f(\omega) + 4f(\omega - h) + f(\omega - 2h)}{8h^2} \quad (2.8)$$

Fig.2.7 The second derivative of the ν_3 band of methyl iodide dissolved in carbon tetrachloride is plotted against frequency. Thin line - second derivative using equation (2.6). Thick line - second derivative using equation (2.8).



Equation (2.8) was still noisy. See Fig 2.7. It was decided one reason for the noise lay in giving weightings of 2,4 or 10 to any individual point thus amplifying any noise associated with that point.

(iii) From Fig 2.6

$$\begin{aligned} f(\omega + 2h) - f(\omega + h) &= 2. a\omega h + 3. ah^2 + bh \\ f(\omega - h) - f(\omega - 2h) &= 2. a\omega h - 3. ah^2 + bh \\ f''(\omega) &= \frac{f(\omega + 2h) - f(\omega + h) - f(\omega - h) + f(\omega - 2h)}{3h^2} \end{aligned} \quad (2.9)$$

Also

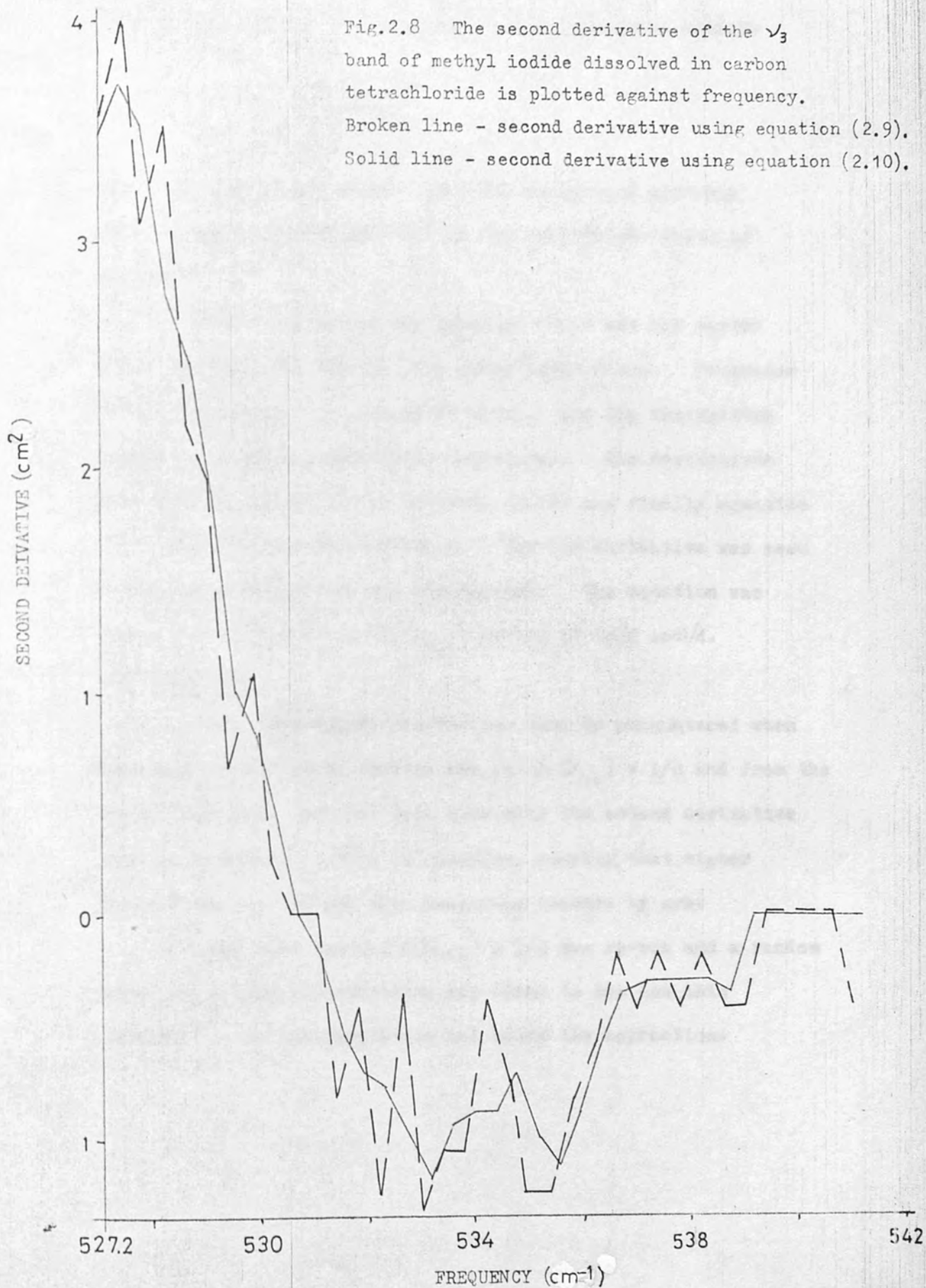
$$\begin{aligned} f(\omega + 3h) - f(\omega + h) &= 4. a\omega h + 8 ah^2 + 2bh \\ f(\omega - h) - f(\omega - 3h) &= 4. a\omega h - 8 ah^2 + 2bh \\ f''(\omega) &= \frac{f(\omega + 3h) - f(\omega + h) - f(\omega - h) + f(\omega - 3h)}{8h^2} \end{aligned} \quad (2.10)$$

Equation (2.9) and (2.10) were both tried and they gave much smoother curves although (2.10) was the better of the two. See Fig 2.8. Higher derivatives can be calculated substituting $f''(\omega)$ for $f(\omega)$ but these higher derivatives have far too much noise to be of any use.

Equation (2.10) was now tested to see what sampling interval was necessary for a spectrum of a given transmitted intensity curve half width to obtain an accurate second derivative in the absence of noise. Programme SECDIV was written which simulated a Lorentzian function and plotted it out on a transmittance scale between 20% and 90%. The algebraic second derivative was calculated to be

$$\begin{aligned} I''(\bar{\nu}) &= \frac{180 X_1 X_3 \exp(-Y)}{z^2} - \frac{720 X_1 X_3^2 D \bar{\nu}^2 \exp(-Y)}{z^2} \\ &+ \frac{360 X_1^2 X_3^2 D^2 \bar{\nu}^2 \exp(-Y)}{z^4} \end{aligned}$$

Fig.2.8 The second derivative of the ν_3 band of methyl iodide dissolved in carbon tetrachloride is plotted against frequency. Broken line - second derivative using equation (2.9). Solid line - second derivative using equation (2.10).



where $D = \ln(90/20)$ and k refers to the Lorentzian profile

$$Y = \exp \left[\frac{D x_1}{1 + x_3 \bar{\nu}^2} \right]$$

$$Z = 1 + x_3 \bar{\nu}^2$$

From Fig. 2.9 it can be seen that for reasonable accuracy about 40 points are needed across the half height width of the band.

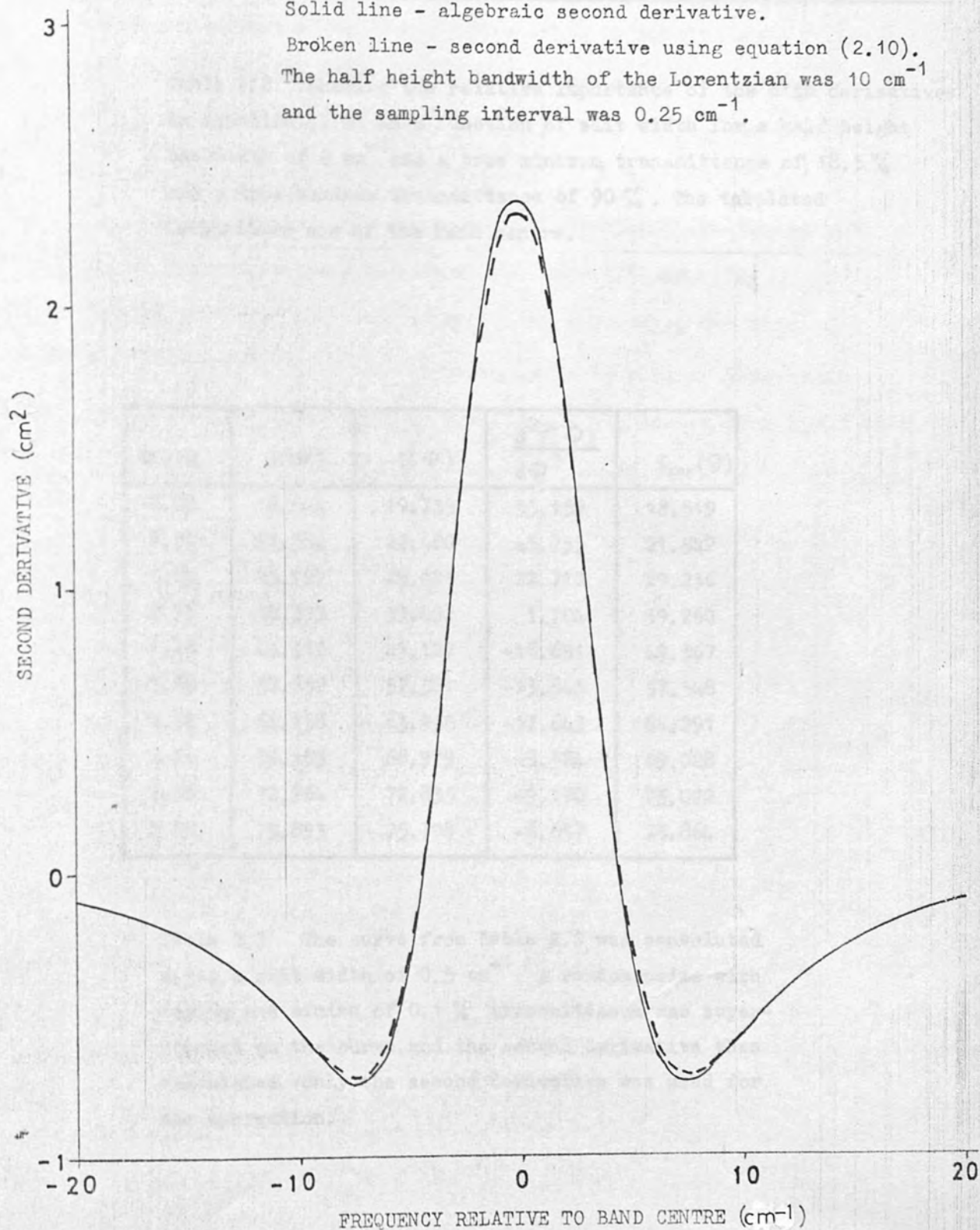
The slit correction equation (2.5) was now tested using the 2nd, 4th, 6th and 8th order derivatives. Programme SECDIV was modified to programme CORSLT and the transmitted intensity curve was accurately convoluted. The derivatives were then calculated using equation (2.10) and finally equation (2.5) used for the deconvolution. The 8th derivative was seen to fluctuate wildly and was disregarded. The equation was tested for different $(s/\Delta \bar{\nu}_{1/2})$ ratios of 1, 1/2 and 1/4. See Table 2.2.

The experimental conditions usually encountered when measuring liquid phase spectra are $(s/\Delta \bar{\nu}_{1/2}) = 1/4$ and from the table it is seen that for this case only the second derivative term is important. This is pleasing, knowing that higher derivatives are useless when measuring spectra by eye.

The case for $(s/\Delta \bar{\nu}_{1/2}) = 1/4$ was re-run and a random noise of $\pm 0.1\%$ transmittance was added to see how this affected the second derivative and hence the correction.

Fig.2.9 A comparison of the algebraic second derivative with that using equation (2.10) for a Lorentzian function plotted on a transmittance scale between 20% and 90%. Solid line - algebraic second derivative.

Broken line - second derivative using equation (2.10). The half height bandwidth of the Lorentzian was 10 cm^{-1} and the sampling interval was 0.25 cm^{-1} .



| $s(\text{cm}^{-1})$ | $I(\bar{\nu}_0) - I'(\bar{\nu}_0)$ (% transmittance) | correction due to the n'th derivative (% transmittance) | | | correction as % of total change due to | |
|---------------------|---|---|-----|-----|--|---------------|
| | | $n = 2$ | 4 | 6 | $n = 2$ | $n = 2, 4, 6$ |
| 2.0 | 13.3 | 7.8 | 2.4 | 0.2 | 59 | 84 |
| 1.0 | 4.4 | 3.7 | 0.5 | 0.1 | 84 | 99 |
| 0.5 | 1.2 | 1.2 | 0.0 | 0.0 | 100 | 100 |

Table 2.2 Showing the relative importance of the n'th derivatives in equation (2.5) as a function of slit width for a half height bandwidth of 2 cm^{-1} and a true minimum transmittance of 18.5% and a true maximum transmittance of 90%. The tabulated intensities are of the band centre.

| $\bar{\nu} - \bar{\nu}_0$ | $I(\bar{\nu})$ | $I'(\bar{\nu})$ | $\frac{d^2 I(\bar{\nu})}{d\bar{\nu}^2}$ | $I_{\text{cor}}(\bar{\nu})$ |
|---------------------------|----------------|-----------------|---|-----------------------------|
| 0.00 | 18.544 | 19.735 | 55.159 | 18.519 |
| 0.32 | 21.386 | 22.480 | 45.733 | 21.542 |
| 0.64 | 29.197 | 29.821 | 22.710 | 29.236 |
| 0.96 | 39.395 | 39.492 | 1.704 | 39.260 |
| 1.28 | 49.312 | 49.127 | -16.651 | 49.367 |
| 1.60 | 57.632 | 57.381 | -13.845 | 57.548 |
| 1.92 | 64.158 | 63.935 | -17.643 | 64.291 |
| 2.24 | 69.153 | 68.979 | -9.384 | 69.028 |
| 2.56 | 72.964 | 72.835 | -9.170 | 73.022 |
| 2.88 | 75.893 | 75.798 | -6.657 | 75.864 |

Table 2.3 The curve from Table 2.2 was convoluted using a slit width of 0.5 cm^{-1} . A random noise with maxima and minima of 0.1% transmittance was superimposed on the curve and the second derivative then calculated. Only the second derivative was used for the correction.

As can be seen from Table 2.3, the second derivative was not too bad and the correction was good. The result was satisfactory and so the above method of slit correction was considered perfectly adequate for the liquid spectra being examined.

The computing time for this latter method is also about twenty times as fast on the computer as the earlier Fourier transform method, taking about two seconds.

When data processing becomes available for the output of the model 325 and a computer time averaged spectrum is obtainable, then this latter method of correcting for slit distortion will be of more importance as it will be extendable to gas phase spectra because the 4th and 6th derivatives could then be smoothed enough to be used for the larger ratio of $(s/\Delta\bar{\nu}_{1/2})$.

Section 2.5 Correction of the Distortion of Infra-red Absorption Bands of Liquids due to Refractive Index effects.

The infra-red absorption bands of liquids are distorted due to the refractive index of the absorbing medium changing in the region of an absorption band. This change in the refractive index is called dispersion. There are two ways in which the refractive index can distort a band but these will not be discussed yet. Some classical theory concerning absorption and dispersion of radiation should first be mentioned. An excellent text for reference is Infra-red Physics by Houghton and Smith (8). The theory is written with respect to S.I. units. The two distortions will be discussed in Sections 2.9 and 2.10.

Transverse components

$$E = E_0 \exp i(\omega t - 2\pi \nu y) \quad (2.12)$$

where $2\pi \nu = \omega/v$ and v is the phase velocity of the radiation. Differentiation of equation (2.12) and then substitution in equation (2.11) yields

$$4\pi^2 \nu^2 \epsilon = \omega^2 \mu (\epsilon - 1 + i\kappa/\omega) \quad (2.13)$$

Also $4\pi^2 \nu^2 \epsilon = \omega^2 \epsilon_0 \epsilon$, ϵ defines the complex dielectric constant. Now the refractive index in a non-absorbing medium is expressed as the ratio of the velocity of the radiation in vacuo to the phase velocity of the radiation. For the case where absorption is taking place a complex refractive index, \hat{n} , is defined as $\hat{n} = n - i\kappa$, where n is the

Section 2.6 The Dispersion Relations

A convenient starting point is one of Maxwell's equations for electromagnetic waves. The electric field strength, E , of the radiation in a given medium is given by

$$\nabla^2 E - \epsilon \mu \frac{\partial^2 E}{\partial t^2} - \mu \sigma \frac{\partial E}{\partial t} = 0 \quad (2.11)$$

t is time

In equation (2.11) $\epsilon = \epsilon_r \epsilon_0$, where ϵ_r is the relative permittivity (or dielectric constant) of the medium and ϵ_0 is the permittivity of free space, $\mu = \mu_r \mu_0$ where μ is permeability and σ is the conductivity of the medium. The solution of equation (2.11) at a point distant l from a fixed origin, measured along the direction of propagation has transverse components

$$E = E_0 \exp i (\omega t - 2\pi \bar{\nu} l) \quad (2.12)$$

where $2\pi \bar{\nu} = \omega / u$ and u is the phase velocity of the radiation. Differentiation of equation (2.12) and then substitution in equation (2.11) yields

$$4\pi^2 \bar{\nu}^2 = \omega^2 \mu (\epsilon - i \sigma / \omega) \quad (2.13)$$

Also $4\pi^2 \bar{\nu}^2 = \omega^2 \epsilon_c \mu$. ϵ_c defines the complex dielectric constant. Now the refractive index in a non-absorbing medium is expressed as the ratio of the velocity of the radiation in vacuo to the phase velocity of the radiation. For the case where absorption is taking place a complex refractive index, \hat{n} , is defined as $\hat{n} = n - i k$, where n is the

real refractive index, $i = (-1)^{1/2}$ and k is the absorption index
 proportion $n - ik = c/v = 2\pi c \bar{\nu}/\omega$ of the electric (2.14)

Also, the square of the complex refractive index is equal
 to the complex dielectric constant.

Squaring equation (2.14) and substituting for
 $4\pi^2 \bar{\nu}^2/\omega^2$ from equation (2.13) we get

$$\begin{aligned} n^2 - k^2 - 2ink &= 4\pi^2 c^2 \bar{\nu}^2/\omega^2 \\ &= c^2 \mu (e - i\sigma/\omega) \end{aligned}$$

Separating the real and imaginary parts we get

$$n^2 - k^2 = c^2 \mu e = c^2 \mu_r \mu_o \epsilon_r \epsilon_o$$

It is a known fact that $c^2 = (\mu_o \epsilon_o)^{-1}$ and so

$$n^2 - k^2 = \mu_r \epsilon_r \quad (2.15a)$$

$$\text{Also } 2nk = c^2 \mu \sigma / \omega = \mu_r \sigma / (\epsilon_o \omega) \quad (2.15b)$$

At infra-red frequencies μ_r is generally unity and
 so n and k can be found for a medium if the dielectric constant
 ϵ_r and conductivity σ are known.

It will now be shown that k arises from attenuation of
 the intensity of the beam, while n controls the phase of the
 radiation passing through the medium. From equations (2.12) and
 (2.14) we have

$$\begin{aligned} E &= E_o \exp i (\omega t - \hat{n} \omega l/c) \\ &= E_o \exp (-k \omega l/c) \exp i \omega (t - nl/c) \end{aligned}$$

The amplitude of the wave is, therefore, attenuated
 proportionally to the absorption index k , while the imaginary
 component describes a sinusoidal wave with phase velocity c/n .

Experimentally we measure intensity, which is proportional to the square of the amplitude of the electric field strength of the radiation, hence in a path length, l , the ratio of the incident radiation intensity I_0 to the emergent intensity I will be

$$I/I_0 = \exp(-2\omega k l/c)$$

$$= \exp(-al)$$
 where a is the absorption coefficient and has units of reciprocal length, whereas k is dimensionless.

charged particles bound to equilibrium positions by Hooke's Law forces, (ii) that these forces are isotropic, and, (iii) experience damping forces proportional to velocity. The equation of motion for such a particle of mass, m , and charge, e , subject to an oscillating electric field of the form $E = E_0 \exp(i\omega t)$ directed along the x axis is thus

$$m \frac{d^2 x}{dt^2} + g \frac{dx}{dt} + 2\omega_0^2 x = e E_0 \exp(i\omega t)$$

in which g is the damping constant. The solution of this equation is

$$x = \frac{(e/a) E}{\omega_0^2 - \omega^2 + i\omega g}$$

The polarization, P , or electric dipole moment per unit volume is equal to Nex , where N is the number of charged particles per unit volume

$$\text{Thus, } P = \frac{(Ne^2/a) E}{\omega_0^2 - \omega^2 + i\omega g} \quad (5.16)$$

Section 2.7

The Lorentz Model of Absorption and Dispersion

In the last section, the relationships between optical and electrical constants were derived but no indication of their actual values or frequency dependence is present. For this, a model expressing the absorption and dispersion mechanism on an atomic scale must be postulated. The Lorentz model (9) is a simple model in which the basic assumptions are (i) that the material contains charged particles bound to equilibrium positions by Hooke's Law forces, (ii) that these forces are isotropic, and, (iii) experience damping forces proportional to velocity. The equation of motion for such a particle of mass, m , and charge, e , subject to an oscillating electric field of the form $E = E_0 \exp(i\omega t)$ directed along the x axis is thus

$$m \frac{d^2x}{dt^2} + mg \frac{dx}{dt} + m \omega_0^2 x = eE$$

in which g is the damping constant. The solution of this equation is

$$x = \frac{(e/m) E}{\omega_0^2 - \omega^2 + i\omega g}$$

The polarisation, P , or electric dipole moment per unit volume is equal to Nex , where N is the number of charged particles per unit volume

$$\text{Thus, } P = \frac{(Ne^2/m) E}{\omega_0^2 - \omega^2 + i\omega g} \quad (2.16)$$

Now $P = (\epsilon_0 - 1) \epsilon_0 E$ and so

$$\epsilon_0 = (n - ik)^2 = 1 + P/(\epsilon_0 E)$$

By substituting P in the above for equation (2.16) we get

$$(n - ik)^2 = 1 + \frac{(Ne^2/m\epsilon_0)}{\omega_0^2 - \omega^2 + i\omega g}$$

Separating the real and imaginary parts

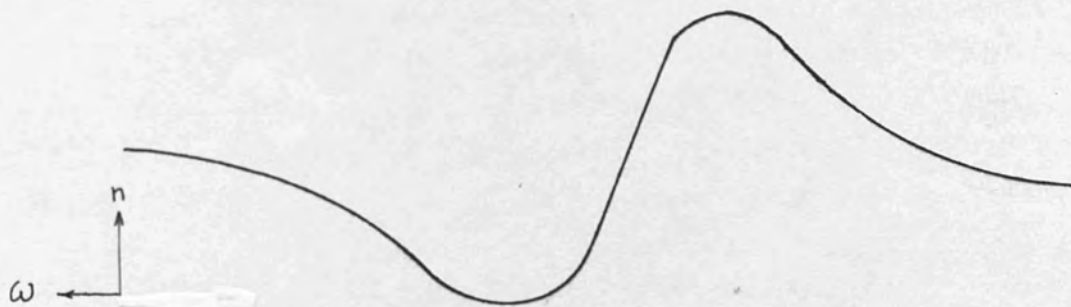
$$n^2 - k^2 = 1 + \frac{(Ne^2/m\epsilon_0) (\omega_0^2 - \omega^2)}{(\omega_0^2 - \omega^2)^2 + \omega^2 g^2} \quad (2.17a)$$

$$2nk = \frac{(Ne^2/m\epsilon_0) \omega g}{(\omega_0^2 - \omega^2)^2 + \omega^2 g^2} \quad (2.17b)$$

In equation (2.17a), if we assume the charge density, N , is small compared with a large frequency, ω , and that k^2 is much smaller than n^2 , then by binomial expansion and retaining only the first term

$$n = 1 + \frac{(Ne^2/m\epsilon_0) (\omega_0^2 - \omega^2)}{2(\omega_0^2 - \omega^2)^2 + 2\omega^2 g^2}$$

and the shape of this function is generally as shown below



In practice this is, in fact, the case. For equation (2.17b), assuming n does not vary in magnitude much compared with k , then $2nk \approx 2k$, and along with large frequency the line shape is seen to be a Lorentzian function. This again agrees the the experimental.

Section 2.8

The Kramers-Kronig Transform

The above has shown that absorption and dispersion are related and, in fact, the refractive index may be obtained from k using the Kramers-Kronig transform, which is

$$n(\nu) = \bar{n} + \frac{2}{\pi} \oint_{\text{band}} \frac{\nu' k(\nu')}{\nu^2 - \nu'^2} d\nu' \quad (2.18)$$

where \bar{n} is a mean refractive index measured in the wings of the band. The stronger the absorption band is, the larger the refractive index change is.

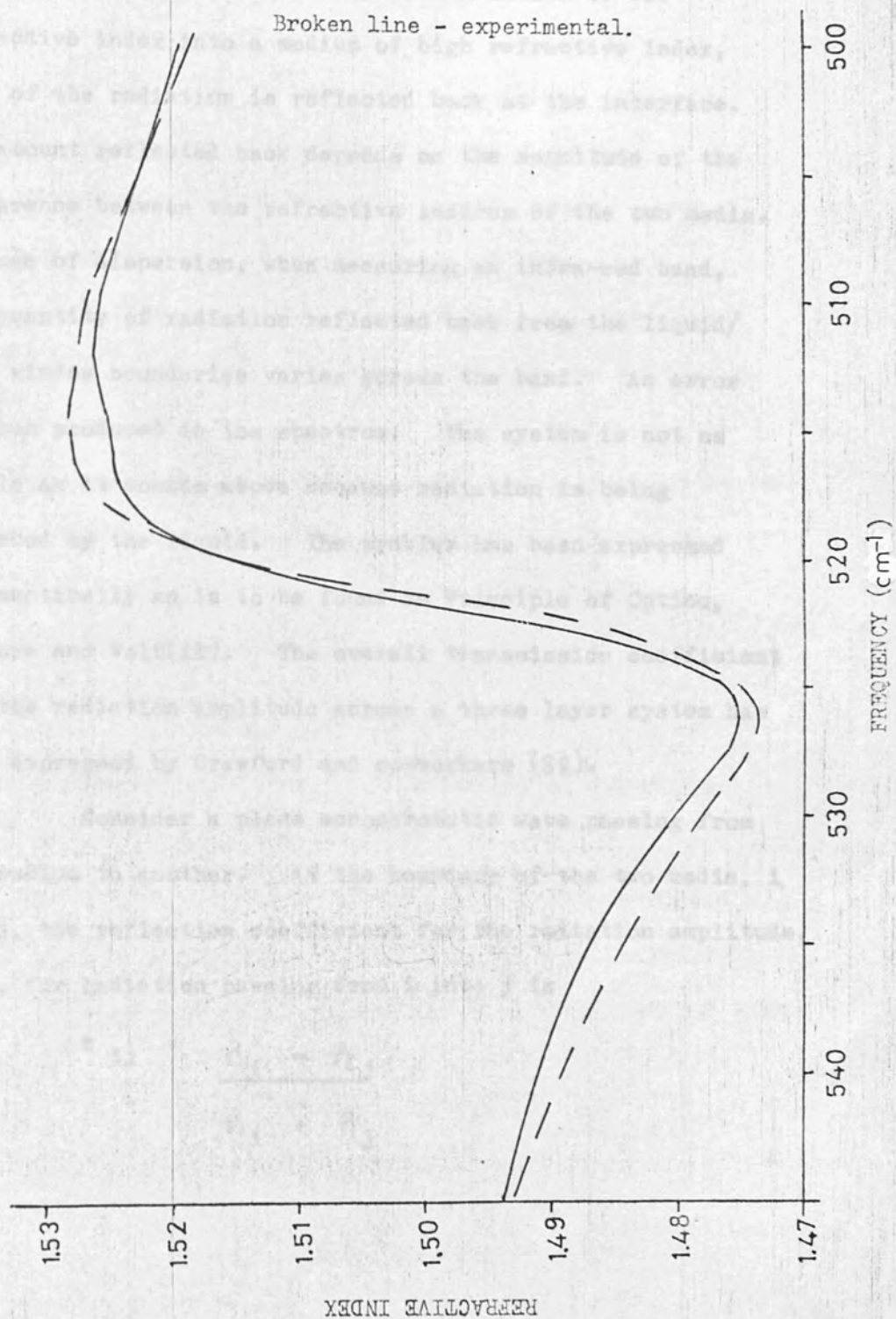
The Kramers-Kronig transform was tested for an experimental spectrum and the calculated refractive indices compared with some literature values recorded by Crawford (41). This also tested the correctness of the computer routine written, which was later utilised in other programmes. The result is to be seen in Fig. 2.10. The refractive indices closely agree.



Fig.2.10 A comparison of the experimentally measured refractive indices of the ν_3 band of methyl iodide with values calculated using the Kramers-Kronig transform.

Solid line - calculated.

Broken line - experimental.



Section 2.9

The Reflection Loss Correction

When radiation passes from a medium of low refractive index into a medium of high refractive index, some of the radiation is reflected back at the interface. The amount reflected back depends on the magnitude of the difference between the refractive indices of the two media. Because of dispersion, when measuring an infra-red band, the quantity of radiation reflected back from the liquid/cell window boundaries varies across the band. An error is thus produced in the spectrum. The system is not as simple as it sounds above because radiation is being absorbed by the liquid. The problem has been expressed mathematically as is to be found in Principle of Optics, by Born and Wolf(11). The overall transmission coefficient for the radiation amplitude across a three layer system has been expressed by Crawford and co-workers (88).

Consider a plane monochromatic wave passing from one medium to another. At the boundary of the two media, i and j, the reflection coefficient for the radiation amplitude, r_{ij} , for radiation passing from i into j is

$$r_{ij} = \frac{\hat{n}_i - \hat{n}_j}{\hat{n}_i + \hat{n}_j}$$

The transmission coefficient is given by

$$r_{ij} = 2\hat{n}_j / (\hat{n}_i + \hat{n}_j)$$

A quantity B is now defined for the absorbing medium

$$B = 2\pi\bar{\nu}\hat{n}_1$$

where $\bar{\nu}$ is the vacuum wavenumber of the radiation. The overall transmission coefficient, t, for a three layer system is given by

$$t = t_{12} t_{23} \exp(iB) / [1 + r_{12} r_{23} \exp(2iB)] \quad (2.19)$$

where media 1 and 3 are the cell windows in the case of an infra-red cell and medium 2 is the absorbing liquid. A spectrometer records the intensity of radiation, which is the square of the amplitude of the radiation, or in the case of complex numbers, is the square of the modulus of the amplitude of the radiation.

$$\text{i.e. } I_{\text{obs}} = |t|^2$$

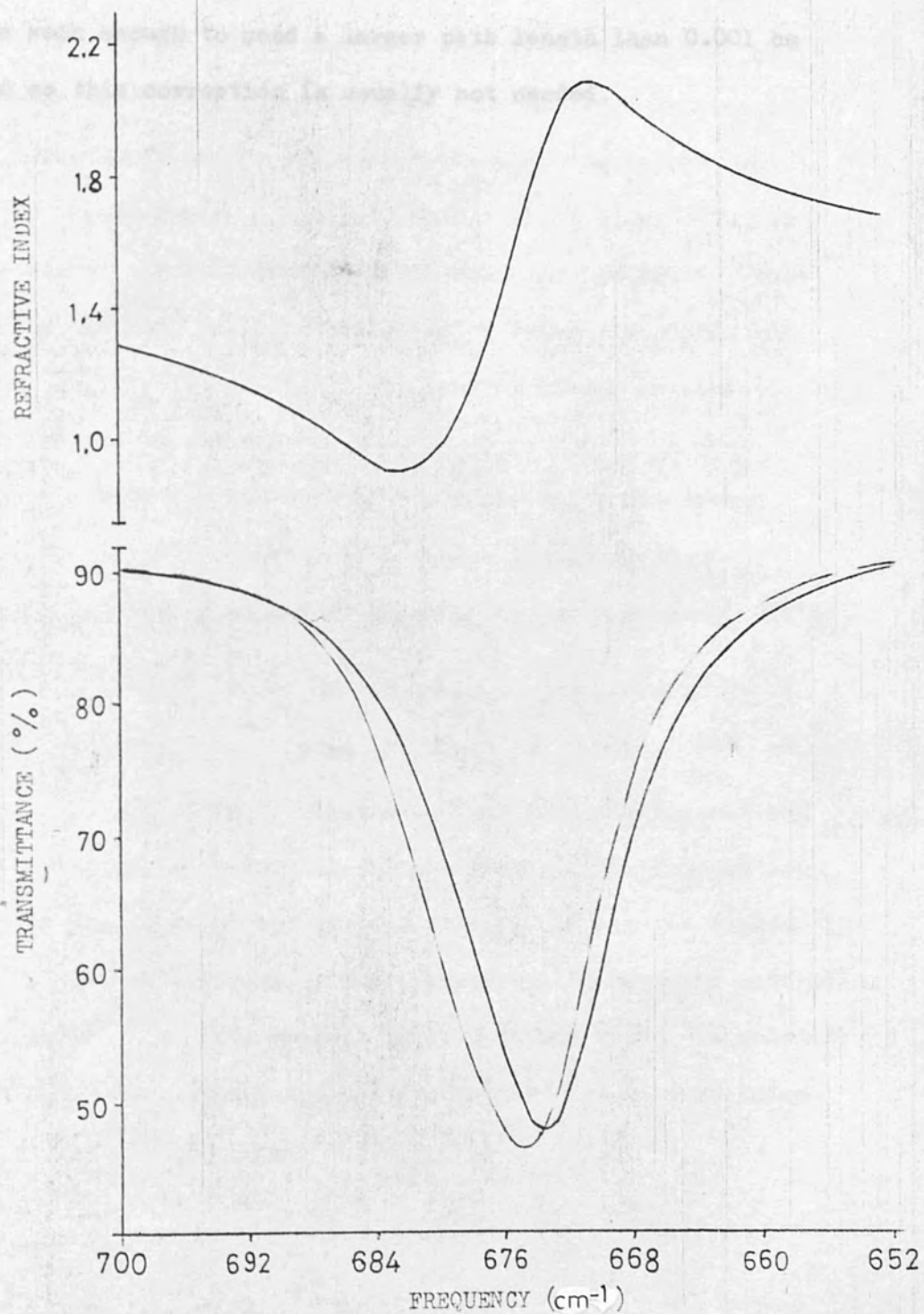
Equation (2.19) gives us the overall transmission coefficient and hence the observed intensity, I_{obs} , but we want to know the intensity arising purely from absorbance, I_{cor} . As can be seen, equation (2.19) cannot be re-arranged to give us I_{cor} . A method was thus worked out to get around this problem.

The distortion of the spectrum, because of reflection loss, is small compared with the magnitude of the true absorbance spectrum. Thus I_{obs} is an approximation to I_{cor} , so it was decided to distort I_{obs} using equation (2.19) to give a calculated intensity, I_{calc} . The distortion ($I_{\text{obs}} - I_{\text{calc}}$) was similar in magnitude to the true distortion ($I_{\text{cor}} - I_{\text{obs}}$) because of I_{cor} and I_{obs} being of similar magnitude. A second approximation to I_{cor} was thus considered to be $I_{\text{obs}} + (I_{\text{obs}} - I_{\text{calc}})$. This quantity was called I_{app} . The intensity I_{app} was distorted using equation (2.19) to give a new I_{calc} and, in turn, a new I_{app} was formed, which was a better approximation than the previous one. A computer programme THFILM was written to perform the above. The refractive indices were calculated using the Kramers-Kronig transform. The above process was cycled five times and it was found that I_{app} became self consistent and was thus equal to I_{cor} . That is, the final I_{app} , when distorted using equation (2.19), gave an exact fit to I_{obs} .

It was seen that the correction to the band shape was not symmetrical and a slight shift to higher frequency was apparent. Fig.2.11 shows this correction applied to the a_{2u} band of liquid benzene.



Fig.2.11 The reflection correction applied to the a_{2u} band of liquid benzene. The experimental intensity and refractive index curves are shown (solid lines) along with the corrected intensity curve (broken line).



Section 2. It was found that the reflection loss correction was negligible when the path length being used (to give a sensible spectrum with a minimum at about 20% transmittance) was greater than 0.001 cm. The majority of infra-red bands are weak enough to need a larger path length than 0.001 cm and so this correction is usually not needed.

The electric field, E , but rather the spectrum, related to the effective field, $E_{eff}(\omega)$, within the medium. The true spectrum may be different from the recorded spectrum. This problem has been fully investigated by Pechoulov, Gizin and Litov (14, 15, 16 and 17). The general theory related to this problem is set out below.

Einstein has derived the probability per second per unit radiation density of a transition being induced between two levels n' and n'' by radiation of frequency $\nu = \omega_{n'n''}$.

$$B_{n''n'}(\nu) = 2\pi^2/15^2 \epsilon_0 \cdot |D_{n'n''}(\nu)|^2$$

where $D_{n'n''}(\nu) = \int (\psi_{n''}^* \vec{\mu} \psi_{n'}) d\tau$

$B_{n''n'}(\nu)$ is the Einstein absorption coefficient and the subscript, o , refers to the gas phase. The integration is over the range of the wavefunction, ψ , and $\vec{\mu}$ is the dipole vector for the molecule. The experimentally measured absorption coefficient, $\epsilon_o(\omega)$, where $\epsilon_o(\omega) = 4\pi\nu k(\omega)/c$, is related to the Einstein absorption coefficient as will be seen below.

Section 2.10 The Theory of the Local Field Correction

When radiation enters a liquid medium the electric field strength, E , changes in a way that is related to properties of the medium including the refractive index (13). A spectrometer does not record the true spectrum related to the electric field, E , but rather the spectrum related to the effective field, $E_{\text{eff}}(\nu)$, within the medium. The true spectrum may be different from the recorded spectrum. This problem has been fully investigated by Bakhshiev, Girin and Libov (14, 15, 16 and 17). The general theory related to this problem is set out below.

Einstein has derived the probability per second per unit radiation density of a transition being induced between two levels m'' and m' by radiation of frequency $\nu_{m''m'}$.

$$B_o(\nu) = 2 \cdot \pi^2 / 3h^2 \epsilon_o \cdot | D_o(\nu) |^2$$

where

$$D_o(\nu) = \int (\psi_{m''}^* \tilde{\mu} \psi_{m'}) d\tau$$

$B_o(\nu)$ is the Einstein absorption coefficient and the subscript, o , refers to the gas phase. The integration is over the range of the wavefunction, ψ , and $\tilde{\mu}$ is the dipole vector for the molecule. The experimentally measured absorption coefficient, $a_o(\nu)$, where $a_o(\nu) = 4\pi\nu k(\nu)/c$, is related to the Einstein absorption coefficient as will be seen below.

The amount of energy absorbed per unit time, $dW_o(\nu)/dt$, within a unit spectral interval and a volume $dV = qdl$, depends on the number of absorbing particles per unit volume, N_o , and the spectral density of the average transition probability $\overline{A_o(\nu)}$

$$\begin{aligned} \frac{dW_o(\nu)}{dt} &= \overline{A_o(\nu)} h\nu N_o dV \\ &= B_o(\epsilon_o E_o^2(\nu)/2) h\nu N_o q dl \quad (2.20) \end{aligned}$$

where $(\epsilon_o E_o^2/2)$ is the volume spectral density of the energy of the light wave in vacuo.

According to the Lambert law of absorption the amount of energy absorbed per unit time is proportional to the thickness of the sample, the absorption coefficient and the radiant flux (the time rate of transfer of the radiant energy).

$$\begin{aligned} \frac{dW_o(\nu)}{dt} &= a_o(\nu) F_o(\nu) dl \\ &= a_o(\nu) c (\epsilon_o E_o^2(\nu)/2) q dl \quad (2.21) \end{aligned}$$

where $F_o(\nu)$ is the spectral density of the radiation flux.

From equations (2.20) and (2.21) we obtain the relation

$$B_o(\nu) = \frac{a_o(\nu) c}{N_o h \nu} \quad (2.22)$$

A different situation exists in the case of a liquid medium. Equation (2.20) becomes

$$\frac{dW(\nu)}{dt} = B(\nu) (\epsilon_o(\nu) E_{\text{eff}}^2(\nu)/2) h\nu N q dl \quad (2.23)$$

where $E_{\text{eff}}(\nu)$ is the effective local field of the light wave acting on the molecule under study. Equation (2.21) becomes

$$\frac{dW(\nu)}{dt} = a(\nu) c n(\nu) (\epsilon_0 E_{\text{av}}^2(\nu)/2) qd1 \quad (2.24)$$

$E_{\text{av}}(\nu)$ is the macroscopic average field of the light wave in the medium. From equations (2.23) and (2.24) we obtain the relation

$$B(\nu) = \frac{a(\nu) c}{h \nu N} \cdot n(\nu) \frac{E_{\text{av}}^2(\nu)}{E_{\text{eff}}^2(\nu)}$$

which may be written, on comparison with equation (2.22) as

$$B(\nu) = \frac{a(\nu) c}{h \nu N} \theta(\nu) \quad (2.25)$$

We thus want to find the form of the function $\theta(\nu)$.

From dielectric theory (18) the effective field vector, \tilde{E}_{eff} at a point in a macroscopic spherical region of volume, V , is related to the macroscopic average field by the general expression

$$\tilde{E}_{\text{eff}} = f_1(\hat{n}) E_{\text{av}} + f_2(\hat{n}) \frac{\tilde{M}}{V} \quad (2.26)$$

Here, $f_1(\hat{n})$ and $f_2(\hat{n})$ are certain functions of the complex refractive index and \tilde{M} is the electric moment vector of the designated region. The first term on the right hand side of equation (2.26) is called the cavity field and takes no account of interactions between molecules. The second term is called

the reactive field, and the reactive field acting on a given molecule is related to its dipole moment by a function which takes into account all forms of interaction between the molecule under investigation and its nearest neighbours.

According to the Lorentz model for an oscillator (9) the effective field is related to the average field by

$$E_{\text{eff}}(\nu) = \left(\frac{\hat{n}^2 + 2}{3} \right) E_{\text{av}}(\nu)$$

The Lorentz model does not allow for a reactive field and uses only the cavity field. From above

$$\frac{E_{\text{av}}^2(\nu)}{E_{\text{eff}}^2(\nu)} = \left| \frac{3}{\hat{n}^2 + 2} \right|^2$$

$$\text{and thus } \theta_L(\nu) = \frac{9n}{(n^2 - k^2 + 2)^2 + 4n^2 k^2} \quad (2.27)$$

The subscript refers to the Lorentz model. We already know how n changes across an absorption band and so $\theta_L(\nu)$ must change as well.

Another model to use is the Onsager-Bottcher model which takes into account a reactive field (19) and this model relates the effective field to the average field by

$$E_{\text{eff}}(\nu) = \left(\frac{3\hat{n}^2}{2\hat{n}^2 + 1} \right) \left(\frac{1}{1 - f\hat{\alpha}} \right) E_{\text{av}}(\nu) \quad (2.28)$$

$$\text{where } f = \frac{2(\hat{n}^2 - 1)}{r^3(2\hat{n}^2 + 1)}$$

r is the Onsager radius of the molecule and $\hat{\alpha}$ is the complex polarisability. The Polarisation of a dielectric consisting of isotropically polar molecules is also related to the electric field strength (18) by

$$E_{av}(\nu) (\hat{n}^2 - 1)/4\pi = N \hat{\alpha} E_{eff}(\nu) \quad (2.29)$$

Removing $\hat{\alpha}$ from equation (2.28) using equation (2.29) we get, on re-arrangement

$$\frac{E_{av}^2(\nu)}{E_{eff}^2(\nu)} = a^2 \left| \frac{2 \hat{n}^2 + 1}{3 a \hat{n}^2 + (\hat{n}^2 - 1)^2} \right|^2$$

where $a = 2 \pi N r^3$. We thus have

$$\theta_B(\nu) = n(\nu) a^2 \left| \frac{2 \hat{n}^2 + 1}{3 a \hat{n}^2 + (\hat{n}^2 - 1)^2} \right|^2 \quad (2.30)$$

The subscript refers to the Bottcher model.

Section 2.11

Application of the Local Field Correction

Programme BAKSHV was written to perform the local field correction. The refractive index was calculated using the Kramers-Kronig transform. The correction was applied to the ν_3 band of methyl iodide. This band is of medium strength ($k_{\max} = 0.054$). The Lorentz model was first used and the resulting band shape was the same as the original, with the same band centre. There was an overall decrease in intensity of 26% though. The Onsager-Bottcher model was then used which required a knowledge of the radius of the molecule. The radius was calculated assuming the liquid consisted of closely packed spheres. In this case there is 26% of void space and the radius of the molecule is obtained from

$$4 \pi r^3 N_A / 3 = 0.74 M_r / \rho \quad (2.31)$$

where N_A is Avogadro's number, M_r is the molecular weight of the substance and ρ is the density of the substance. The equation was tested for carbon tetrachloride and a radius of 3.05 Å obtained, which compared with a literature value (17) of 3.0 Å. The methyl iodide molecule may be considered almost spherical because of the larger iodine atom. The radius of the molecule calculated by equation (2.31) was 2.6 Å. The number of absorbing particles per unit volume was calculated from

$$N = N_A / (M_r / \rho)$$

where M_r / ρ is the molar volume.

With this model, programme BAKSHV yielded the result that the band shape and position were unchanged but the overall intensity reduced by 33%.

The programme was re-run for a much more intense band, namely the a_{2u} band of benzene at 674 cm^{-1} . This band has $k_{\text{max}} = 1.1$. The Lorentz model yielded a narrower band at higher frequency which was far more symmetric than before the correction. The half height bandwidth was reduced from 11.1 cm^{-1} to 9.5 cm^{-1} . The band centre shifted from 674.8 cm^{-1} to 677.4 cm^{-1} . The integrated intensity of the band, Γ , fell from $34.0 \pm 4.0 \text{ dm}^3 \text{ mol}^{-1} \text{ cm}^{-1}$ to $27.0 \pm 4.0 \text{ dm}^3 \text{ mol}^{-1} \text{ cm}^{-1}$. This compares favourably with the integrated intensity for the band measured in dilute solution in cyclohexane of $21.5 \pm 2.1 \text{ dm}^3 \text{ mol}^{-1} \text{ cm}^{-1}$. The band measured in dilute solution in cyclohexane is free from the need for correction.

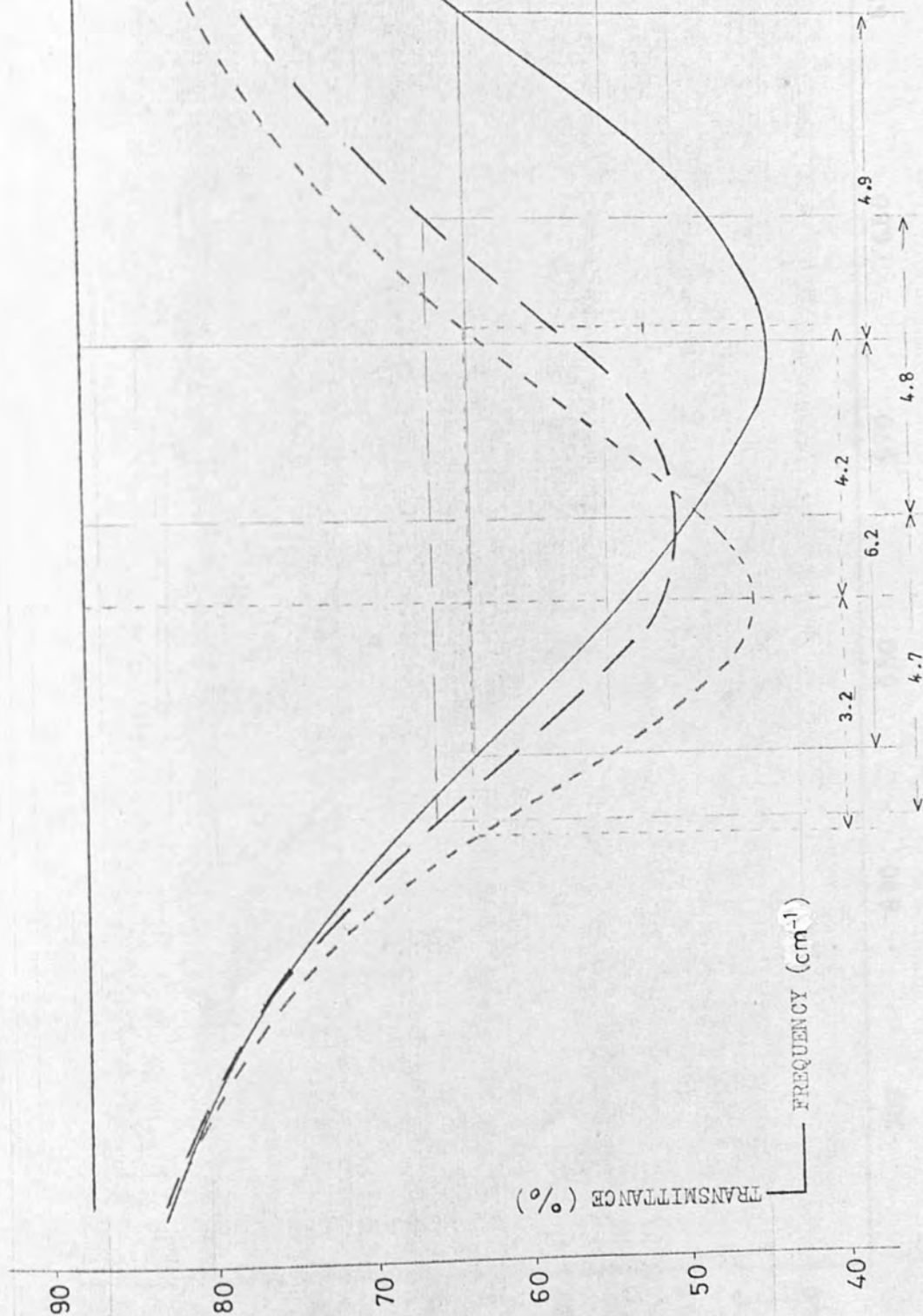
The a_{2u} band was then corrected using the Onsager-Bottcher model and the result was a band which was more asymmetric than before the correction. The band centre was shifted to 678.8 cm^{-1} and the half height bandwidth reduced to 7.4 cm^{-1} . The reason for the asymmetry probably lies in the need for a molecular radius. The value used was calculated using equation (2.31) and is obviously inaccurate because benzene is a flat molecule. The results are shown in Fig. 2.12 and Fig. 2.13. In Fig. 2.12 the original and corrected transmitted intensity curves are compared and their evenness about their respective band centres is indicated using the bandwidths at half height. Fig. 2.13 shows the whole band after correction using the Lorentz model, to get the overall picture.

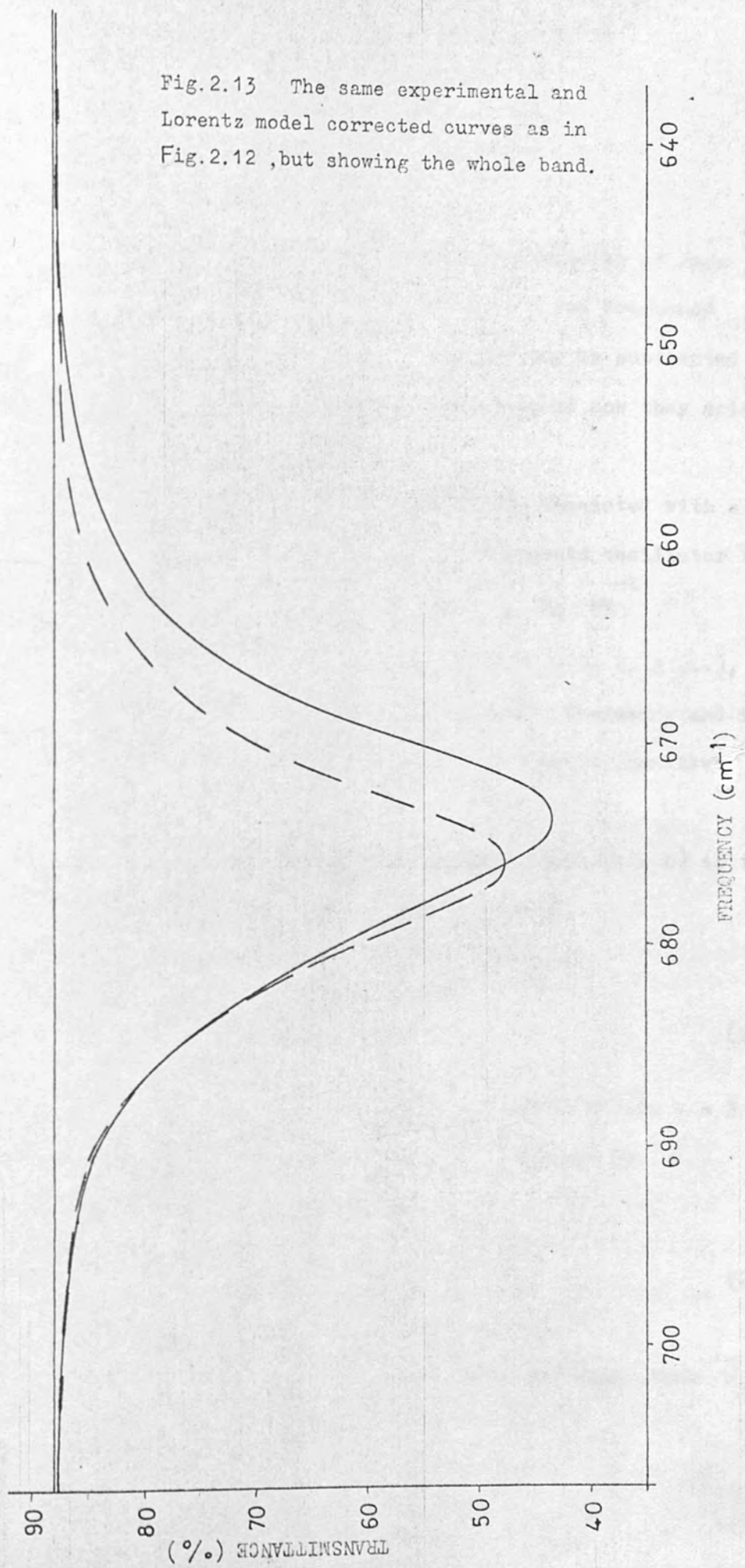
Fig.2.12 The a_{2u} band of liquid benzene and the correction for the local field.

Solid line - experimental (after the reflection loss correction).

Long dashed line - correction using the Lorentz model.

Short dashed line - correction using the Onsager-Bottcher model.





Section 2.12

Hot Bands

Infra-red absorption bands at frequencies of less than 1000 cm^{-1} tend to have hot bands to the low frequency side of the band centre. These hot bands may be subtracted out of the measured band after consideration of how they arise in the spectrum.

The eigenvalues of the energy, E , connected with a particular vibration are given for an anharmonic oscillator by

$$\bar{E} = E/hc = (v + \frac{1}{2})\bar{\nu}_e - (v + \frac{1}{2})^2 \bar{\nu}_e x_e \text{ cm}^{-1}$$

where v is the vibrational quantum number ($v = 0, 1, 2 \dots$), $\bar{\nu}_e$ is the (hypothetical) equilibrium oscillation frequency and x_e is the anharmonicity constant. x_e is a small, positive constant.

For a transition from the ground state ($v = 0$) to the $v = 1$ state, the band centre, $\bar{\nu}_1$, is given by

$$\begin{aligned} \bar{\nu}_1 &= \bar{\nu}_e - 2 \bar{\nu}_e x_e \\ &= \bar{\nu}_e (1 - 2 x_e) \text{ cm}^{-1} \end{aligned} \quad (2.32)$$

For a transition from the $v = 1$ state to the $v = 2$ state (a hot band) the band centre, $\bar{\nu}_2$, is given by

$$\begin{aligned} \bar{\nu}_2 &= \bar{\nu}_e - 4 \bar{\nu}_e x_e \\ &= \bar{\nu}_1 - 2 x_e \text{ cm}^{-1} \end{aligned} \quad (2.33)$$

The hot band is thus seen to be at a lower frequency than $\bar{\nu}_1$.

The number of molecules occupying the $v = 1$ state, N_1 , is determined by the Boltzmann expression

$$N_1 = \frac{N g_1 \exp \left(-hc \left[\left(1 + \frac{1}{2}\right) \bar{\nu}_e - \left(1 + \frac{1}{2}\right)^2 \bar{\nu}_e x_e \right] / kT \right)}{Z}$$

where k is the Boltzmann constant, T is the temperature, N is the total number of molecules, g_1 is the degeneracy of the energy state and Z is the partition function given by

$$Z = \sum_i g_i \exp (-E_i/kT)$$

The number of molecules occupying the $v = 2$ state is given by

$$N_2 = \frac{N g_2 \exp \left(-hc \left[\left(2 + \frac{1}{2}\right) \bar{\nu}_e - \left(2 + \frac{1}{2}\right)^2 \bar{\nu}_e x_e \right] / kT \right)}{Z}$$

The ratio of the populations of the two energy states is thus obtained.

$$\frac{N_1}{N_2} = \frac{g_1 \exp \left(-hc \left[\left(1 + \frac{1}{2}\right) \bar{\nu}_e - \left(1 + \frac{1}{2}\right)^2 \bar{\nu}_e x_e \right] / kT \right)}{g_2 \exp \left(-hc \left[\left(2 + \frac{1}{2}\right) \bar{\nu}_e - \left(2 + \frac{1}{2}\right)^2 \bar{\nu}_e x_e \right] / kT \right)} \quad (2.34)$$

If, as an approximation, we let $x_e = 0$, then equation (2.34) reduces to

$$\frac{N_1}{N_2} = \left(g_1 / g_2 \right) \exp (+hc \bar{\nu}_e / kT) \quad (2.35)$$

To get a rough idea of the dependence of the intensity of hot bands on frequency consider equation (2.35) and a vibration at 500 cm^{-1} . The $v = 1$ and $v = 2$ states are non-degenerate and assume the temperature is 313° K (the temperature in the sample compartment of the P.E. 325).

$$\begin{aligned}\frac{N_1}{N_2} &= \exp(500 hc/kT) \\ &= 10.7\end{aligned}$$

At 1000 cm^{-1} we find

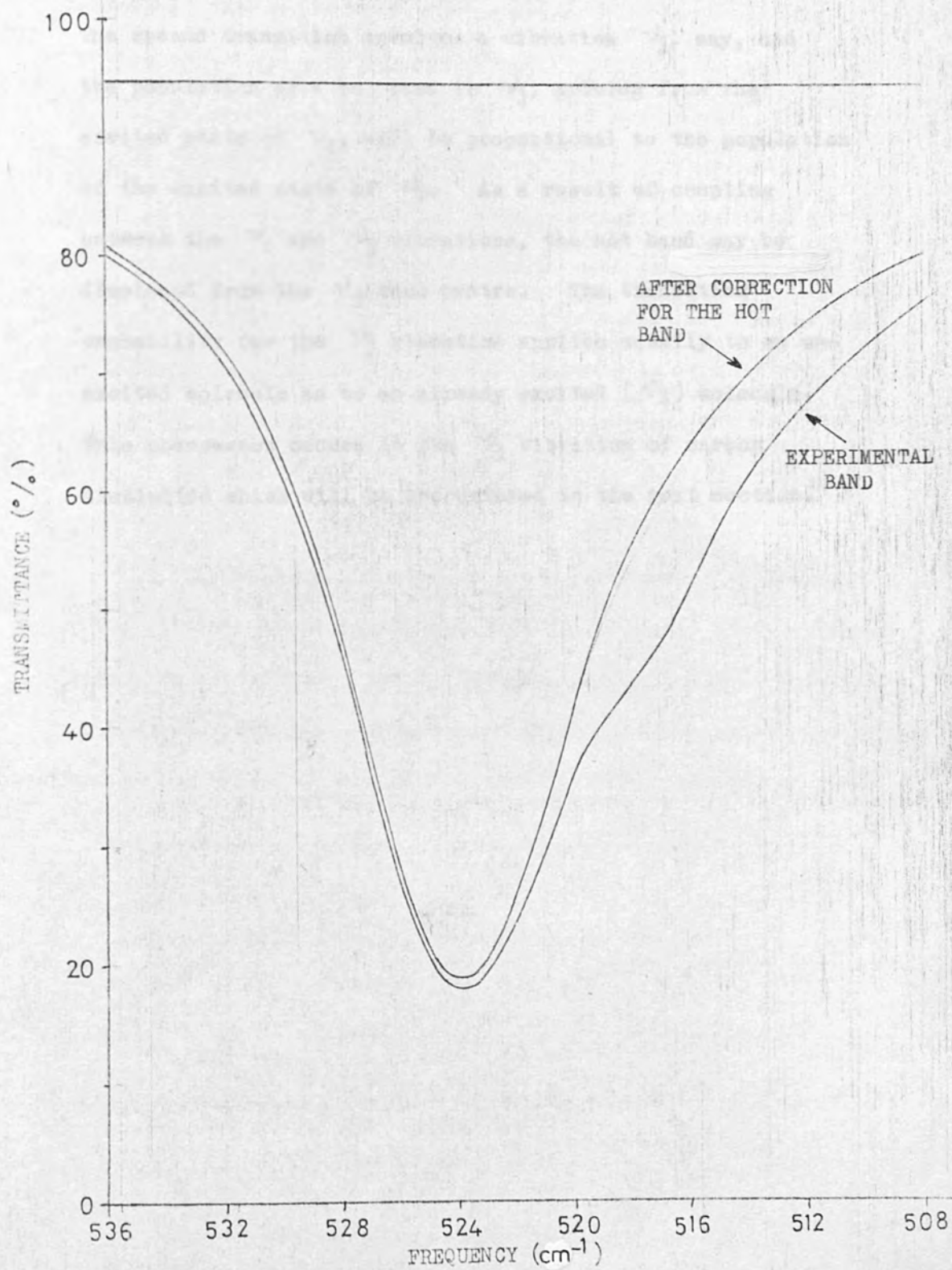
$$\begin{aligned}\frac{N_1}{N_2} &= \exp(1000 hc/kT) \\ &= 99.6\end{aligned}$$

Thus we see that around 500 cm^{-1} we may expect a hot band of about 10% of the intensity of the fundamental, whereas at 1000 cm^{-1} the hot band is only about 1% of the intensity of the fundamental.

The ν_3 band of methyl iodide at 523.6 cm^{-1} was measured in the liquid phase. This is the lowest frequency fundamental of methyl iodide. A definite underlying band was present at around 518 cm^{-1} . The exact centre of this hot band was not resolved and so the gas phase was turned to. The gas phase infrared spectrum resolves the hot band and shows it to be 6.5 cm^{-1} to the low frequency side of the main band. The separation will remain the same on going into the liquid phase and so the hot band in the liquid phase was centred on 517.1 cm^{-1} .

The numerical values of χ_e and $\bar{\nu}_e$ were obtained using equations (2.32) and (2.33). The ratio of the populations of the $v = 1$ and $v = 2$ energy states was obtained using equation (2.34). This yielded $N_1/N_2 = 10.7$. A good approximation to the shape of the hot band was the measured band shape. The hot band was accordingly removed and the result is shown in Fig. 2.14. The result was a good smooth and symmetric band.

Fig. 2.14 The ν_3 band of methyl iodide liquid showing the hot band to the low frequency side of the main band. After removal of this hot band the corrected band is far more symmetric.



There is also another, less usual, type of hot band that occurs. This latter type arises from a transition from the excited state of a low lying vibration, ν_i , which has a relatively high equilibrium population. The second transition involves a vibration ν_j , say, and the population of a hot band in ν_j , arising from the excited state of ν_i , will be proportional to the population of the excited state of ν_i . As a result of coupling between the ν_i and ν_j vibrations, the hot band may be displaced from the ν_j band centre. The transition probability for the ν_j vibration applies equally to an unexcited molecule as to an already excited (ν_i) molecule. This phenomenon occurs in the ν_3 vibration of carbon disulphide which will be encountered in the next section.

| Atom | Isotope | % abundance |
|----------|------------------|-------------|
| Hydrogen | ^1H | 99.98 |
| | ^2H | 0.01 |
| Carbon | ^{12}C | 98.89 |
| | ^{13}C | 1.11 |
| Fluorine | ^{19}F | 100.00 |
| Sulphur | ^{32}S | 95.00 |
| | ^{34}S | 4.76 |
| Iodine | ^{127}I | 100.00 |
| | ^{131}I | 0.00 |

Table 2.4

Section 2.13 Isotopic Shifts

The effect that an isotope has on a spectrum is observed in the following simple analogy. If one considers a spring which has a small weight oscillating on the end of it, if this weight is then replaced by a heavy weight, this heavy weight will oscillate at a slower rate. This analogy holds for vibrations in molecules and the force constant, f , for a given vibration remains constant, when substituting one isotope for another, which is analogous to using the same spring. The vibration, ν_a , arising from an isotope, a , is given by

$$\nu_a = 1/2\pi (f/\mu_a)^{1/2}$$

where μ_a is the reduced mass of the system, which is the same as for a classic spring.

The need to correct for isotopes depends, of course, on the relative abundance of them for a particular atom. During the course of this work the different atoms encountered in various solutes were hydrogen, carbon, sulphur, iodine and fluorine.

These atoms have the following natural isotopic abundances (20).

| Atom | Isotope | % abundance |
|----------|------------------|-------------|
| Hydrogen | H ¹ | 99.99 |
| | H ² | 0.01 |
| Carbon | C ¹² | 98.89 |
| | C ¹³ | 1.11 |
| Fluorine | F ¹⁹ | 100.00 |
| Sulphur | S ³² | 95.00 |
| | S ³³ | 0.76 |
| | S ³⁴ | 4.22 |
| Iodine | I ¹²⁷ | 100.00 |

Table 2.4

An isotopic abundance of about 1% will not appreciably affect a spectrum and the effect certainly could not be detected in a liquid phase spectrum. From Table 2.4 it can be seen that sulphur is the only atom encountered with an isotope of appreciable abundance. The molecule looked at was carbon disulphide. It will be instructive to carry out the correction for this particular molecule.

Carbon disulphide is a linear triatomic molecule and the ν_3 band at 1522 cm^{-1} was measured in carbon tetrachloride solution. The low frequency side of this band had a large shoulder arising from a hot band and isotopes. The S^{33} isotope will be neglected in the correction and so we have S^{32} and S^{34} .

The probabilities for different isotopic molecules are shown below.

$$\begin{aligned} \text{CS}^{32} \text{S}^{32} & \text{ will have an abundance of } (0.9500 \times 0.9500) = 0.9025 \\ \text{CS}^{32} \text{S}^{34} & \text{ will have an abundance of } (0.9500 \times 0.0422) \times 2 = 0.0802 \\ \text{CS}^{34} \text{S}^{34} & \text{ will have an abundance of } (0.0422 \times 0.0422) = 0.0018 \end{aligned}$$

The relative abundances of these three molecules is thus 500 : 45 : 1. The $\text{CS}^{34} \text{S}^{34}$ isotope may be disregarded, and so we have 11.1 : 1 for the former two isotopes. The isotopic band may be removed in the same way as a hot band. We now need to know the position of the isotopic band. We first have to calculate the force constant for the vibration. This is done using the following 2 x 2 determinant (21), where the symbols employed are shown in the diagram



$$\begin{vmatrix} f_1 - 4\pi^2 \nu^2 m_1 (m_2^2 + 2m_2 m_3 + m_3^2 + m_1 m_2 + m_1 m_3) / M^2 & -4\pi^2 \nu^2 m_1 (2m_3^2 + 2m_1 m_3 + 2m_2 m_3) / 2M^2 \\ -4\pi^2 \nu^2 m_1 (2m_3^2 + 2m_1 m_3 + 2m_2 m_3) / 2M^2 & f_2 - 4\pi^2 \nu^2 m_3 (m_2^2 + 2m_1 m_2 + m_1^2 + m_2 m_3 + m_1 m_3) / M^2 \end{vmatrix} = 0$$

The determinant was first solved for $f = f_1 = f_2$, using $\nu = 1522 \times 3 \times 10^{10}$ Hz, $m_1 = m_3 = 32 / N_A$, $m_2 = 12 / N_A$ and $M = 76 / N_A$. The result was $f = 43.715 \times 10^5$ dynes.cm⁻¹ or $f = 6.905 \times 10^5$ dynes.cm⁻¹. A typical force constant for this type of vibration should be of the order of magnitude of 10^5 dynes.cm⁻¹, and so the latter result was used. The determinant was then solved again to obtain the frequency of the CS³²S³⁴ vibration using $f = f_1 = f_2 = 6.905$ dynes.cm⁻¹, $m_1 = 32 / N_A$, $m_3 = 34 / N_A$ and $M = 78 / N_A$. The result was $\nu = 1518.2 \times 3 \times 10^{10}$ Hz or $\nu = 595.0 \times 3 \times 10^{10}$ Hz. The former is obviously the true answer here.

Another point to be considered is the symmetry of the carbon disulphide with respect to exchange of sulphur nuclei (or inversion about the centre of symmetry, which is the carbon atom). We must consider the total wavefunction of the molecule, ψ , which is the product of the wavefunctions shown below.

$$\psi = \psi_e \psi_v \psi_r$$

where ψ_e is the electronic wavefunction, ψ_v is the vibrational wavefunction and ψ_r is the rotational wavefunction. Dealing only with the system $S^{32}CS^{32}$ we must first consider what happens to the individual wavefunctions on inversion about the centre of symmetry. For the molecule in its ground state electronic configuration the electronic wavefunction is totally symmetric on inversion. The vibrational wavefunction depends on the magnitude of the internuclear distance and hence is symmetric to inversion. Rotational energy levels are quantised and the energy levels are associated with the rotational quantum number, J , where $J = 0, 1, 2, 3, 4 \dots$. The rotational wavefunction can change sign on inversion in which case it is said to be antisymmetric. Even values of the rotational quantum number, J , are associated with the symmetric wavefunctions, and odd values of J with the antisymmetric wavefunctions. The total wavefunction may thus change sign on inversion and this is dependent solely on the rotational wavefunction. The nuclear spin of the end atoms must now be considered. If the end atoms have a zero or integral nuclear spin quantum number the total wavefunction must not change sign on inversion. S^{32} has a nuclear spin quantum number of 0, and so for the total wavefunction to not change sign on inversion, odd value of J rotational energy levels must be absent. The alternate rotational energy levels are seen to be absent in the gas phase spectrum of $S^{32}CS^{32}$ (22).

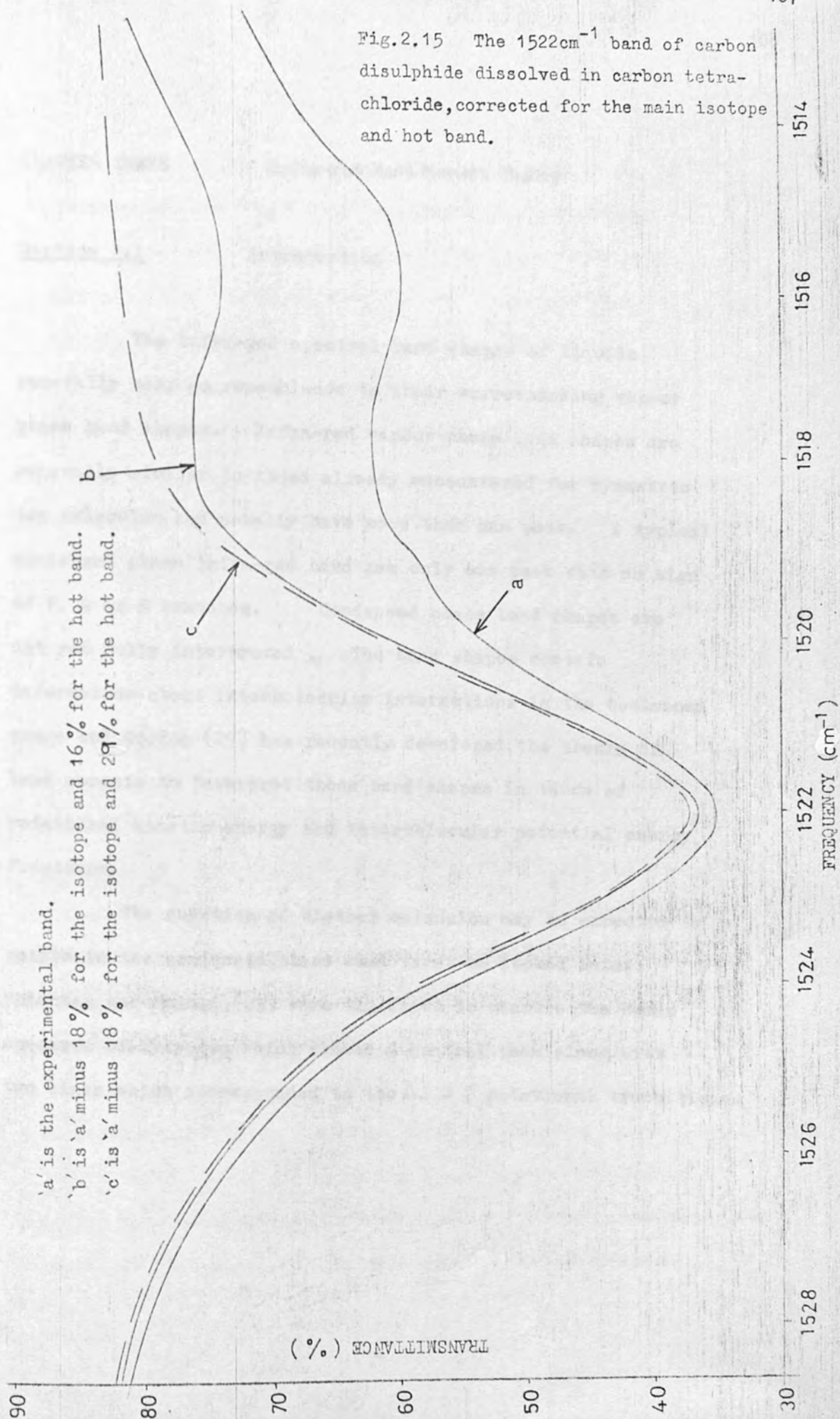
If one of the sulphurs is now changed for the isotope S^{34} , the symmetry of the molecule is lost and the above rules do not apply. This means that all rotational energy levels are now present and there is, effectively, a doubling of intensity compared with before. (Further reading to expand on this very condensed version on the subject of symmetry and wavefunctions may be found in reference (5)). ~~The above all leads up to the point that although the isotopic ratio of $CS^{32}S^{32}$ to $CS^{32}S^{34}$ is 11.1:1, the intensity ratio in the spectrum will be 5.55:1.~~

The shoulder of the 1522 cm^{-1} band is not all due to the isotope. There is also a hot band at 6.4 cm^{-1} to lower frequency of the main band, arising from the excited molecules of the ν_2 fundamental at 395 cm^{-1} (22). The intensity of this relative to the main part of the ν_3 band was calculated to be 29% using equation (2.34).

The hot band and isotopic band were subtracted out of the experimental band and the resulting band was more symmetric and the hot band was fully removed. See Fig. 215. The hot band was fully removed using a relative intensity of 29%. 1522

~~_____~~
~~_____~~
~~_____~~ The overall band shape was very symmetric after subtracting away the hot band and isotopic band.

The programme used to remove the isotopic band and the hot band was HOTBND.



CHAPTER THREE Infra-red Band Moment Theory

Section 3.1 Introduction

The infra-red spectral band shapes of liquids generally bear no resemblance to their corresponding vapour phase band shapes. Infra-red vapour phase band shapes are generally similar to those already encountered for symmetric top molecules and usually have more than one peak. A typical condensed phase infra-red band has only one peak with no sign of P, Q or R branches. Condensed phase band shapes are not yet fully interpreted. The band shapes contain information about intermolecular interactions in the condensed phase and Gordon (25) has recently developed the theory of band moments to interpret these band shapes in terms of rotational kinetic energy and intermolecular potential energy functions.

The question of whether molecules may be expected to rotate in the condensed phase must first be looked into. McLennan and McLeod (23) were the first to measure the Raman spectrum of hydrogen which showed a central peak along with two lines which corresponded to the $\Delta J = 2$ rotational transitions.

One peak arose from the lowest rotational level of ortho hydrogen and the other from the lowest rotational level of para hydrogen. The positions of both of these peaks were virtually unaltered from the gas phase spectrum. Much work has since been done on this molecule, with the conclusion that rotation does take place in the condensed phase. The moment of inertia of hydrogen is very small compared with other molecules and so the separation of adjacent rotation-vibration energy levels is large. Hence, although the rotational fine structure is broadened out due to the increased rate of collision by going into the condensed phase, the fine structure is not smeared out. With larger molecules, if rotation does take place in the condensed phase, collision broadening would smear the structure out so that it could not be resolved anyway. The general contour of a P and an R branch in the infra-red spectrum of liquid hydrogen chloride has been observed by West (24), and it was later shown that, when increasing the pressure on hydrogen chloride gas, the P and R branches fine structure first smeared out to a contour and then a forbidden "Q" branch started to rise near the gaseous band centre. On going into the liquid state there was no abrupt change in the spectrum. Using argon and nitrogen as diluents, different size "Q" branches were observed, suggesting that the effect of the added gas was not merely due to its rate of collision with the hydrogen chloride but also caused by more specific interactions. Hydrogen chloride

dissolved in liquid nitrogen gave a spectrum with an intense "Q" branch whereas, in argon, the P and R branches were dominant. Larger molecules than hydrogen chloride have not generally given rise to similar spectra but this, again, may be explained by the size of the moment of inertia of larger molecules such that the P and R branches would be completely smeared out. In the condensed phase, vibrational energy levels are slightly diminished and so there is usually an overall shift of the band to lower frequency. The problem of whether, and how much larger molecules rotate in the condensed phase cannot be solved merely by looking at the shape of the condensed phase spectrum.

Section 3.2

Band Moment Theory and the Odd Order Moments

There is a lot of information contained in condensed phase spectra concerning intermolecular forces and intermolecular motion. According to Gordon (25), some of this information may be obtained through analysis of the moments of the band intensity about the band centre. The j 'th order ($j = 1, 2, 3 \dots$) band moment, $M(j)$ is defined as

$$M(j) = \frac{\int_{\text{band}} (\bar{\nu} - \bar{\nu}_0)^j k(\bar{\nu}) d\bar{\nu}}{\int_{\text{band}} k(\bar{\nu}) d\bar{\nu}} \quad (3.1)$$

The denominator is an integrated area of the band which will be called Γ and is present to normalise out the intensity of the band so that the moments depend purely on the band contour. Gordon has calculated expressions for the first, second, third and fourth moments. He did this by considering the commutators $[H, \mu]$, where H is the total rotation - vibration Hamiltonian, and calculating the average of an operator in the initial state using commutator algebra. Gordon made a few simple approximations for the system. It was assumed that the binding within the molecule in the condensed phase was strong compared with intermolecular interactions. This means that the internal degrees of freedom (electronic and nuclear) move rapidly compared to overall molecular rotations and centre of mass

translational motions. Hence the total state vector for the whole system may be written approximately as a product of an external state and an internal state. The external state depends on the centre of mass co-ordinates and on the direction of the principal axis of inertia of all the molecules. The internal state depends on the internal degrees of freedom of all the molecules, and parametrically on the external state. The second approximation was to take the internal state as a simple product of those for each of the molecules. This approximation holds for dilute solutions where spectroscopically active molecules are separated. Thirdly, it was assumed that the external state had no influence on the magnitude of the internal transition moment or its direction relative to the principal molecular axis of inertia. Fourthly, it was assumed that the vibrational ground state was the only one populated thermally, so no allowance was made for hot bands.

The odd order moments are essentially a measure of the asymmetry in a band. The odd order moment of an even function is zero because the moment of the high frequency side is cancelled out by the low frequency side. The first moment is useful because it may be used to locate the true band centre of an asymmetric band, which may not be the position of maximum absorption. Provided the wings of a band are not badly overlapped, the value obtained for the first moment for an

asymmetric band is a small number, of the order of one wavenumber, which is the frequency displacement of the absorption band maximum from the true internal molecular transition. The first moment may thus be used to calculate the true band centre which is then utilised in the calculation of higher order moments.

The third order moment is a measure of the true asymmetry of a band with respect to its true band centre. The third moment of an asymmetric band need not be zero if the true band centre is used because of differences in the contours on either side of the band.

The intermolecular potential energy of the gas is considered to be the same for the ground state and the first excited state in the infra-red region if there is no frequency shift between the vapour and condensed phases.

The average molecular rotational kinetic energy is fixed in the gaseous and condensed phases by the equipartition theorem which states that, on heating a gas, the energy taken up equally by all its degrees of freedom is $\frac{1}{2}kT$ per molecule for each translational or rotational co-ordinate and $\frac{1}{2}kT$ per molecule for each vibration. The equation for energy of rotation has the form $E = I_x \omega_x^2/2 + I_y \omega_y^2/2 + I_z \omega_z^2/2$ where I_x is the moment of inertia about the x axis. Since each term in the energy expression is proportional to the square of a velocity component, each term on the average would have its equal share of energy. Thus the total average rotational energy of a non-

Section 3.3

The Second Moment - Gordon's Formulation

The second moment of a band is one measure of its width. There are two types of term in the second moment expression :-

- a) The fluctuation of the difference between intermolecular potential energies in the excited state and the ground state, averaged in the initial external state.
- b) The rotational kinetic energy terms.

The intermolecular potential energies may be considered to be the same for the ground state and the first excited state in the infra-red region if there is no frequency shift between the vapour and condensed phases.

The average molecular rotational kinetic energy is fixed in the gaseous and condensed phases by the equipartition theorem which states that, on warming a gas, the gas takes up energy (ergs) in all its degrees of freedom of $kT/2$ per molecule for each translational or rotational co-ordinate and kT per molecule for each vibration. The equation for energy of rotation has the form $E = I_x \omega_x^2/2 + I_y \omega_y^2/2 + I_z \omega_z^2/2$ where I_x is the moment of inertia about the x axis. Since each term in the energy expression is proportional to the square of a velocity component, each term on the average should have its equal share of energy. Thus the total average rotational energy of a non-

linear molecule is $3 kT/2$ ($2 kT/2$ for a linear molecule) and this energy is retained (but redistributed) in going from the gas phase to the condensed phase.

Gordon's equation for the second moment of the contour of a condensed phase infra-red band is set out below.

The units are cm^{-2} .

$$\begin{aligned}
 M_p(z) = & 2/x \left[(\bar{m}_y^{-2} + \bar{m}_z^{-2}) \frac{(B_p(x))^2}{B_o(x)} + (\bar{m}_x^{-2} + \bar{m}_z^{-2}) \frac{(B_p(y))^2}{B_o(y)} \right. \\
 & \left. + (\bar{m}_x^{-2} + \bar{m}_y^{-2}) \frac{(B_p(z))^2}{B_o(z)} \right] + (\text{Tr } B_p)^2 - 2(\bar{m} \cdot B_p \cdot \bar{m}) (\text{Tr } B_p) \\
 & + (\bar{m} \cdot B_p \cdot B_p \cdot \bar{m}) + 1/x \left[\frac{\Delta B(x)}{B_o(x)} + \frac{\Delta B(y)}{B_o(y)} + \frac{\Delta B(z)}{B_o(z)} \right] \quad (3.2) \\
 & (\text{Tr } B_p - \bar{m} \cdot B_p \cdot \bar{m}) + 1/(4x^2) \left[3 \left[\left(\frac{\Delta B(x)}{B_o(x)} \right)^2 + \left(\frac{\Delta B(y)}{B_o(y)} \right)^2 \right. \right. \\
 & \left. \left. + \left(\frac{\Delta B(z)}{B_o(z)} \right)^2 \right] + 2 \left[\frac{\Delta B(x) \Delta B(y)}{B_o(x) B_o(y)} + \frac{\Delta B(x) \Delta B(z)}{B_o(x) B_o(z)} + \frac{\Delta B(y) \Delta B(z)}{B_o(y) B_o(z)} \right] \right] \\
 & \left[\frac{\langle \text{m.s.s.m} (V_p - V_o)^2 \rangle}{\langle \text{m.s.s.m} \rangle} - \frac{\langle \text{m.s.s.m} (V_p - V_o) \rangle^2}{\langle \text{m.s.s.m} \rangle^2} \right] / (hc)^2
 \end{aligned}$$

In the above, ρ is the excited vibrational state and σ is the vibrational ground state, $x = (hc/kT)cm$, \bar{m} is a unit vector along the direction of the transition dipole having components about the x, y and z axes of inertia of $\bar{m}_x, \bar{m}_y, \bar{m}_z$, B is a diagonal matrix formed from the rotational constants B(x), B(y), B(z) along the three axes of inertia, ΔB is the difference between the rotational constants in the excited state and ground state, Tr is the abbreviation for taking the trace of a matrix, which is the sum of the terms along the leading diagonal. V_ρ and V_σ are the intermolecular potential energies for p'th excited state and the ground state. S is the shielding tensor which relates the average field of the radiation in the medium to the local field. The final term of equation (3.2) is called the shift fluctuation term. The present state of the knowledge of intermolecular forces precludes giving this term an accurate value, but Gordon states that this term should be much smaller than the dynamic terms in the equation. This term will thus be neglected. The equation is now seen to be independent of intermolecular forces and contains purely dynamic terms. To get a feel for the magnitude of these terms consider methyl iodide at a temperature of 300 °K undergoing a vibrational transition from the $v = 0$ state to the $v = 1$ state, with a vibrational transition dipole directed along the z axis. This means that $\bar{m}_z = 1$ and $\bar{m}_x = \bar{m}_y = 0$.

The rotational constants (26) are :-

$$B_0(x) = B_0(y) = B_0 = 0.2502 \text{ cm}^{-1}$$

$$B_0(z) = A_0 = 5.119 \text{ cm}^{-1}$$

$$B_1(x) = B_1(y) = B_1 = 0.2484 \text{ cm}^{-1}$$

$$B_1(z) = A_1 = 5.069 \text{ cm}^{-1}$$

$$\Delta B = 0.0018 \text{ cm}^{-1}$$

$$\Delta A = 0.050 \text{ cm}^{-1}$$

Taking the different terms of equation (3.2) in order we have :-

$$a) \quad 2/x \left[(\bar{m}_y^2 + \bar{m}_z^2) \frac{B_1^2}{B_0} + (\bar{m}_x^2 + \bar{m}_z^2) \frac{B_1^2}{B_0} + \right.$$

$$\left. (\bar{m}_x^2 + \bar{m}_y^2) \frac{A_1^2}{A_0} \right]$$

$$= 4 B_1^2 / B_0 x$$

$$= 205.54 \text{ cm}^{-2}$$

$$b) \quad (\text{Tr } B_1)^2 - 2(\bar{m} \cdot B_1 \cdot \bar{m}) (\text{Tr } B_1) + (\bar{m} \cdot B_p \cdot B_p \cdot \bar{m})$$

Now the trace of matrix B_1 is given by

$$\text{Tr} \begin{pmatrix} B_1 & 0 & 0 \\ 0 & B_1 & 0 \\ 0 & 0 & A_1 \end{pmatrix} = 2B_1 + A_1$$

and so we have

$$(2B_1 + A_1)^2 - 2 \begin{pmatrix} 0 & 0 & 1 \end{pmatrix} \begin{pmatrix} B_1 & 0 & 0 \\ 0 & B_1 & 0 \\ 0 & 0 & A_1 \end{pmatrix} \begin{pmatrix} 0 \\ 0 \\ 1 \end{pmatrix} (2B_1 + A_1)$$

$$\begin{aligned}
& + \begin{pmatrix} 0 & 0 & 1 \end{pmatrix} \begin{pmatrix} B_1 & 0 & 0 \\ 0 & B_1 & 0 \\ 0 & 0 & A_1 \end{pmatrix} \begin{pmatrix} B_1 & 0 & 0 \\ 0 & B_1 & 0 \\ 0 & 0 & A_1 \end{pmatrix} \begin{pmatrix} 0 \\ 0 \\ 1 \end{pmatrix} \\
& = (4B_1^2 + A_1^2 + 4A_1 B_1) - 2(2A_1 B_1 + A_1^2) + A_1^2 \\
& = 4B_1^2 \\
& = 0.25 \text{ cm}^{-2}
\end{aligned}$$

$$\begin{aligned}
\text{c) } & 1/x \left[\frac{\Delta B}{B_0} + \frac{\Delta B}{B_0} + \frac{\Delta A}{A_0} \right] (\text{Tr } B_1 - \bar{m} \cdot B_1 \cdot \bar{m}) \\
& = 2B_1 / x \left[\frac{2\Delta B}{B_0} + \frac{\Delta A}{A_0} \right] \\
& = 2.50 \text{ cm}^{-2}
\end{aligned}$$

$$\begin{aligned}
\text{d) } & 1/(4x^2) \left[3 \left[\left(\frac{\Delta B}{B_0} \right)^2 + \left(\frac{\Delta B}{B_0} \right)^2 + \left(\frac{\Delta A}{A_0} \right)^2 \right] + \right. \\
& \left. 2 \left[\frac{\Delta B}{B_0} \frac{\Delta B}{B_0} + \frac{\Delta A}{A_0} \frac{\Delta B}{B_0} + \frac{\Delta A}{A_0} \frac{\Delta B}{B_0} \right] \right] \\
& = 1/(4x^2) \left[8 \left(\frac{\Delta B}{B_0} \right)^2 + 3 \left(\frac{\Delta A}{A_0} \right)^2 + 4 \left(\frac{\Delta A}{A_0} \frac{\Delta B}{B_0} \right) \right] \\
& = 10.78 \text{ cm}^{-2}
\end{aligned}$$

Collecting these four terms together we have

$$\begin{aligned}
M_1(2) & = 205.54 + 0.25 + 2.50 + 10.78 \text{ cm}^{-2} \\
& = 219.07 \text{ cm}^{-2}
\end{aligned}$$

The first term is seen to be the dominant one, and from the form of the other terms it is seen that this will generally be the case. The first term is thus an approximation to the second moment. This term also involves the term (kT/hc) which is kinetic energy expressed in wavenumbers and so the second moment is related to the rotational energy through the rotational constants

$$\text{e.g. } M_1(2) \sim 4 \left(\frac{kT}{hc} \right) B_1$$

$$\text{Rotational kinetic energy } \left(\frac{kT}{hc} \right) \sim \frac{M_1(2)}{4 B_1}$$

The rotational kinetic energy is (kT/hc) and not $(3kt/2hc)$. This is because, for a symmetric top molecule, although the molecule may be rotating about all three axes of inertia, the rotational about the z axis is not observed because the molecular dipole is not rotating in that case. An observation that the experimentally measured condensed phase second moment is equal to that predicted by equation (3.2) is a confirmation that molecules rotate in the condensed phase. This does not mean that there is free rotation though. The molecules would be colliding all the time, which would hinder rotation, but the total rotational kinetic energy would be conserved to give us the classical second moment. Gordon's formulation of the second moment takes no account of the Coriolis interaction for an E band.

To check Gordon's formulation against that from a gas phase approach, the second moment of a parallel band of a symmetric top molecule was recalculated from the gas phase equations and compared with equation (3.2). If the results agreed, the gas phase approach was to be used for a perpendicular transition of a symmetric top molecule, taking the Coriolis constant into account.

calculated using

$$M(\nu) = \frac{1}{2} \sum_{J,K} (J - K)^2 \nu_{J,K}$$

The transition probabilities for parallel and perpendicular transitions of symmetric top molecules have been derived by Zoni and London (27) and by Hefner and Badawak (28). These are the terms in $\sum_{J,K} A_{J,K} \exp(-F_{J,K} / kT)$. Here $F_{J,K}$ is the rotational term value of the ground state, J is the quantum number determining the total angular momentum of the system, K is the quantum number determining the component of this angular momentum about the unique axis of the molecule, $\nu = (hc/kT)$, $A_{J,K}$ is a term whose value depends on the rotational quantum numbers J and K , and $g_{J,K}$ is the statistical weight of the lower state which depends on the selection rules.

| Allowed transition for a parallel band | Value of $A_{J,K} g_{J,K}$ |
|--|--|
| R branch $J, K \rightarrow J+1, K$ | $(2 - \delta_{K,0}) (J+K+1) (J-K+1) / (J+1)$ |
| Q branch $J, K \rightarrow J, K$ | $(2 - \delta_{K,0}) (2J+1) K^2 / (J+1)$ |
| P branch $J, K \rightarrow J-1, K$ | $(2 - \delta_{K,0}) (J^2 - K^2) / J$ |

Section 3.4The Second Moment - A Gas Phase Approach
for Symmetric Top Molecules

Equations for the transition probabilities and transition frequencies of rotation - vibration spectra of symmetric top molecules are known, and so calculation of the theoretic spectrum is easy. The second moment is then calculated using

$$M(2) = \frac{\int_{\text{band}} k(\bar{\nu}) (\bar{\nu} - \bar{\nu}_0)^2 d\bar{\nu}}{F}$$

The transition probabilities for parallel and perpendicular transitions of symmetric top molecules have been derived by Honl and London (27) and by Reiche and Rademaker (28). These are the terms in $A_{J,K} g_{J,K} \exp(-F_v(J,K) x)$. Here $F_{J,K}$ is the rotational term value of the ground state, J is the quantum number determining the total angular momentum of the system, K is the quantum number determining the component of this angular momentum about the unique axis of the molecule, $x = (hc/kT)$, $A_{J,K}$ is a term whose value depends on the rotational quantum numbers J and K , and $g_{J,K}$ is the statistical weight of the lower state which depends on the selection rules.

| <u>Allowed transition for a parallel band</u> | <u>Value of $A_{J,K} g_{J,K}$</u> |
|---|---|
| R branch $J, K \rightarrow J + 1, K$ | $(2 - \delta_{K,0}) (J + K + 1) (J - K + 1) / (J + 1)$ |
| Q branch $J, K \rightarrow J, K$ | $(2 - \delta_{K,0}) (2J + 1) K^2 / (J(J + 1))$ |
| P branch $J, K \rightarrow J - 1, K$ | $(2 - \delta_{K,0}) (J^2 - K^2) / J$ (3.3) |

Notice that the sum of $g_{J,K}$ for a given J, K over the P, Q and R branches is $(2J + 1)$, the well known degeneracy for each rotational energy level. $\delta_{K,0}$ is the Kronecker delta function which is equal to 1 when $K = 0$ and is equal to 0 when $K \neq 0$. For simplicity we will assume that $\delta_{K,0} = 0$ throughout, as it does not produce any significant change in the spectrum. The $A_{J,K}$ term may thus be removed as it is then normalised out by the integrated intensity anyway. Also the summation will be from $J = 0$ to $J = \infty$, irrespective of whether there is a $J = 0$ ground state for the different P, Q and R branches. This again will not significantly affect the result.

The rotation vibration energy of a symmetric top molecule in a vibrational energy level of quantum number v is given by

$$F_v(J,K) = B_v J(J+1) + (A_v - B_v) K^2 \text{ cm}^{-1}$$

and so we can now calculate the second moment using equation (3.3) and the above for a transition from the ground state to the $v = 1$

state. The units of the second moment are cm^{-2} and are omitted

from the algebra. $\sum_{J,K}$ is used to represent $\sum_{J=0}^{\infty} \sum_{K=-J}^J$

and $\exp(J,K)$ is used to represent $\exp(-F_v(J,K)x)$. Also the

sum over all the transition probabilities $\sum_{J=0}^{\infty} \sum_{K=-J}^J g_{J,K}$

$\exp(-F_v(J,K)x)$ will be called Q_r .

$$\begin{aligned}
 Q_r M(2) = & \sum_{J,K} (B_1 (J+1)(J+2) - B_0 J(J+1) + Z)^2 \\
 & (J^2 - K^2 + 2J + 1)/(J+1) \exp(J, K) + \\
 & (B_1 J(J+1) - B_0 J(J+1) + Z)^2 (2J+1)K^2 / \\
 & (J(J+1)) \exp(J, K) + (B_1 J(J-1) - \\
 & B_0 J(J+1) + Z)^2 (J^2 - K^2)/J \exp(J, K)
 \end{aligned}$$

Where the summation $\sum_{J,K}$ is over all terms on the right hand side of the equation and $Z = ((A_1 - B_1) K^2 - (A_0 - B_0) K^2)$. Writing ΔB in place of $(B_1 - B_0)$ and multiplying throughout by $J(J+1)$ we get

$$\begin{aligned}
 Q_r J(J+1) M(2) & = \sum_{J,K} \left[(\Delta B J(J+1) + B_1 2(J+1) + Z)^2 \right. \\
 & (J(J+1)^2 - JK^2) + (\Delta B J(J+1) + Z)^2 \\
 & (2J+1)K^2 + (\Delta B J(J+1) - 2B_1 J + Z)^2 \\
 & \left. (J^2 - K^2)(J+1) \right] \exp(J, K)
 \end{aligned}$$

Squaring the frequency terms and collecting together terms common to the P, Q and R branches gives :-

$$\begin{aligned}
 Q_T J(J+1) M(2) &= \sum_{J,K} \left[(\Delta B)^2 J^2 (J+1)^2 \left[J(J+1)^2 \right. \right. \\
 &\quad \left. \left. - J K^2 + (2J+1) K^2 + (J^2 - K^2)(J+1) \right] \right. \\
 &\quad \left. + Z^2 \left[J(J+1)^2 - J K^2 + (2J+1) K^2 \right. \right. \\
 &\quad \left. \left. + (J^2 - K^2)(J+1) \right] \right. \\
 &\quad \left. + 4B_1^2 \left[(J+1)^2 (J(J+1)^2 - J K^2) \right. \right. \\
 &\quad \left. \left. - J^2 (J^2 - K^2)(J+1) \right] \right. \\
 &\quad \left. + 4\Delta B B_1 J(J+1) \left[(J+1)(J(J+1))^2 \right. \right. \\
 &\quad \left. \left. - J K^2 \right] - J(J^2 - K^2)(J+1) \right] \\
 &\quad \left. + 2\Delta B Z J(J+1) \left[J(J+1)^2 - J K^2 + \right. \right. \\
 &\quad \left. \left. (2J+1) K^2 + (J^2 - K^2)(J+1) \right] \right. \\
 &\quad \left. + 4 B_1 Z \left[(J+1)(J(J+1))^2 - J K^2 \right] - \right. \\
 &\quad \left. J(J^2 - K^2)(J+1) \right] \exp(J,K)
 \end{aligned}$$

Multiplying out the different terms in J and K leads to many terms cancelling each other out. Collecting the remaining terms together we have

$$\begin{aligned}
 Q_T M(2) &= \sum_{J,K} \left[(\Delta B)^2 J^2 (J+1)^2 (2J+1) + Z^2 (2J+1) \right. \\
 &\quad \left. + 4 B_1^2 (2J+1) (J(J+1) + 1 - K^2) \right. \\
 &\quad \left. + 4\Delta B B_1 J(J+1) (2J+1) + 2\Delta B Z J \right. \\
 &\quad \left. (J+1) (2J+1) + 4 B_1 Z (2J+1) \right] \exp(J,K)
 \end{aligned}$$

Expanding and re-arranging the equation we get

$$Q_r M(2) = \sum_{J, K} (2J + 1) \cdot \left[\begin{array}{l} (\Delta B)^2 J^2 (J + 1)^2 + (\Delta(A - B))^2 K^4 \\ + 4 B_1^2 (J(J + 1) + 1 - K^2) \\ + 4 \Delta B B_1 J(J + 1) + 2 \Delta B \Delta(A - B) \\ J(J + 1) K^2 \\ + 4 B_1 \Delta(A - B) K^2 \end{array} \right] \exp(-F_0(J, K)x) \quad (3.4)$$

The problem now is to convert from a summation to an integration or a series expansion. The term Q_r is called the rotational partition function for a symmetric top molecule and collecting the $g_{J,K}$ terms together we have

$$Q_r = \sum_{J=0}^{\infty} \sum_{K=-J}^J (2J + 1) \cdot \exp(-F_v(J, K)x) \quad (3.5)$$

Kassel (30) has computed Q_r and also expressed it as a series expansion. He also differentiated this series expansion of Q_r with respect to different parameters and obtained sums of the form we need above. He defined sums, $S(f)$, to be

$$S(f) = \sum_{J=0}^{\infty} \sum_{K=-J}^J f(2J+1) \exp(-F_V(J, K) x)$$

and $Q_r = S(1) = \pi^{1/2} \sigma^{3/2} \exp(\sigma/4) (\beta + 1)^{-1/2}$

$$\left[1 + (1/12) \beta (\beta + 1)^{-1} \sigma + (7/480) \beta^2 (\beta + 1)^{-2} \sigma^2 + \dots \right] \quad (3.6)$$

where $\beta = (A/B_V - 1)$ and $\sigma = B_V x$. Using this nomenclature equation (3.5) becomes

$$S(1) = \sum_{J, K} (2J+1) \exp(-J(J+1)\sigma - \beta \sigma K^2)$$

and differentiation of this equation with respect to β gives

$$\frac{\partial S(1)}{\partial \beta} = \sum_{J, K} - (2J+1) \sigma K^2 \exp(-J(J+1)\sigma - \beta \sigma K^2) \quad (3.7)$$

The right hand side of equation (3.7) is equal to $-\sigma S(K^2)$ so we will now differentiate equation (3.6) with respect to β

$$\frac{\partial S(1)}{\partial \beta} = \frac{\partial}{\partial \beta} \left(\pi^{1/2} \sigma^{3/2} \exp(\sigma/4) \right)$$

$$\cdot \left[(\beta + 1)^{-1/2} + (1/12) \beta (\beta + 1)^{-3/2} \sigma + \dots \right]$$

$$= \pi^{1/2} \sigma^{3/2} \exp(\sigma/4) \left[-1/2 (\beta + 1)^{-3/2} + (1/12) (-3/2) \beta (\beta + 1)^{-5/2} \sigma + (1/12) (\beta + 1)^{-3/2} \sigma + \dots \right]$$

$$= -1/2 \pi^{1/2} \sigma^{3/2} \exp(\sigma/4) (\beta + 1)^{-3/2} \\ \left[1 + (1/12) 3 \beta (\beta + 1)^{-1} \sigma - \sigma/6 \right] \\ = -1/2 \pi^{1/2} \sigma^{3/2} \exp(\sigma/4) (\beta + 1)^{-3/2} \\ \left[1 + (1/12) (\beta + 1)^{-1} (\beta - 2) \sigma + \dots \right]$$

On comparison with equation (3.7) we now get

$$S(K^2) = 1/2 \pi^{1/2} \sigma^{5/2} \exp(\sigma/4) (\beta + 1)^{-3/2} \\ \left[1 + (1/12) (\beta + 1)^{-1} (\beta - 2) \sigma + \dots \right]$$

In a similar way all of the summations we need may be obtained by differentiation of $S(1)$. All the sums we need are set out below in modern nomenclature.

$$S(1) = X \left[1 + \frac{B_0 x}{12} - \frac{B_0^2 x}{12 A_0} + \frac{7x^2}{480} \left(B_0^2 - \frac{2 B_0^3}{A_0} + \frac{B_0^4}{A_0^2} \right) + \dots \right]$$

$$S(K^2) = \frac{X}{2A_0 x} \left[1 + \frac{B_0 x}{12} - \frac{B_0^2 x}{4 A_0} + \dots \right] \quad (3.8)$$

$$S(J(J+1)) = \frac{X}{B_0 x} \left[1 + \frac{B_0}{2A_0} = \frac{B_0 x}{4} + \frac{B_0^2 x}{8 A_0} - \frac{B_0^3 x}{8 A_0^2} + \dots \right]$$

$$S(J^2 (J+1)^2) = \frac{X}{4B_0^2 x^2} \left[8 + \frac{4B_0}{A_0} + \frac{3B_0^2}{A_0} - 2 B_0 x \right. \\ \left. - \frac{B_0^2 x}{A_0} + \frac{5 B_0^3 x}{4 A_0^2} + \frac{21 B_0^4 x}{4 A_0^3} \right]$$

$$S(K^4) = \frac{X}{4 A_0^2 x^2} \left[3 + \frac{B_0 x}{4} - \frac{5 B_0^2 x}{4 A_0} + \dots \right]$$

$$S(J(J+1)K^2) = \frac{X}{4 A_0 B_0 x^2} \left[2 + \frac{3 B_0}{A_0} - \frac{B_0 x}{2} + \frac{3 B_0^2 x}{4 A_0} - \frac{5 B_0^3 x}{4 A_0^2} + \dots \right] \quad (3.8)$$

$$\text{where } X = \left(\frac{\pi}{A_0 B_0^2 x^3} \right)^{1/2} \exp \left(-\frac{B_0 x}{4} \right)$$

Equation (3.4) may now be solved for the various summations. Retaining only the terms of lowest order in the rotational constants, after substitution in (3.8) and dividing by π , we get

$$M(2) = (\Delta B)^2 \left(\frac{2}{B_0^2 x^2} + \frac{1}{A_0 B_0 x^2} + \frac{3}{4 A_0^2 x^2} \right)$$

$$+ (\Delta(A-B))^2 \left(\frac{3}{4 A_0^2 x^2} \right) + B_1^2$$

$$\left(\frac{4}{B_0 x} + \frac{8}{3} + \frac{2 B_0}{3 A_0} \right)$$

$$+ \Delta B B_1 \left(\frac{4}{B_0 x} + \frac{2}{A_0 x} \right) + \Delta B \Delta(A-B)$$

$$\left(\frac{1}{A_0 B_0 x^2} + \frac{3}{2 A_0^2 x^2} \right)$$

$$+ \Delta(A-B) \frac{2 B_1}{A_0 x}$$

Writing $\Delta A - \Delta B$ in place of $\Delta(A - B)$, and re-arranging we get

$$\begin{aligned}
 M(2) = & B_1^2 \left(\frac{4}{B_0 x} + \frac{8}{3} + \frac{2 B_0}{3 A_0} \right) + \frac{(\Delta B)^2}{x^2} \left(\frac{2}{B_0^2} \right) \\
 & + \frac{(\Delta A)^2}{x^2} \left(\frac{3}{4 A_0^2} \right) + \frac{\Delta A \Delta B}{x^2} \left(\frac{1}{A_0 B_0} \right) + \frac{\Delta B B_1}{x} \left(\frac{4}{B_0} \right) \\
 & + \frac{B_1 \Delta A}{x} \left(\frac{2}{A_0} \right) \text{ cm}^{-2} \quad (3.9)
 \end{aligned}$$

We thus have an expression for the second moment of a gas phase parallel band for a symmetric top molecule.

Gordon's equation for a parallel band of a symmetric top molecule has already been derived in stages and can be written

$$\begin{aligned}
 M(2) = & B_1^2 \left(\frac{4}{B_0 x} + 4 \right) + \frac{(\Delta B)^2}{x^2} \left(\frac{2}{B_0^2} \right) \\
 & + \frac{(\Delta A)^2}{x^2} \left(\frac{3}{4 A_0^2} \right) + \frac{\Delta A \Delta B}{x^2} \left(\frac{1}{A_0 B_0} \right) + \frac{\Delta B B_1}{x} \left(\frac{4}{B_0} \right) \\
 & + \frac{B_1 \Delta A}{x} \left(\frac{2}{A_0} \right) \text{ cm}^{-2} \quad (3.10)
 \end{aligned}$$

There is only one very small difference between equations (3.9) and (3.10) and that is equation (3.10) contains the term $4 B_1^2$ instead of $(8/3 + 2 B_0/3 A_0) B_1^2$.

This result is seen as a proof that Gordon's formulation is correct.

There is, however, one thing that Gordon's formulation lacks, and that is allowance for coupling of rotations and vibrations in a degenerate transition, in the form of the Coriolis constant, ξ . For a degenerate band (E band in the case of symmetric top molecules, which have doubly degenerate bands) the equation for the rotational energy levels is modified to

$$F_v(J, K) = B_v J(J+1) + (A_v - B_v)K^2 \mp 2A_v \xi K$$

ξ may have any one value ranging from -1 to +1

and gives rise to a whole range of band shapes

(31), and one can expect the second moment to change a lot as well. It was decided to calculate the equation for the second moment of a perpendicular band for a symmetric top molecule (all the E bands are perpendicular bands).

The derived equation can then be compared with Gordon's equation to see how the Coriolis coupling generally affects his formulation.

The allowed transitions and statistical weights for a perpendicular transition are set out below.

Allowed transition for a perpendicular band Value of $g_{J, K}$

$$J, |K| \rightarrow J+1, |K| \pm 1 \quad (J \pm K + 1) (J \pm K + 2) / (J + 1)$$

$$J, |K| \rightarrow J, |K| \pm 1 \quad (2J + 1) (J \mp K) (J \pm K + 1) / (J (J + 1))$$

$$J, |K| \rightarrow J-1, |K| \pm 1 \quad (J \mp K) (J \mp K - 1) / J$$

Using the same tabulation as for the parallel transition case we have

$$\begin{aligned} Q_r M(2) = & \sum_{J, K} \left[\left[\Delta B J (J + 1) + 2 B_1 (J + 1) + Z + (A_1 - B_1) (2K + 1) \right. \right. \\ & \left. \left. - 2 \zeta A_1 (K + 1) \right]^2 (J + K + 1) (J + K + 2) / (J + 1) \right. \\ & + \left[\Delta B J (J + 1) + 2 B_1 (J + 1) + Z + (A_1 - B_1) (2K - 1) \right. \\ & \left. + 2 \zeta A_1 (K - 1) \right]^2 (J - K + 1) (J - K + 2) / (J + 1) \\ & + \left[\Delta B J (J + 1) + Z + (A_1 - B_1) (2K + 1) - 2 \zeta A_1 (K + 1) \right]^2 \\ & (2J + 1) (J - K) (J + K + 1) / (J (J + 1)) \\ & + \left[\Delta B J (J + 1) + Z + (A_1 - B_1) (2K - 1) + 2 \zeta A_1 (K - 1) \right]^2 \\ & (2J + 1) (J + K) (J - K + 1) / (J (J + 1)) \\ & + \left[\Delta B J (J + 1) - 2 B_1 J + Z + (A_1 - B_1) (2K + 1) - \right. \\ & \left. 2 \zeta A_1 (K + 1) \right]^2 (J - K) (J - K - 1) / J \\ & + \left[\Delta B J (J + 1) - 2 B_1 J + Z + (A_1 - B_1) (2K - 1) + \right. \\ & \left. 2 \zeta A_1 (K - 1) \right]^2 (J + K) (J + K - 1) / J \Big] \exp(J, K) \end{aligned}$$

After multiplying out the above and simplifying

we get :-

$$Q_r M(2) = \sum_{J,K} 4 (2J+1) \left[B_1^2 (2J(J+1) - 2K^2 + 1) \right. \\ + 4 \bar{A}_1^2 (K^2) \\ + \bar{A}_1^2 + 2 \bar{A}_1 B_1 + 2 (B_1 + \bar{A}_1) \Delta(A-B) (K^2) \\ + (\Delta(A-B))^2 (K^4) + (\Delta B)^2 (J^2 (J+1)^2) \\ \left. + 2 (B_1 + \bar{A}_1) \Delta B (J(J+1)) \right] \exp(J,K) \quad (2.10)$$

where $\bar{A}_1 = A_1 (1 - \xi)$ and $\bar{\bar{A}}_1 = A_1 (1 - 2\xi)$. These sums can again be solved as before using series expansions. This was carried out with the following results

$$M(2) = B_1^2 \left(\frac{2}{B_0 x} + \frac{1}{3} + \frac{B_0}{3 A_0} \right) + \bar{A}_1^2 + 2 \bar{A}_1 B_1 \\ + (\Delta(A-B))^2 \left(\frac{3}{4 A_0^2 x^2} \right) + \frac{(\Delta B)^2}{x^2} \\ \left(\frac{2}{B_0^2} + \frac{1}{A_0 B_0} + \frac{3}{4 A_0^2} \right) \\ + \frac{\Delta B}{x} (B_1 + \bar{A}_1) \left(\frac{2}{B_0} + \frac{1}{A_0} \right) + \Delta(A-B) \\ (B_1 + \bar{A}_1) / (A_0 x) \\ + \bar{\bar{A}}_1^2 \left(\frac{2}{A_0 x} - \frac{B^2}{3 A_0^2} \right)$$

Expanding all these terms we get :-

$$\begin{aligned}
M(2) = & \frac{2 B_1^2}{B_0 x} + \frac{2 \bar{A}_1^2}{A_0 x} + \bar{A}_1^2 + 2 \bar{A}_1 B_1 + \frac{B_1^2}{3} \\
& + \frac{2 \bar{A}_1 \Delta B}{B_0 x} + \frac{2 B_1 \Delta B}{B_0 x} + \frac{\bar{A}_1 \Delta A}{A_0 x} + \frac{B_1 \Delta A}{A_0 x} \quad (3.11) \\
& + \frac{2}{x^2} \left(\frac{\Delta B}{B_0} \right)^2 + \frac{3}{4 x^2} \left(\frac{\Delta A}{A_0} \right)^2 - \frac{3}{2 x^2} \left(\frac{\Delta A \Delta B}{A_0^2} \right) \\
& + \frac{3}{2 x^2} \left(\frac{\Delta B}{A_0} \right)^2 + \frac{1}{x^2} \left(\frac{\Delta B^2}{A_0 B_0} \right) + \frac{B_1^2 B_0}{3 A_0} - \frac{\bar{A}_1^2 B_1^2}{3 A_0^2}
\end{aligned}$$

We now have an equation for the second moment of a perpendicular band for a symmetric top molecule, and want to compare this with the equation using Gordon's formulation. To solve equation (3.2) we have $\bar{m}_z = 0$, $\bar{m}_x = 1$ or 0 and $\bar{m}_y = 0$ or 1 respectively. Taking each term in turn, as before, we have

$$\begin{aligned}
a) \quad & 2/x \left[(\bar{m}_y^2 + \bar{m}_z^2) \frac{B_1^2}{B_0} + (\bar{m}_x^2 + \bar{m}_z^2) \frac{B_1^2}{B_0} \right. \\
& \left. + (\bar{m}_x^2 + \bar{m}_y^2) \frac{A_1^2}{A_0} \right]
\end{aligned}$$

$$= \frac{2 B_1^2}{B_0 x} + \frac{2 A_1^2}{A_0 x}$$

$$b) \quad (2B_1 + A_1)^2 - 2 \begin{pmatrix} \bar{m}_x & \bar{m}_y & \bar{m}_z \end{pmatrix} \begin{pmatrix} B_1 & 0 & 0 \\ 0 & B_1 & 0 \\ 0 & 0 & A_1 \end{pmatrix} \begin{pmatrix} \bar{m}_x \\ \bar{m}_y \\ \bar{m}_z \end{pmatrix} (2B_1 + A_1)$$

$$+ \begin{pmatrix} \bar{m}_x & \bar{m}_y & \bar{m}_z \end{pmatrix} \begin{pmatrix} B_1 & 0 & 0 \\ 0 & B_1 & 0 \\ 0 & 0 & A_1 \end{pmatrix} \begin{pmatrix} B_1 & 0 & 0 \\ 0 & B_1 & 0 \\ 0 & 0 & A_1 \end{pmatrix} \begin{pmatrix} \bar{m}_x \\ \bar{m}_y \\ \bar{m}_z \end{pmatrix} \quad (3-22)$$

$$= 4B_1^2 + A_1^2 + 4B_1 A_1 - 4B_1^2 - 2A_1 B_1 + B_1^2$$

$$= A_1^2 + 2A_1 B_1 + B_1^2$$

$$c) \quad \frac{1}{x} \left(\frac{\Delta B}{B_0} + \frac{\Delta B}{B_0} + \frac{\Delta A}{A_0} \right) \left[(2B_1 + A_1) - \begin{pmatrix} \bar{m}_x & \bar{m}_y & \bar{m}_z \end{pmatrix} \right]$$

$$\left[\begin{pmatrix} B_1 & 0 & 0 \\ 0 & B_1 & 0 \\ 0 & 0 & A_1 \end{pmatrix} \begin{pmatrix} \bar{m}_x \\ \bar{m}_y \\ \bar{m}_z \end{pmatrix} \right]$$

$$= \frac{1}{x} \left(\frac{2\Delta B}{B_0} + \frac{\Delta A}{A_0} \right) (A_1 + B_1)$$

$$d) \quad \frac{1}{4x^2} \left[3 \left[\left(\frac{\Delta B}{B_0} \right)^2 + \left(\frac{\Delta B}{B_0} \right)^2 + \left(\frac{\Delta A}{A_0} \right)^2 \right] + 2 \left[\left(\frac{\Delta B}{B_0} \right)^2 + \left(\frac{\Delta A \Delta B}{A_0 B_0} \right) \right] \right.$$

$$\left. + \left(\frac{\Delta A \Delta B}{A_0 B_0} \right) \right] = \frac{1}{4x^2} \left[8 \left(\frac{\Delta B}{B_0} \right)^2 + 3 \left(\frac{\Delta A}{A_0} \right)^2 + 4 \left(\frac{\Delta A \Delta B}{A_0 B_0} \right) \right]$$

Collecting all these terms together we have

$$\begin{aligned}
 M(2) = & \frac{2 B_1^2}{B_0 x} + \frac{2 A_1^2}{A_0 x} + A_1^2 + 2 A_1 B_1 + B_1^2 \\
 & + \frac{2 A_1 \Delta B}{B_0 x} + \frac{2 B_1 \Delta B}{B_0 x} + \frac{A_1 \Delta A}{A_0 x} + \frac{B_1 \Delta A}{A_0 x} \\
 & + \frac{2}{x^2} \left(\frac{\Delta B}{B_0} \right)^2 + \frac{3}{4x^2} \left(\frac{\Delta A}{A_0} \right)^2 + \frac{1}{x^2} \left(\frac{\Delta A \Delta B}{A_0 B_0} \right)
 \end{aligned} \tag{3.12}$$

Equations (3.11) and (3.12) may now be compared and are seen to be almost identical for the case when $\xi = 0$ ($\xi = 0$ in equation (3.12) by virtue of its absence). There are a few minor differences which are set out below.

Terms in equation (3.11)

$$\frac{B_1^2}{3A_0} - \frac{\bar{A}_1^2 B_1^2}{3A_0}$$

$$- \frac{3}{2x^2} \left(\frac{\Delta A \Delta B}{A_0^2} \right)$$

$$\frac{3}{2x^2} \left(\frac{\Delta B}{B_0} \right)^2 + \frac{1}{x^2} \left(\frac{\Delta B^2}{A_0 B_0} \right)$$

$$+ \frac{B_1^2 B_0}{3A_0}$$

Terms in equation (3.12)

$$B_1^2$$

$$\frac{1}{x} \left(\frac{\Delta A \Delta B}{A_0 B_0} \right)$$

Methyl iodide will again be used as a numerical example.

Putting $\zeta = 0.0$ and using equation (3.11) we get

$$\begin{aligned}
 M(2) &= 102.77 + 2091.72 + 25.69 + 2.52 \\
 &+ 0.02 + 15.20 + 0.74 + 10.32 \\
 &+ 0.50 + 4.49 + 3.11 - 0.22 \\
 &+ 0.01 + 0.11 + 0.00 - 0.02 \text{ cm}^{-2}
 \end{aligned}$$

$$M(2) = 2257.5 \text{ cm}^{-2}$$

The terms in disagreement with equation (3.12) add up to -0.1 cm^{-2} and so are negligible in this case. The two different terms in equation (3.12) add up to only 3 cm^{-2} .

The discrepancies in the equation are possibly due to the degree of accuracy to which the series expansion to get equation (3.11) was taken.

We now want to see the effect of the Coriolis constant on the second moment, so using methyl iodide and $\zeta = -1$ in equation (3.11) we get, keeping the terms in the same order for comparison with the above :-

$$\begin{aligned}
 M(2) &= 102.77 + 8366.88 + 231.25 + 7.55 \\
 &+ 0.02 + 45.59 + 0.74 + 30.95 \\
 &+ 0.50 + 4.49 + 3.11 - 0.22 \\
 &+ 0.01 + 0.11 + 0.00 - 0.08 \text{ cm}^{-2}
 \end{aligned}$$

$$M(2) = 8793.67 \text{ cm}^{-2}$$

And for $\xi = +1$ we have

$$\begin{aligned}
 M(2) &= 102.77 + 0.0 - 25.69 - 2.52 \\
 &+ 0.02 - 15.20 + 0.74 - 10.32 \\
 &+ 0.50 + 4.49 + 3.11 - 0.22 \\
 &+ 0.01 + 0.11 + 0.00 + 0.02 \text{ cm}^{-2}
 \end{aligned}$$

$$M(2) = 57.82 \text{ cm}^{-2}$$

So, for methyl iodide, a hypothetical perpendicular band could have a second moment ranging from 57.82 up to 8793.67 cm^{-2} .

The Coriolis coupling constant has a huge effect on the second moment, and so a measure of the second moment can, conversely, yield the Coriolis coupling constant to a high degree of accuracy.

This can apply to a gaseous band of unknown ξ , or to condensed phase bands. For condensed phase bands it is not known whether Coriolis coupling is affected by the frequent collisions and the inability of the molecule to rotate freely. Picking out the major terms in equation (3.11) we have

$$M(2) = \frac{2 B_1^2}{B_0 x} + \frac{2 \bar{A}_1^2}{A_0 x} + \bar{A}_1^2 + \frac{2 \bar{A}_1 \Delta B}{B_0 x} + \frac{\bar{A} \Delta B}{A_0 x}$$

From expanding this equation and re-arrangement we get the following quadratic, which can be solved for ξ .

$$\begin{aligned} \mathcal{J}^2 \left(\frac{2A_1^2}{A_0 x} + 4A_1^2 \right) - \mathcal{J} \left(\frac{4A_1^2}{A_0 x} + 4A_1^2 + \frac{2A_1 \Delta B}{B_0 x} + \frac{2A_1 \Delta B}{A_0 x} \right) \\ + (A_1^2 + \frac{2B_1^2}{B_0 x} + \frac{2A_1^2}{A_0 x} + \frac{2A_1 \Delta B}{B_0 x} + \frac{A_1 \Delta B}{A_0 x} - M(2)) = 0.0 \end{aligned} \quad (3.13)$$

is much more complicated than the one above. It can be simplified

by using the classical rotational constants, i.e. the

Equation (3.13) can be solved using the formula

$$(\text{root}) = \frac{-b \pm (b^2 - 4ac)^{1/2}}{2a}$$

Only one of the roots obtained from this equation should make sense. A small computer routine was written to solve equation (3.13) for \mathcal{J} . The correctness of the routine was checked by solving for the Coriolis constant in a computer simulated spectrum of the ν_6 band of methyl iodide, given a Coriolis constant of zero. The result obtained was 0.004 which implies that any results from the equation are accurate to two decimal places. Experimental second moments will be considered in later chapters.

of rotation around x, y and z. V is the angle dependent part of the intermolecular potential energy. The average, represented by the brackets $\langle \dots \rangle$, is over the six-dimensional Boltzmann distribution for the rotational and translational co-ordinates. For a freely rotating molecule, i.e. in the gas phase, there is no intermolecular

Section 3.5

The Fourth Moment

The fourth moment has been developed by Gordon (32) and is much more complicated than the second moment. To simplify matters, Gordon used classical rotational constants, i.e. the upper and lower vibrational states have identical rotational constants, $B_1 = B_0 = B$. His result is set out below

$$\begin{aligned}
 M(4) = & 4/x^2 \left[2 (\text{Tr } B)^2 - 3 \text{Tr } B \cdot B + 7 \bar{m} \cdot B \cdot B \cdot \bar{m} \right. \\
 & - 6 (\bar{m} \cdot B \cdot \bar{m}) (\text{Tr } B) + (\text{Tr } B^{-1}) (\text{Tr } B) (\text{Tr } B \cdot B) \\
 & - (\text{Tr } B^{-1}) (\text{Tr } B \cdot B \cdot B) - (\text{Tr } B^{-1}) (\text{Tr } B) (\bar{m} \cdot B \cdot B \cdot \bar{m}) \\
 & + (\text{Tr } B^{-1}) (\bar{m} \cdot B \cdot B \cdot B \cdot \bar{m}) + 4 \langle (OV) \cdot B \cdot B \cdot \\
 & \left. (OV) \rangle - 4 \langle (\bar{m} \cdot B \cdot OV)^2 \rangle \right] \text{cm}^{-4} \quad (3.14)
 \end{aligned}$$

O is an operator whose components O_x , O_y and O_z along the axes of inertia x , y and z represent derivatives with respect to angles of rotation around x , y and z . V is the angle dependent part of the intermolecular potential energy. The average, represented by the brackets $\langle \rangle$, is over the classical Boltzmann distribution for the rotational and translational co-ordinates. For a freely rotating molecule, i.e. in the gas phase, there is no intermolecular

potential energy and thus $OV = 0.0$. The potential energy terms contribute if the intermolecular forces depend on the angles describing the orientation of the active molecule. $(OV)^2$ is the square of the torque acting on the molecule hindering rotation. Numerically, the square of the torque is defined by

$$(OV)^2 = \left(\frac{\partial V}{\partial \theta} \right)^2 + \operatorname{cosec}^2 \theta \left(\frac{\partial V}{\partial \phi} \right)^2$$

where θ and ϕ are the usual angles defined when using polar co-ordinates (θ is the angle subtended about the z axis and ϕ is the angle subtended about the x axis). The terms involving (OV) in the fourth moment expression are clearly positive, so the hindering of rotation leads to a larger than classical (freely rotating) fourth moment.

Equation (3.14) was checked by computing the fourth moment from a simulated gas phase band contour of methyl iodide using $B = 0.2502 \text{ cm}^{-1}$, $A = 5.119 \text{ cm}^{-1}$ and $T = 300^\circ \text{K}$. In this case ($OV = 0$). A parallel transition was used and the fourth moment was calculated to be 88733 cm^{-4} .

Solving equation (3.14) for the above transition we

get

$$\begin{aligned} M(4) = & 4/x^2 (8B^2 + 2A^2 + 8AB - 6B^2 - 3A^2 \\ & + 7A^2 - 12AB - 6A^2 + 10B^2 + 4B^3/A \\ & + 4AB + 5A^2 + 2AB + 2A^3/B - 4B^2 \\ & - 2A^3/B - 2B^3/A - A^2 - 5A^2 - 2AB \\ & - 2A^3/B + 2A^3/B + A^2) \end{aligned}$$

Which simplifies to

$$M(4) = 4/x^2 (8B^2 + 2B^3/A) \quad (3.15)$$

$$M(4) = 87750 \text{ cm}^{-4}.$$

The two values for the fourth moment closely agree, the former probably being larger because of small errors in the integration using the trapezium rule.

The importance of the fourth moment lies in determining the mean squared torque acting on the molecule $\langle (OV)^2 \rangle$. This can usually be done experimentally through comparison of the second and fourth moments, providing the rotational constants are known.

e.g. For a linear molecule and a parallel transition with rotational constants

$$B(x) = B, \quad B(y) = B, \quad B(z) = 0 \quad \text{we have :-}$$

$$M(2) = 4B (kT/hc)$$

$$M(4) = 4 (kT/hc)^2 (8B^2) + 4B^2 \langle (OV)^2 \rangle$$

$$\Rightarrow M(4) = 2 M(2)^2 + 4B^2 \langle (OV)^2 \rangle$$

$$\langle (OV) \rangle = \left(\frac{M(4) - 2 M(2)^2}{4B^2} \right)^{\frac{1}{2}} \text{ cm}^{-1}$$

Here the mean torque is about the x and y axes. Experimental fourth moments and molecular torques will be considered in a later chapter.

CHAPTER FOURExperimental Vapour and Condensed Phase
Second Moments and Condensed Phase Band
ShapesSection 4.1The Determination of the Coriolis Constant
of an "e" Band of a Symmetric Top Molecule
from the Vapour Phase Second Moment

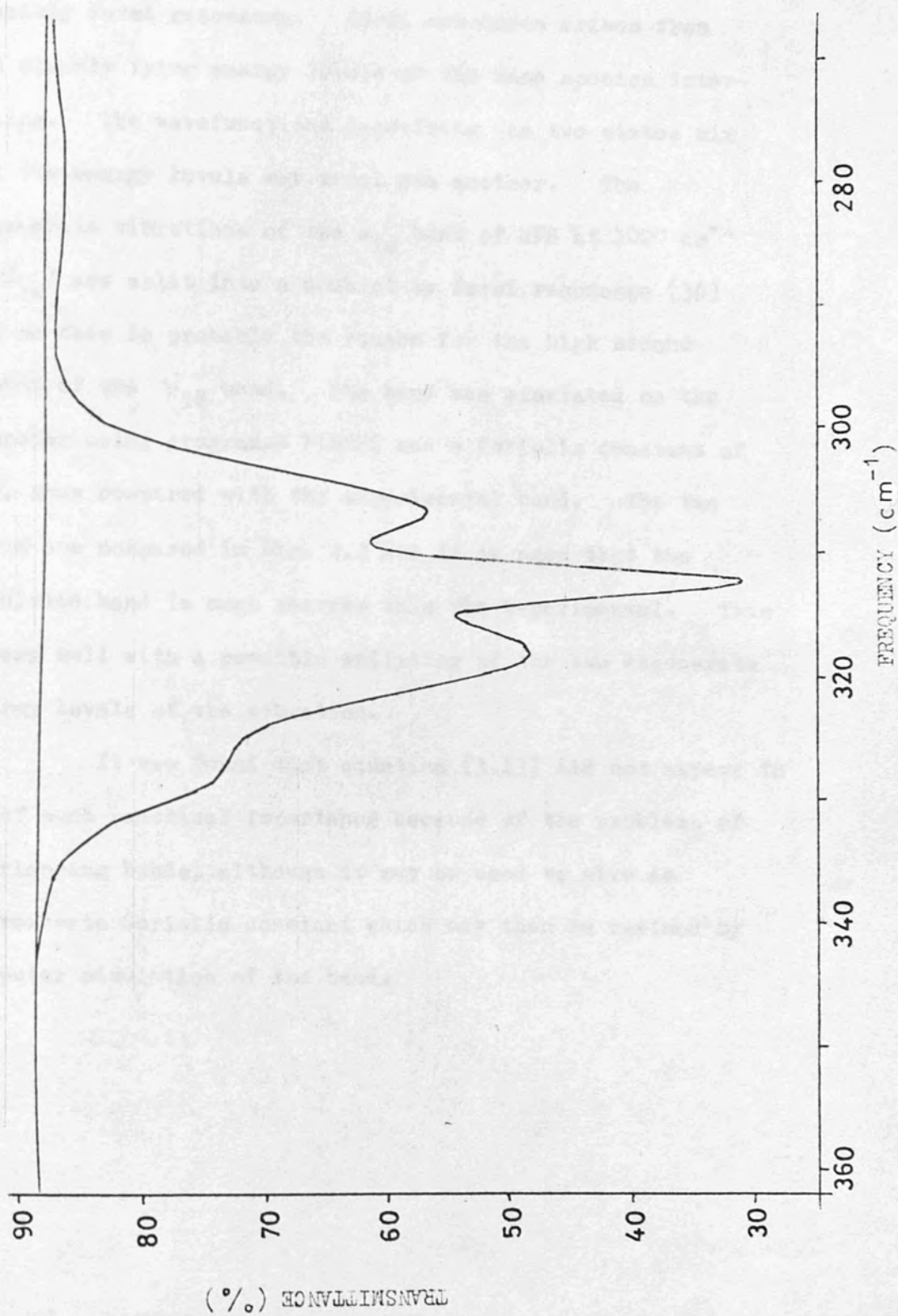
In the previous chapter it was shown that the Coriolis constant of a doubly degenerate band of a symmetric top molecule could be calculated from the second moment of the band and the rotational constants. This equation should be particularly useful for bands of molecules with large moments of the inertia about the three axes, for which the rotational fine structure is merged into a single contour. The Coriolis constant may be determined by a trial and error method of computer simulation of the experimental band. Alternatively, it can be determined from the second moment using equation (3.13) which is easy to use. A smooth contour was needed to calculate the moments from, because a band like the ν_6 band of methyl iodide would be very difficult to measure owing to the numerous strong Q branches. A handicap with using "large" molecules to give smooth contours was that there were generally more fundamentals resulting in overlapping of bands. Overlapping bands were no use because the $(\bar{\nu} - \bar{\nu}_0)^2$ term in the second moment expression means that terms out in the wings of a band make a significant contribution to the second moment. Another

drawback was that degenerate bands of symmetric top molecules tend to be broader than the non-degenerate bands, making overlapping of bands more likely.

A fairly good molecule to use was hexafluorobenzene (HFB). This has two reasonably well separated e_{1u} bands. The first is the ν_{20} band at 3125 cm^{-1} and the second the ν_{18} band at 1533 cm^{-1} . The ν_{20} band is shown in Fig. 4.1. It was measured at a pressure of $1.05 \times 10^4 \text{ Pa}$, which is the vapour pressure of HFB at 300°K , in a 10 cm gas cell with polythene windows. The wings of the band are not very good but, because the wings of bands are approximately Gaussian in nature and decay rapidly, an estimate of the error in the recorded second moment after drawing corrected wings on the spectrum is 20%. The second moment was calculated to be $40 \pm 8 \text{ cm}^{-2}$. The calculation was performed on the computer using the trapezium rule on equation (3.1). Use of equation (3.13) then resulted in an estimated Coriolis constant of -0.9 ± 0.3 . This compares with a Coriolis constant determined by Wheatley (36) of -0.6 .

The ν_{18} band was then looked at. A Coriolis constant for this band was not recorded by Wheatley. The spectrum of this band was measured in a 10 cm gas cell with KBr windows and at a pressure of about $5 \times 10^2 \text{ Pa}$. The second moment of the band was calculated to be $60 \pm 10 \text{ cm}^{-2}$ and the Coriolis constant obtained was -1.5 ± 0.3 . The maximum value

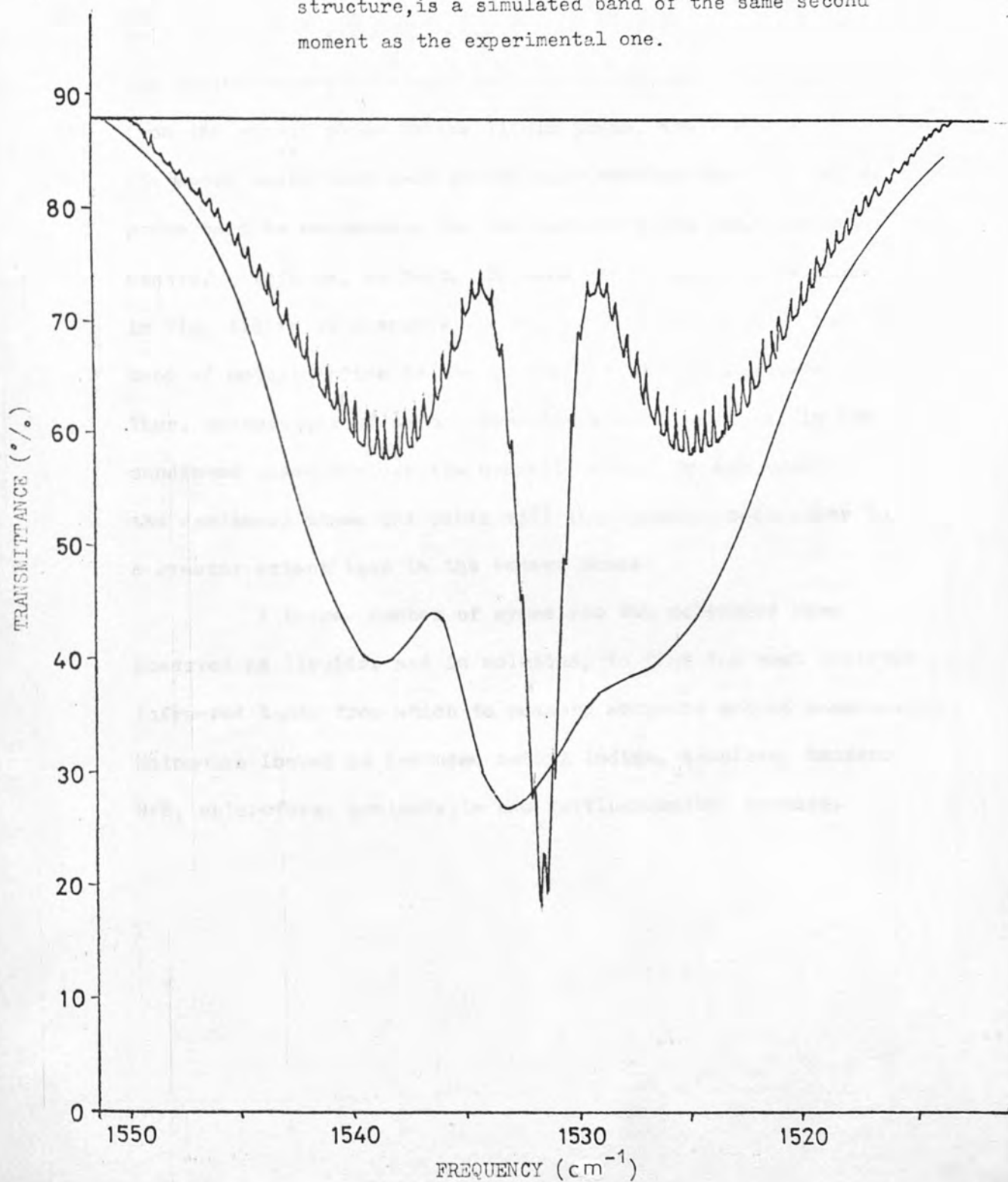
Fig.4.1 The 315 cm^{-1} band of hexafluorobenzene, measured in a 10 cm gas cell, at a pressure of 1.05×10^4 Pa.



that $|S|$ should be is 1.0, and so it was suspected that another broadening mechanism was perturbing the band, possibly Fermi resonance. Fermi resonance arises from two closely lying energy levels of the same species interacting. The wavefunctions describing the two states mix and the energy levels may repel one another. The degenerate vibrations of the e_{1u} band of HFB at 1020 cm^{-1} (ν_{1a}) are split into a doublet by Fermi resonance (36) and so this is probably the reason for the high second moment of the ν_{18} band. The band was simulated on the computer using programme PLESPC and a Coriolis constant of 1.5, then compared with the experimental band. The two bands are compared in Fig. 4.2 and it is seen that the simulated band is much sharper than the experimental. This agrees well with a possible splitting of the two degenerate energy levels of the vibration.

It was found that equation (3.13) did not appear to be of much practical importance because of the problems of overlapping bands, although it may be used to give an approximate Coriolis constant which may then be refined by computer simulation of the band.

Fig.4.2 The 1533 cm^{-1} band of hexafluorobenzene. The broad band is the experimentally measured one, measured in a 10 cm gas cell, at a pressure of about $5 \times 10^2\text{ Pa}$. The sharp band, with the rotational fine structure, is a simulated band of the same second moment as the experimental one.

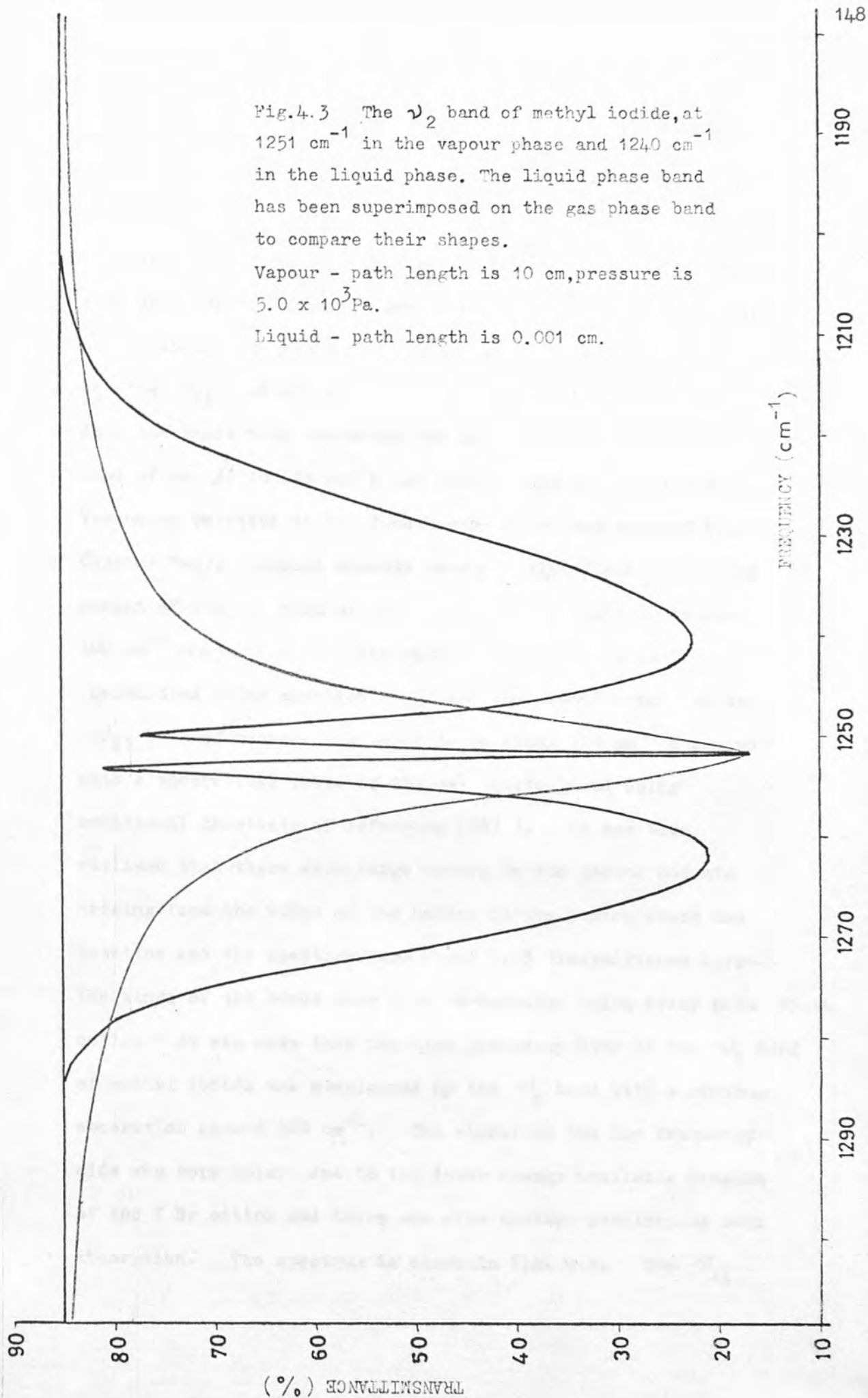


Section 4.2

Experimental Second Moments and Band Shapes in the Condensed Phase

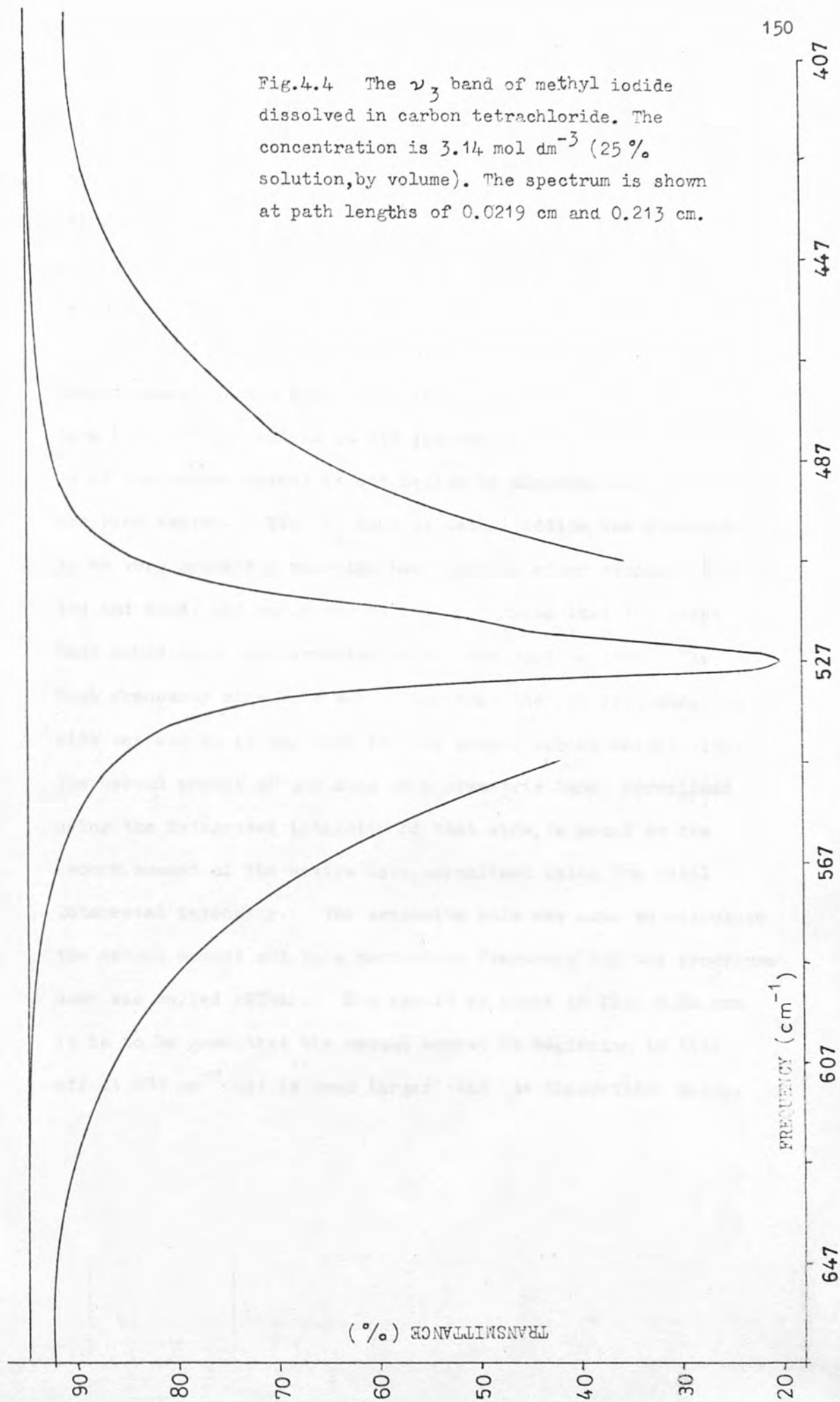
When going into the condensed phase, the intense part of an infra-red band becomes much narrower and the half height bandwidth is generally reduced five-fold. If the second moment of a band is to stay constant in going from the vapour phase to the liquid phase, the wings of the condensed phase band must extend much further than the vapour phase band to compensate for the reduced width near the band centre. This is, in fact, the case and an example is shown in Fig. 4.3 which compares the overall band contours of the ν_2 band of methyl iodide in the vapour and condensed phases. Thus, measurement of second moments is more difficult in the condensed phase because the overall bandwidths are greater in the condensed phase and bands will thus overlap each other to a greater extent than in the vapour phase.

A large number of symmetric top molecules were observed as liquids, and in solution, to find the most isolated infra-red bands from which to measure accurate second moments. Molecules looked at included methyl iodide, iodoform, benzene, HFB, chloroform, acetonitrile and trifluoromethyl bromide.



The least overlapped bands were the ν_3 band of methyl iodide at 527 cm^{-1} and the ν_{11} band of benzene at 674 cm^{-1} . Both of these bands are non-degenerate and produced good spectra with wings that approached zero absorption. The ν_3 band of methyl iodide was measured in solution in carbon tetrachloride and the ν_{11} band of benzene as solution in cyclohexane. Both the bands were corrected for slit distortion. The ν_3 band of methyl iodide had a hot band at 6.4 cm^{-1} to lower frequency relative to the fundamental which was removed (see Chapter Two). Second moments were calculated and the second moment of the ν_3 band of methyl iodide was found to be about 300 cm^{-2} compared with a theoretical value of 210 cm^{-2} (calculated using equation (3.9)) and the second moment of the ν_{11} band of benzene was found to be about 110 cm^{-2} compared with a theoretical value of 163 cm^{-2} (calculated using rotational constants of reference (36)). It was then realised that there were large errors in the second moments arising from the wings of the bands, in the region where the baseline and the spectrum were about 0.5% transmittance apart. The wings of the bands were thus re-measured using wider path length cells. It was seen that the high frequency side of the ν_3 band of methyl iodide was overlapped by the ν_6 band with a minimum absorption around 660 cm^{-1} . The signal on the low frequency side was very noisy due to the lower energy available because of the K Br optics and there was also another overlapping weak absorption. The spectrum is shown in Fig. 4.4. The ν_{11}

Fig.4.4 The ν_3 band of methyl iodide dissolved in carbon tetrachloride. The concentration is 3.14 mol dm^{-3} (25% solution, by volume). The spectrum is shown at path lengths of 0.0219 cm and 0.213 cm.



band of benzene was found to be overlapped on the high frequency side but the low frequency side was clear excepting a small kink in the near wing. The spectrum is shown in Fig. 4.5 and Fig. 4.6.

Unless the wings of a band go to zero, the second moment of the band is infinite because of the term $(\bar{\nu} - \bar{\nu}_0)^2$ and so it was decided to plot the build-up of the second moment as a function of distance away from the band centre. The ν_3 band of methyl iodide was observed to be very symmetric near the band centre, after removal of the hot band, and so it was decided to assume that the ideal band would have been symmetric about the band centre. The high frequency side wing was better than the low frequency side one and so it was used for the second moment calculation. The second moment of one side of a symmetric band, normalised using the integrated intensity of that side, is equal to the second moment of the entire band, normalised using the total integrated intensity. The trapezium rule was used to calculate the second moment out to a particular frequency and the programme used was called EXTRAP. The result is shown in Fig. 4.7a and it is to be seen that the second moment is beginning to tail off at 400 cm^{-2} but is much larger than the theoretical value.



Fig. 4.5 The 674 cm^{-1} band of benzene dissolved in cyclohexane. The concentration is 0.192 mol dm^{-3} (1.5% solution, by volume). The spectrum is shown at path lengths of 0.0041 cm and 0.0485 cm . The far wings of the band were run at a slightly higher concentration of 0.943 mol dm^{-3} (7% solution by volume) and using a path length of 0.0968 cm . These are to be seen in Fig. 4.6.

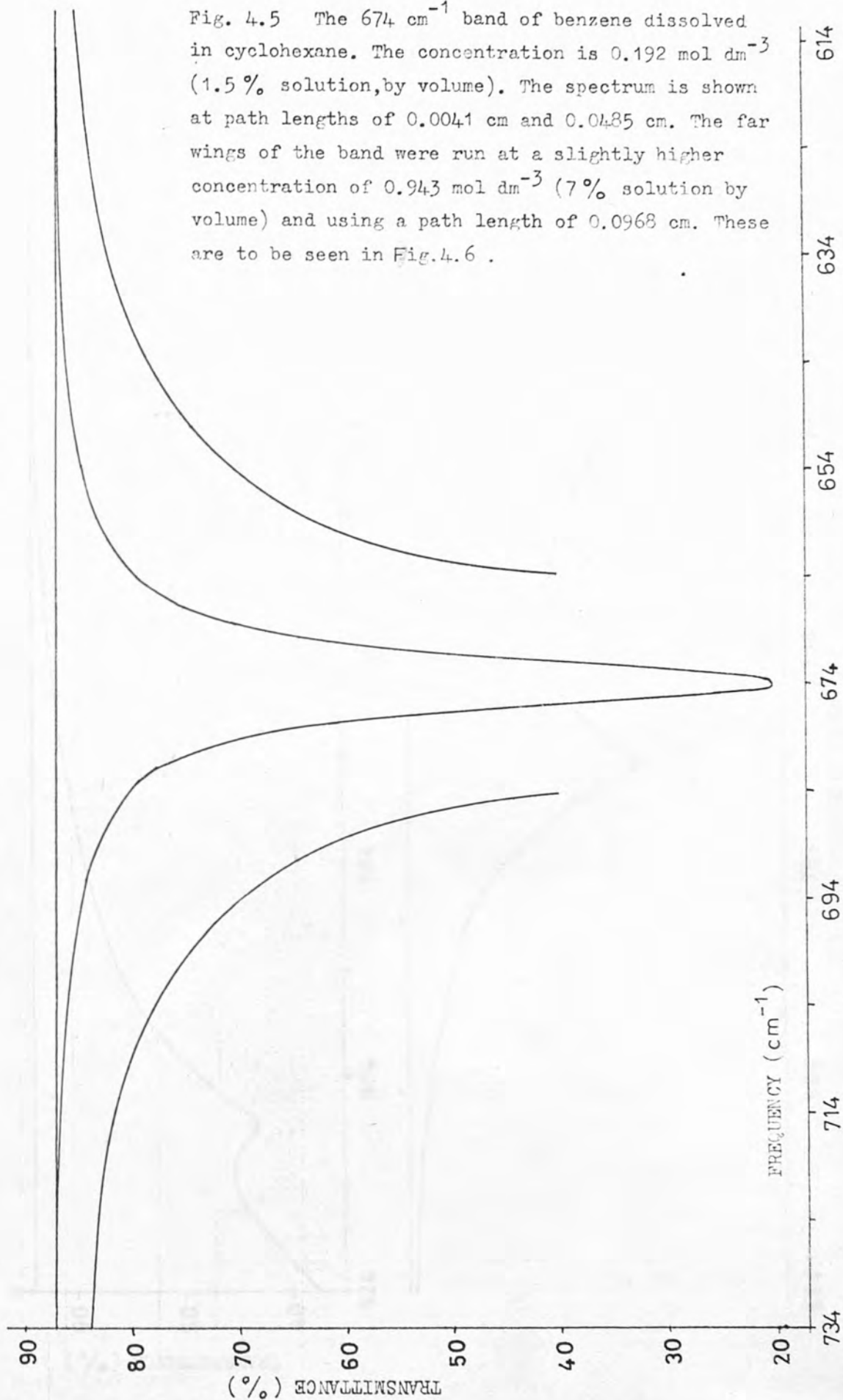
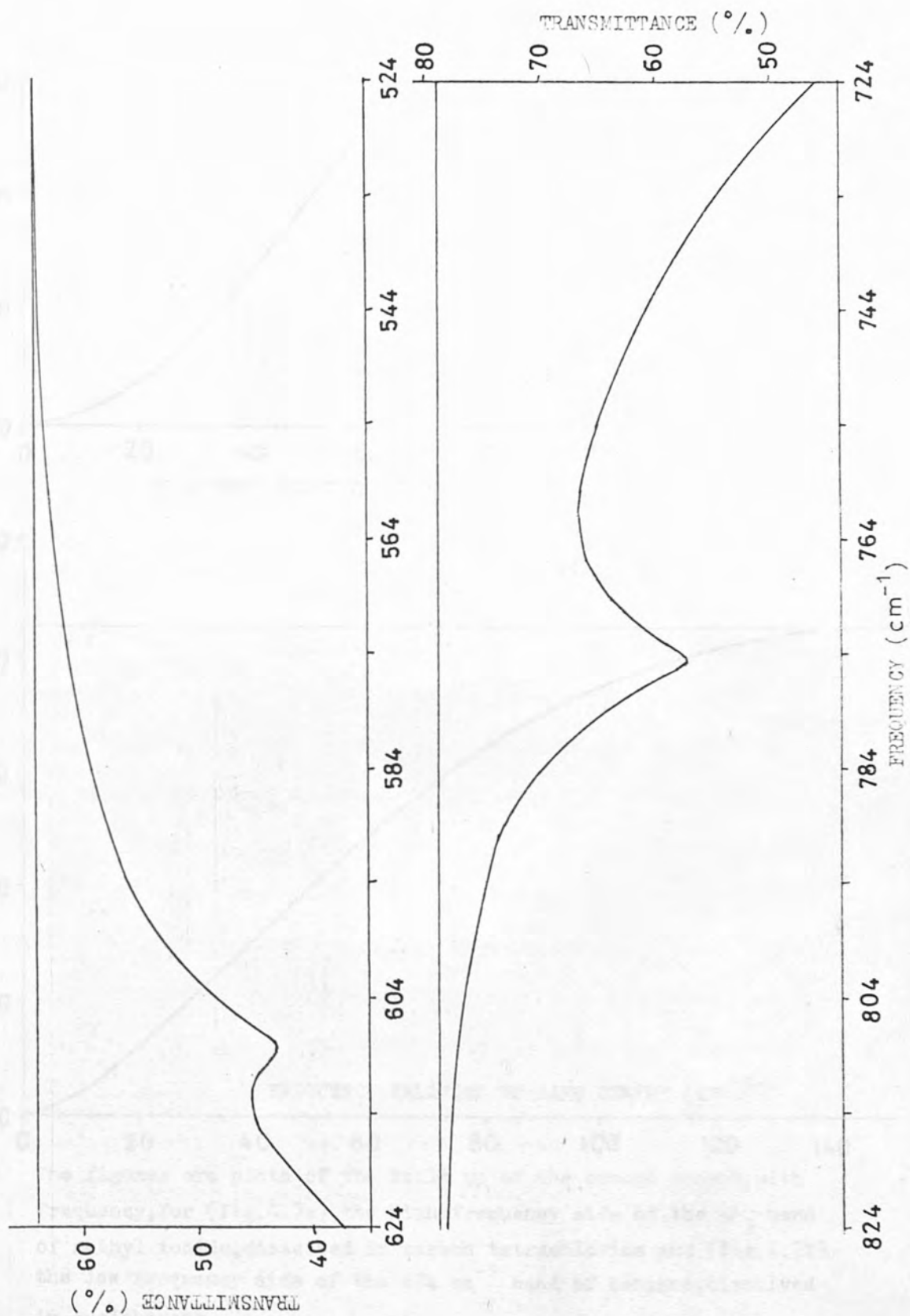
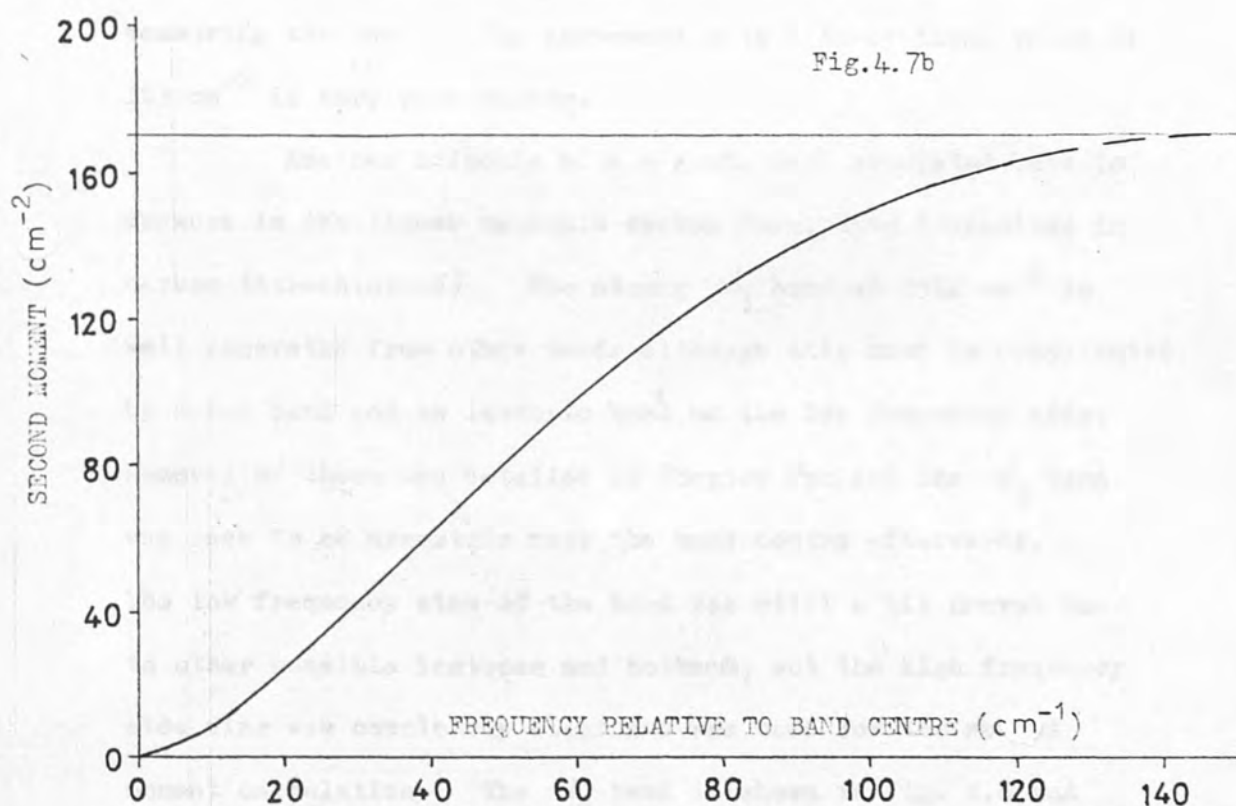
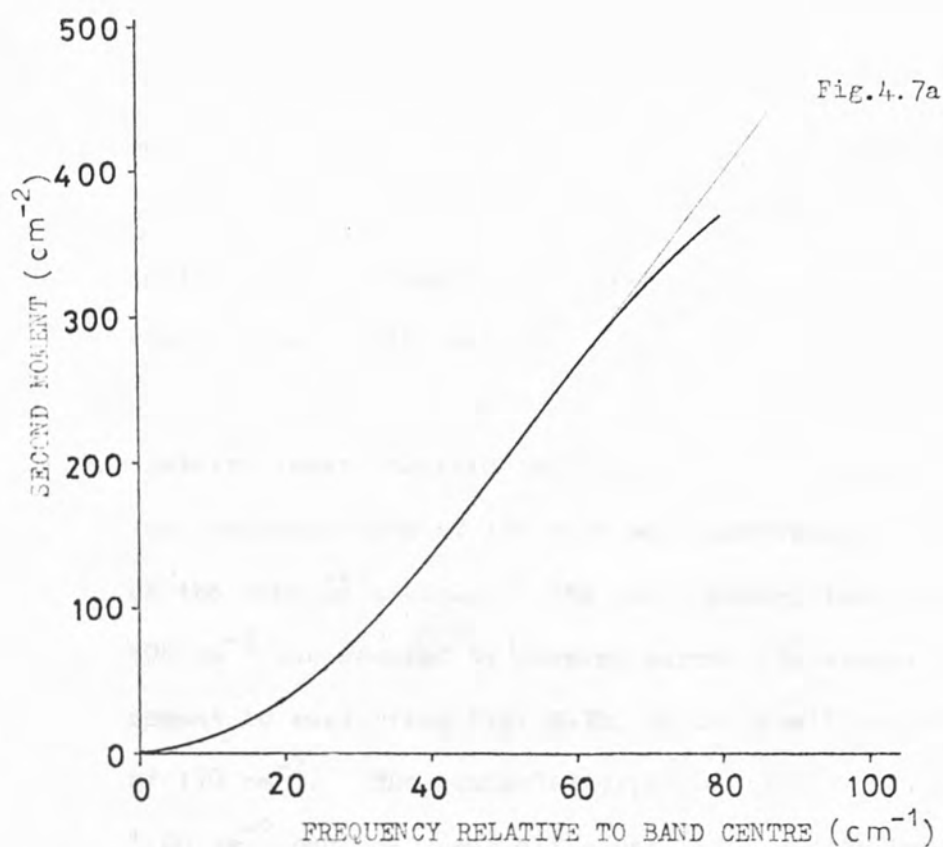


Fig.4.6 The far wings of the 674 cm^{-1} band of benzene dissolved in cyclohexane (see Fig.4.5 for details).



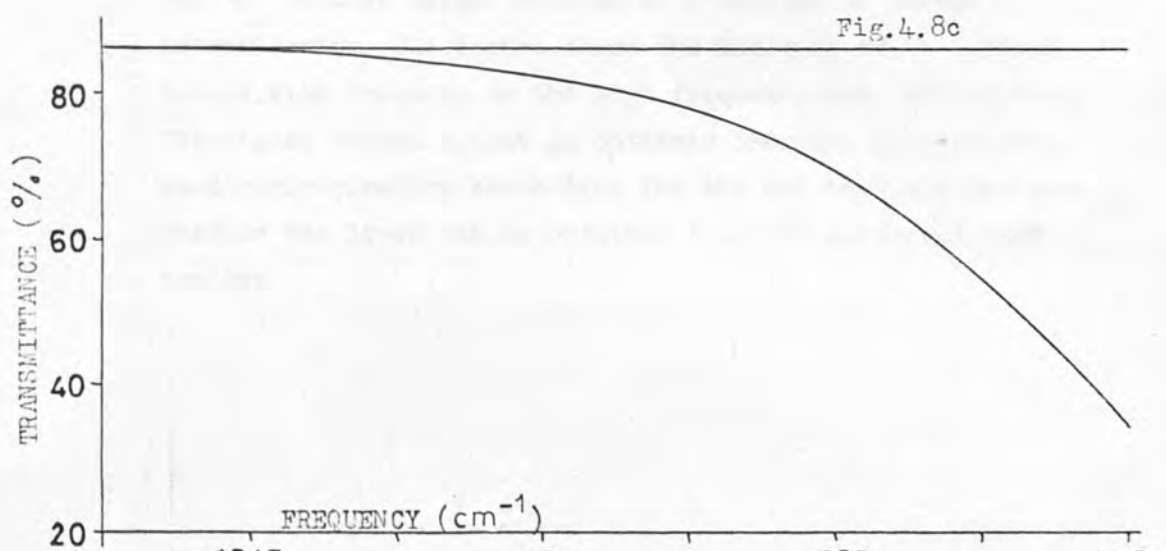
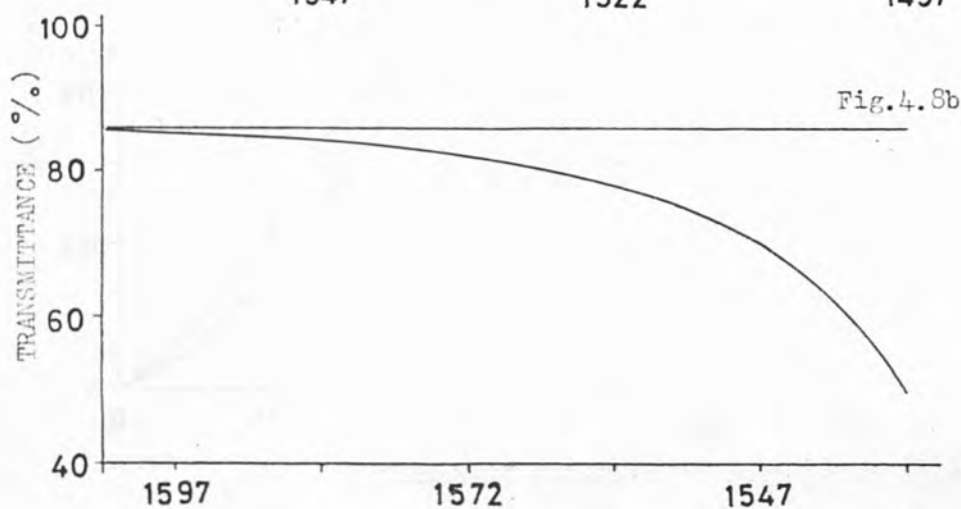
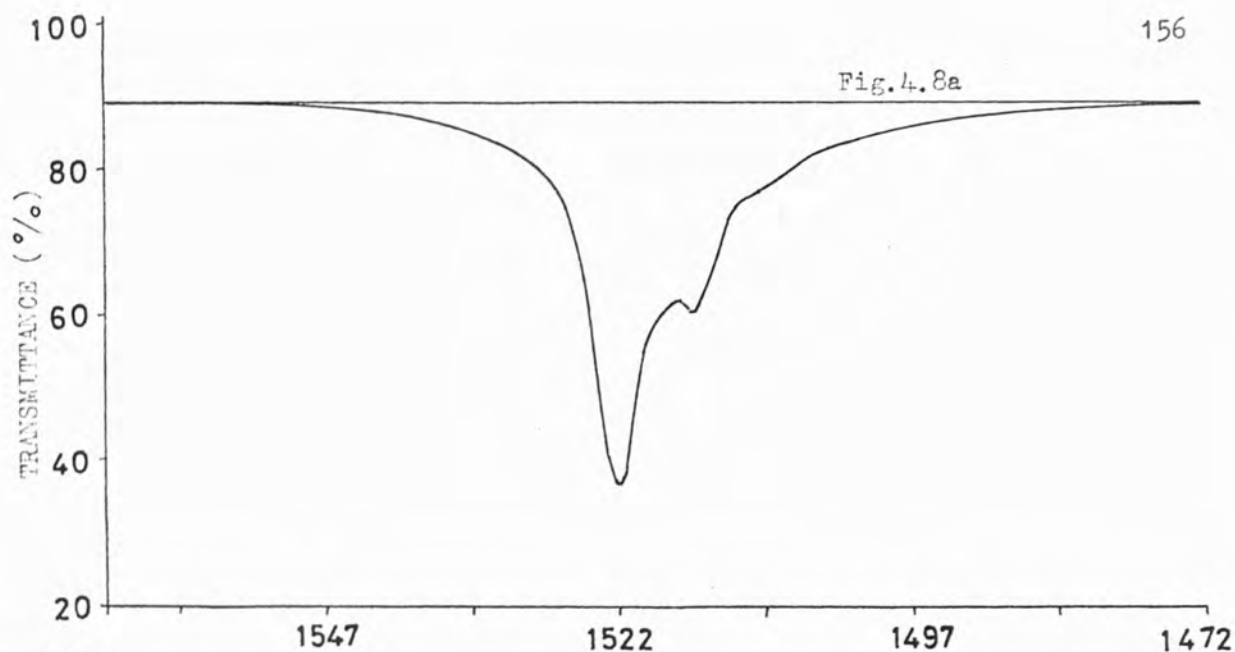


The figures are plots of the build up of the second moment, with frequency, for (Fig. 4.7a) the high frequency side of the ν_3 band of methyl iodide, dissolved in carbon tetrachloride and (Fig. 4.7b) the low frequency side of the 674 cm^{-1} band of benzene, dissolved in cyclohexane.

This is probably due to the overlapping ν_6 band. Separation of the ν_3 and ν_6 bands is thus desirable, but to do this we need to know the shape of an isolated absorption band. This will be dealt with later.

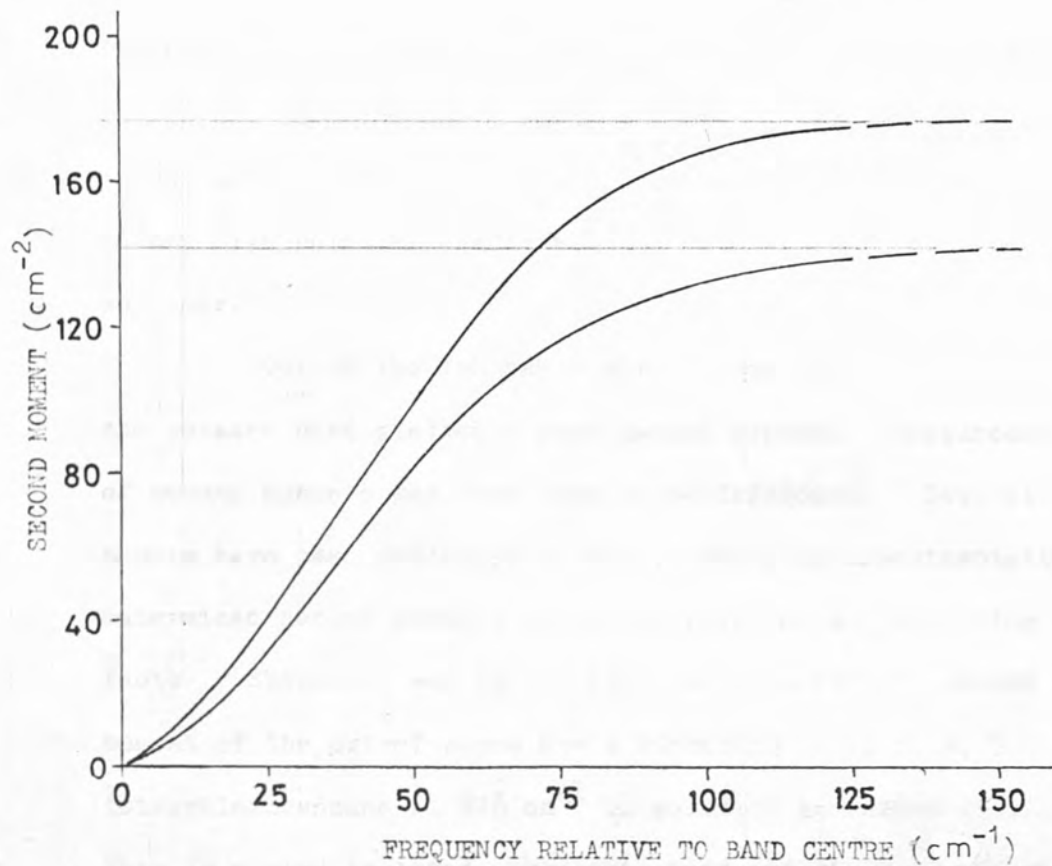
The ν_{11} band of benzene was also seen to be symmetric near the band centre and so the second moment of the low frequency side of the band was considered to be representative of the band as a whole. The small absorption in the wing near 608 cm^{-1} was removed by drawing across its wings. The second moment is seen, from Fig. 4.7b, to be levelling off to a value of 170 cm^{-2} . The estimated experimental error in this is only $\pm 20 \text{ cm}^{-2}$ because three different path lengths were used in measuring the band. The agreement with a theoretical value of 163 cm^{-2} is very encouraging.

Another molecule with a good, well separated band to measure is the linear molecule carbon disulphide (dissolved in carbon tetrachloride). The strong ν_3 band at 1522 cm^{-1} is well separated from other bands although this band is complicated by a hot band and an isotopic band on the low frequency side. Removal of these was detailed in Chapter Two and the ν_3 band was seen to be symmetric near the band centre afterwards. The low frequency side of the band was still a bit uneven due to other possible isotopes and hotbands, but the high frequency side wing was completely clear and was used for the second moment calculation. The ν_3 band is shown in Fig. 4.8 and the second moment growth curve in Fig 4.9.



The ν_3 band of carbon disulphide dissolved in carbon tetrachloride
 Fig.4.8a - concentration is $0.0664 \text{ mol dm}^{-3}$ (0.4 % solution, by volume),
 path length is 0.0042 cm. Fig.4.8b - concentration is $1.654 \text{ mol dm}^{-3}$
 (10 % solution, by volume), path length is 0.002 cm. Fig.4.8c - conc-
 entration is $1.654 \text{ mol dm}^{-3}$ (10 % solution, by volume), path length is
 0.023 cm.

Fig.4.9



The ν_3 band of carbon disulphide dissolved in carbon tetrachloride. The figure shows the build up of the second moment, with frequency, on the high frequency side of the band. The higher second moment is obtained from the experimental band contour, before correcting for the hot band and isotopes, whereas the lower one is obtained from the corrected band contour.

The theoretical second moment was calculated to be 92 cm^{-2} . The experimental second moment was 180 cm^{-2} before removal of the hot band and isotope and 140 cm^{-2} afterwards, with an estimated experimental error of $\pm 20 \text{ cm}^{-2}$. This was a rather disappointing result because this wing of the band was so clear.

Out of the two bands with a good clear wing only the benzene band yielded a good second moment. Measurement of second moments was thus seen to be difficult. Several papers have been published in the journals on experimentally determined second moments and these revealed the following facts. Shimosawa and Wilson (37) had measured the second moment of the out-of-plane C—H vibration of 1, 2, 4, 5 tetrachlorobenzene at 878 cm^{-1} in solution in carbon disulphide. This is a good isolated, symmetric band and yielded a second moment of 13.7 cm^{-2} compared with a theoretical value of 18.2 cm^{-2} . This band had not been re-measured with a thicker cell to obtain the wings of the band more accurately, though. It was decided to re-examine this band. This showed that the wings contained three weak absorptions and also that the carbon disulphide solvent had an absorption in the low frequency wing at 856 cm^{-1} which was intense enough to produce an error in the wing, even when using a variable path length cell in the reference beam.

Ideal allowance for the weak absorptions would probably have yielded the theoretical second moment, but the errors involved in removing these absorptions were considered too large to be able to quote a second moment with an error of less than one hundred per cent.

Bonn and co-workers (38) have measured the ν_2 absorption band of molten sodium nitrate at a series of temperatures and each experimental second moment was about half the theoretical value. The authors did point out that this was, in their opinion, due to inaccuracies in the measurement of the wings of the band, which were not re-measured using a thicker sample.

Cabana and co-workers (39) have measured the ν_3 and ν_4 absorption bands of liquid methane with the aim of obtaining the mean squared torque acting on the molecule, from comparison of the second and fourth moments. Second moments were calculated from a single path length spectrum and if the second moment did not agree with the theoretical, the uncertainty in the baseline was assumed to be the cause for this error. The base line was thus raised, or lowered, to give a band which yielded the theoretical second moment. The fourth moment was then measured from this band and the mean squared torque obtained from the equation :-

$$\left[M(4) - 2.5 M(2) \right] \frac{3 I^2}{2} = \langle \tau^2 \rangle$$

This equation only applies to spherical top molecules where I is the moment of inertia. Figures quoted in the communication showed that raising the base line by 0.15% transmittance raised the second moment by 8.5%, raised the fourth moment by 20.4% and raised $\langle \tau^2 \rangle$ by 25.7%. The mean squared torque is thus very sensitive to movement of the base line. It is not clear whether making the experimental second moment fit the theoretical value in order to obtain a mean squared torque from the fourth moment is justified, but the errors involved appear to be huge.

Rothschild (40) has followed Cabana and co-workers in fitting a theoretical second moment to a band in order to get the fourth moment. Favelukes and co-workers (41) have stated that the errors in calculating second moments for the ν_3 and ν_6 bands of methyl iodide are too large for them to be of any worth.

Measurement of second moments is thus very difficult and it is necessary to try and deduce the nature of ^{the} shape of infra-red band contours in the condensed phase to enable overlapping bands to be accurately separated. It is also possible that other relaxation mechanisms are broadening particular bands. This will be dealt with in Chapter Seven.

Section 4.3Statistical Analysis of the Condensed
Phase Contours of Infra-red Bands - I

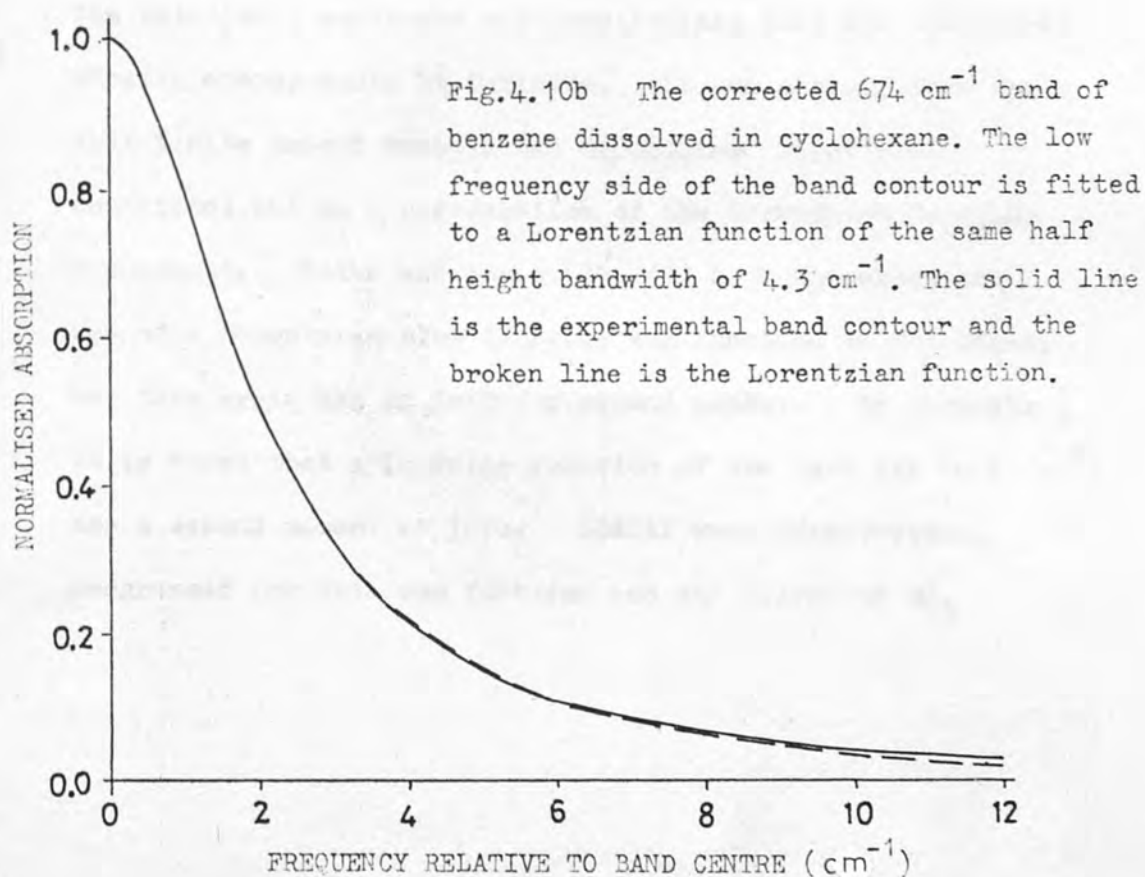
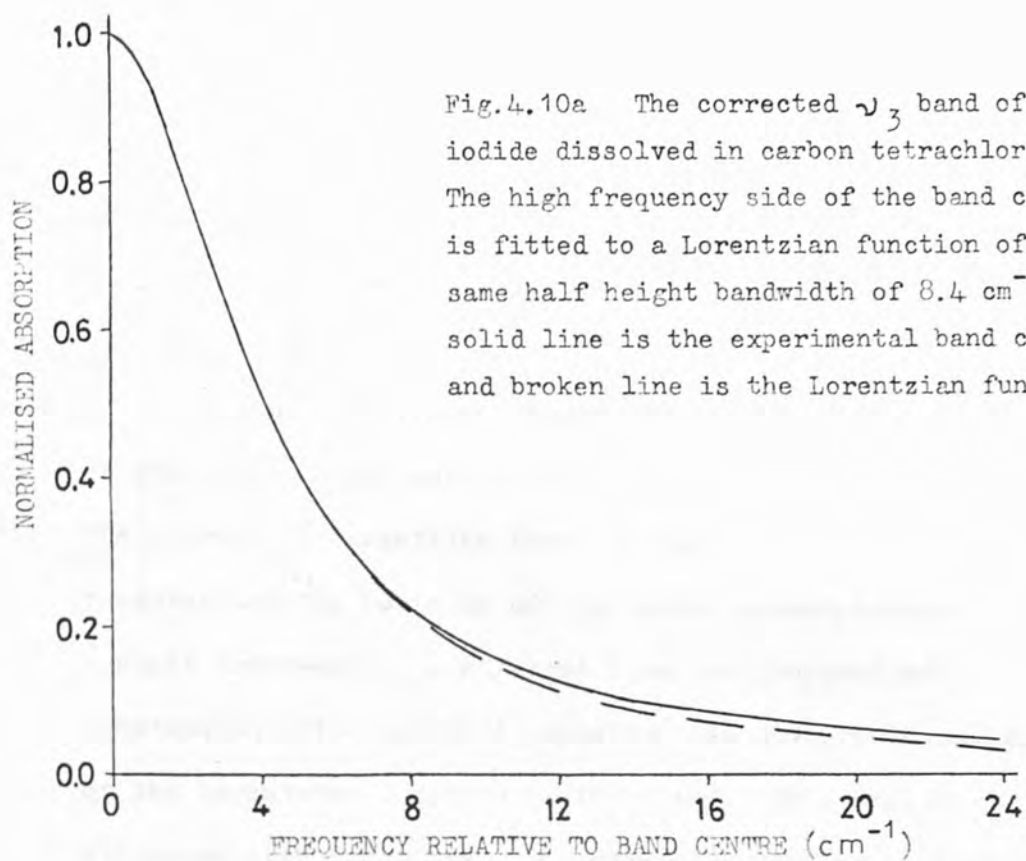
It has been realised for many years that a symmetric, condensed phase infra-red absorption band is essentially a Lorentzian function. Ramsey (35) assumed that the Lorentzian function fitted a true band contour in order to correct for slit distortion. Poor resolution and instrumentation had prevented much work being done on band shapes until the last twenty years. Abramowitz and Bauman made a comprehensive survey of a series of spherical top molecules (42) using a high resolution instrument with a spectral slit width of one wavenumber. Their conclusions were that the observed symmetric bands of liquids and solutions fitted a Lorentzian function well and that any asymmetric bands were also asymmetric in the vapour phase, due to intramolecular perturbations. Consequently they concluded that non-directional molecular interactions in a solution (using a spherical top as solvent) lead to symmetric bands.

The origin of the Lorentzian function goes back to the Lorentz model for absorption (43). Lorentz assumed that the atom, or molecule, absorbed, or emitted, at a discrete frequency during the time between collisions.

Radiation stopped abruptly when collisions occurred and the energy became wholly kinetic. The time intervals between collisions were considered to be large compared with the duration of a collision. The effect of the collision was such that all the pre-existing orientations were obliterated and the molecules became randomly oriented with respect to the radiation. The way in which the Lorentz model leads to a Lorentzian function is summarised well in a review article by Seshadri and Jones (44). Later Van Vleck and Weisskopf (45) suggested that, after collision, the molecules would tend to retain a selection of low energy orientation with respect to the field. This does not effect the Lorentzian function in the infra-red region though, as it involves the term $\bar{\nu} / \bar{\nu}_0$, which is ~ 1 throughout an infra-red band.

A programme was written to fit the best Lorentzian function to an infra-red band (LORGAP). The corrected ν_3 band of methyl iodide dissolved in carbon tetrachloride was used and the following results observed. The Lorentzian function was a good fit near the band centre but the experimental contour did not fall off as fast as the Lorentzian after about 10 cm^{-1} from the band centre. See Fig. 4.10a. The ν_{11} band of benzene dissolved in cyclohexane was looked at and this band fitted well to a

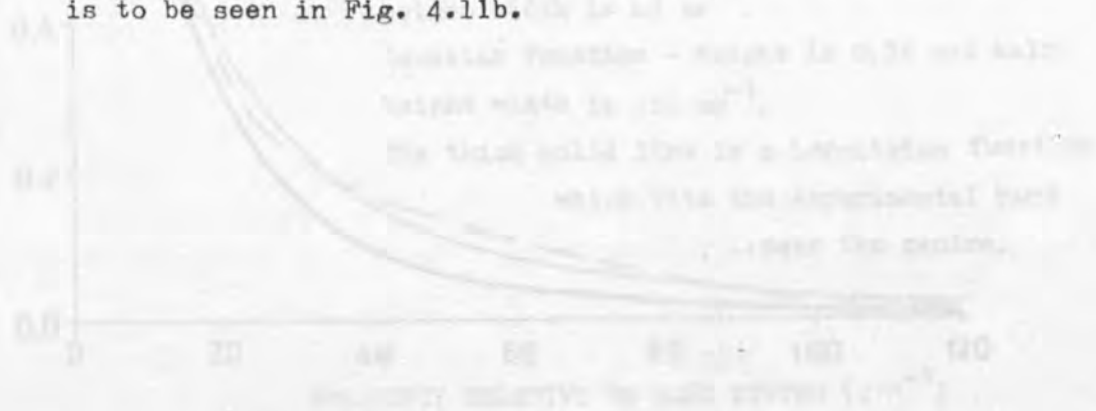


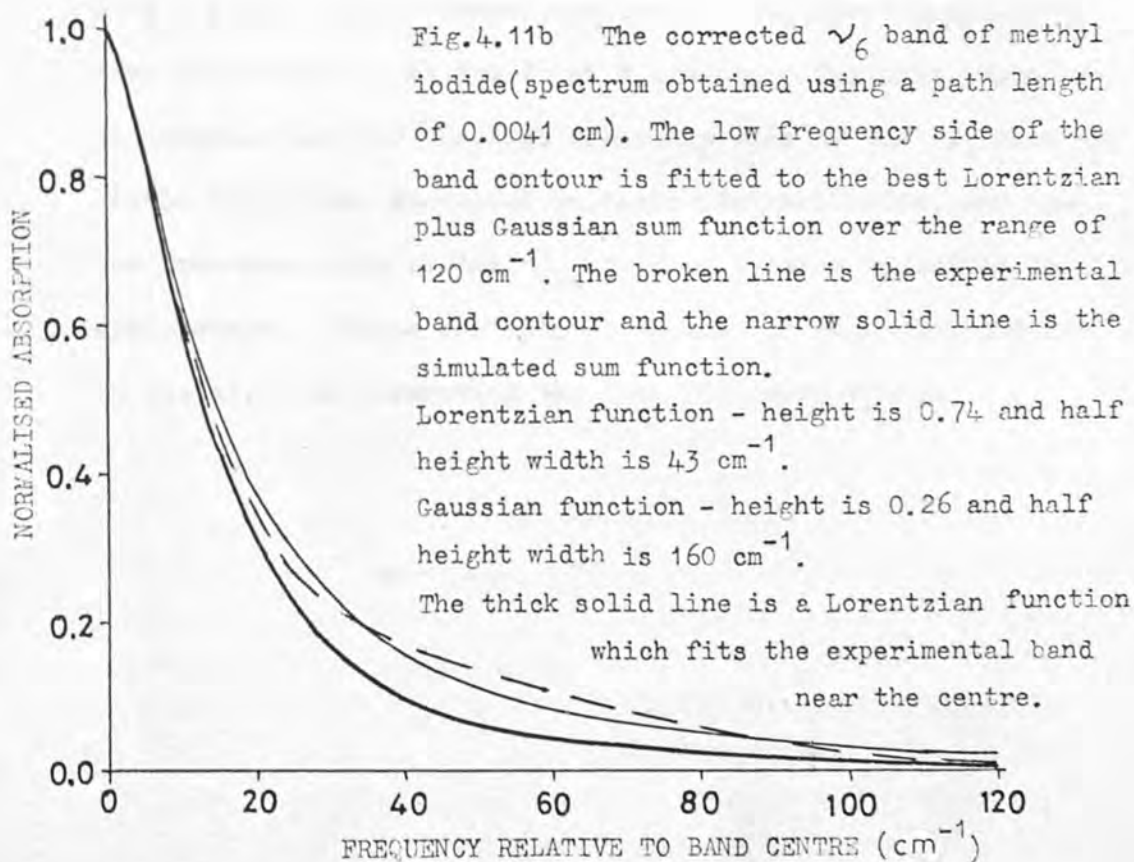
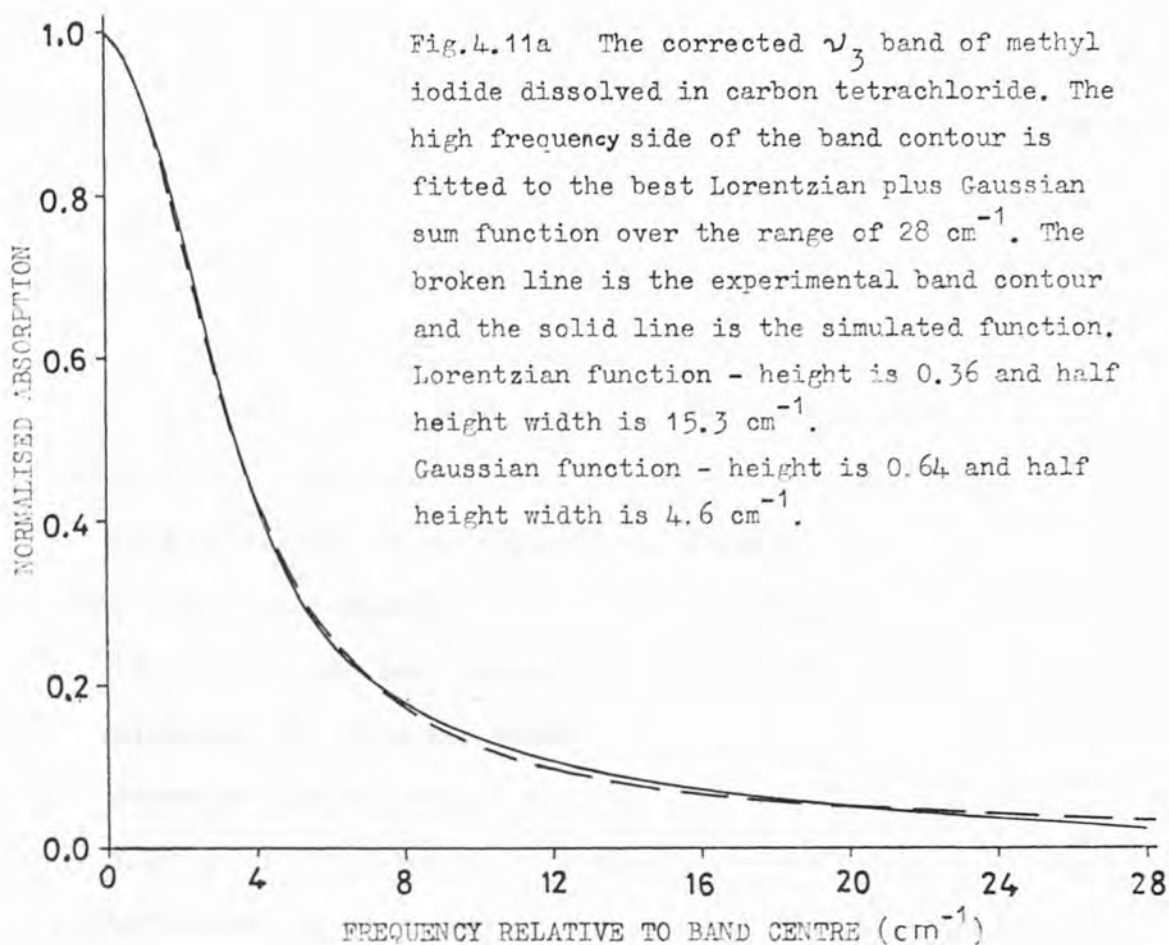


Lorentzian function near the band centre, but did not fall off as fast as the Lorentzian in the near wing. It then fell off faster than a Lorentzian in the far wing. See Fig. 4.10b.

It thus appeared that a Lorentzian function fitted an absorption band near the band centre, but not out in the wings. A Lorentzian function was simulated on the computer and the build-up of the second moment plotted against frequency. A straight line was produced of constant positive gradient, showing that the second moment of the Lorentzian function is infinite. This applies to all Lorentzian functions. A Lorentzian with an infinite second moment is not consistent with Gordon's theory. The second moment is related to the rotational kinetic energy through the rotational constants and this implies that the rotational kinetic energy could be infinite. It has already been shown that finite second moments can be obtained under ideal conditions and so a perturbation of the Lorentzian function was sought. Pitha and Jones (46, 47) have suggested the use of a Lorentzian plus Gaussian sum function to fit bands, but this again has an infinite second moment. In Appendix I it is shown that a Gaussian function of the form $\exp(-s \bar{\nu}^2)$ has a second moment of $1/2s$. LORGAP was, nevertheless, programmed for this sum function and the corrected ν_3

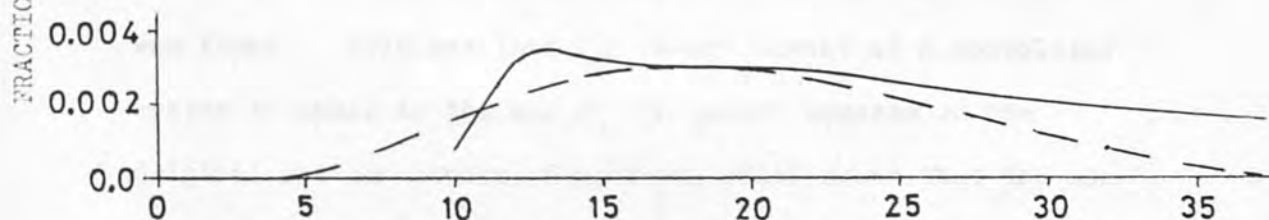
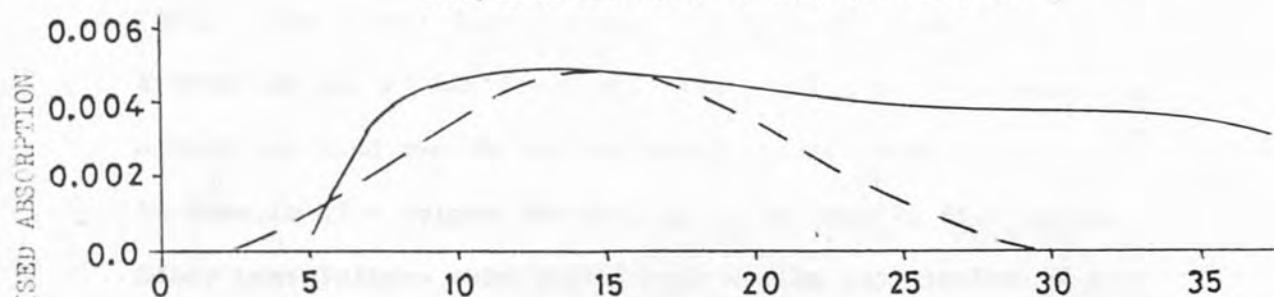
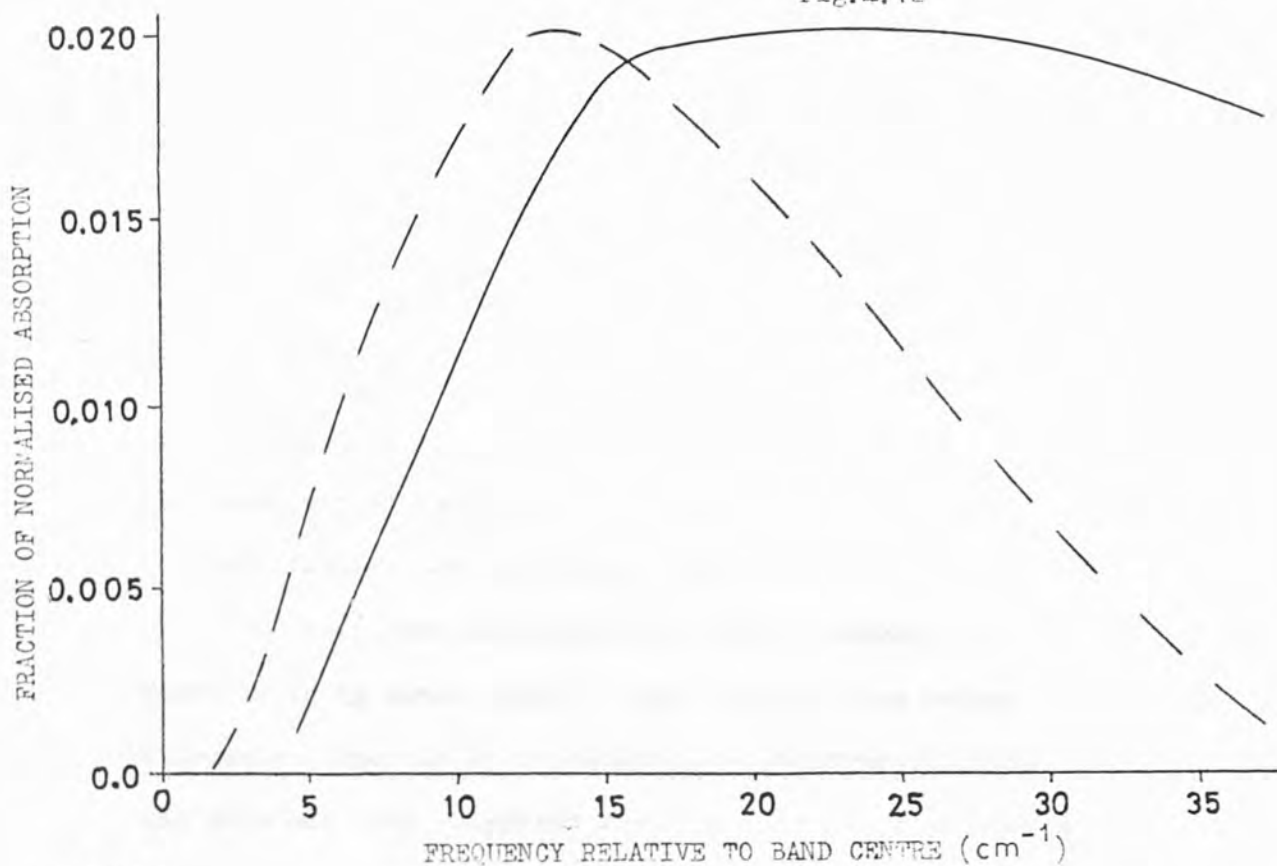
band of methyl iodide dissolved in carbon tetrachloride was fitted to the best sum function, using all ranges of relative intensities and bandwidths for the two functions. Only the first 28 cm^{-1} of the high frequency side of the band were used and a least - squares criterion used for fitting the best simulated curve to the experimental. The best fit is shown in Fig. 4.11a and was not considered satisfactory. Similar poor results were obtained for the ν_3 band of carbon disulphide and the ν_{11} band of benzene. The ν_6 band of liquid methyl iodide was also considered, whose gas phase spectrum is well behaved. The band was measured as the pure liquid because no suitable non-absorbing solvent could be found. The band is overlapped on the high frequency side by the ν_2 band, but is symmetric near the band centre. The band is also only slightly overlapped in the low frequency wing and so the low frequency side of the band was used for the fitting. The band is seen, in Fig. 4.11b, to be much more intense in the near wing than the Lorentzian function that fitted near the band centre. This looked like a good case for fitting to the sum of a Lorentzian plus Gaussian function but the best fit was not at all good, as is to be seen in Fig. 4.11b.





There may still be a Gaussian character in the absorption band contours of non-degenerate vibrations (and degenerate vibrations with a P, Q, R type structure) in the form of the smoothed contours of P and R branches, which may manifest themselves as a double Gaussian function. The P and R branches have zero intensity near the band centre and so a Lorentzian function was calculated for the high frequency side of the ν_3 band of methyl iodide, which fitted the band exactly at half-height. This Lorentzian function was extended to 40 cm^{-1} from the band centre and the difference between the intensity of this function and the experimental contour was calculated. This difference was then plotted out to see if there was an underlying R branch. The result is shown in Fig. 4.12 along with the gas phase R branch contour. The excess intensity does not appear to be due to an R branch. The same procedure was carried out for the high frequency side of the ν_3 band of carbon disulphide dissolved in carbon tetrachloride, and the low frequency side of the ν_{11} band of benzene dissolved in cyclohexane. These are also to be seen in Fig. 4.12 and are no better, thus disproving the idea for these cases.

Fig.4.12



The solid lines in the figures show the excess intensity in the near wings, of three parallel bands of different molecules in solution, over the intensity of a Lorentzian which fits the band contour near the centre. The top figure is for the high frequency side of the ν_3 band of methyl iodide, the middle for the high frequency side of the ν_3 band of carbon disulphide, and the bottom for the low frequency side of the 674 cm^{-1} band of benzene. The broken lines are the smoothed P or R branch contours of the vapours.

A Lorentzian times Gaussian product function (46, 47) was then considered for the above four bands. It is known that the near wings of the bands are more intense than the Lorentzian function that fits near the band centre, and so this product function cannot yield the experimental band shape, because the product will fall off faster than the original function in all cases.

A further means of perturbing a Lorentzian function is by convolution. When this is done using a Gaussian function it is called a Voight function (48) and this has been suggested for band fitting in reference (44). The Voight function was investigated using computer simulation and it was found that the Lorentzian behaviour around the band centre was destroyed by the convolution. An example of a Voight function is to be seen in Fig. 4.13a. Other convolutions were tested such as the convolution of a Gaussian function with a back-to-back exponential function ($\exp - (s | \bar{\nu} |)$). No close fits to the experimental bands were obtained, but an interesting property of the convolution was found. This was that the second moment of a convoluted system is equal to the sum of the second moments of the original and convoluting functions, which means that the convolution of a Lorentzian and another function produces a function with an infinite second moment. Further evidence against the convolution is to be found in Chapter Five.

An interesting way of depicting band contours was employed. This involved re-arranging the equation of the function that was meant to fit a contour, to give the equation of a straight line. In this way, deviation from a straight line showed how the contour behaved in relation to the function.

The equation of a Lorentzian function may be written as :-

$$k_L(\bar{\nu}) = x_1 / (1 + x_3 (\bar{\nu} - \bar{\nu}_0)^2)$$

$$\Rightarrow x_1 / k_L(\bar{\nu}) = 1 + x_3 (\bar{\nu} - \bar{\nu}_0)^2 \quad (4.1)$$

x_1 normalises $k_L(\bar{\nu})$ and so a plot of $x_1 / k_L(\bar{\nu})$ against $(\bar{\nu} - \bar{\nu}_0)^2$ is a straight line of slope x_3 and intercept 1.0. The convolutions of Fig. 4.13a were plotted out using the above "Lorentzian axes" in Fig. 4.13b. The broken line appears to be a straight line, but the Lorentzian in this case was convoluted by a Gaussian function of one third of the half height bandwidth, so that the Lorentzian function was not particularly altered.

The equation of a Gaussian function may be written as :-

$$k_G(\bar{\nu}) = x_1 \exp(-s_1 (\bar{\nu} - \bar{\nu}_0)^2)$$

$$\Rightarrow -\ln[k_G(\bar{\nu}) / x_1] = s_1 (\bar{\nu} - \bar{\nu}_0)^2 \quad (4.2)$$

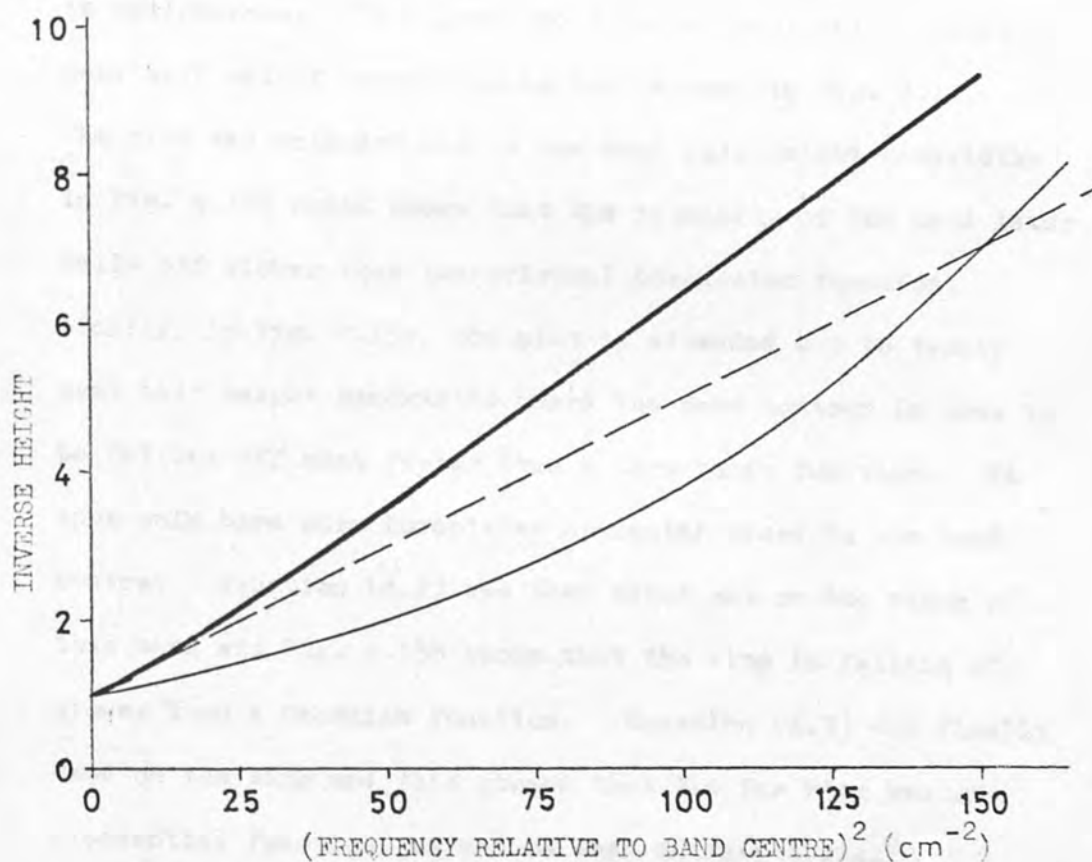
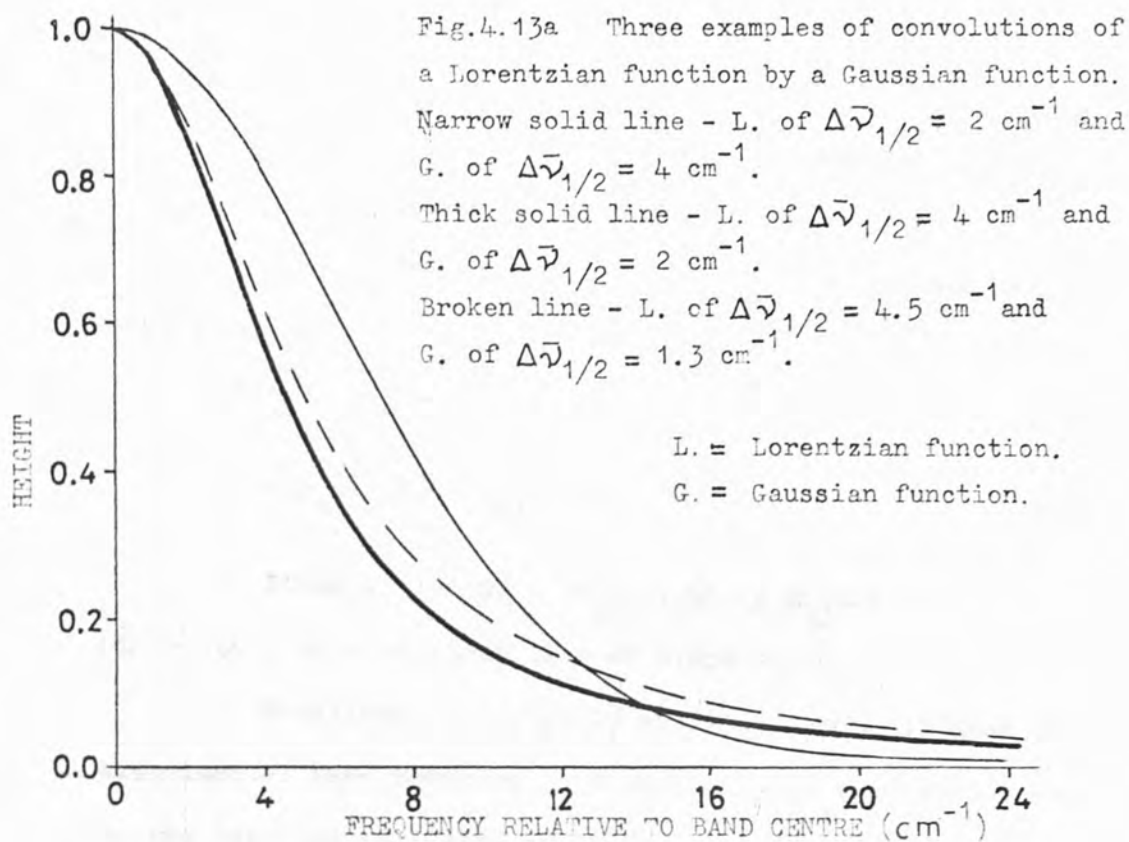


Fig.4.13b The three curves of fig.4.13a are plotted to show any Lorentzian function character as a straight line.

Hence a plot of $-\ln k_G(\bar{\nu})/x_1$ against $(\bar{\nu} - \bar{\nu}_0)^2$ is a straight line of slope s_1 .

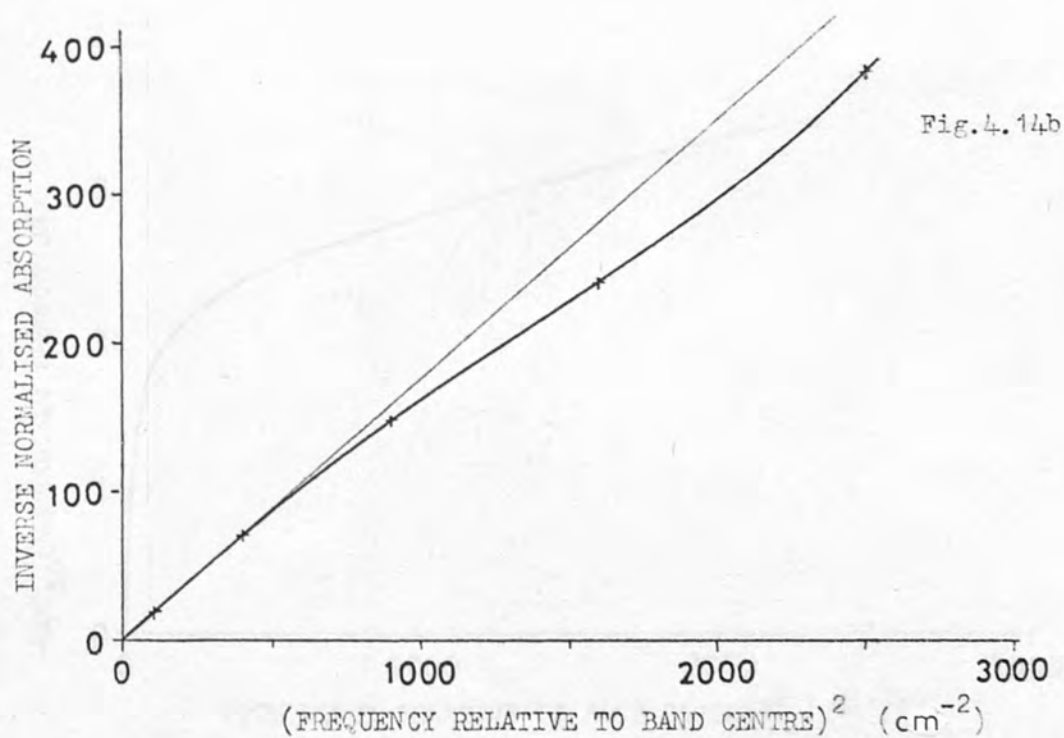
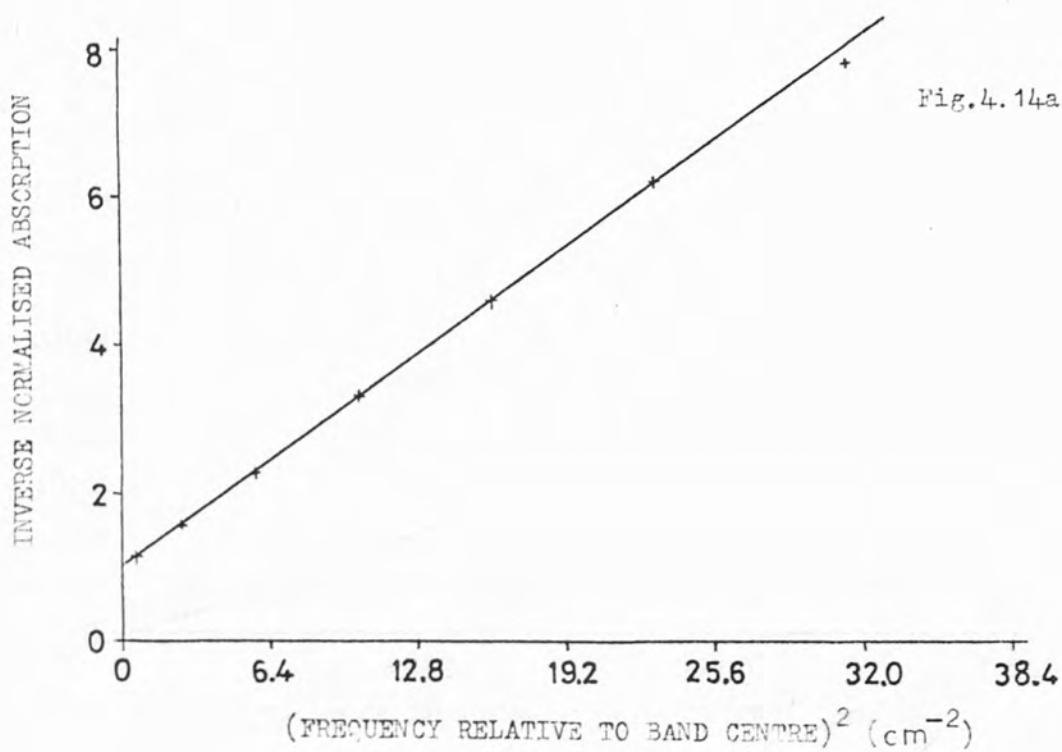
The equation of an exponential function may be written as :-

$$k_e(\bar{\nu}) = x_1 \exp(-s_2 |\bar{\nu} - \bar{\nu}_0|)$$

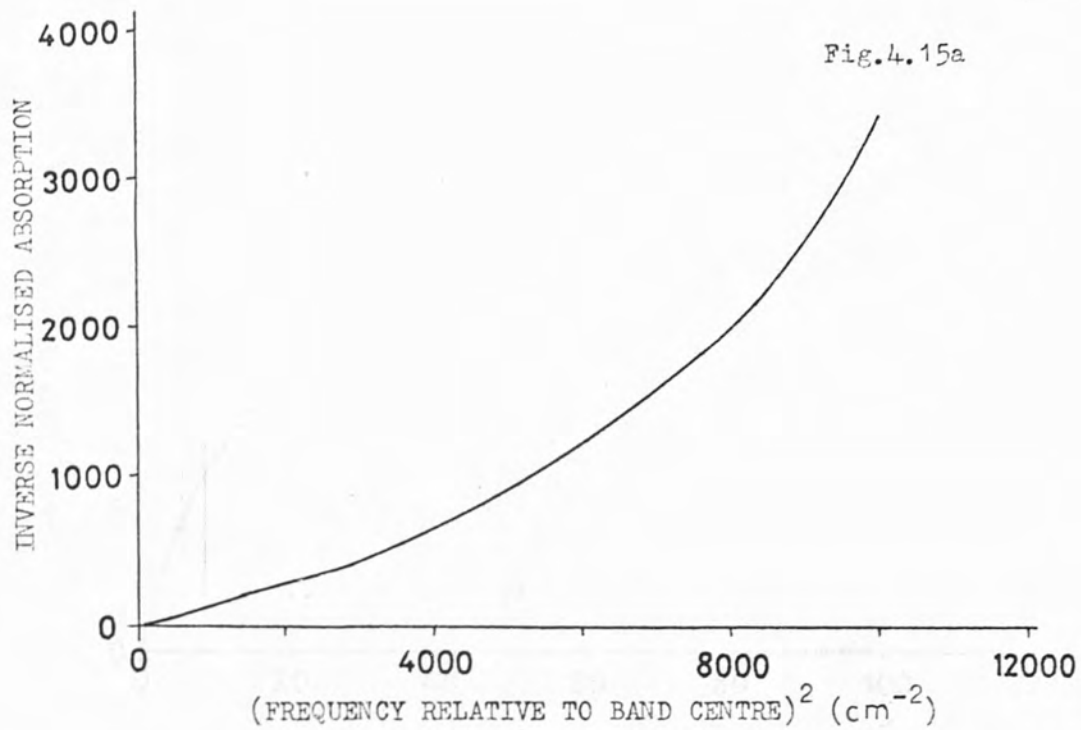
$$-\ln[k_e(\bar{\nu})/x_1] = s_2 |\bar{\nu} - \bar{\nu}_0| \quad (4.3)$$

Hence a plot of $-\ln[k_e(\bar{\nu})/x_1]$ against $|\bar{\nu} - \bar{\nu}_0|$ is a straight line of slope s_2 .

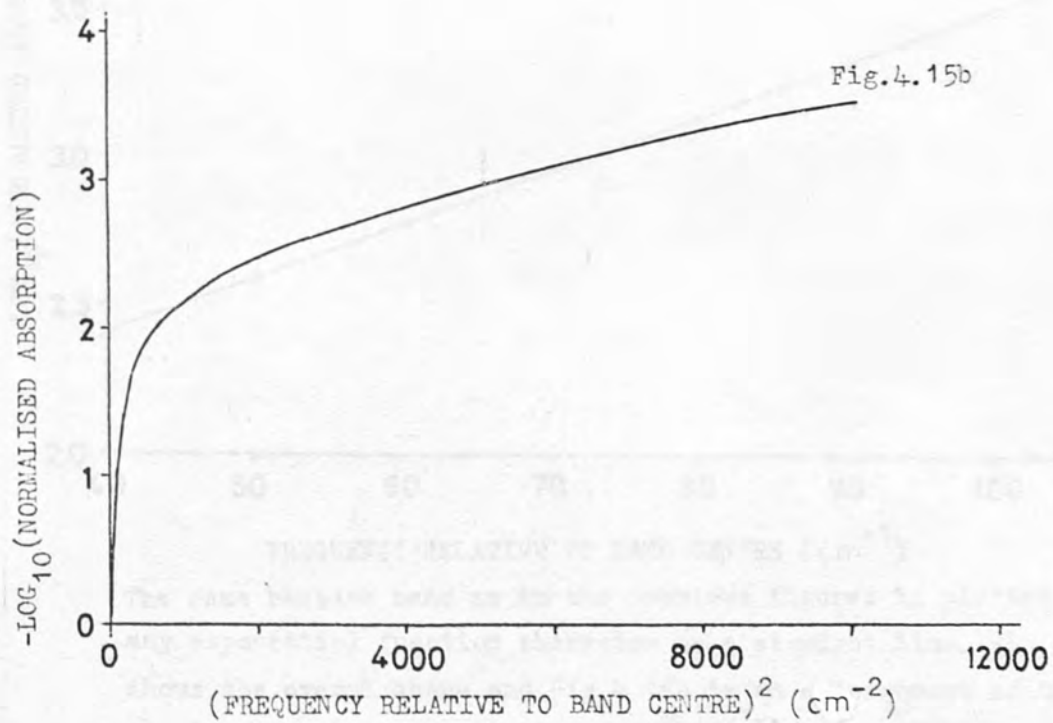
Equations (4.1), (4.2) and (4.3) were all used on experimental band contours. Equation (4.1) was first used on the low frequency side of the ν_{11} band of benzene dissolved in cyclohexane. This produced a linear plot out to about two semi half height bandwidths as can be seen in Fig. 4.14a. The plot was extended out to ten semi half height bandwidths in Fig. 4.14b which shows that the intensity of the band later falls off slower than the original Lorentzian function. Finally, in Fig. 4.15a, the plot is extended out to twenty semi half height bandwidths where the band contour is seen to be falling off much faster than a Lorentzian function. We thus only have pure Lorentzian character close to the band centre. Equation (4.2) was then tried out on the wings of this band and Fig. 4.15b shows that the wing is falling off slower than a Gaussian function. Equation (4.3) was finally used on the wing and this showed that the far wing was an exponential function, as can be seen in Fig. 4.16a.



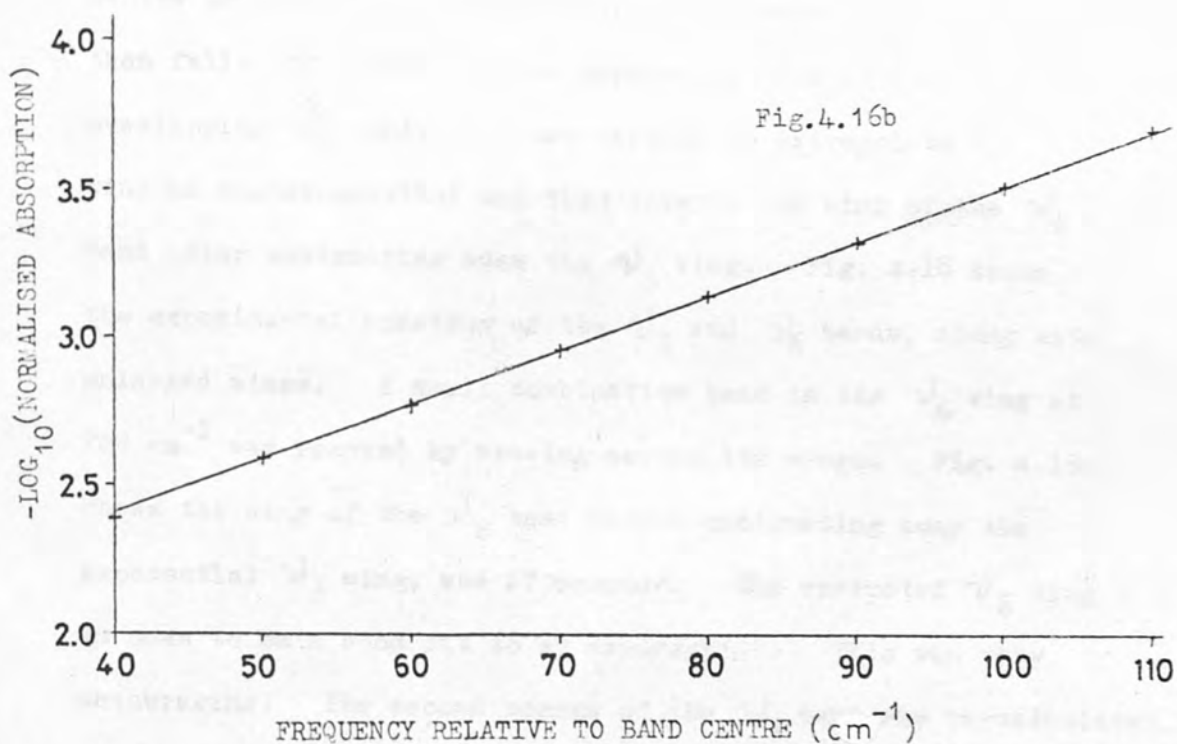
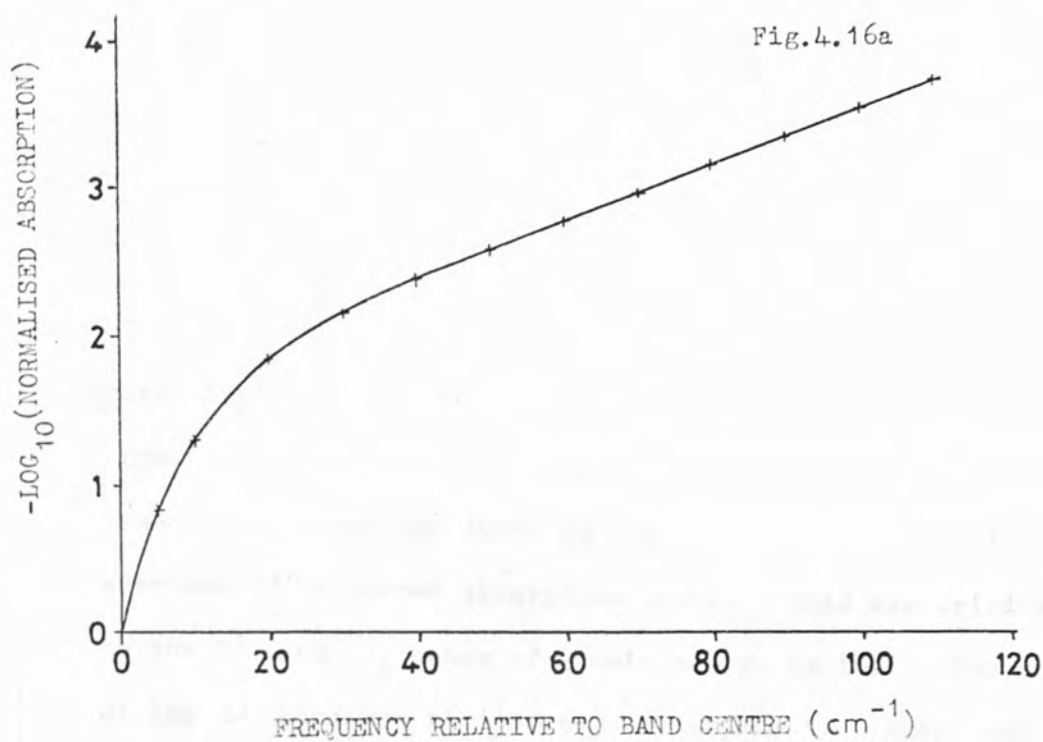
The plots show the Lorentzian function character of the low frequency side of the 674 cm^{-1} band of benzene, dissolved in cyclohexane. The half height bandwidth is 4.3 cm^{-1} .



Continuation of the Lorentzian function plot of Fig. 4.14b .



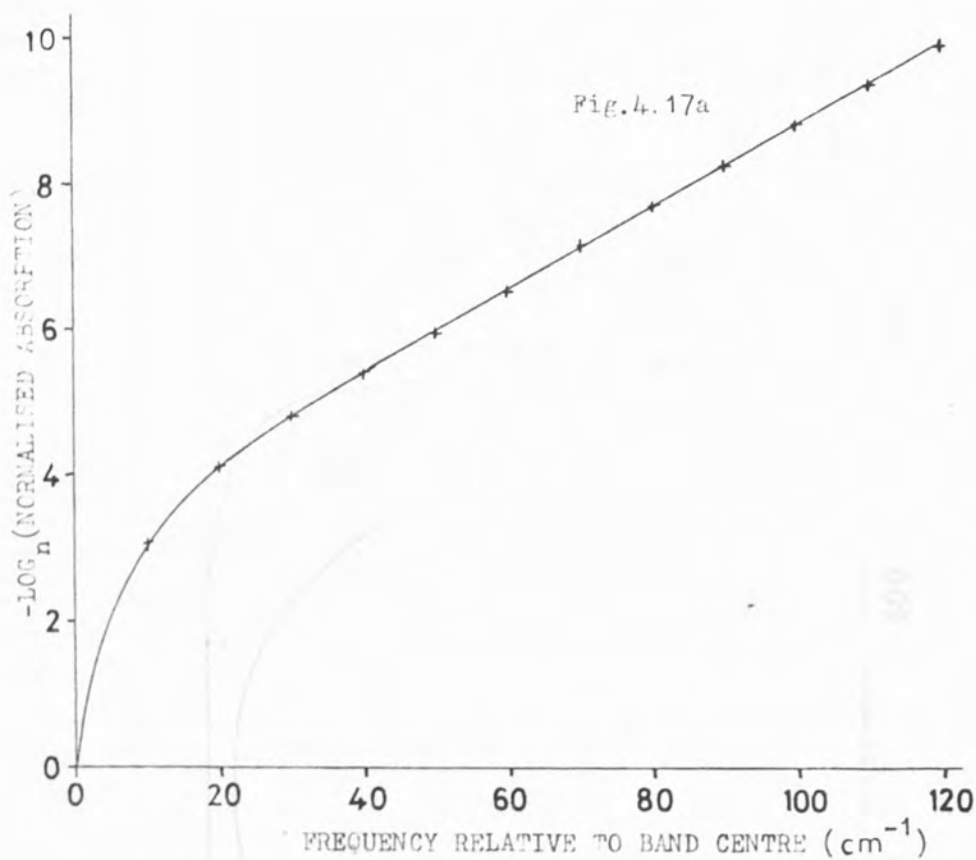
The same benzene band as above, plotted to show any Gaussian function character as a straight line.



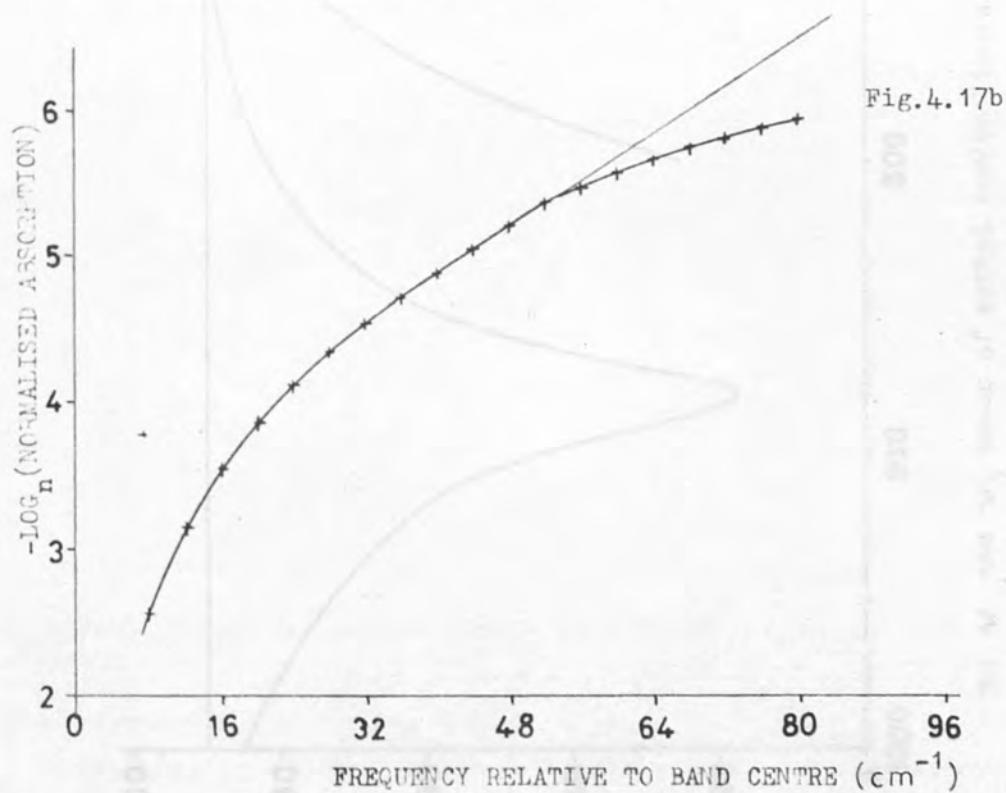
The same benzene band as in the previous figures is plotted to show any exponential function character as a straight line. Fig.4.16a shows the overall shape and Fig.4.16b is an enlargement of the wing showing how closely it follows an exponential.

An enlarged diagram is shown in Fig. 4.16b, where it is seen that the graph is very linear.

The wing on the high frequency side of the ν_3 band of carbon disulphide dissolved in carbon tetrachloride was next plotted out on "exponential axes" and it can be seen from Fig. 4.17a that this wing too, is exponential. This exponential behaviour leads to the possibility of separating overlapping infra-red absorption bands. This was tried out on the ν_3 and ν_6 bands of liquid methyl iodide. The wing of the ν_3 band was plotted out on "exponential axes" and is to be seen in Fig. 4.17b. From about 32 cm^{-1} from the band centre to 52 cm^{-1} the wing appears to be exponential, and then falls off slower than an exponential due to the overlapping ν_6 band. It was decided to extrapolate this wing as the exponential and then observe the wing of the ν_6 band after subtracting away the ν_3 wing. Fig. 4.18 shows the experimental spectrum of the ν_3 and ν_6 bands, along with enlarged wings. A small combination band in the ν_6 wing at 720 cm^{-1} was removed by drawing across its wings. Fig. 4.19a shows the wing of the ν_6 band before subtracting away the exponential ν_3 wing, and afterwards. The corrected ν_6 wing is seen to be a good fit to an exponential. This was very encouraging. The second moment of the ν_3 band was re-calculated using the exponential wing extrapolated out to 200 cm^{-1} from the band centre and found to be about 700 cm^{-2} .

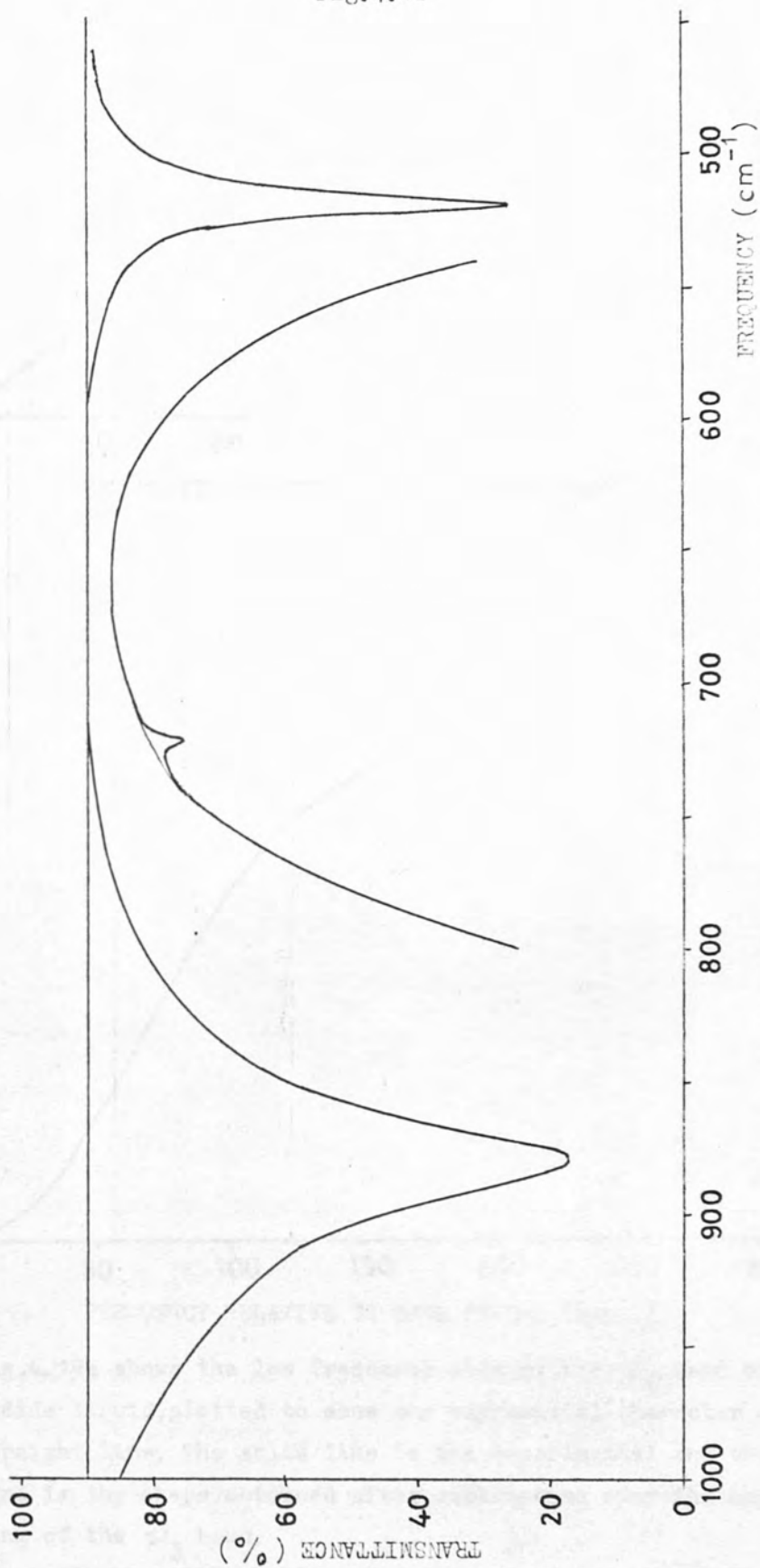


The high frequency side of the ν_3 band of carbon disulphide, dissolved in carbon tetrachloride, is plotted to show any exponential character as a straight line.



The high frequency side of the ν_3 band of liquid methyl iodide is plotted to show any exponential character as a straight line. The, apparently, straight part is extrapolated into the far wing.

Fig.4.18



The ν_6 and ν_3 bands of methyl iodide liquid. The main spectrum was run using a path length of 0.004 cm and the wings enlarged using a path length of 0.054 cm.

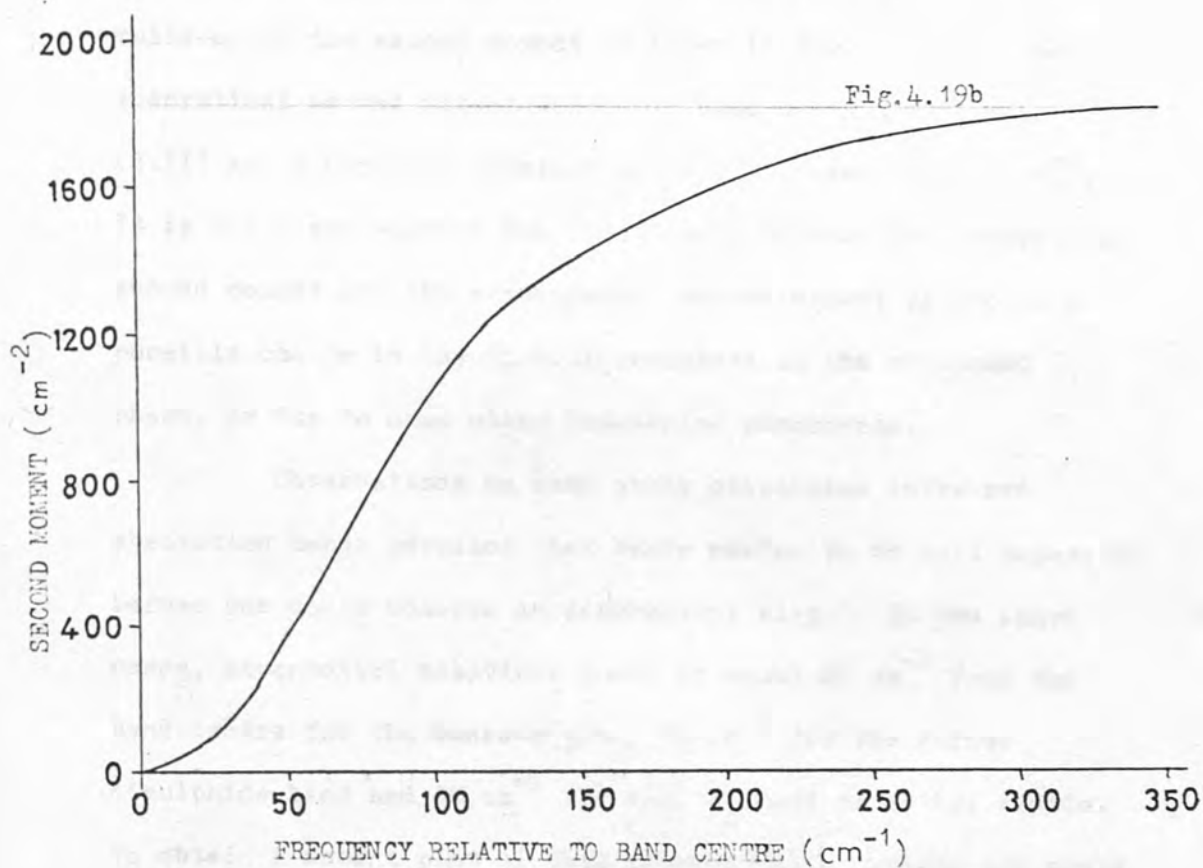
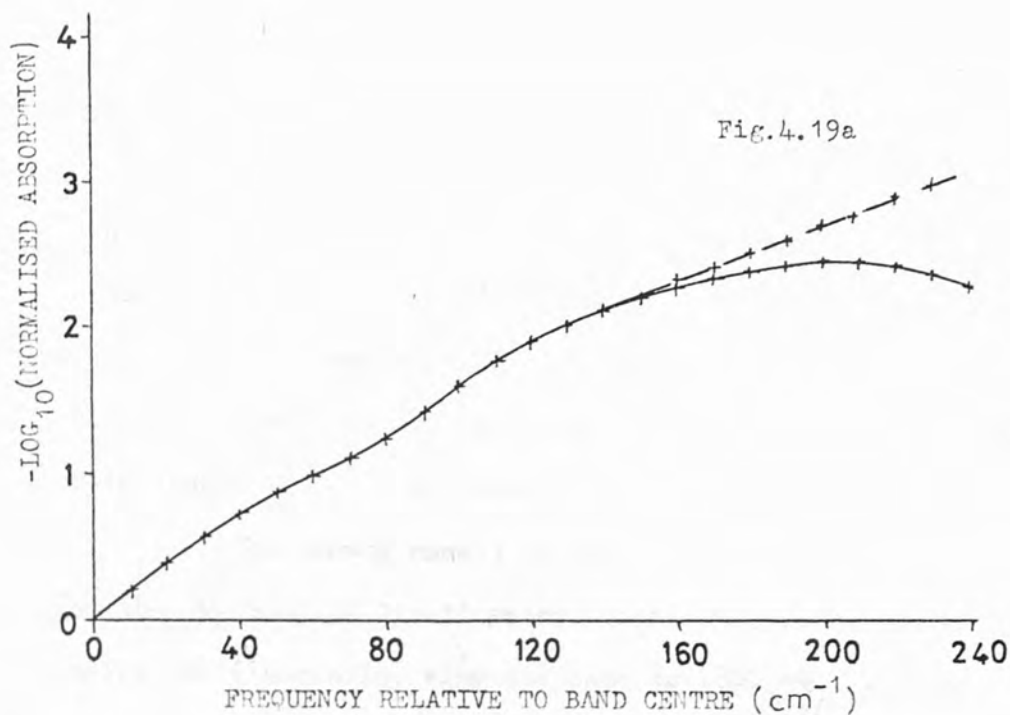


Fig.4.19a shows the low frequency side of the ν_6 band of methyl iodide liquid, plotted to show any exponential character as a straight line. The solid line is the experimental and the broken line is the shape obtained after subtracting away the exponential wing of the ν_3 band.

Fig.4.19b shows the build up of the second moment of the band obtained from the corrected curve of fig.4.19a.

The experimental error in this (assuming the wing is exponential) is probably $\pm 200 \text{ cm}^{-2}$. The second moment is thus much higher than the theoretical value of 210 cm^{-2} , although this measurement was for the pure liquid. This problem will be discussed in a later chapter.

The second moment of the low frequency side of the ν_6 band of liquid methyl iodide was calculated using the exponential wing and came to 1800 cm^{-2} with an estimated experimental error of $\pm 200 \text{ cm}^{-2}$. A plot of the build-up of the second moment is shown in Fig. 4.19b. The theoretical second moment was calculated using equation (3.11) and a Coriolis constant of 0.21 and came to 1440 cm^{-2} . It is not clear whether the discrepancy between the theoretical second moment and the experimental second moment is due to a possible change in the Coriolis constant in the condensed phase, or due to some other broadening phenomenon.

Observations on some other overlapped infra-red absorption bands revealed that bands needed to be well separated before one could observe an exponential wing. In the above cases, exponential behaviour began at about 40 cm^{-1} from the band centre for the benzene band, 30 cm^{-1} for the carbon disulphide band and 30 cm^{-1} for the ν_3 band of methyl iodide. To obtain a decent plot of this exponential behaviour one would need to go out to about 60 cm^{-1} for these bands, without any overlapping bands interfering. Even this requirement is difficult to meet in most cases and this requirement may be expected to be

for a greater distance out from the band centre for wider bands, e.g. 200 cm^{-1} for the ν_6 band of methyl iodide.

The state of the statistical band shape analysis so far was not very satisfactory. It was seen in the literature (41) that the Fourier transformation of an infra-red band contour may yield further information about the band shapes. This will be discussed in the proceeding chapter.

It was shown by Kubo (42) that the R.R.E. frequency spectrum is the Fourier transform of the correlation function of the modulation angles of a doublet consisting of two interacting spins, one of which is the rotating spin. It was also pointed out analogously, in the infra-red, that the absorption spectrum is the Fourier transform of the correlation function of the orientation angles of the transition dipole moment vector.

A correlation function, $C(t)$, is defined by the equation -

$$C(t) = \langle \mu(t) \mu(0) \rangle$$

The brackets represent an ensemble average and $\mu(t)$ and $\mu(0)$ are two vectors describing some state of the system at times t and 0 respectively. In most spectroscopic applications μ and $\mu(0)$ refer to the transition dipole moment vector.

CHAPTER FIVEFourier Transformation on Infra-Red
Band ContoursSection 5.1Derivation of the Relationship between
the Transition Dipole Moment Correlation
Function and the Frequency Spectrum

Fourier transformation has been applied to nuclear magnetic resonance (N.M.R.) spectra for several years to observe the time decay of the spectra. It was shown by Kubo (49) that the N.M.R. frequency spectrum is the Fourier transform of the correlation function of the orientation angles of a vector connecting a pair of interacting spins, one of which is the relaxing spin. Kubo also implied that analogously, in the infra-red, the absorption spectrum is the Fourier transform of the correlation function of the orientation angles of the transition dipole moment vector.

A correlation function, $C(\tau + t)$, is defined by the equation :-

$$C(\tau + t) = \langle F(\tau) G(\tau + t) \rangle$$

The brackets represent an ensemble average and $F(\tau)$, $G(\tau + t)$ are two vectors describing some state of the system at times τ and $\tau + t$ respectively. In most spectroscopic applications interest is in situations where F and G refer

to the same vector property, in which case $C(\tau + t)$ is called the autocorrelation function.

Gordon developed the infra-red theory (50) to investigate what an infra-red spectral band shape can tell us about molecular motion, and in particular molecular rotation. Interpretation of spectroscopic information is usually based on assignment of lines in a spectrum to transitions, induced by the measuring radiation, between the various quantum states of the system. We may call this conventional spectroscopic view the Schrodinger picture, since attention is focused on the energy levels of the system, rather than on its time development. There are several drawbacks to this method of interpretation. There may be so many transitions that interpretation is difficult, or the lines may blend together to form a continuous band. This is usually the case in dense gases, liquids, solutions and many solids. The assignment of individual lines is impossible. The intensity distribution, determined by all the many - molecule wavefunctions of the system, is essentially impossible to calculate. Also, there is no classical analogy of a single quantum state so that, even for systems which are described reasonably well by classical mechanics, the Schrodinger picture does not allow any classical correspondence to be exploited.

However, the Heisenberg picture of quantum mechanics provides a powerful interpretive tool for spectra of complicated systems. By focusing attention on the time development of the system, rather than on its quantum states, the above difficulties may be avoided. Interpretation of unresolved lines is possible and the interpretation is easily visualised in terms of molecular motion in the system. Also, a classical correspondence exists which may be exploited for systems which approach classical behaviour. The Heisenberg picture of spectroscopy leads naturally to the consideration of a spectrum as the Fourier transform of an appropriate time autocorrelation function. As already mentioned in Chapter One, a Fourier transform may be inverted, and so we can get from the experimental frequency spectrum to the time autocorrelation function. The transition dipole moment vector must be a simple molecular property, uninfluenced by the others in the system, so ideally we should use dilute solutions. Thus, if the short time and long time behaviour of the system is different, the two are isolated in the autocorrelation function but, in the frequency spectrum, the intensity at a particular frequency includes contributions from the entire time development of the autocorrelation function.

In infra-red spectroscopy equilibrium is very rapidly attained and since measurements are made over times much longer than the relaxation times it follows that the autocorrelation function of the transition dipole $C(\zeta, t)$ does not vary with ζ and can be replaced by $C(0, t)$ or just $C(t)$. The way in which the autocorrelation function is related to the frequency spectrum has been set out by Gordon (50) and also by Steele (51).

The absorption coefficient, $k(\bar{\nu})$, can be related to the Einstein transition probability for a transition from a state "i" to a state "j". Expressed in Dirac notation we have :-

$$k(\bar{\nu}) = \left(\frac{2\pi^2}{3ch} \right) \sum_{i,j} N_i \left| \langle i | \hat{\epsilon} \cdot \mu | j \rangle \right|^2 \cdot \delta(\bar{\nu}_{ji} - \bar{\nu}) \quad (5.1)$$

where $\hat{\epsilon}$ is a unit vector along the direction of the electric field of the incident radiation of frequency $\bar{\nu}$, μ is the total electric dipole moment operator for the molecules in the system, N_i is the number of molecules in the initial state "i" within the ensemble, and $\bar{\nu}_{ji}$ is the frequency for transition from state "i" to state "j". The summation is

taken over all states such that the transitions $j \leftarrow i$ have transition frequencies within the bandwidth under consideration.

The Kronecker delta $\delta(\bar{\nu}_{ji} - \bar{\nu})$ is present to formally

express that the transition probability is zero unless

$$E_j - E_i = hc \bar{\nu}_{ji} = hc \bar{\nu} .$$

Equation (5.1) may be converted to the Heisenberg form by introducing the Fourier expansion of the Kronecker delta :-

$$\delta(\bar{\nu}) = 1/2\pi \int_{-\infty}^{+\infty} \exp(i 2 \pi c \bar{\nu} t) dt$$

in which case we now have

$$k(\bar{\nu}) = \left(\frac{\pi}{3 ch} \right) \sum_{ij} N_i | \langle i | \hat{e} \cdot \mu | j \rangle \langle j | \hat{e} \cdot \mu | i \rangle \int_{-\infty}^{+\infty} \exp \left[\frac{2 \pi i t}{h} (E_j - E_i) - 2 \pi i c \bar{\nu} t \right] dt \quad (5.2)$$

Now, in the Heisenberg formulation, the eigenvalues are taken as time independent with the operators $\xi(t)$ varying as

$$\xi(t) = \exp(2 \pi i H t/h) \xi \exp(-2 \pi i H t/h)$$

Also,

$$\exp(-2\pi i H t/h) |i\rangle = \exp(-2\pi i E_i t/h) |i\rangle$$

$$\text{and } \langle j | \exp(2\pi i H t/h) = \langle j | \exp(2\pi i E_j t/h)$$

Replacing the dipole operator of equation (5.2)

using the above we have :-

$$\mu(t) = \exp(2\pi i H t/h) \mu(0) \exp(-2\pi i H t/h) \quad (5.3)$$

and using the completeness relation $\sum_j |j\rangle \langle j| = 1$

we get :-

$$k(\bar{\nu}) = \left(\frac{\pi}{3ch}\right) \int_{-\infty}^{+\infty} \exp(-2\pi i c \bar{\nu} t)$$

$$\sum_i N_i \langle i | \hat{\epsilon} \cdot \mu(0) \hat{\epsilon} \cdot \mu(t) | i \rangle dt$$

The sum over all "i" is simply the equilibrium average

$$\langle \hat{\epsilon} \cdot \mu(0) \hat{\epsilon} \cdot \mu(t) \rangle$$

For an isotropic sample, the same result is obtained if we average over all the three polarisation directions of the radiation and we obtain :-

$$k(\bar{\nu}) = \left(\frac{\pi}{3ch}\right) \int_{-\infty}^{+\infty} \langle \mu(0) \cdot \mu(t) \rangle dt$$

$$\langle \mu(0) \cdot \mu(t) \rangle dt$$

It is usual to express the transition dipole correlation function in terms of a unit vector, "u", along the direction of the transition dipole moment. The term correlation function, rather than autocorrelation function, is employed here because cross terms between different molecules are inherent in the ensemble average unless we have dilute solutions. Normalising to unit area we get :-

$$k(\bar{\nu})/\Gamma = 1/2\pi \int_{-\infty}^{+\infty} \exp(-i 2\pi c \bar{\nu} t)$$

$$\langle u(0) \cdot u(t) \rangle dt$$

If we are interested in the relaxation of a particular vibrational transition dipole moment we must have a reference frequency to work from, which will be the band centre in this work. The final expression is thus :-

$$k(\bar{\nu})/\Gamma = 1/2\pi \int_{-\infty}^{+\infty} \exp(-i 2\pi c (\bar{\nu} - \bar{\nu}_0)t)$$

$$t) \langle u(0) \cdot u(t) \rangle dt$$

and the inverse Fourier relationship is defined as

$$\langle u(0) \cdot u(t) \rangle = \frac{\int_{\text{band}} k(\bar{\nu}) \exp(i 2\pi c (\bar{\nu} - \bar{\nu}_0)t) d\bar{\nu}}{\Gamma}$$

(5.4)

The above equations express the Heisenberg description of the infra-red band shape. The distribution of absorption frequencies about the vibrational frequency is the Fourier transform of the average motion of the transition dipole moment. In general, a correlation function will contain cross terms between transition dipole moments of different molecules and, because of these, one cannot simply interpret the dipole correlation function. When the observed molecules are dissolved in a solvent, so that they are well separated from each other, these cross terms disappear and we are left with the autocorrelation function. The autocorrelation function at time = t describes the average projection of a molecule's vibrational transition dipole moment on that at time = 0. This assumes that the vibrational motion of the molecule is separable from the rotational motion, as in the Born - Oppenheimer approximation, and $|\mu|$ is constant during the time scale being investigated (see Chapters Seven for more observations on vibrational relaxation).

From vector algebra we know that for two vectors A and B:-

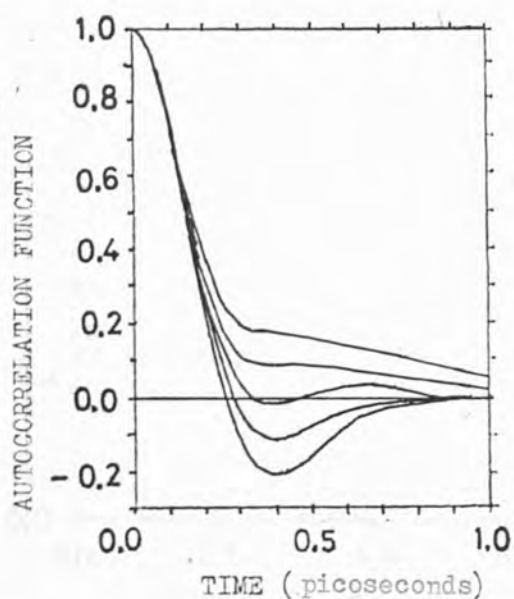
$$A \cdot B = |A| \times |B| \cos \theta$$

where $|A| = (A_x^2 + A_y^2 + A_z^2)^{\frac{1}{2}}$ is the magnitude of the vector and θ is the angle between the two vectors.

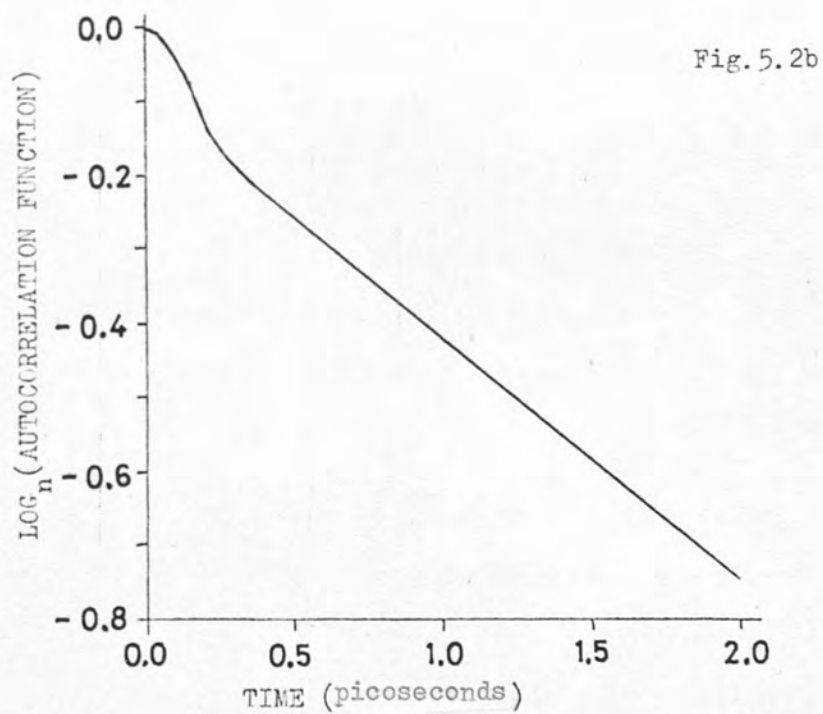
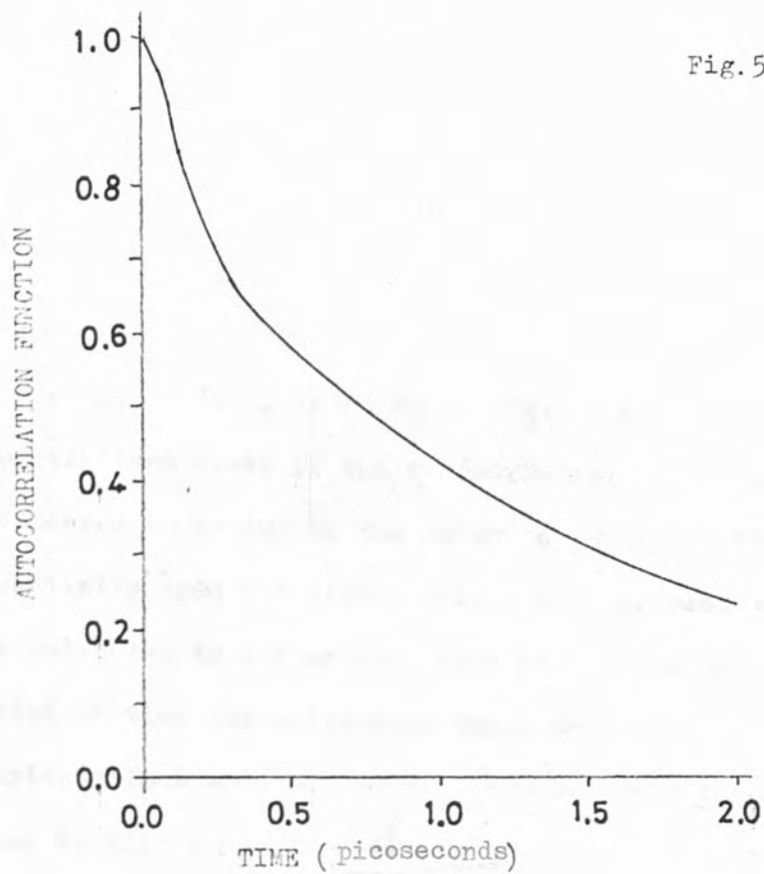
If we are dealing with unit vectors we have simply $A \cdot B = \cos \theta$. So, to determine the autocorrelation function, we determine the dot product of a unit vector along the direction of a transition dipole moment at time = t , compared with a reference time = 0. We do this for each molecule of the ensemble and take the average result. This then tells us the average cosine of the rotational angle, θ , the molecules of the ensemble have traversed in a time t .

For molecules in the gas phase collisions occur which damp this cosine wave exponentially with time (in Chapter One it was mentioned that collision broadening leads to a Lorentzian line shape, which Fourier transforms to an exponential in the time domain). Gordon (50) showed how the autocorrelation function for carbon monoxide changed in going from the gas phase to the solution phase. The general trend is shown in Fig. 5.1. The negative values of the autocorrelation function are from the molecule having rotated over 90° and thus having a negative cosine. The figure shows that the rotational autocorrelation function decays more slowly for a solution. This can be visualised as a hindering of rotation from neighbouring molecules. Steele (52) has shown that, at short times, a Gaussian type decay of the autocorrelation function may be expected. A typical autocorrelation function of a solution is shown in Fig. 5.2a. (This was calculated

Fig. 5.1



The figure shows a range of transition dipole autocorrelation functions for the infrared band of carbon monoxide in different environments. The top curve is carbon monoxide dissolved in chloroform (liquid), then the next one is carbon monoxide in carbon tetrachloride (liquid), then carbon monoxide in n-heptane (liquid), then carbon monoxide in argon (gas, 5.1×10^7 Pa), and finally carbon monoxide in argon (gas, 2.7×10^7 Pa).



The figures show the autocorrelation function of the ν_3 band of carbon disulphide dissolved in carbon tetrachloride.

using EXTRAP). The initial curve is approximated to a Gaussian decay, but this later turns into an exponential. It is usual to plot the logarithm of the autocorrelation function against time so that the exponential part is seen as a straight line, as shown in Fig. 5.2b. The initial Gaussian type decay of the autocorrelation function is considered to be due to the molecules in the system enjoying essentially free rotation. For about 0.2 psec the bulk of the molecules do not undergo hard collisions but after this period of time the collisions begin to dominate the reorientations and the decay curve goes over to an exponential decay (1 picosecond = 10^{-12} sec).

Section 5.2

The Short and Long Time Behaviour of the Autocorrelation Function

The main reason for Fourier analysis of a band shape is so that the short and long time motions of the molecular system may be considered separately. The behaviour of the autocorrelation function at short times can be approximated by a power series expansion. Returning to equation (5.4)

$$C(t) = \frac{\int_{\text{band}} k(\bar{\nu}) \exp(i 2 \pi c (\bar{\nu} - \bar{\nu}_0) t) d\bar{\nu}}{\Gamma}$$

The series expansion of an exponential is

$$\exp(x) = \sum_{n=0}^{\infty} x^n / n!$$

and so we have :-

$$C(t) = \sum_{n=0}^{\infty} (i 2 \pi c t)^n / n! \cdot \frac{\int_{\text{band}} (\bar{\nu} - \bar{\nu}_0)^n k(\bar{\nu}) d\bar{\nu}}{\Gamma}$$

This may be re-written as

$$C(t) = \sum_{n=0}^{\infty} (i 2 \pi c t)^n / n! \cdot M(n)$$

where $M(n)$ is the n 'th moment of the normalised frequency spectrum. So at short times we have, for a symmetric band :-

$$C(t) = 1 - \frac{(2 \pi c)^2}{2!} M(2) t^2 + \frac{(2 \pi c)^4}{4!} M(4) t^4 - \dots \quad (5.5)$$

From our knowledge of second and fourth moments it is seen that at very short times the autocorrelation function depends primarily on the second moment. As an example, use the second and fourth moments for an ideal parallel band of methyl iodide in the vapour phase, i.e. $M(2) = 219 \text{ cm}^{-2}$ and $M(4) = 87750 \text{ cm}^{-4}$. (See Chapter Three). Let the short time be 0.05 psec, in which case we get

$$C(t) = 1 - 0.009326 + 0.000029$$

The term in $M(4)$ is negligible compared with the term in $M(2)$. The fourth moment in the condensed phase is not expected to be much larger and so, at very short times, the autocorrelation function should not change in going from the gas phase to the solution phase.

At really short times the $M(4)$ term may be neglected and so, at zero time the gradient is given by

$$dC(t)/dt = -(2\pi c)^2 M(2) t = 0.$$

and the second derivative is

$$d^2 C(t)/dt^2 = -(2\pi c)^2 M(2) \quad (5.6)$$

This latter equation may be useful in later work for determining second moments although, of course, any moments in the above equations are identical to the moments of the frequency spectrum. Equation (5.6) was found to be correct when tested on an experimental autocorrelation function.

At 0.2 psec equation (5.5) becomes

$$C(t) = 1 - 0.037304 + 0.007372$$

and the term in $M(4)$ is much more important and, at a later time, dominates $M(2)$ term.

This series expansion of equation (5.5) may be used to prove that the second moment of a convoluted system is equal to the sum of the second moments of the original functions. This can be done by multiplying the autocorrelation functions (series expansions) of the original functions together and taking the second derivative at zero time.

The long time behaviour of the autocorrelation function is exponential in character and Favro (53) has reported a general theory of rotational diffusion for the transition dipole autocorrelation function. A random re-orientation process, by random small angle jumps, was shown to lead to the exponential decay observed and the gradient of the natural logarithmic plot of the exponential was shown to be related to the rotational diffusion constants D_x , D_y , D_z . For a symmetric top molecule, the constant of the exponential decay of the $C(t)$ curve of a parallel band, $\beta(a)$, is related to the rotational diffusion constant concerned with rotation about the x axis (and the y axis), i.e.

$$D_x = \beta(a) / 2 \text{ psec}^{-1} = D_y \quad (5.7)$$

and for a perpendicular band we have

$$D_z = \beta(e) - (\beta(a)/2) \text{ psec}^{-1} \quad (5.8)$$

Hence we can compare rates of rotational diffusion about the different axes.

The autocorrelation function of a red laser line is shown in Fig. 5.1a. It is a smooth curve which decays exponentially from 1.0 at $t=0$ to about 0.1 at $t=10$ psec. The autocorrelation function of the ν_3 band of liquid methyl iodide is shown in Fig. 5.1b along with the autocorrelation function for carbon tetrachloride solution. The two autocorrelation functions are almost identical, indicating that there is probably little association in the liquid. The autocorrelation function of the ν_6 band of liquid methyl iodide is shown in Fig. 5.3b, which is probably also similar to the solution phase one. The autocorrelation function of the ν_{11} band of benzene dissolved in cyclohexane is shown in Fig. 5.4, along with the autocorrelation function of the vapor.

In further interpretation of these autocorrelation functions, it will be informative to compare those for the ν_3 and ν_6 bands of liquid methyl iodide. The autocorrelation function at time t is a measure of the cosine of the angle θ which the transition dipole moment has covered through in that time. If we look at the autocorrelation functions of the ν_3 and ν_6 bands of liquid methyl iodide we can see that, for

Section 5.3Autocorrelation Functions -
Experimental Results

Autocorrelation functions of a range of infra-red absorption bands were calculated and plotted out on a logarithmic scale against time. All the autocorrelation functions exhibited the same general shape of a Gaussian-like function at short times and then an exponential decay after about 0.4 psec. The autocorrelation function of the ν_3 band of liquid methyl iodide is shown in Fig. 5.3a along with the autocorrelation function for carbon tetrachloride solution. The two autocorrelation functions are almost identical, indicating that there is probably little association in the liquid. The autocorrelation function of the ν_6 band of liquid methyl iodide is shown in Fig. 5.3b, which is probably also similar to the solution phase one. The autocorrelation function of the ν_{11} band of benzene dissolved in cyclohexane is shown in Fig. 5.4, along with the autocorrelation function of the vapour.

As regards interpretation of these autocorrelation functions, it will be informative to compare those for the ν_3 and ν_6 bands of liquid methyl iodide. The autocorrelation function at time = t is a measure of the cosine of the angle (θ) which the transition dipole moment has moved through in that time. If we look at the autocorrelation functions of the ν_3 and ν_6 bands of liquid methyl iodide we can see that, for

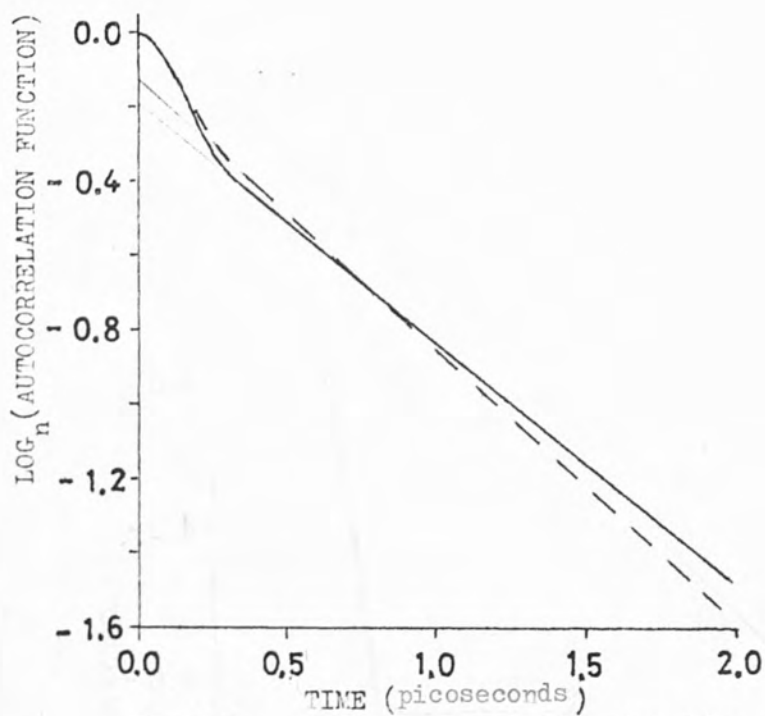


Fig. 5.3a The autocorrelation function of the ν_3 band of methyl iodide liquid (solid line) and solution in carbon tetrachloride (broken line).

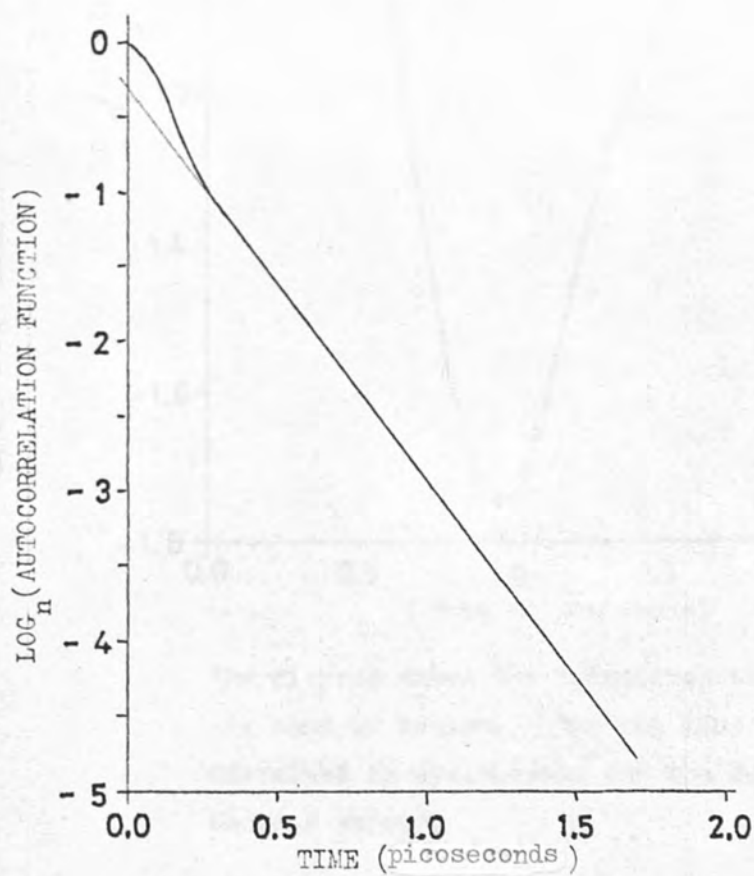
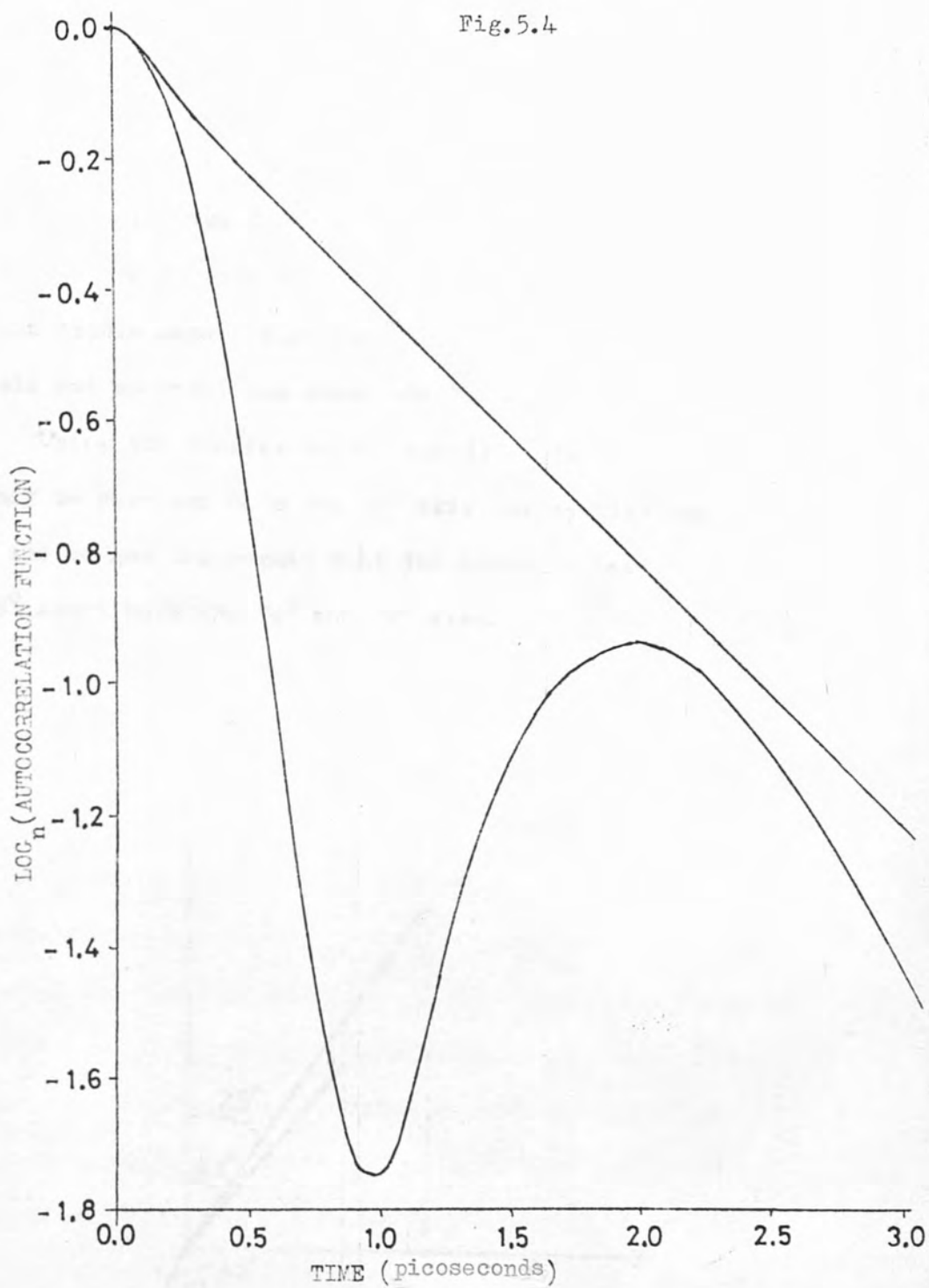
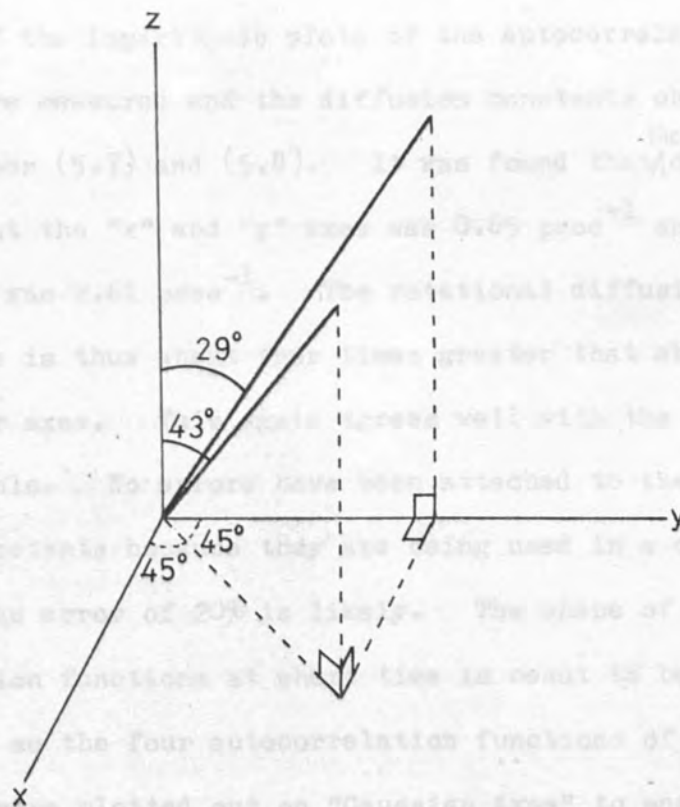


Fig. 5.3b The autocorrelation function of the ν_6 band of liquid methyl iodide.



The diagram shows the autocorrelation function of the ν_{11} band of benzene. The top line is that for benzene dissolved in cyclohexane and the bottom line that for benzene vapour.

approximately 0.25 psec, the molecule enjoys essentially free rotation. The autocorrelation value at this time is 0.73 for the ν_3 band and 0.41 for the ν_6 band. The arc cosines of these values are 43° and 65° . Now, a parallel band has a transition dipole moment directed along the "z" axis of the molecule and so rotations about the "x" and "y" axes are observed. Using the diagram below, the 43° relative to the "z" axis may be resolved onto the "y" axis (or equally the "x" axis) and we get the result that the molecule has rotated 29° about both the "x" and "y" axes.



A perpendicular band has a transition dipole moment directed along the "x" or "y" axis. Let it be the "y" axis here. Rotations observed are thus about the "x" and "z" axes. We know that rotation about the "x" axis is 29° , and so rotation about the "z" axis was calculated to be 50° . Thus it is seen that, on average, a molecule in liquid methyl iodide rotates freely 29° about the "x" and "y" axes and 50° about the "z" axis before a disruptive collision alters the motion. This result should not be taken too literally, but it nevertheless agrees well with the geometry of the molecule and its moments of inertia.

The rotational diffusion constants were then calculated for these two bands. The gradients of the straight line parts of the logarithmic plots of the autocorrelation functions were measured and the diffusion constants obtained using equations (5.7) and (5.8). It was found that ^{the} diffusion constant about the "x" and "y" axes was 0.65 psec^{-1} and about the "z" axis was 2.61 psec^{-1} . The rotational diffusion about the main axis is thus about four times greater than about the perpendicular axes. This again agrees well with the geometry of the molecule. No errors have been attached to these diffusion constants because they are being used in a comparative manner, but an error of 20% is likely. The shape of the autocorrelation functions at short time is meant to be Gaussian and so the four autocorrelation functions of Fig. 5.2, 5.3 and 5.4 were plotted out on "Gaussian Axes" to see if they

yielded a straight line. The results are shown in Fig. 5.5. None of these autocorrelation functions is a good fit to a Gaussian. Some authors in the literature have shown autocorrelation functions which were good fits to the Fourier transforms of the Gaussian functions which yielded the theoretical second moment. Rothschild (54) had obtained a good fit for the ν_3 band of methyl iodide. However, Rothschild had lowered the base line of the experimental frequency spectrum to give the correct second moment. It has already been shown that the autocorrelation function at short time is related to the second moment, so a reasonable fit may be expected on these grounds. Also, by lowering the base line, one can expect a Gaussian nature to be forced into the wings of a quasi Lorentzian band. To illustrate this point a Lorentzian function of half height bandwidth equal to 20 cm^{-1} was calculated out to 100 cm^{-1} from the band centre. The second moment of this band and the Fourier transform were calculated. The short time decay was plotted out for comparison with the Fourier transform of a Gaussian function of the same second moment. This is to be seen in Fig. 5.6a. The Lorentzian was turned into a transmittance curve between 90% and 20%. The baseline was then lowered to 89.12% so that the last point in the wings was zero. The second moment and Fourier transform of the contour obtained from this system were calculated and the short

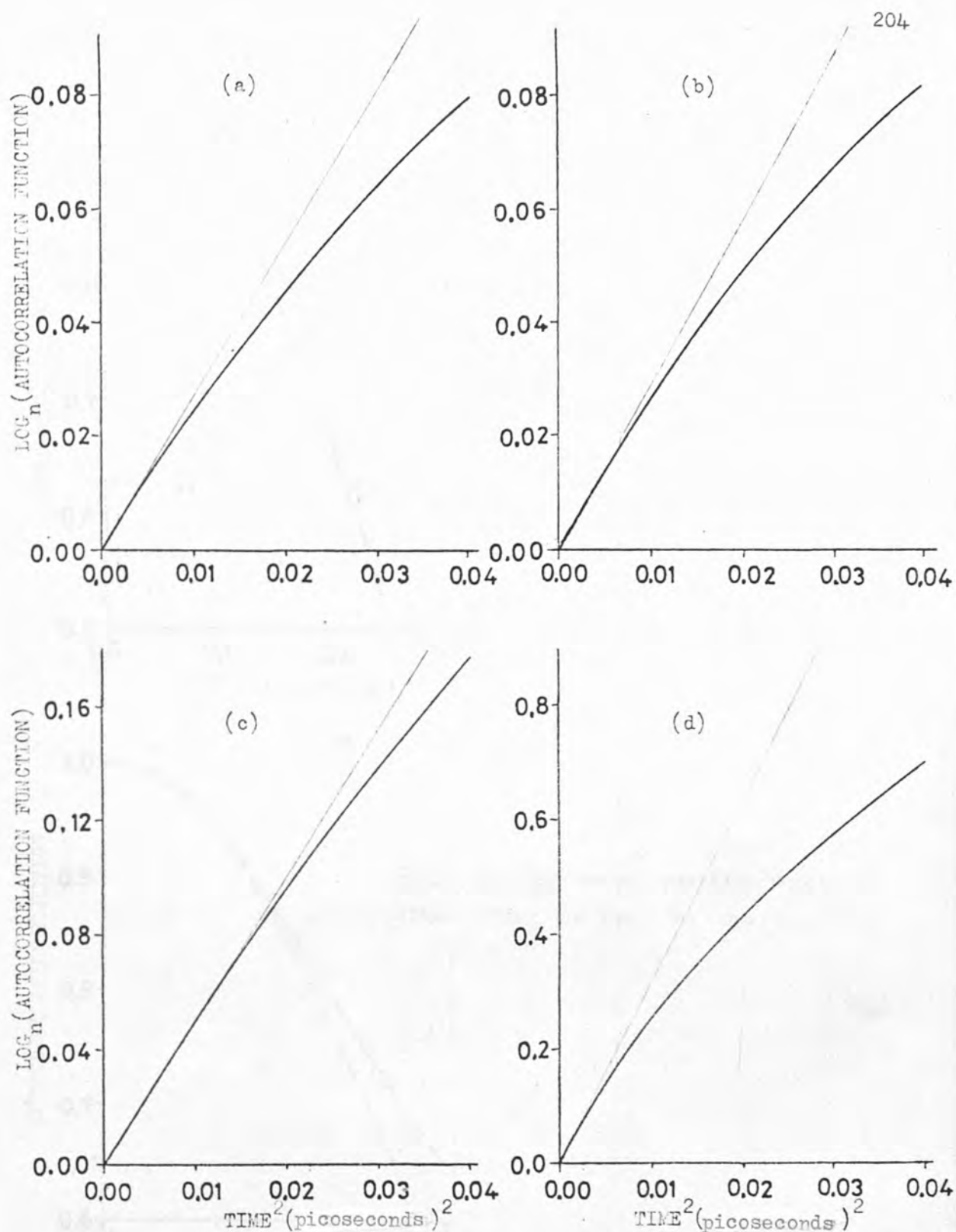


Fig.5.5 All the axes of the above graphs are of the same variables.

The straight lines are Gaussian functions drawn tangentially to the curves at zero time. (a) is for the ν_3 band of carbon disulphide

(b) is for the ν_{11} band of benzene (c) is for the ν_3 band of liquid methyl iodide and (d) is for the ν_6 band of methyl iodide.

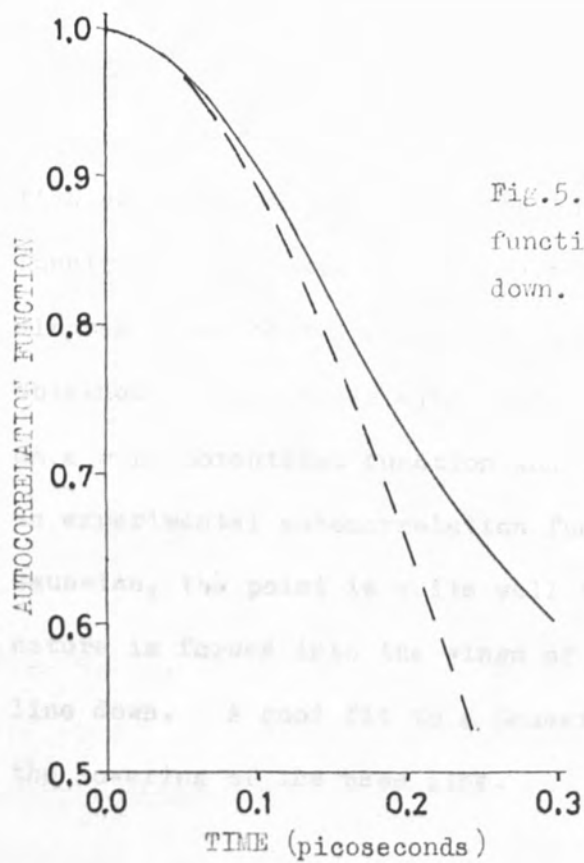


Fig.5.6a The autocorrelation function before moving the baseline down.

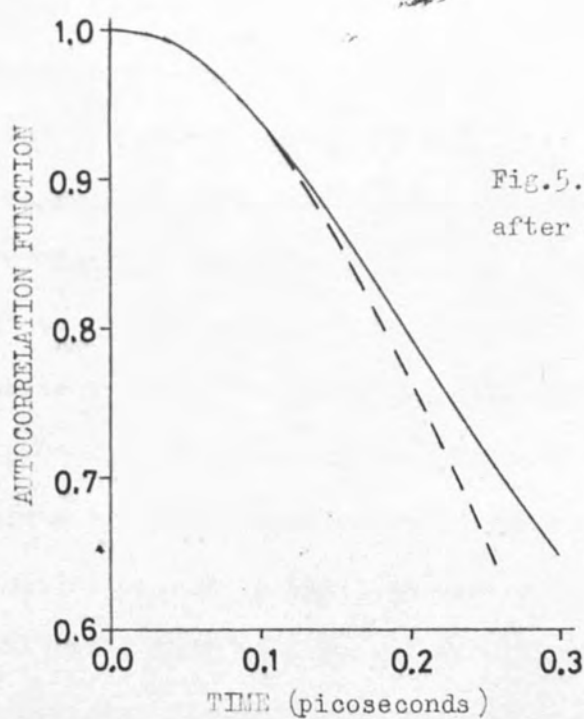


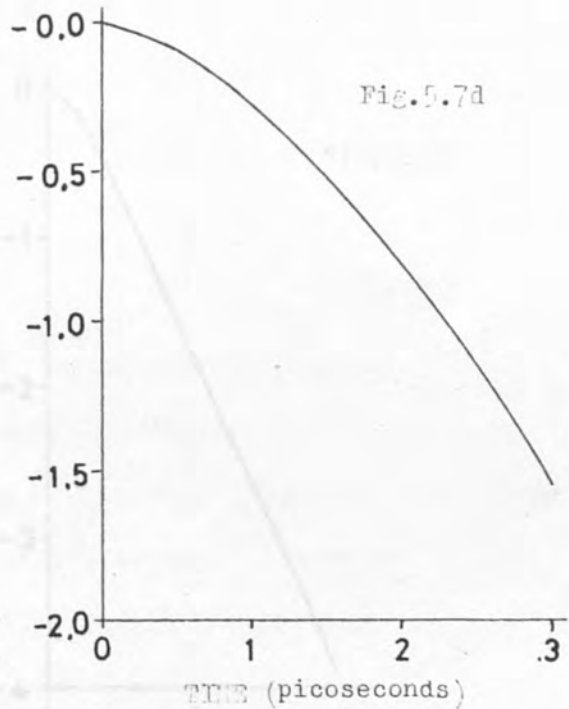
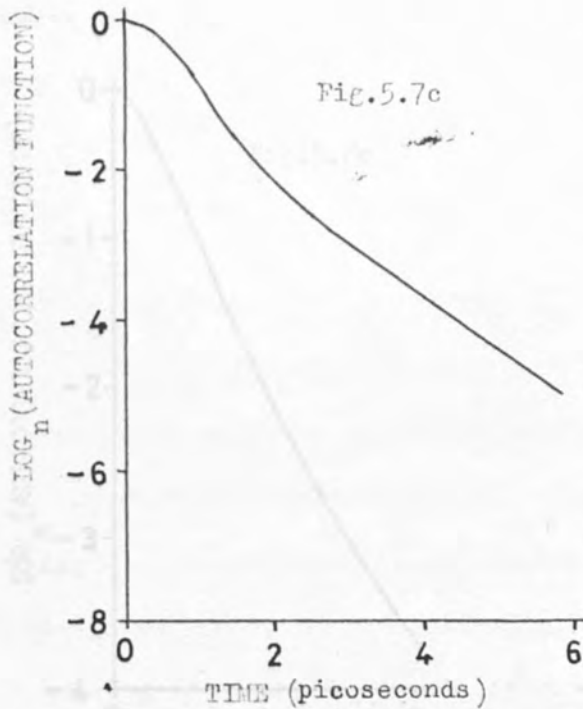
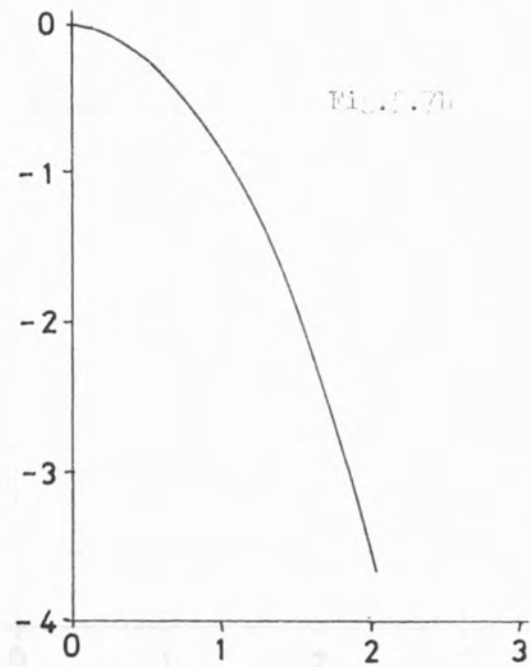
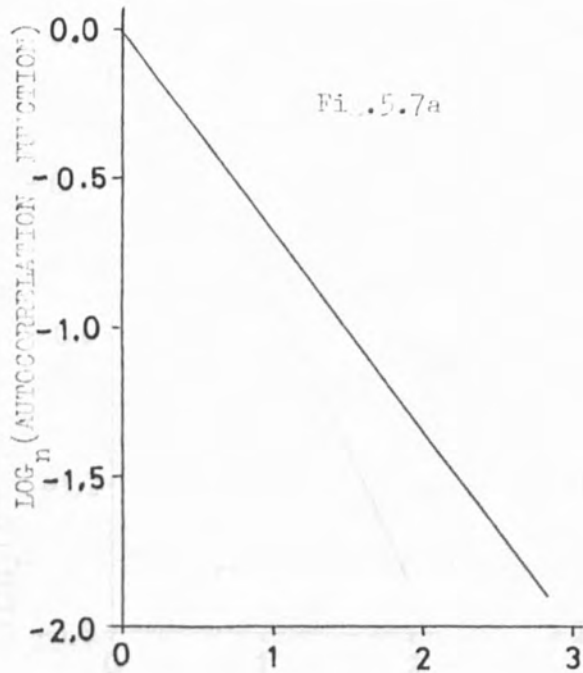
Fig.5.6b The autocorrelation function after moving the baseline down.

In both the above diagrams the solid line is the simulated curve and the broken line is a Gaussian function of the same second moment.

time decay is compared with the Fourier transform of a Gaussian function of the same new second moment in Fig. 5.6b. This diagram shows that a closer fit to a Gaussian function was obtained. Bearing in mind that this calculation was performed on a pure Lorentzian function and that the short time decay of an experimental autocorrelation function does resemble a Gaussian, the point is quite well illustrated that a Gaussian nature is forced into the wings of a band by moving the base line down. A good fit to a Gaussian function does not justify the lowering of the base line.

Section 5.4Statistical Analysis of the Condensed
Phase Contours of Infra-Red Bands - II

Fourier transformation has provided a powerful tool in gleaning more information about molecular motion in the condensed phase. Pictorial Fourier transforms may now be used to help solve the problem of infra-red band shapes. These Fourier transforms were calculated using EXTRAP. Fig. 5.7 shows the Fourier transforms of various Lorentzian and Gaussian functions, and their sums and products. The only function like the experimental is the Lorentzian plus Gaussian sum function. An extremely broad Gaussian function added to a narrow Lorentzian function would have a Fourier transform similar to the experimental, but we already know that the second moment of a Lorentzian function is infinite. The product of a Lorentzian and an exponential decay is shown in Fig. 5.8 and is not like the experimental. Fig. 5.8 also shows the general picture obtained from various convolutions of Lorentzian, Gaussian and exponential functions, none of which fit the experimental picture. This is to be expected, since a convolution in the frequency domain is a multiplication in the time domain, and so the only convolution that will show an exponential character at long time will be of a Lorentzian function with another Lorentzian function.



The above four autocorrelation functions are for different combinations of a Lorentzian function (L) of $\Delta\nu_1 = 7.2 \text{ cm}^{-1}$ and a Gaussian function (G) of $\Delta\nu_1 = 16.0 \text{ cm}^{-1}$.
 Fig. 5.7a - L only. Fig. 5.7b - G only. Fig. 5.7c - L + G
 when given the same initial intensity. Fig. 5.7d - L x G.

Fig. 5.7c is for $L = 5$, where L has $\Delta\nu_1 = 5 \text{ cm}^{-1}$ and G has $\Delta\nu_1 = 7 \text{ cm}^{-1}$. Fig. 5.7d is for $G = 2$, where G has $\Delta\nu_1 = 10 \text{ cm}^{-1}$ and L has $\Delta\nu_1 = 7 \text{ cm}^{-1}$.

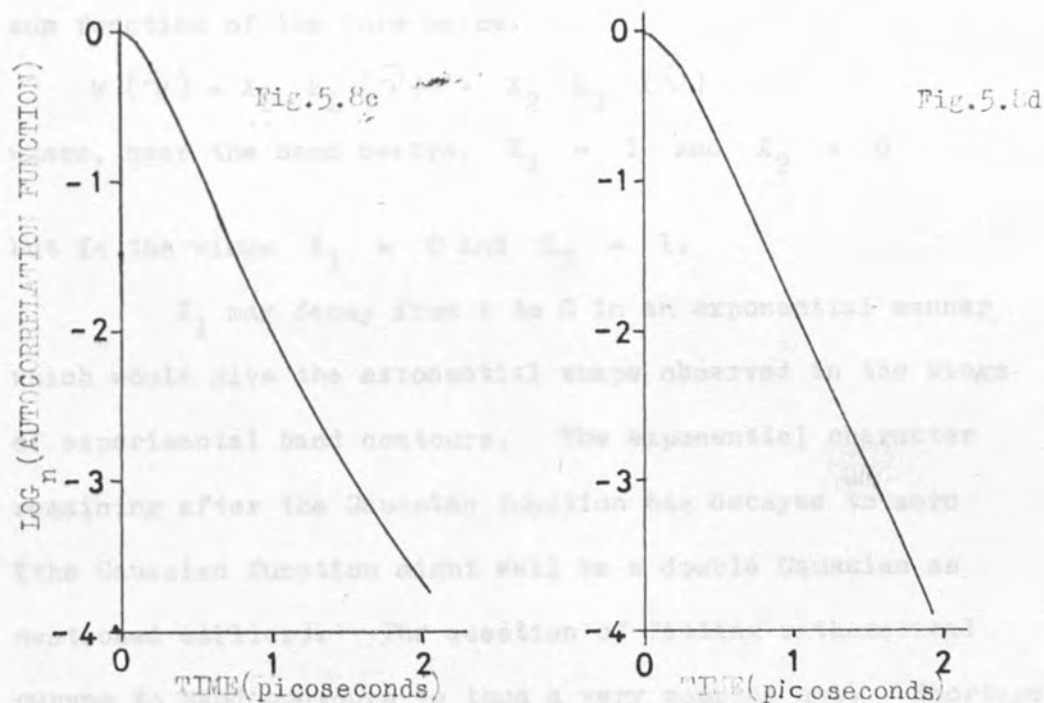
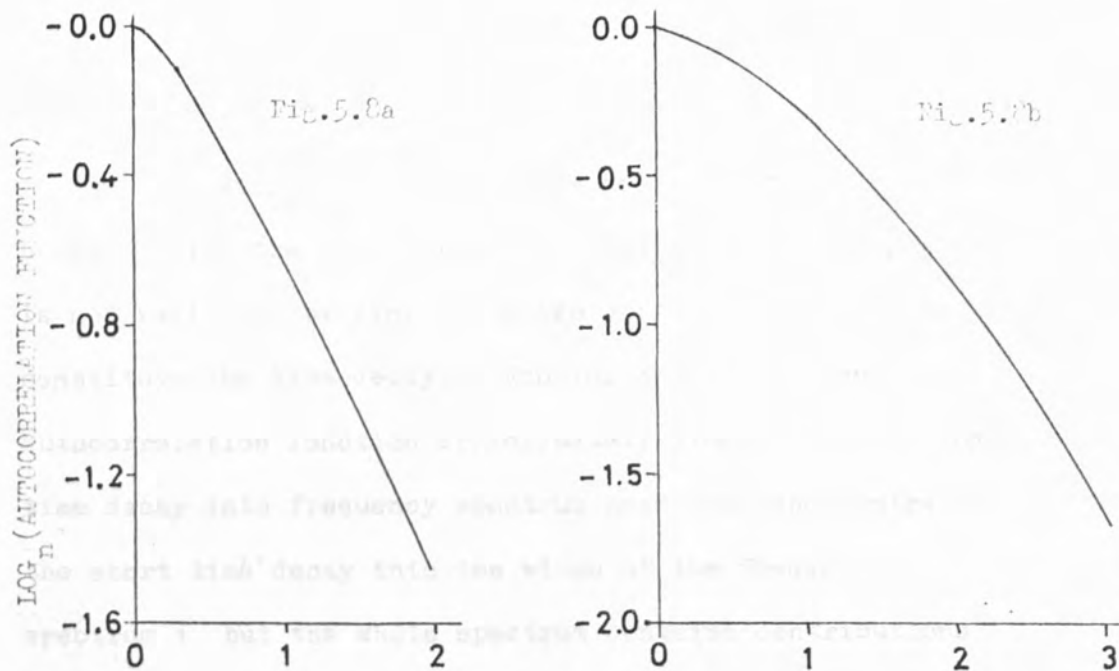


Fig. 5.8a is for a $L \times$ exponential function (E), where L has $\Delta\bar{\nu}_1 = 10 \text{ cm}^{-1}$ and E has $\Delta\bar{\nu}_2 = 20 \text{ cm}^{-1}$. The other figures are of convolutions (represented by *). Fig. 5.8b is for $L * G$, where L has $\Delta\bar{\nu}_1 = 5 \text{ cm}^{-1}$ and G has $\Delta\bar{\nu}_1 = 5 \text{ cm}^{-1}$. Fig. 5.8c is for $L * E$, where L has $\Delta\bar{\nu}_1 = 5 \text{ cm}^{-1}$ and E has $\Delta\bar{\nu}_1 = 7 \text{ cm}^{-1}$. Fig. 5.8d is for $G * E$, where G has $\Delta\bar{\nu}_1 = 10 \text{ cm}^{-1}$ and E has $\Delta\bar{\nu}_1 = 7 \text{ cm}^{-1}$.

A simple function cannot be fitted to infra-red bands. From the autocorrelation functions obtained, this is not really surprising since two different decay curves constitute the time decay. Fourier transformation of the autocorrelation function approximately transforms the long time decay into frequency spectrum near the band centre and the short time decay into the wings of the frequency spectrum ; but the whole spectrum contains contributions from both. The best approximation to an infra-red band shape can thus be expected to be a Lorentzian plus Gaussian sum function of the form below.

$$k(\bar{\nu}) = X_1 k_L(\bar{\nu}) + X_2 k_G(\bar{\nu})$$

where, near the band centre, $X_1 = 1$ and $X_2 = 0$

but in the wings $X_1 = 0$ and $X_2 = 1$.

X_1 may decay from 1 to 0 in an exponential manner which would give the exponential shape observed in the wings of experimental band contours. The exponential character remaining after the Gaussian function has decayed to zero (the Gaussian function might well be a double Gaussian as mentioned earlier). The question of fitting mathematical curves to band contours is thus a very complex one. Shortage of time prevented any further work exploring the above ideas. The above ideas may work, but the original objective of fitting a curve to a band contour was so that different bands

could be separated from each other, in order to calculate band moments. The mathematical equation to fit a band accurately will probably be so complicated that the band will have to be well separated in the first place to obtain all the parameters.

Although the band shapes of the
solved, the way in which the band
the band shapes of the same molecule were
different solvents. Several types of
binary solutions containing solvents such as ethyl iodide,
acetonitrile, carbon disulfide, carbon tetrachloride,
cyclohexane and benzene. The general result was that band
shapes did not alter to any noticeable extent in different
polar and non-polar solvents. There was one outstanding
exception to this observation though. Certain vibrations
of benzene were greatly broadened out when benzene was
dissolved in a polar solvent. This broadening was accompanied
by a shift to higher frequency compared with the band centres
in non-polar solvents. The results obtained from ethyl iodide
as solvent are set out below and are compared with those for
cyclohexane as solvent.

CHAPTER SIXBroadening of Infra-Red Band Shapes
and Weak Molecular Complexes
in Benzene SystemsSection 6.1

Initial Survey

Although the band shape problem has not been solved, the work so far may be utilised in analysis of the band shapes of the same molecule dissolved in different solvents. Several spectra were run of dilute binary solutions containing solvents such as methyl iodide, acetonitrile, carbon disulphide, carbon tetrachloride, cyclohexane and benzene. The general result was that band shapes did not alter to any noticeable extent in different polar and non-polar solvents. There was one outstanding exception to this observation though. Certain vibrations of benzene were greatly broadened out when benzene was dissolved in a polar solvent. This broadening was accompanied by a shift to higher frequency compared with the band centres in non-polar solvents. The results obtained from methyl iodide as solvent are set out below and are compared with those for cyclohexane as solvent.

| Band | $C_6 H_{12}$ | | $CH_3 I$ | |
|-----------------------|-----------------------------|---|-----------------------------|---|
| | $\bar{\nu}_0$ (cm^{-1}) | $\Delta\bar{\nu}_{\frac{1}{2}}$ (cm^{-1}) | $\bar{\nu}_0$ (cm^{-1}) | $\Delta\bar{\nu}_{\frac{1}{2}}$ (cm^{-1}) |
| ν_{11} | 674.6 | 4.3 | 680.1 | 7.4 |
| $\nu_5 + \nu_{17}$ | 1952.9 | 9.6 | 1960.2 | 16.0 |
| $\nu_{10} + \nu_{17}$ | 1808.3 | 9.7 | 1816.0 | 15.7 |
| $\nu_{10} + \nu_{11}$ | 1517 | ~ 8 | 1526 | ~ 16 |

The $\nu_{10} + \nu_{11}$ combination band was on the edge of the strong ν_{19} band (at 1482 cm^{-1}) so the data for this band is approximate.

It was found that the above broadened bands all concerned vibrations out of the plane of the benzene ring. There are, in fact, seven observable bands of this nature in the infra-red. These vibrations are shown in reference (3) and are listed below, along with frequencies of the band centres for the pure liquid and the symmetry species for the vibration.

- (1) ν_{11} band at 675 cm^{-1} (a_{2u})
- (2) ν_{10} band at 850 cm^{-1} (e_{1g})
- (3) ν_{17} band at 969 cm^{-1} (e_{2u})
- (4) ν_5 band at 991 cm^{-1} (b_{2g})
- (5) $\nu_{10} + \nu_{11}$ combination band at 1525 cm^{-1} (e_{1u})

(6) $\nu_{10} + \nu_{17}$ combination band at 1819 cm^{-1} (e_{1u})

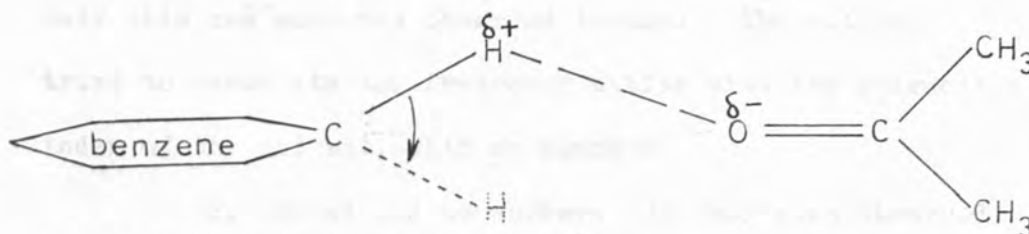
(7) $\nu_5 + \nu_{17}$ band at 1960 cm^{-1} (e_{1u})

The ν_{10} , ν_{17} , and ν_5 bands were all much weaker (inactive for unperturbed benzene molecules) than the other out-of-plane bands and could not be observed accurately in any solvents. Thus, all the observable out-of-plane bands have broadened out.

The ν_{11} , $\nu_5 + \nu_{17}$ and $\nu_{10} + \nu_{17}$ bands were all measured accurately in a series of polar and non polar solvents. There appeared to be a general trend of the more polar the solvent, the higher the frequency of the band centre was and the broader the band was. Before proceeding further a survey was made of the literature to see if these observations were original. The experimental results will be returned to later.

These observations were not original. La Lau (76) reported that the γ mode for the hydrogens of several aromatic compounds (hydrogens wagging out of the plane of the aromatic ring, ν_{11} band in benzene) dissolved in acetone and acetonitrile experienced shifts to higher, rather than lower, frequency compared with the gas phase. He explained the

shifts as being due to an electrostatic interaction between the positively charged hydrogens and the negatively charged oxygen or nitrogen of the polar solvent as outlined in the diagram below.



The C-H bond is vibrating at 90° to the planar benzene ring.

Calculations based on this idea lead to predicted frequency shifts which were very close to the experimentally observed ones. This model is considered unsatisfactory though, because it would lead to similar frequency shifts for the in-plane vibrations in this crude form.

Cole and Michell (72) reported that the hydrogen γ mode of aromatic compounds, with a single alkyl substituent group on the ring, gave anomalously broad bands when the alkyl group was a long "straight chain" such as n-butyl.

However, the band was not broad when the substituent was a *t*-butyl group. The reason for this broadening could not be explained. Cole and Michell (73) later measured the hydrogen δ mode of several aromatic compounds dissolved in different solvents and found that the bands were sometimes broadened out and shifted to higher frequency. Only this one mode was observed though. The authors tried to correlate the frequency shifts with the refractive index of the solvent, with no success.

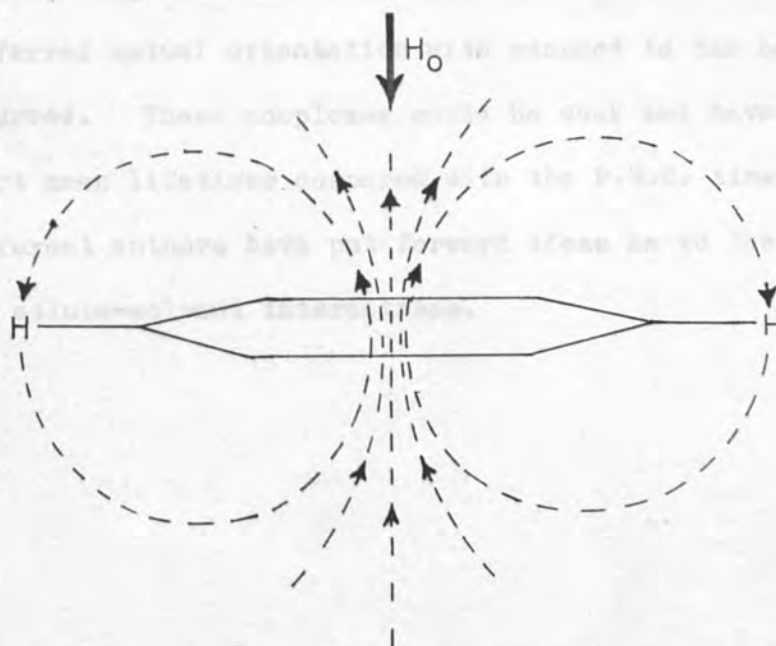
P. Dorval and co-workers (79) had also observed the frequency shifts for the out-of-plane modes of benzene, thiophene, furan and *N*-methyl-pyrrole in polar solvents. Frequency shifts were related to charges on the polar solvent using the ideas of La Lau. The frequency shifts for two of the aromatics in different solvents were plotted against each other and appeared to follow a linear relationship.

The rest of the work found in the literature concerning interactions between benzene and solvents concerned proton magnetic resonance (P.M.R.) which will be discussed in the next section.

Section 6.2Proton Magnetic Resonance Evidence
for Interaction between Benzene and
Various Solvents

P.M.R. spectra of benzene solutions of various solvents have been studied by many workers and the observations made are set out below.

W. Schneider (55) recorded P.M.R. shifts of the proton in chloroform to higher magnetic field, when the solvent was changed from "inert" cyclohexane to benzene. The reason given for this was that a large anisotropy in the magnetic susceptibility of the benzene was caused by the applied magnetic field, H_0 . The diagram below shows how, when H_0 is applied normal to the plane of the benzene ring, a circular current is induced which, in turn, generates a secondary magnetic field opposed in direction to that of the applied field.



The broken lines represent the secondary magnetic field.

Consequently, the resonance for a proton of the benzene ring will be shifted to lower magnetic field. However, a proton above or below the ring will have its resonance shifted to higher magnetic field. Schneider observed that the magnitude of the shifts of proton resonances of polar solutes in benzene tended to be proportional to the permanent electric dipole of the solute molecule. He believed that rotational averaging of the solute molecule took place, with no particular preferred orientation and consequently decided that the molar volume of the solute was of importance, because this determined the mean distance of approach to the benzene molecule. Fig. 6.1 shows a plot of P.M.R. shifts against electric dipole moments divided by molar volume. The plot is seen to be roughly linear (although chloroform is an exception) implying that dipole induced interactions mainly account for the shifts. Later authors suggested that a specific interaction involving a preferred mutual orientation with respect to the benzene occurred. These complexes would be weak and have very short mean lifetimes compared with the P.M.R. timescale. Different authors have put forward ideas as to the nature of the solute-solvent interactions.

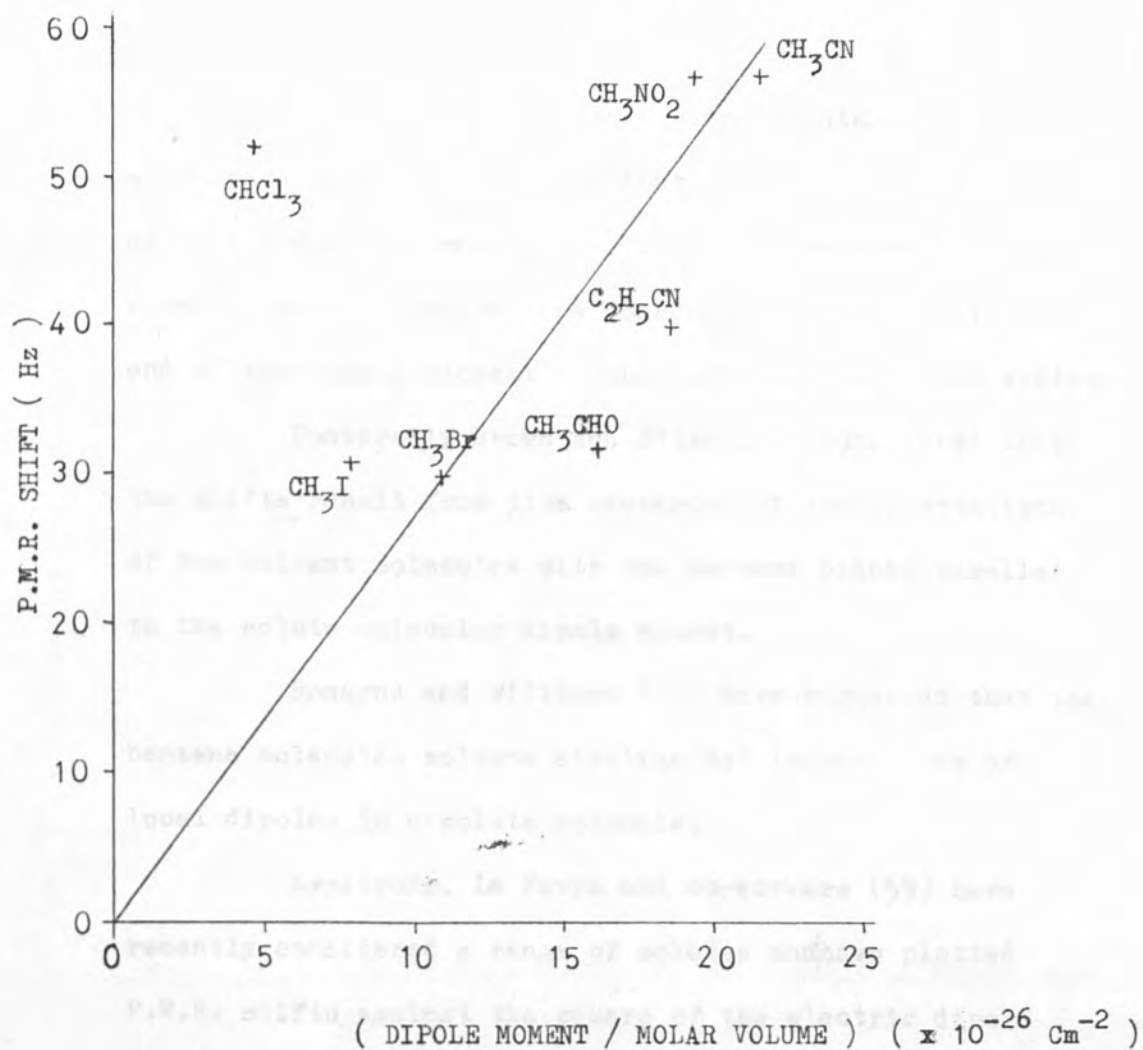


Fig.6.1 This graph is taken from data in reference (55) and is a plot of P.M.R. shifts of the above solutes dissolved in benzene, measured relative to their P.M.R. shifts in neopentane. The shifts are for the CH_3 group, excepting chloroform, and were measured in a field of 60 MHz .

Ledaal (56) inferred that benzene interacts with a polar solvent in such a way that the electric dipole axis of the solute molecule is located along the six-fold symmetry axis of the benzene molecule, with the positive end of the dipole closest to the benzene π electron system.

Conversely Brown and Stark (57) considered that the shifts result from time averaging of the orientations of the solvent molecules with the benzene planes parallel to the solute molecular dipole moment.

Ronayne and Williams (58) have suggested that the benzene molecules solvate electron deficient sites of local dipoles in a solute molecule.

Armstrong, Le Fevre and co-workers (59) have recently considered a range of solutes and have plotted P.M.R. shifts against the square of the electric dipole moment of the solute molecules, and obtained a rough straight line correspondence for a series of molecules such as CH_3I , CH_3Br , CH_3NO_2 and CH_3CN . A plot for these molecules is to be seen in Fig. 6.2. These co-workers go on to say that the series of molecules H C X_3 preferentially orientate with their dipole axes along the six-fold axis of the benzene molecule, with their proton nearest to the π electron layer. These associations being energetically favourable, but not exclusive. The CH_3X series of molecules are not thought to have a preferred orientation.

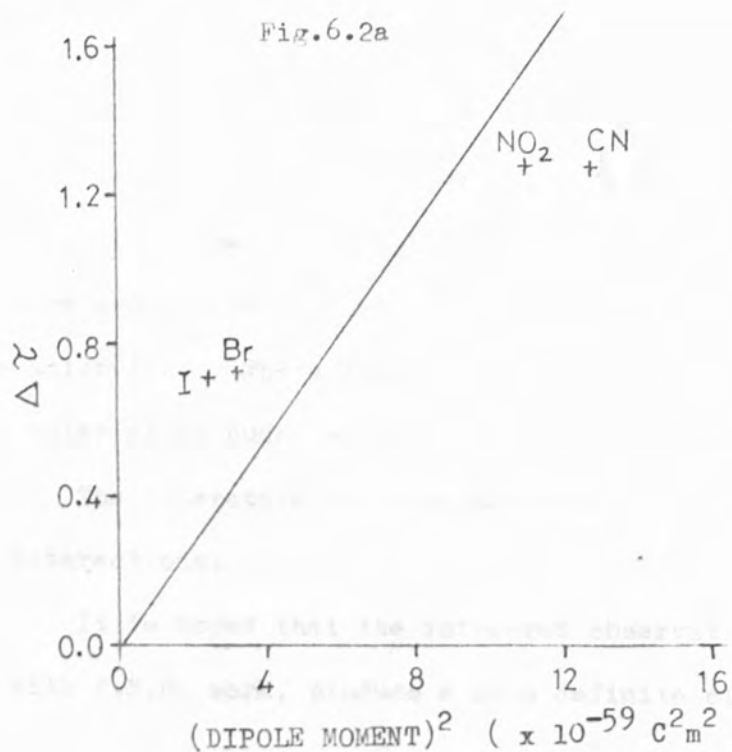
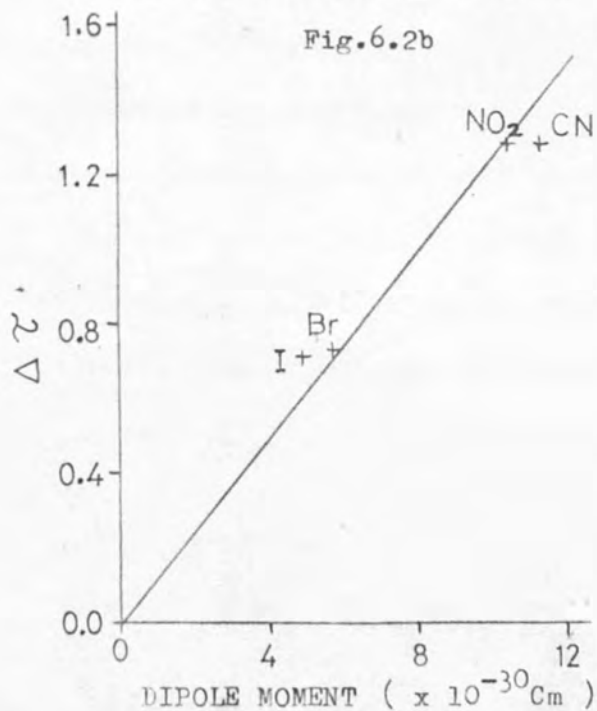


Fig.6.2a shows the chemical shifts for the protons in the series of molecules CH_3X , where $\text{X}=\text{Br}, \text{I}, \text{NO}_2$ and CN . These chemical shifts, $\Delta\tau$, are for benzene as solvent and are measured relative to 1,4 dioxane. The present author has replotted this data against the dipole moment and the result is shown below in Fig.6.2b. This plot is seen to be a better approximation to a straight line.



Homer and Cook (60) have suggested that, rather than interactions being through the molecular dipole moment, that there are interactions through local dipoles of the solute molecules. These local dipoles being due to highly polar atoms such as chlorine and oxygen.

The literature is thus undecided on the nature of these interactions.

It is hoped that the infra-red observations may, along with P.M.R. work, produce a more definite picture.

Section 6.3Correlation of Experimental Bandwidths
and Frequency Shifts with Macroscopic
Physical Properties of the Solvent

Table 6.1 shows the complete range of solvents used in measuring the ν_{11} band of benzene. Carbon disulphide, carbon tetrachloride and 1,4 dioxane have been added to my own list of solvents because these solvents are referred to in the P.M.R. work. Some of these bands were measured using three different path lengths to obtain accurate wings, but not all the solvents were transparent enough for this. The $\nu_5 + \nu_{17}$ and $\nu_{10} + \nu_{17}$ combination bands were measured using only one path length because both of these bands are overlapped quite badly. These two bands are listed in Table 6.2. The $\nu_{10} + \nu_{11}$ band was not measured because of the large errors involved. Tables 6.1 and 6.2 list the half height bandwidths and frequency of the different band centres.

A series of graphs was plotted for these three bands in an analogous fashion to that in the P.M.R. work.

1. The half height bandwidths were plotted against the dipole moment of the solute molecule to observe any dependence. These graphs are to be seen in Fig. 6.3a, 6.3c and 6.3e.

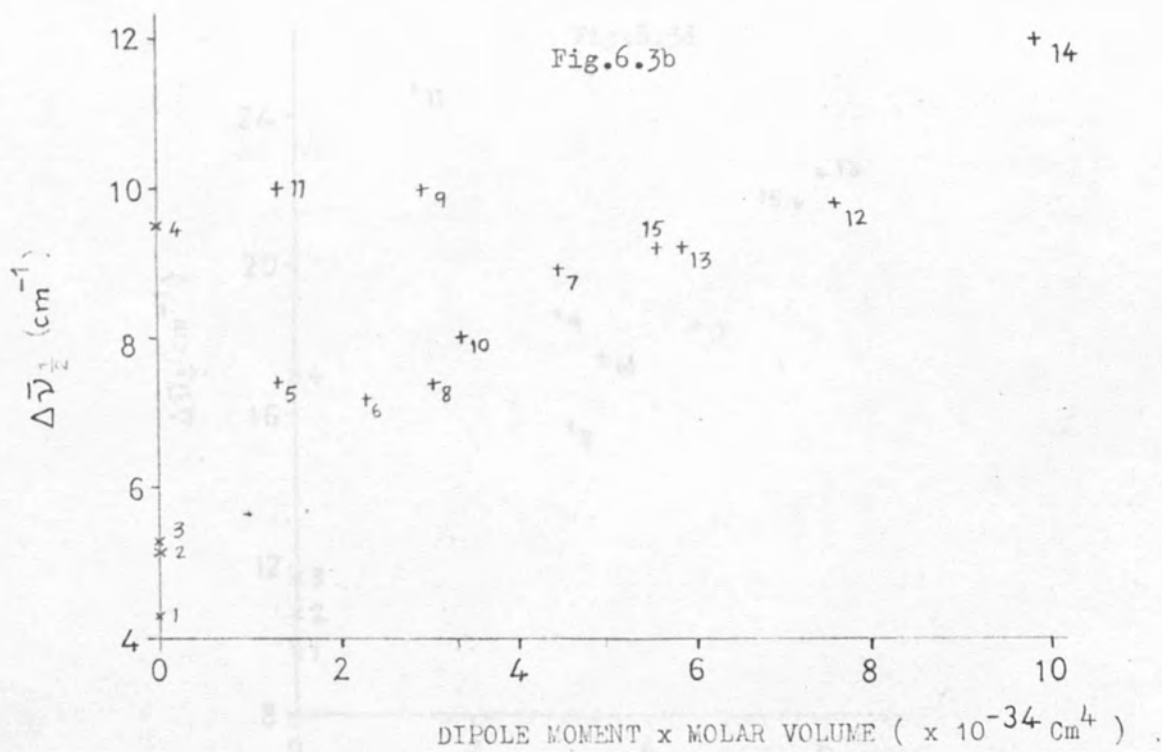
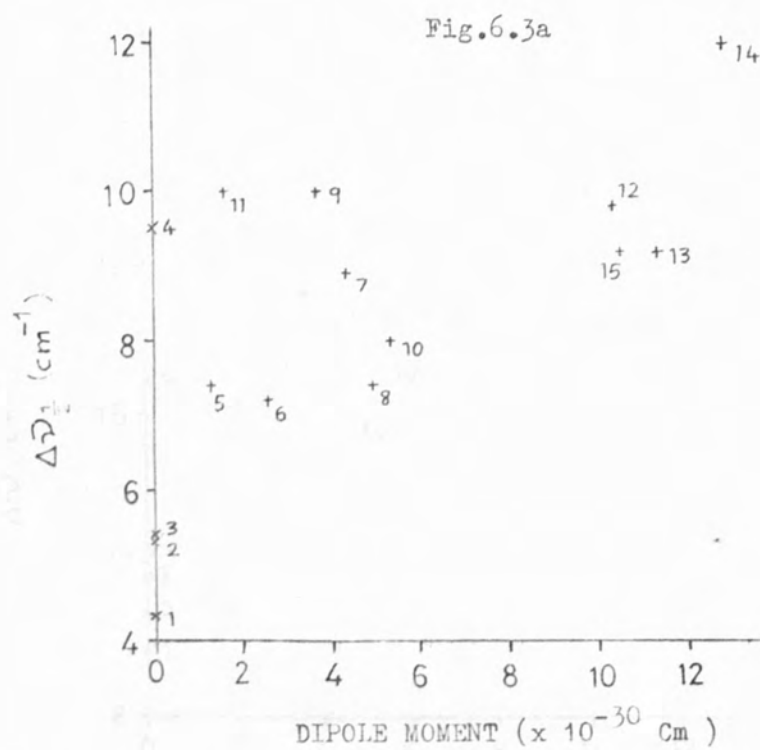
| SOLVENT AND REFERENCE NUMBERS | CONCENTRATION (mol dm ⁻³) | BAND CENTRE (cm ⁻¹) | $\Delta \nu_{1/2}$ (cm ⁻¹) | DIPOLE MOMENT (x 10 ⁻³⁰ cm) AT 25° | DIPOLE MOMENT x MOLAR VOLUME (x 10 ⁻³⁴ cm ⁴) | MOLAR POLARIS- ATION (x 10 ⁴ m ³) AT 25° |
|---|---|-------------------------------------|--|---|--|--|
| 1 C ₆ H ₁₂ | 0.260 | 674.6 | 4.3 | 0.00 | 0.00 | 2.754 |
| 2 CS ₂ | 0.342 | 675.2 | 5.3 | 0.00 | 0.00 | 2.113 |
| 3 CCl ₄ | 0.335 | 676.2 | 5.4 | 0.00 | 0.00 | 2.822 |
| 4 C ₆ H ₆ (1) | 11.202 | 677.6 | 9.5 | 0.00 | 0.00 | 2.670 |
| 5 C ₆ H ₅ CH ₃ | 0.416 | 678.2 | 7.4 | 1.23 | 1.31 | 3.349 |
| 6 C ₂ HCl ₃ | 0.325 | 678.6 | 7.2 | 2.57 | 2.30 | 3.988 |
| 7 (C ₂ H ₅) ₂ O | 0.358 | 679.1 | 8.9 | 4.33 | 4.49 | 5.460 |
| 8 CH ₃ I | 0.375 | 680.1 | 7.4 | 4.93 | 3.07 | 4.152 |
| 9 CHCl ₃ | 0.384 | 681.3 | 10.0 | 3.66 | 2.95 | 4.498 |
| 10 CH ₂ Cl ₂ | 0.440 | 682.6 | 8.0 | 5.33 | 3.41 | 4.667 |
| 11 C ₄ H ₈ O ₂ | 0.336 | 684.9 | 10.0 | 1.57 | 1.33 | 2.435 |
| 12 (CH ₃) ₂ CO | 0.408 | 685.1 | 9.8 | 10.37 | 7.60 | 6.405 |
| 13 CH ₃ CN | 0.381 | 686.8 | 9.2 | 11.30 | 5.90 | 4.812 |
| 14 C ₃ H ₇ NO | 0.520 | 687.8 | 12.0 | 12.83 | 9.88 | — |
| 15 CH ₃ NO ₂ | 0.390 | 688.4 | 9.2 | 10.47 | 5.62 | 4.974 |

Table 6.1 lists all the solvents used in investigating the ν_{11} band of benzene. The reference numbers of the solvents are used in later graphs. The dipole moments, molar volumes and molar polarisations are for the pure solvents.

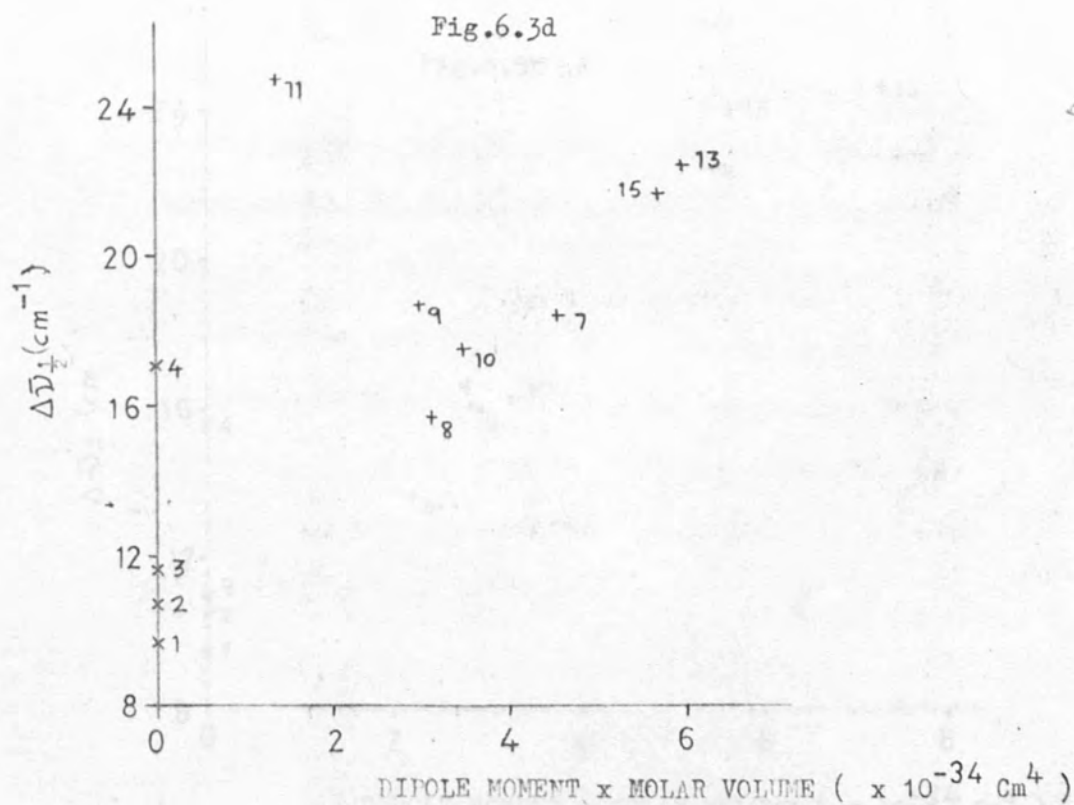
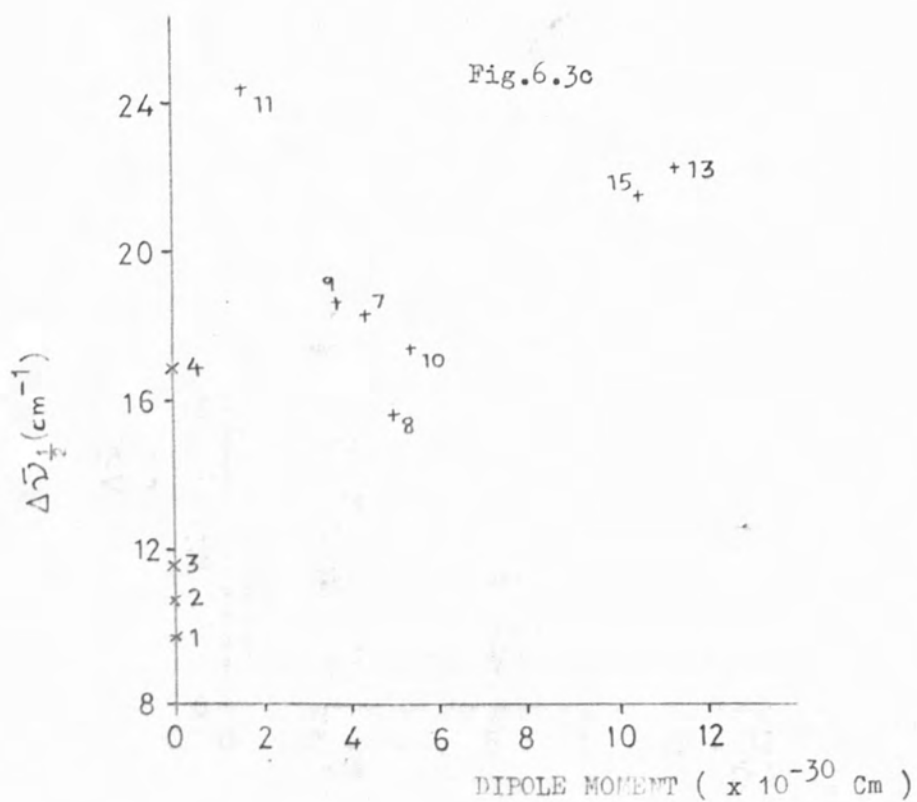
Table 6.2

| SOLVENT AND REFERENCE NUMBER | APPROXIMATE CONCENTRATION (mol dm^{-3}) | $\nu_{10} + \nu_{17}$ BAND | | $\nu_5 + \nu_{17}$ BAND | |
|--------------------------------------|--|---------------------------------------|---|---------------------------------------|---|
| | | $\bar{\nu}_0$ (cm^{-1}) | $\Delta\bar{\nu}_{1/2}$ (cm^{-1}) | $\bar{\nu}_0$ (cm^{-1}) | $\Delta\bar{\nu}_{1/2}$ (cm^{-1}) |
| 1 C_6H_{12} | 0.63 | 1808.3 | 9.7 | 1952.9 | 9.6 |
| 2 CS_2 | 0.63 | 1808.6 | 10.7 | 1952.7 | 10.5 |
| 3 CCl_4 | 0.65 | 1813.0 | 11.6 | 1952.2 | 11.0 |
| 4 $\text{C}_6\text{H}_6(1)$ | 11.20 | 1815.1 | 17.0 | 1960.0 | 15.5 |
| 5 $\text{C}_6\text{H}_5\text{CH}_3$ | — | — | — | — | — |
| 6 C_2HCl_3 | 0.76 | — | — | 1958.9 | 13.7 |
| 7 $(\text{C}_2\text{H}_5)_2\text{O}$ | 0.63 | 1814.6 | 18.4 | — | — |
| 8 CH_3I | 0.63 | 1816.0 | 15.7 | 1960.2 | 16.0 |
| 9 CHCl_3 | 0.57 | 1818.7 | 18.7 | 1962.1 | 16.1 |
| 10 CH_2Cl_2 | 0.63 | 1821.3 | 17.5 | 1964.7 | 16.2 |
| 11 $\text{C}_4\text{H}_8\text{O}_2$ | 0.63 | 1822.8 | 24.5 | — | — |
| 12 $(\text{CH}_3)_2\text{CO}$ | 0.63 | — | — | 1968.6 | 24.7 |
| 13 CH_3CN | 0.91 | 1827.2 | 22.4 | 1971.8 | 24.1 |
| 14 $\text{C}_3\text{H}_7\text{NO}$ | — | — | — | — | — |
| 15 CH_3NO_2 | 0.67 | 1828.8 | 21.7 | 1972.5 | 22.8 |

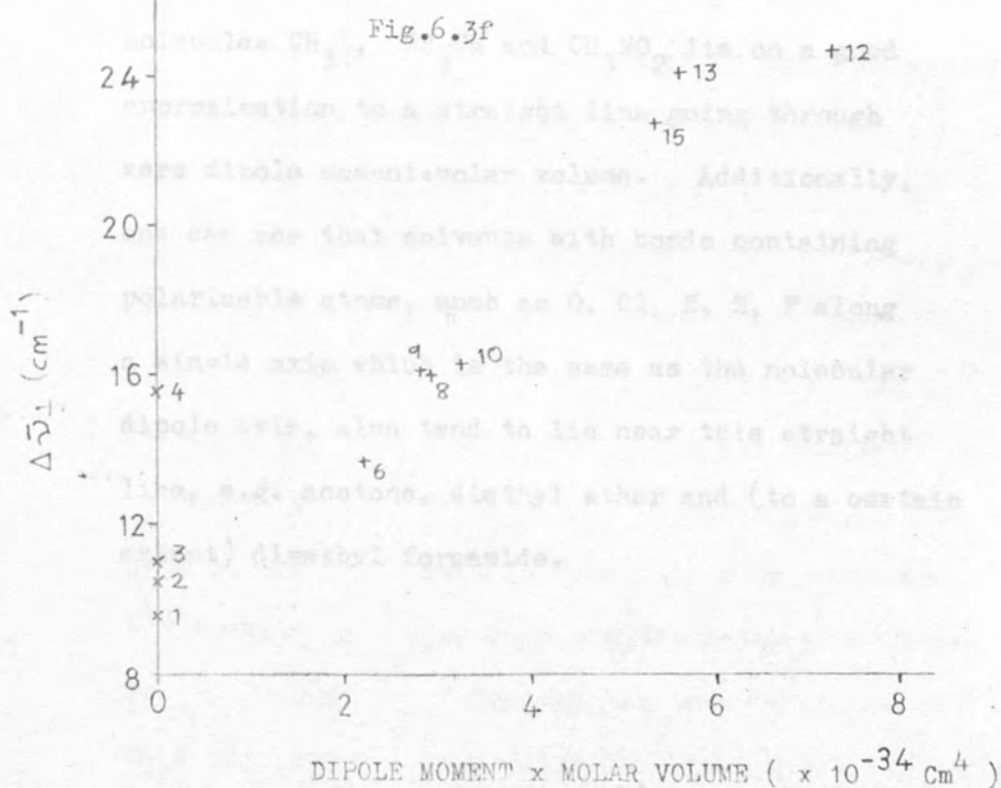
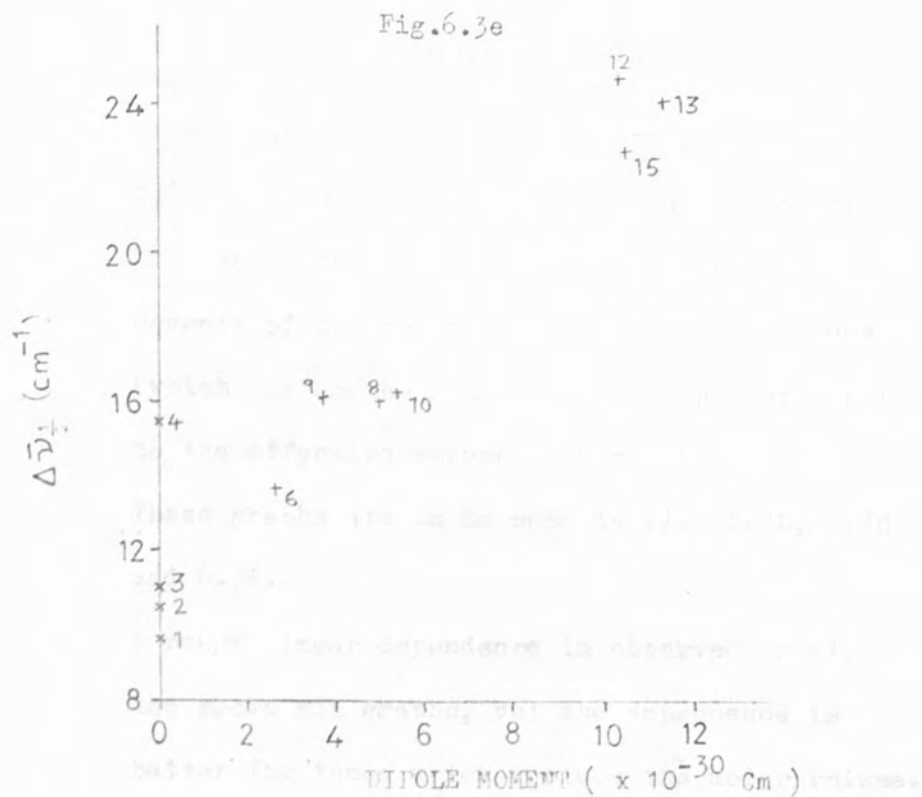
Table 6.2 lists the band centres and half height bandwidths of the $\nu_{10} + \nu_{17}$ and $\nu_5 + \nu_{17}$ combination bands of benzene in different solvents.



Both the plots are for the ν_{11} band of benzene in various solvents.



Both the plots are for the $\nu_{10} + \nu_{17}$ band of benzene in various solvents.



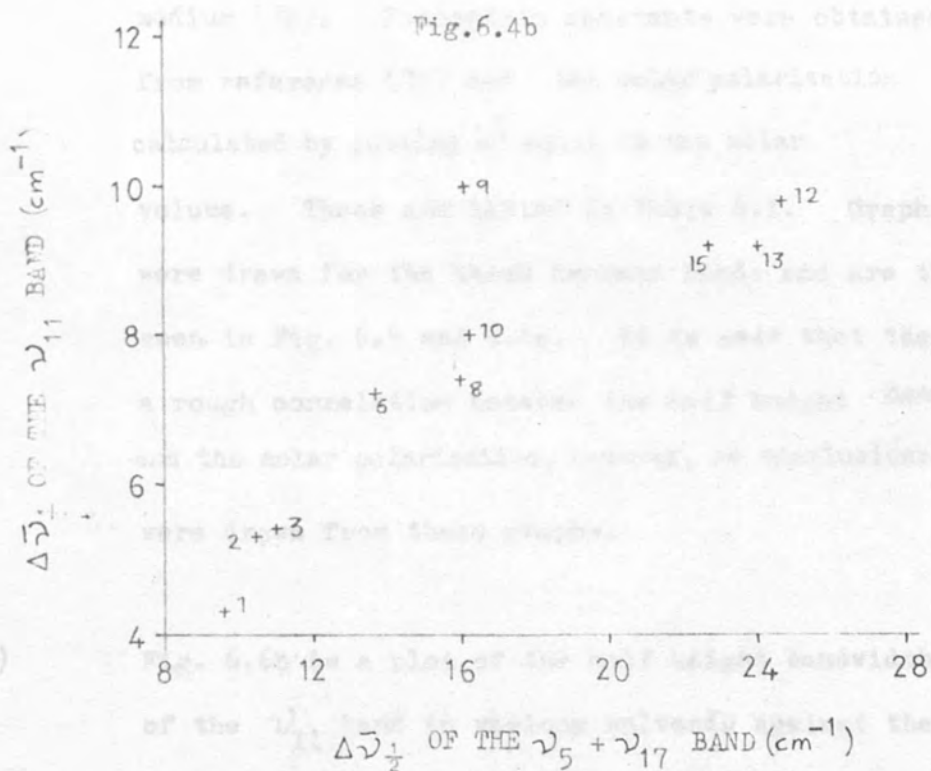
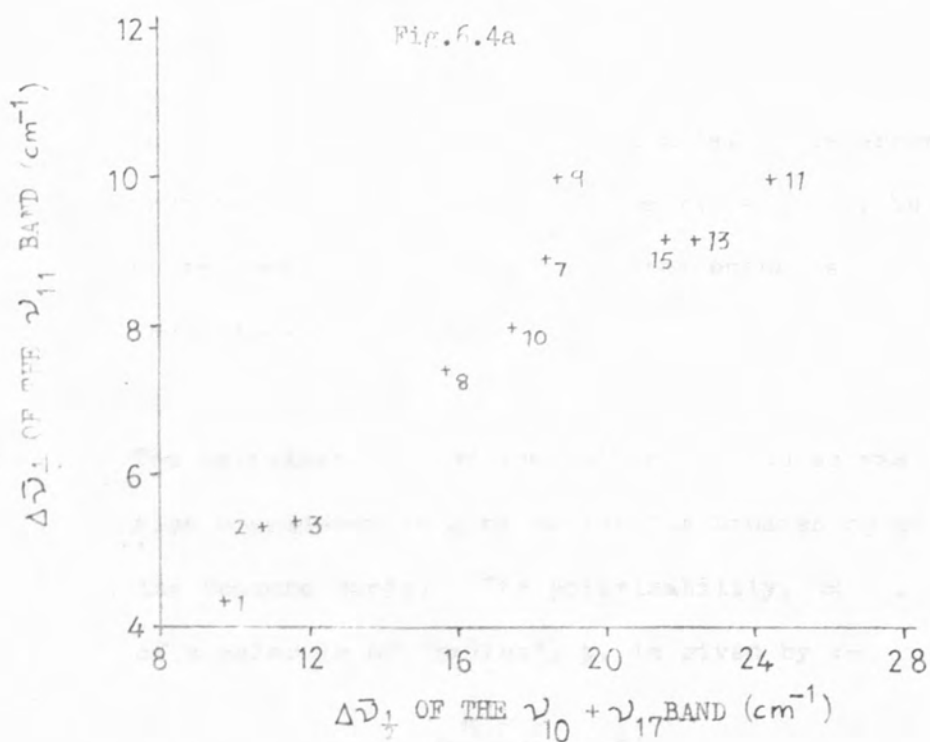
Both the plots are for the $\nu_5 + \nu_{17}$ band of benzene in various solvents.

2. It was decided to introduce some kind of molecular shape factor into the above graphs. This was done by multiplying the dipole moments of the solvents by their molar volume (which may be thought of as being proportional to the effective volume of a molecule). These graphs are to be seen in Fig. 6.3b, 6.3d and 6.3f.

A rough linear dependence is observed in all the above six graphs, but the dependence is better for those which include the molar volume. Consider the latter three graphs. With the aid of a rule it will be seen that the group of molecules CH_3I , CH_3CN and CH_3NO_2 lie on a good approximation to a straight line going through zero dipole moment \times molar volume. Additionally, one can see that solvents with bonds containing polarisable atoms, such as O, Cl, N, S, F along a single axis which is the same as the molecular dipole axis, also tend to lie near this straight line, e.g. acetone, diethyl ether and (to a certain extent) dimethyl formamide.

Assuming that the inclusion of the molar volume is valid and that the improved results are not fortuitous, it would appear that the first order effect causing the broadening is due to the molecular dipole moment of the solvent. There is clearly a second order effect which is probably due to "local dipoles" in the solvent molecule. For example, carbon tetrachloride has a zero molecular dipole moment but all the C - Cl bonds are highly polar and may have a short range interaction with the benzene. As an illustration of this idea consider 1,4 dioxane. Hypothetically this molecule looks like two dimethyl ether molecules associated together. Dimethyl ether has a molecular dipole moment of 4.33 Cm, so let a hypothetical dipole moment for 1,4 dioxane be of this magnitude. In this case the points on the graphs for 1,4 dioxane lie much closer to the proposed straight lines. For liquid benzene and aromatic solvents it is imagined that the π electron layers are somehow interacting but this case will be neglected for the time being. Of the molecules with dipole moments, 1,4 dioxane and chloroform are the major exceptions in the graphs. 1,4 dioxane has been accounted for on a hypothetical basis, but this does not apply to chloroform. This molecule is a special case and will be dealt with separately in a later section.

(3) The combination bands of benzene that were broadened out, were broadened out to a greater extent than the ν_{11} band. Fig. 6.4a is a plot of the half height bandwidths of the ν_{11} band, in a particular solvent, against those of the $\nu_{10} + \nu_{17}$ combination band. Fig. 6.4b is a similar plot for the ν_{11} band against the $\nu_5 + \nu_{17}$ combination band. These two graphs are seen to be of a roughly linear nature. The gradients of these graphs were calculated, using the method of least squares, along with the standard deviation. The results were that Fig. 6.4a yielded a gradient of 0.398 ± 0.037 and Fig. 6.4b yielded a gradient of 0.301 ± 0.035 . The reciprocals of these gradients are 2.51 and 3.33 respectively. It is thought that these gradients show that the magnitude of the broadening of the bands is linearly dependent upon the frequency. For example, for the $\nu_{10} + \nu_{17}$ band and cyclohexane as solvent, $674/0.398 = 1693 \text{ cm}^{-1}$ and including the error limits we get $1700 \pm 170 \text{ cm}^{-1}$. The experimental frequency for this band is 1808 cm^{-1} and thus lies within this estimate. For the $\nu_5 + \nu_{17}$ band we get an estimated frequency of $2240 \pm 300 \text{ cm}^{-1}$. The experimental frequency for this band is 1953 cm^{-1}



The plots are for benzene in various solvents.

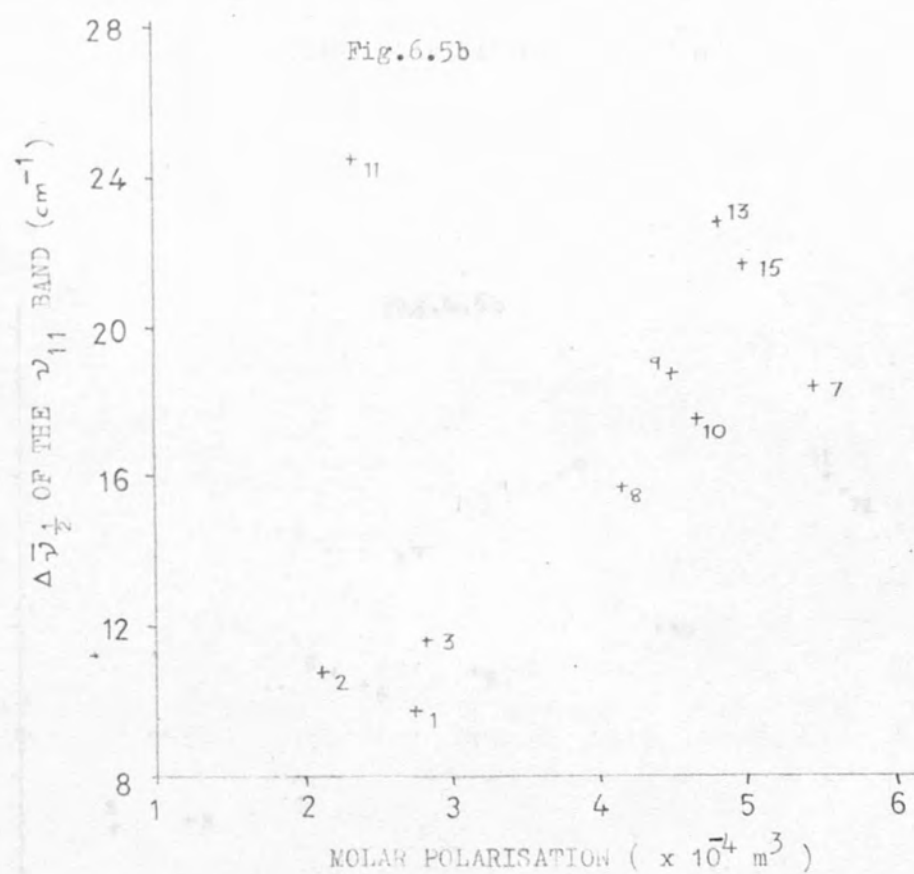
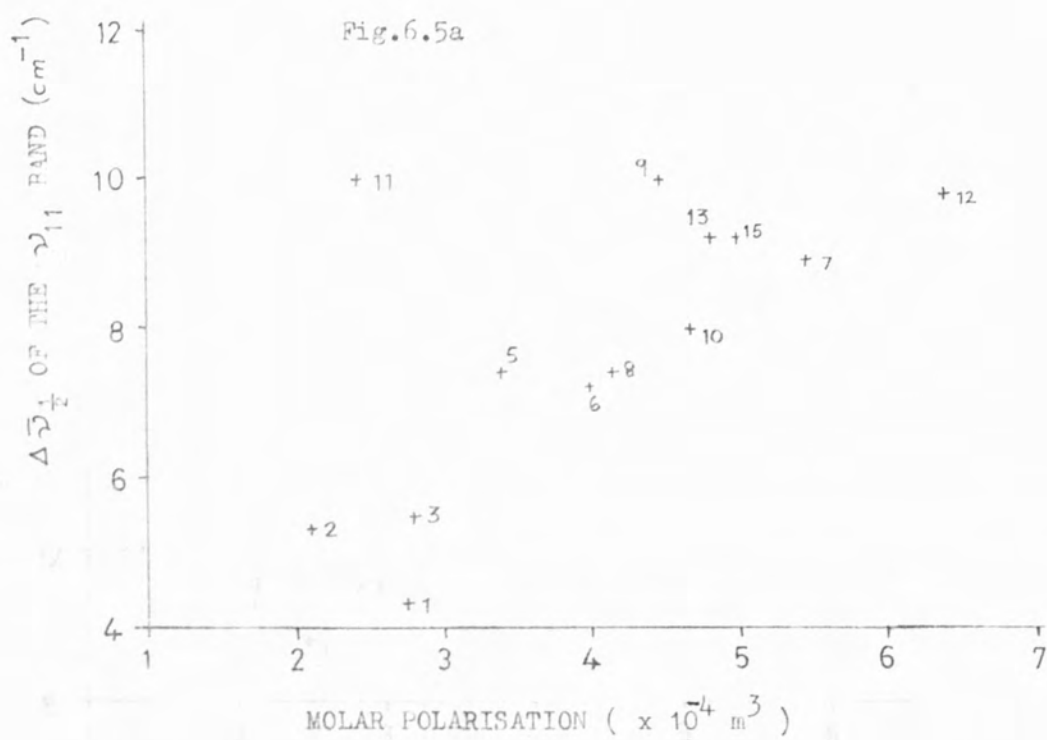
and is within range of this estimate. The errors involved in this calculation are rather high, but a frequency dependence of the broadening is indicated.

- (4) The polarisability of the solvent molecules was also considered as a cause for the broadening of the benzene bands. The polarisability, α , of a molecule of "radius", a , is given by :-

$$\alpha = \left(\frac{\epsilon - 1}{\epsilon + 2} \right) a^3$$

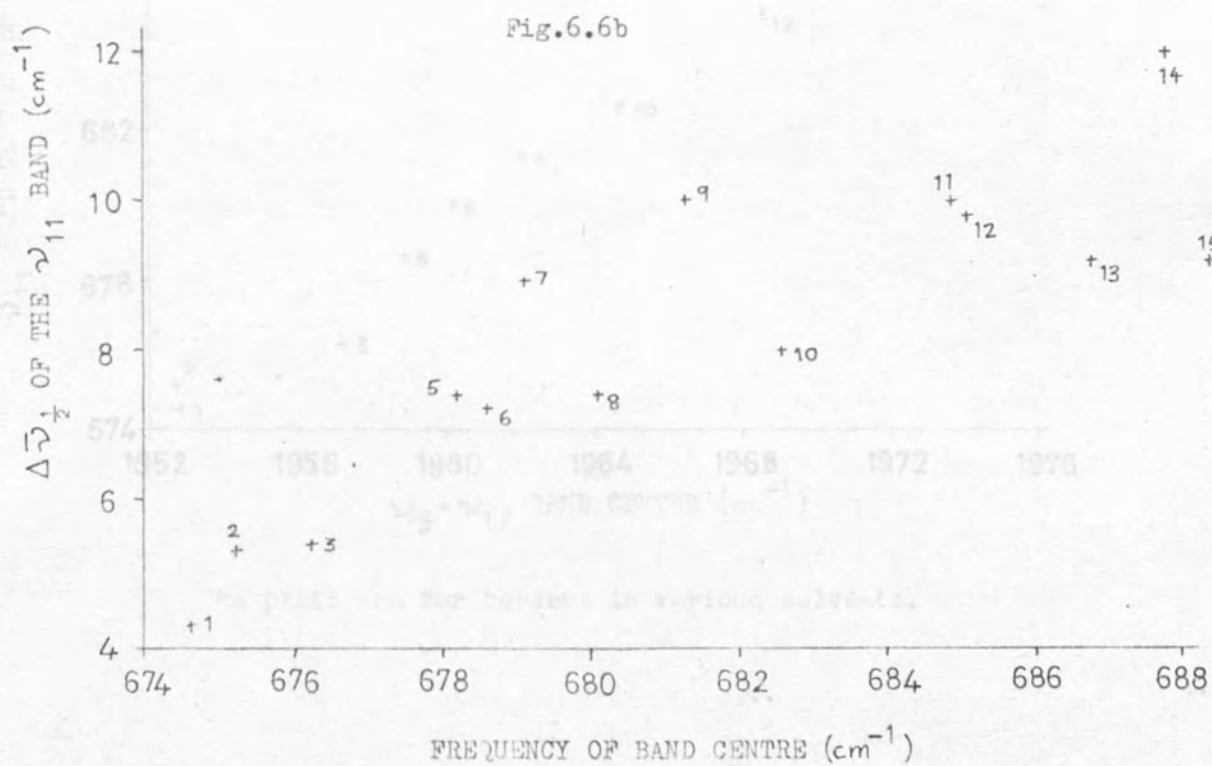
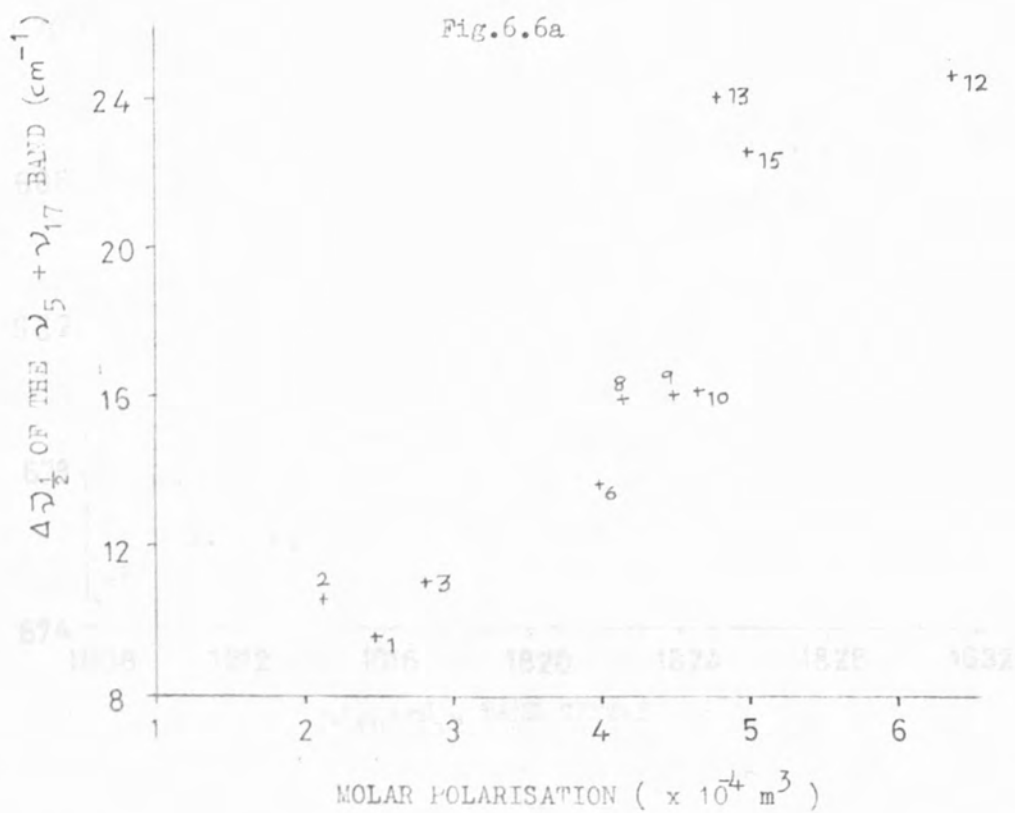
where ϵ is the dielectric constant of the solvent medium (74). Dielectric constants were obtained from reference (75) and the molar polarisation calculated by putting a^3 equal to the molar volume. These are listed in Table 6.1. Graphs were drawn for the three benzene bands and are to be seen in Fig. 6.5 and 6.6a. It is seen that there is a rough correlation between the half height bandwidth and the molar polarisation, however, no conclusions were drawn from these graphs.

- (5) Fig. 6.6b is a plot of the half height bandwidth of the ν_{11} band in various solvents against the frequency of the band centre. There is seen to be only a rough correlation between the two so, again, no conclusions were drawn.

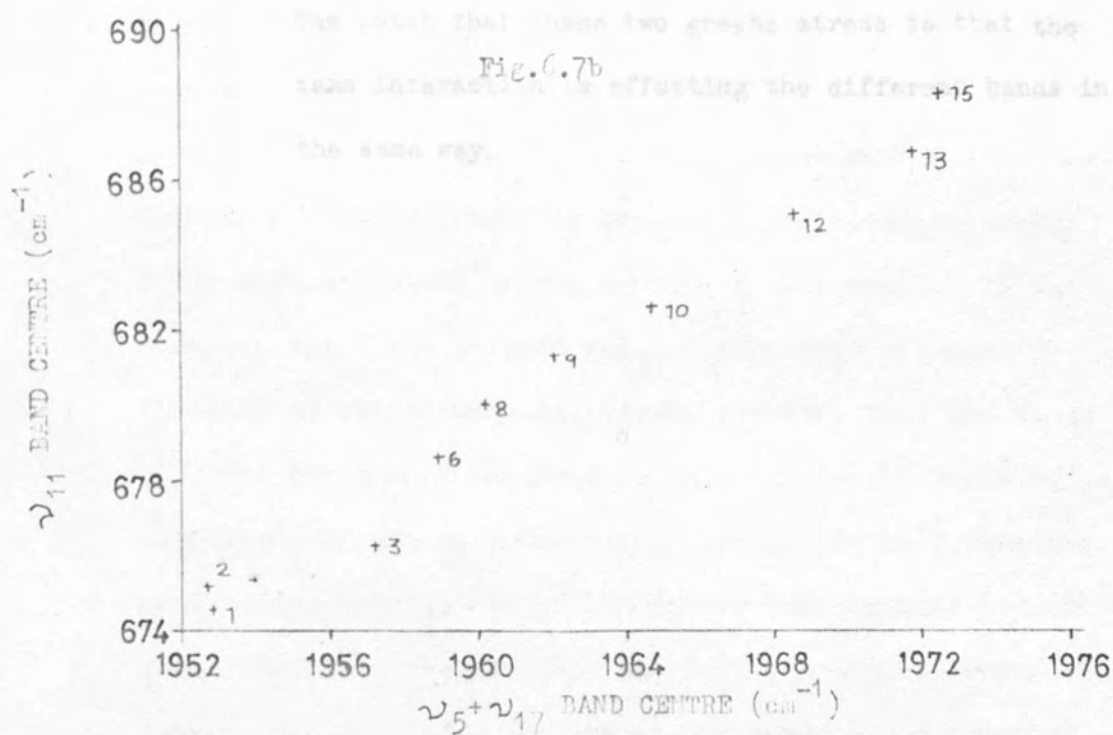


The plots are for benzene in various solvents.

The plots are for benzene in various solvents.



The plots are for benzene in various solvents.



The plots are for benzene in various solvents.

(6) The frequency of the band centre of the ν_{11} band in a particular solvent was plotted against the band centre for the $\nu_{10} + \nu_{17}$ combination band (Fig. 6.7a) and against the frequency for the $\nu_5 + \nu_{17}$ combination band, (Fig. 6.7b).

Both of the plots are seen to be fairly good straight lines. The gradients of these two graphs were both approximately 1.4 and so no connection between the magnitude of the frequency shifts and the frequencies of the different bands is apparent.

The point that these two graphs stress is that the same interaction is effecting the different bands in the same way.

The case of measuring second and fourth moments of the ν_{11} band of benzene in isotopic solvents, which did not absorb in the region of this band. In the cases in which the solvent did not absorb at all (and in the case of liquid benzene) it was observed that the wings of these bands were asymmetric in character. These wings were extrapolated as exponentials out to 100 cm^{-1} from the band centre and the second and fourth moments both determined using EXTRAP. The plots of the build-up of the second and fourth moments showed that, when the second moments had levelled off to a finite value, the fourth moments were still increasing, although these too levelled off later. Table 5.1 shows the

Section 6.4Measurement of the Second and Fourth Moments of the ν_{11} Band of Benzene in Different Solvents

According to Gordon's theory on second moments, the second moment of the ν_{11} band of benzene should not change appreciably in different solvents, despite the huge changes in the band-width. This is because the second moment is related to the rotational kinetic energy, and is independent of intermolecular interactions, although it is affected by a fluctuation in the frequency shift. Conversely the fourth moment of the band is largely determined by the mean squared torque acting on the benzene molecule, hindering rotation.

An attempt was made at measuring second and fourth moments of the ν_{11} band of benzene in selected solvents, which did not absorb in the region of this band. In the cases in which the solvent did not absorb at all (and in the case of liquid benzene) it was observed that the wings of these bands were exponential in character. These wings were extrapolated as exponentials out to 300 cm^{-1} from the band centre and the second and fourth moments both determined using EXTRAP. The plots of the build-up of the second and fourth moments showed that, when the second moments had levelled off to a finite value, the fourth moments were still increasing, although these too levelled off later. Table 6.3 shows the

results obtained. It is seen that the fourth moments vary over a much larger range than the second moments. The error in the fourth moments is estimated to be double the error in the second moments. The whole question of errors is rather vague because it has been assumed that the wing of a band is an exponential out to zero absorption. The low frequency side of the ν_{11} band of liquid benzene accurately follows an exponential decay from 630 cm^{-1} to 560 cm^{-1} , but measurements beyond 560 cm^{-1} are very much limited in accuracy. The wing is exponential as far as the measurements can be taken.

The equation for the fourth moment of a parallel band of a symmetric top molecule was determined, from equation (3.14) to be :-

$$M(4) = 4/x^2 (8B^2 + 2B^3/A) + 4B^2 (OV)^2$$

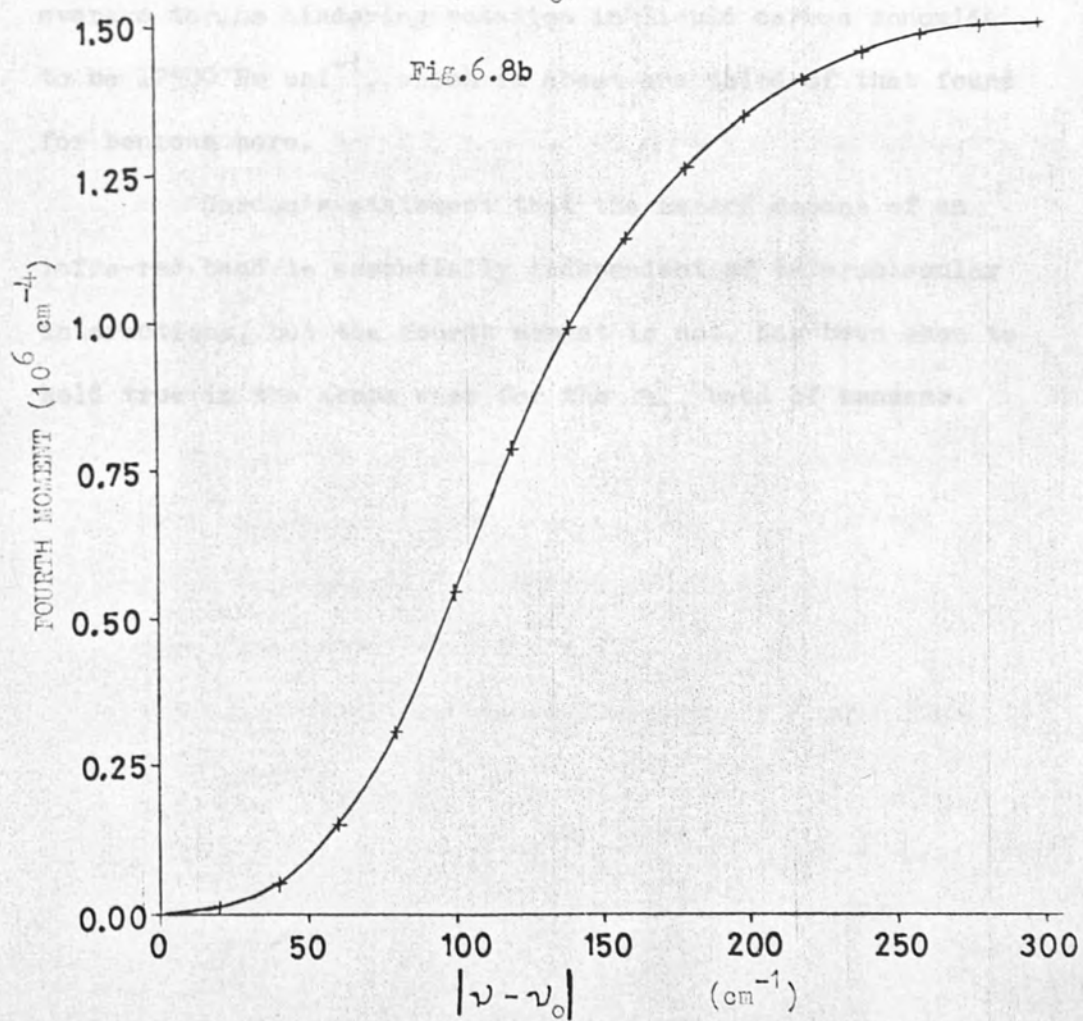
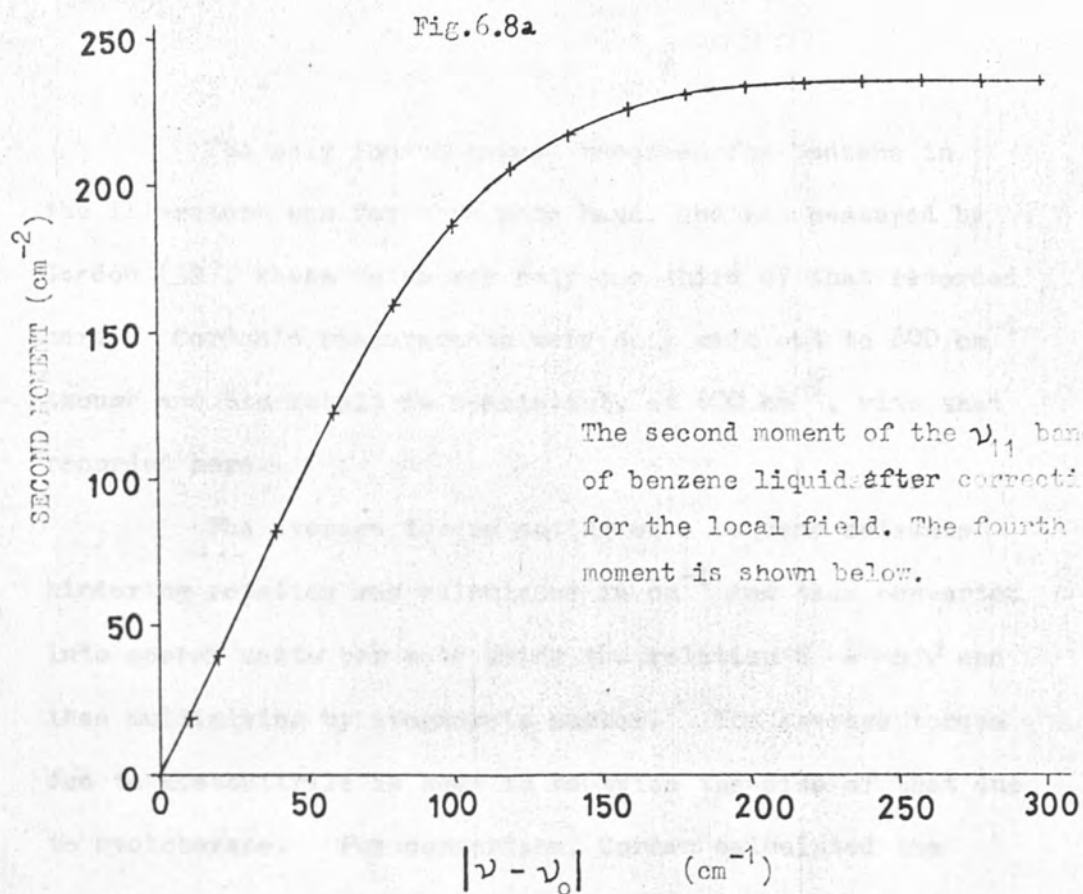
For the benzene molecule we have :-

$$(OV)^2 = \left[M(4) - 4/x^2 (8 \times 0.1894^2 + 2 \times 0.1894^3 / 0.0947) \right] / (4 \times 0.1894^2)$$

The square roots of the mean squared torque is listed in Table 6.3 for the four cases which were considered accurate enough to measure. The build-up of the second and fourth moments against frequency are compared for liquid benzene in Fig. 6.8.

| SOLVENT AND REFERENCE NUMBER | INTEGRATED INTENSITY ($\text{dm}^3 \text{mol}^{-1}$ cm^{-1}) | SECOND MOMENT (cm^{-2}) | FOURTH MOMENT ($\times 10^6$ cm^{-4}) | ROOT MEAN SQUARED TORQUE ($\times 10^4$ N m mol^{-1}) |
|--------------------------------------|--|--|---|---|
| 1 C_6H_{12} | 21.5 ± 2.1 | 180 ± 20 | 1.0 ± 0.2 | 3.04 ± 0.32 |
| 2 CS_2 | — | | | |
| 3 CCl_4 | 21.2 ± 2.1 | | | |
| 4 $\text{C}_6\text{H}_6(1)$ | 27.0 ± 4.0 | 235 ± 20 | 1.5 ± 0.3 | 3.77 ± 0.42 |
| 5 $\text{C}_6\text{H}_5\text{CH}_3$ | 20.6 ± 2.1 | | | |
| 6 C_2HCl_3 | 20.2 ± 2.0 | | | |
| 7 $(\text{C}_2\text{H}_5)_2\text{O}$ | — | | | |
| 8 CH_3I | 20.2 ± 2.0 | 300 ± 50 | 3.3 ± 1.0 | 5.69 ± 0.93 |
| 9 CHCl_3 | 19.6 ± 2.0 | | | |
| 10 CH_2Cl_2 | — | | | |
| 11 $\text{C}_4\text{H}_8\text{O}_2$ | — | | | |
| 12 $(\text{CH}_3)_2\text{CO}$ | 18.0 ± 1.8 | | | |
| 13 CH_3CN | 18.2 ± 1.8 | 340 ± 50 | 3.6 ± 1.0 | 5.93 ± 0.77 |
| 14 $\text{C}_3\text{H}_7\text{NO}$ | — | | | |
| 15 CH_3NO_2 | — | | | |

Table 6.3 lists some constants for the ν_{11} band of benzene in different solvents.



The only fourth moment recorded for benzene in the literature was for this same band, and was measured by Gordon (32), whose value was only one third of that recorded here. Gordon's measurements were only made out to 600 cm^{-1} though and his result is consistent, at 600 cm^{-1} , with that recorded here.

The average torque acting on a benzene molecule hindering rotation was calculated in cm^{-1} and then converted into energy units per mole using the relation $E = h\nu$ and then multiplying by Avogadro's number. The average torque due to acetonitrile is seen to be twice the size of that due to cyclohexane. For comparison, Gordon calculated the average torque hindering rotation in liquid carbon monoxide to be $12500 \text{ Nm mol}^{-1}$, which is about one third of that found for benzene here.

Gordon's statement that the second moment of an infra-red band is essentially independent of intermolecular interactions, but the fourth moment is not, has been seen to hold true in the above case for the ν_{11} band of benzene.

Section 6.5Broadening and the ν_{11} Band

The question of the shape of the broadened band contours will now be dealt with. A plot on "Lorentzian axes" of the central part of the ν_{11} band of benzene dissolved in methyl iodide is to be seen in Fig. 6.9. The contour is seen not to be a Lorentzian function near the band centre. From Table 6.3 it is seen that the integrated intensities of the benzene band in different solvents are fairly constant, despite the huge changes in the bandwidth. Also the far wings of the bands are of an exponential nature and the second moments of the broadened bands are not a great deal larger than those for the narrow bands. All these facts point to the broadened band contour being a convolution of the unperturbed narrow band contour, by an exponential decay function. The reasoning behind this is that :

- a) convolution re-distributes intensity without changing the total intensity
- b) the second moment of a convoluted band is equal to the sum of the second moments of the original band and the convoluted band. The second moment of an exponential function is finite and has been calculated in Appendix I.
- c) the wings of the broadened bands remain exponential in character

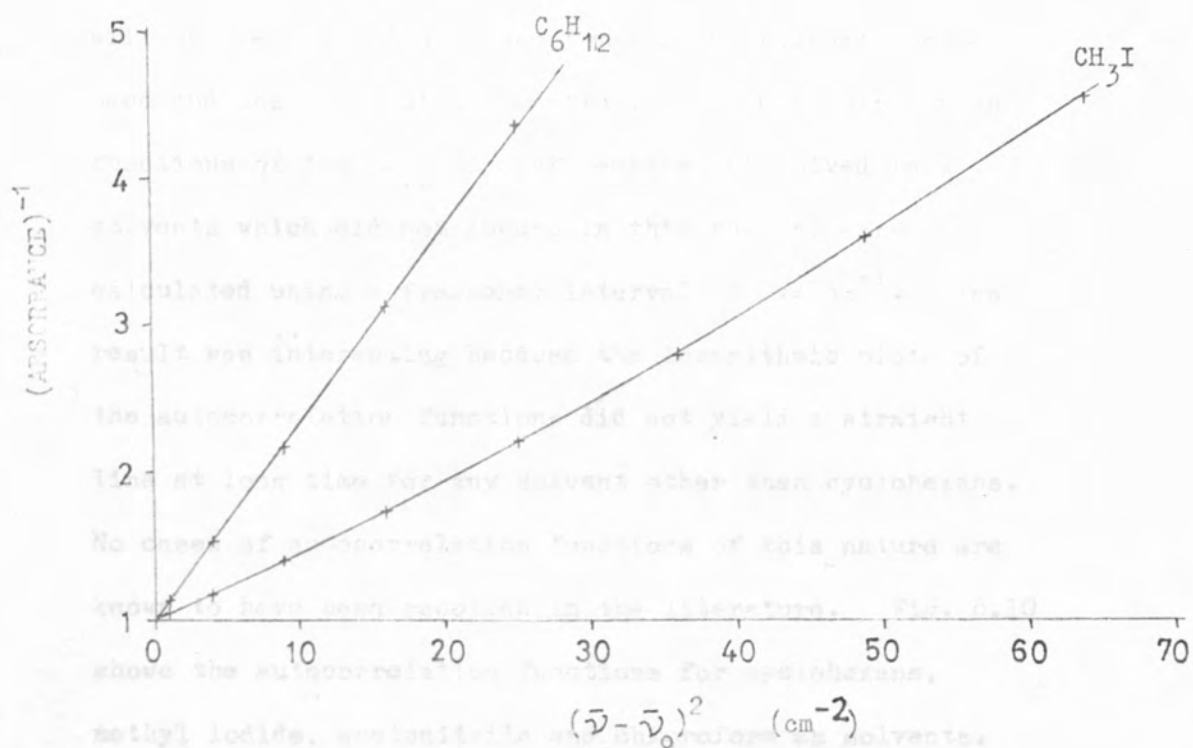


Fig. 6.9 The plots are of the low frequency side of the ν_{11} band of benzene dissolved in cyclohexane and dissolved in methyl iodide. The Lorentzian function character of the two bands is compared.

To investigate the proposed exponential convolution, the ratio of the autocorrelation function for methyl iodide as solvent to that for cyclohexane as solvent, was later. An exponential convolution in the frequency domain is a multiplication by a Lorentzian in the time domain. Thus, the inverse of the above ratio was

Assuming we do have an exponential convolution then the Fourier transform of the broadened band contour will be the product of those for the unperturbed narrow band and the convoluting function. The autocorrelation functions of the ν_{11} band of benzene, dissolved in solvents which did not absorb in this region, were calculated using a frequency interval of 0.4 cm^{-1} . The result was interesting because the logarithmic plots of the autocorrelation functions did not yield a straight line at long time for any solvent other than cyclohexane. No cases of autocorrelation functions of this nature are known to have been recorded in the literature. Fig. 6.10 shows the autocorrelation functions for cyclohexane, methyl iodide, acetonitrile and chloroform as solvents. Fig. 6.11 shows those for acetone, carbon tetrachloride and the pure liquid. The autocorrelation function for chloroform as solvent appears to be different from the others, as it crosses them. This case will be dealt with in a later section.

To investigate the proposed exponential convolution, the ratio of the autocorrelation function for methyl iodide as solvent to that for cyclohexane as solvent, was taken. An exponential convolution in the frequency domain is a multiplication by a Lorentzian in the time domain. Thus, the inverse of the above ratio was

Fig.6.10 The plots are for the ν_{11} band of benzene in various solvents.

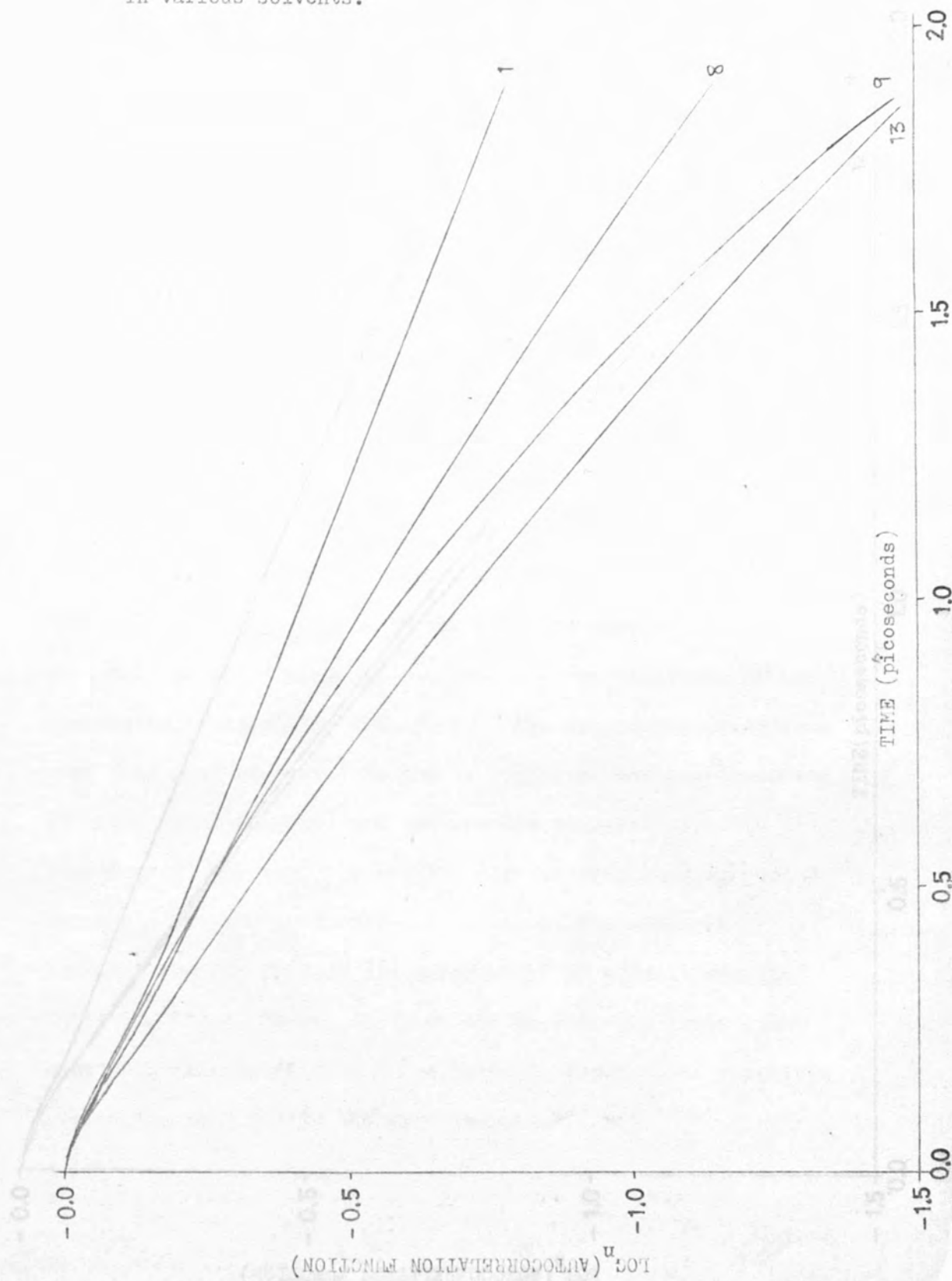
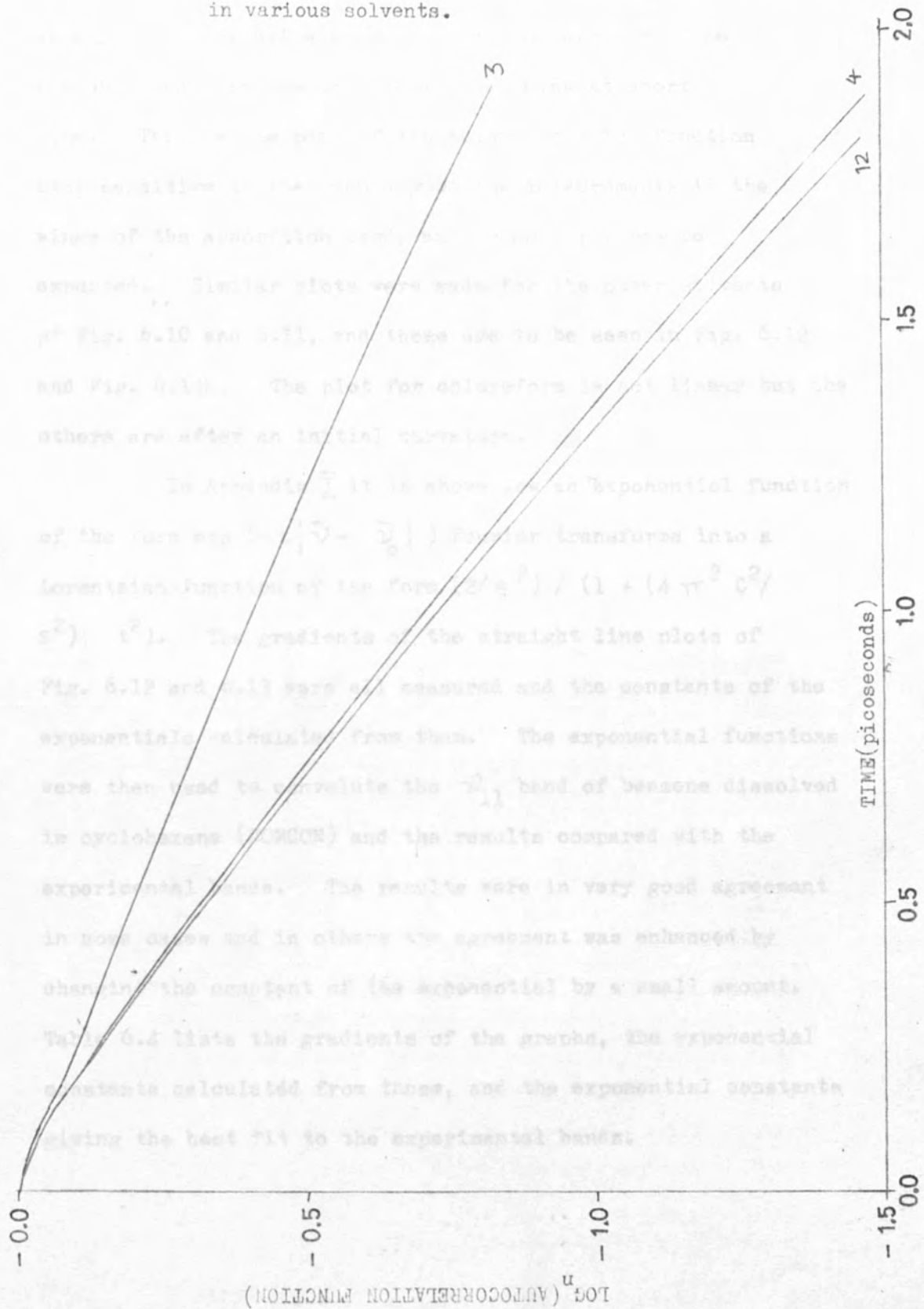


Fig. 6.11 The plots are for the ν_{11} band of benzene in various solvents.



plotted against $(\text{time})^2$, to see if a straight line was obtained. Fig. 6.13a shows that a good straight line was obtained with the only deviation being at short time. This is the part of the autocorrelation function most sensitive to the accuracy of the measurements in the wings of the absorption band, and so an error may be expected. Similar plots were made for the other solvents of Fig. 6.10 and 6.11, and these are to be seen in Fig. 6.12 and Fig. 6.13b. The plot for chloroform is not linear but the others are after an initial curvature.

In Appendix I it is shown how an exponential function of the form $\exp(-s|\bar{\nu} - \bar{\nu}_0|)$ Fourier transforms into a Lorentzian function of the form $(2/s^2) / (1 + (4\pi^2 c^2 / s^2) t^2)$. The gradients of the straight line plots of Fig. 6.12 and 6.13 were all measured and the constants of the exponentials calculated from them. The exponential functions were then used to convolute the ν_{11} band of benzene dissolved in cyclohexane (COMCON) and the results compared with the experimental bands. The results were in very good agreement in some cases and in others the agreement was enhanced by changing the constant of the exponential by a small amount. Table 6.4 lists the gradients of the graphs, the exponential constants calculated from these, and the exponential constants giving the best fit to the experimental bands.

Fig. 6.12

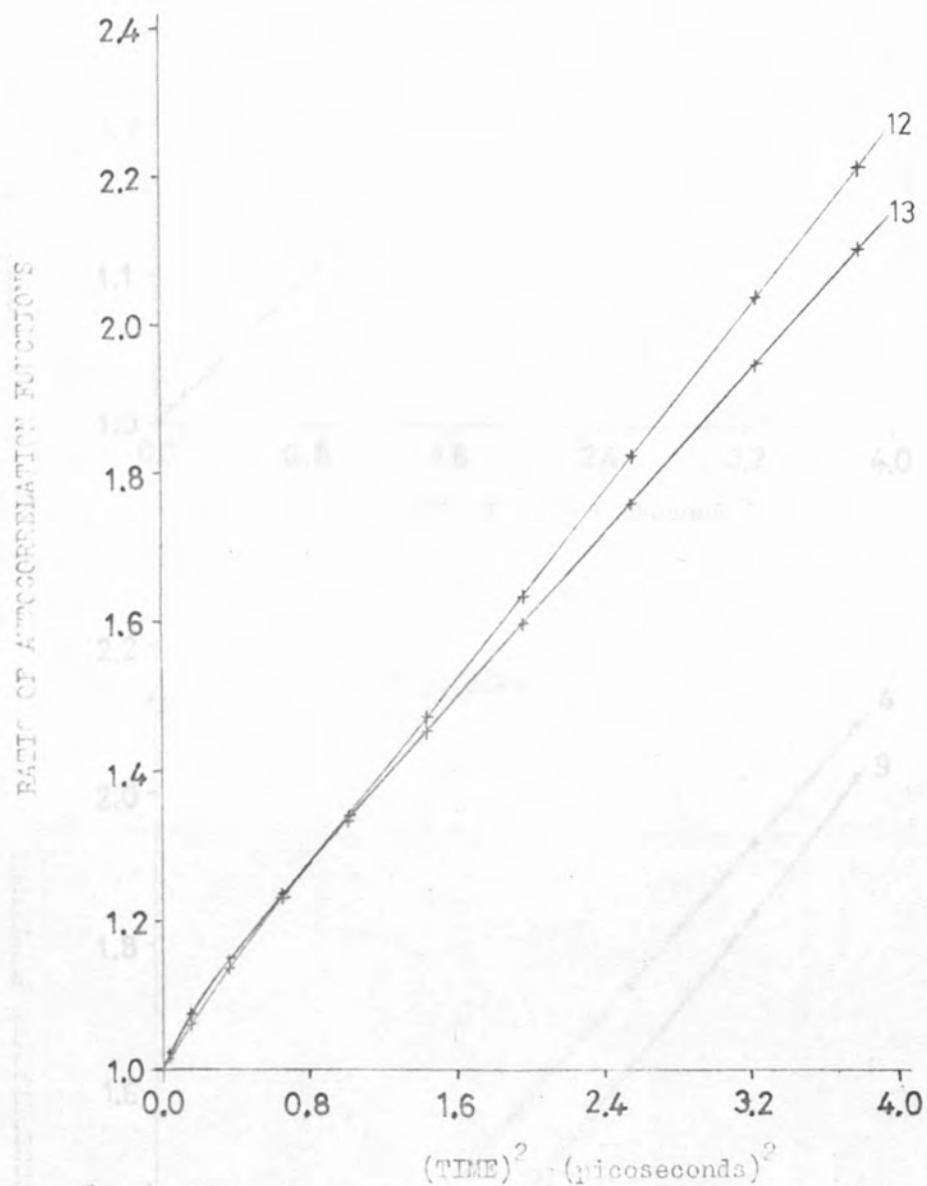


FIG. 6.12/13a/13b are all plots for the ν_{11} band of benzene in different solvents. The ratio of the autocorrelation function for cyclohexane as solvent to that for the solvents numbered in the graphs is plotted to see if it resembles a Lorentzian function.

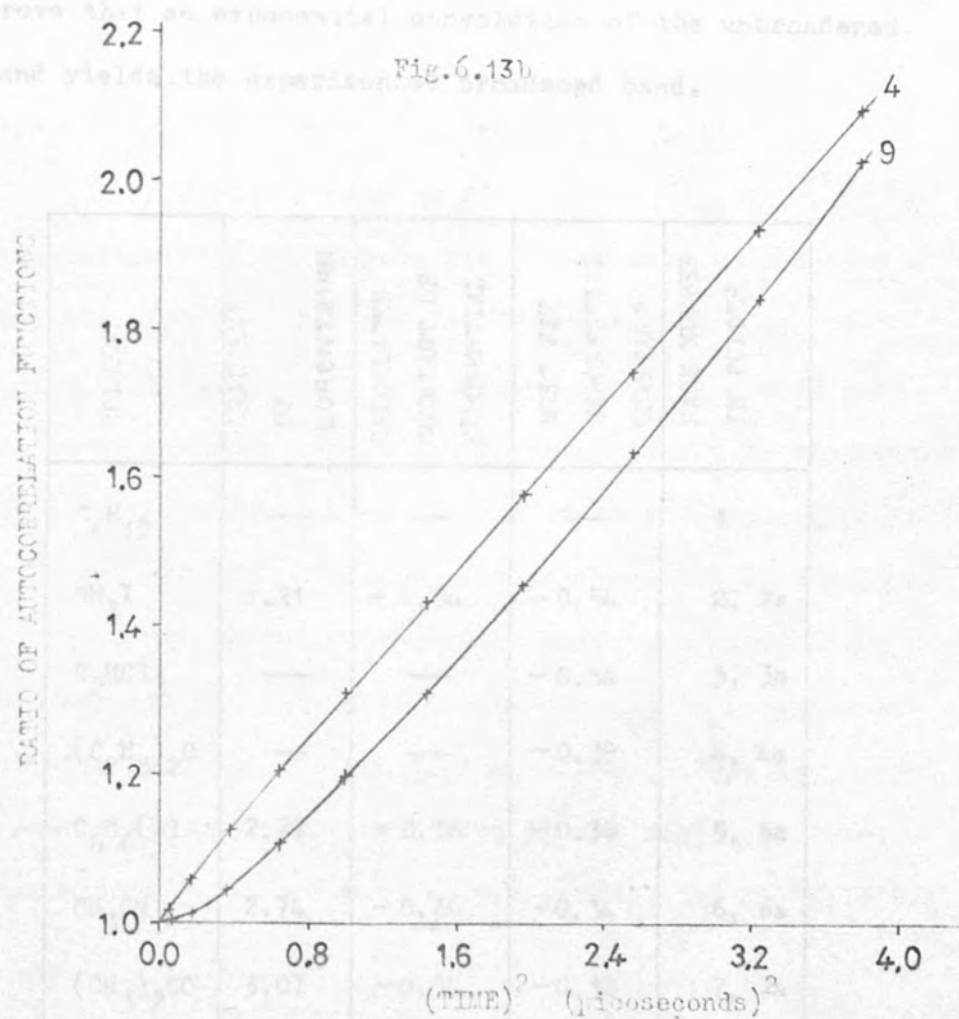
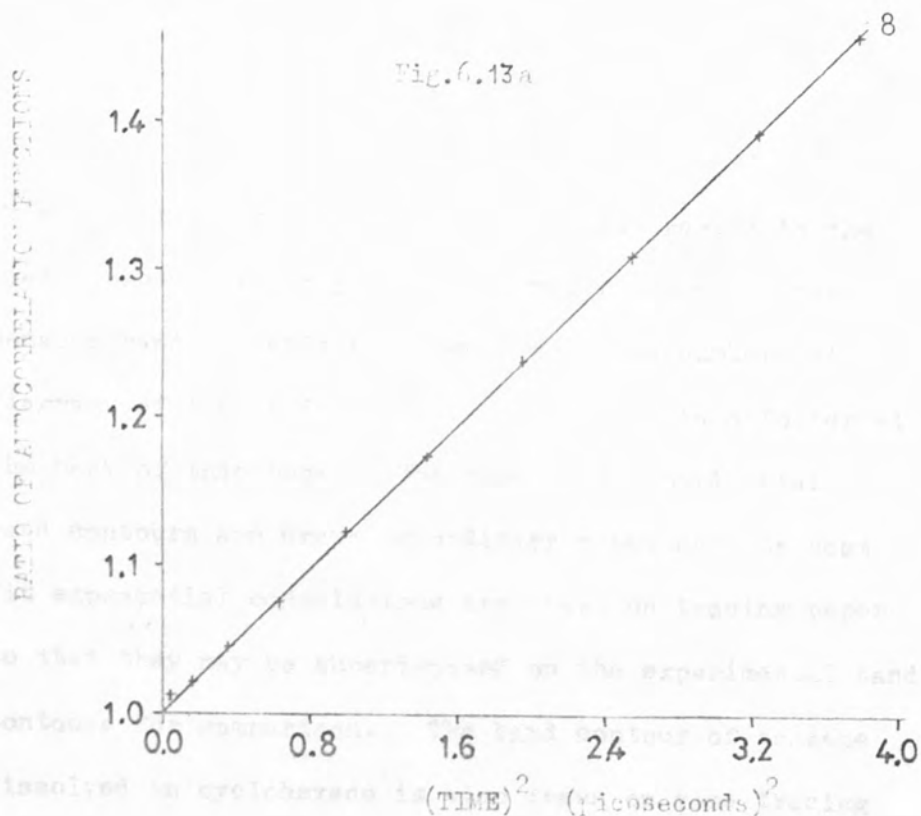


Table 6.4

Trichloroethylene and diethyl ether are present in the list because they only absorb in the far wing of the benzene band. Table 6.4 also lists page numbers of diagrams of the band contours to be found in a folder at the back of this book. The broadened experimental band contours are drawn on ordinary paper and the best fit exponential convolutions are drawn on tracing paper so that they may be superimposed on the experimental band contours for comparison. The band contour of benzene dissolved in cyclohexane is also drawn on some tracing paper for comparison. It is considered that the results prove that an exponential convolution of the unbroadened band yields the experimental broadened band.

| SOLVENT | GRADIENT OF LORENTZIAN | CALCULATED CONSTANT OF EXPONENTIAL | BEST FIT EXPONENTIAL CONSTANT | PAGE NUMBER IN FOLDER |
|---------------|------------------------------|--|-------------------------------------|--------------------------|
| C_6H_{12} | — | — | — | 1 |
| CH_3I | 1.21 | - 0.54 | - 0.54 | 2, 2a |
| C_2HCl_3 | — | — | - 0.54 | 3, 3a |
| $(C_2H_5)_2O$ | — | — | - 0.39 | 4, 4a |
| $C_6H_6(1)$ | 2.77 | - 0.36 | - 0.36 | 5, 5a |
| CH_3CN | 2.74 | - 0.36 | - 0.34 | 6, 6a |
| $(CH_3)_2CO$ | 3.07 | - 0.34 | - 0.32 | 7, 7a |

Table 6.4

Section 6.6

Broadening and the Combination Bands

The $\nu_5 + \nu_{17}$ and $\nu_{10} + \nu_{17}$ combination bands of benzene could not have their Fourier transforms calculated accurately to determine the constant for an exponential to broaden them with, because of overlapping bands. The two bands had to be dealt with on a trial and error basis. Another drawback was that these bands could not be accurately measured in cyclohexane. This did not prevent the work from going ahead because the convolution has the property of association, and the convolution of an exponential function by another exponential yields an exponential. Thus, the accurate spectra for benzene dissolved in carbon tetrachloride were used as a starting place for the broadening.

The high frequency side of the $\nu_{10} + \nu_{17}$ combination band of benzene has a weak band in the near wing and also the high and low frequency sides of the $\nu_5 + \nu_{17}$ combination band of benzene each have a weak band in the near wing. These can be seen clearly in the contours of these bands for carbon tetrachloride solutions (in folder at back of book). These weak bands were not strong enough to contribute in intensity at the band centres of these bands but they did not have large frequency shifts in different solvents like the two combination bands. This meant that a good fit could not be achieved in the region of these weak bands. The solvents used are tabulated in Table 6.5

along with the constants of the exponentials used for the convolution and the page numbers of the diagrams in the folder. The exponential convolutions again fit the experimental broadened bands well.

| BAND NUMBER | SOLVENT | CONSTANT OF EXPONENTIAL | PAGE NUMBER IN FOLDER |
|-----------------------|---------------------------|-------------------------|-----------------------|
| $\nu_{10} + \nu_{17}$ | CCl_4 | — | 8 |
| | $\text{C}_6\text{H}_6(1)$ | -0.26 | 9, 9a |
| | CHCl_3 | -0.20 | 10, 10a |
| $\nu_5 + \nu_{17}$ | CCl_4 | — | 11 |
| | C_2HCl_3 | -0.45 | 12, 12a |
| | $\text{C}_6\text{H}_6(1)$ | -0.32 | 13, 13a |
| | CHCl_3 | -0.29 | 14, 14a |
| | CH_3CN | -0.13 | 15, 15a |

Table 6.5

Section 6.7

Three Component Solutions

Cyclohexane was added to the solution of benzene and methyl iodide and the ν_{11} band was re-measured. This was done for a series of dilutions by cyclohexane. There was a decrease in the bandwidth and the frequency lowered towards that for cyclohexane solution. Table 6.6 shows the results for a series of concentrations and also shows how the percentage change in the shift and percentage change in the bandwidth vary with percentage of cyclohexane present. It is to be seen that $\bar{\nu}_0$ changes roughly linearly with the concentration of cyclohexane, but the broadening remains comparatively larger. The fact that the broadening decreases implies that the interaction is of an electrostatic nature, rather than a separate complex but, because the bandwidth does not decrease as fast as the frequency shift there is the possibility that the methyl iodide may have a preferred orientation relative to benzene, in such a position that it is remote from the hydrogens of the benzene ring. This would appear consistent with the methyl iodide sitting above the π electron layer of the benzene as shown in Fig. 6.14a.

| BAND CENTRE OF ν_{11} BAND (cm^{-1}) | $\Delta \bar{\nu}_{\frac{1}{2}}$ (cm^{-1}) | CONCENTRATION OF C_6H_{12} (mol dm^{-3}) | % SHIFT OF BAND CENTRE RELATIVE TO CH_3I AND C_6H_{12} | % CHANGE IN $\Delta \bar{\nu}_{\frac{1}{2}}$ RELATIVE TO CH_3I AND C_6H_{12} | % OF MOLES OF C_6H_{12} PRESENT |
|---|--|---|---|--|---|
| 680.10 | 7.4 | 0.000 | 0.0 | 0.0 | 0.0 |
| 677.85 | 7.0 | 4.550 | 40.9 | 12.9 | 49.5 |
| 676.05 | 6.2 | 7.329 | 73.7 | 38.7 | 79.7 |
| 675.40 | 5.4 | 8.139 | 85.5 | 64.5 | 88.5 |
| 675.00 | 4.7 | 8.633 | 92.7 | 87.1 | 93.9 |
| 674.75 | 4.4 | 8.980 | 97.3 | 96.8 | 97.6 |
| 674.60 | 4.3 | 9.196 | 100.0 | 100.0 | 100.0 |

Table 6.6 shows how the band centre and half height bandwidth of the ν_{11} band of benzene vary when going from methyl iodide as solvent to cyclohexane as solvent via three component solutions.

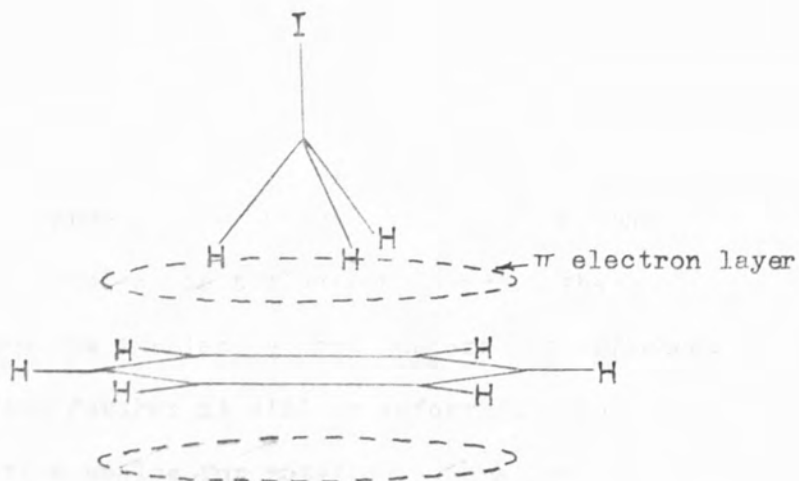


Fig.6.14a depicts a molecule of methyl iodide sitting on the π electron layer of benzene with its dipolar axis perpendicular to the plane of the ring.

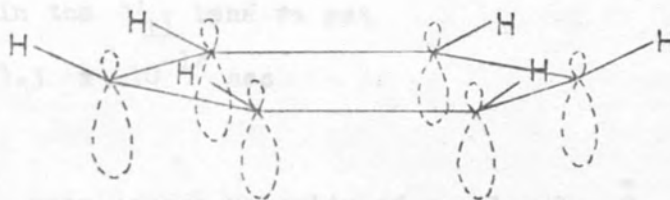


Fig.6.14b shows the probable rehybridisation of the π electron layer of benzene during the waggling mode vibration of the hydrogens.

Section 6.8

Conclusions

The intermolecular interaction producing the broadening must involve the π electron layer of the benzene, because the in-plane vibrations are not affected. Before proceeding further it will be informative to calculate the time scales for rotation, vibration and translation of a molecule. Using benzene as an example we have :-

a) From Chapter Five we know that a molecule of benzene would take about 2 psec per revolution if it were freely rotating.

b) Energy of vibration is given by the equation :-

$$E = \left(v + \frac{1}{2}\right) h\nu$$

So, for the out-of-plane wag of the hydrogens of benzene in the ν_{11} band we get

$$1/\nu = 3.3 \times 10^{-14} \text{ sec}$$

c) The root mean square velocity of a molecule, \bar{C} , is given by the equation :-

$$\bar{C} = (3 kT/m)^{1/2}$$

where m is the mass of the molecule. For benzene, this is equal to $3.1 \text{ \AA} \text{ psec}^{-1}$. The diameter of the benzene ring is about 5 \AA and so this velocity is quite slow on a molecular scale for the time scale of picoseconds we are dealing with.

Thus, on a timescale of 0 to 2 psec, many vibrations take place. Rotations are much slower at the order of 2 psec per rotation and translations are considered as slow enough for a solvent molecule to interact with the benzene.

It has proved difficult to explain the exponential convolution obtained. There is nothing in the literature of this nature. Pure vibrational and relaxation is said to lead to a Lorentzian line shape (70). The following ideas are being put forward which may or may not be realistic.

It is considered that vibrational energy is being transferred to the solvent molecules. This comes about through the formation of a weak "pseudo complex" from an electrostatic attraction between the positive end of the dipolar solvent and the π electron layer of the benzene ring.

The points in the P.M.R. graph of Fig.6.1 for CH_3I , CH_3NO_2 , CH_3CN and CHCl_3 may be seen to parallel those points in the infra-red graphs of Fig.6.3. The timescale for P.M.R. is about 10^{-6} sec compared with 10^{-12} sec for infra-red. It follows that the P.M.R. results indicate that these "pseudo complexes" may exist for 10^{-6} sec or more. Assume that a solvent molecule is trapped for a time of this magnitude but which is also proportional to its dipole moment. During this time many vibrations take place and there is the possibility of transfer of vibrational energy. Now, it has been suggested (81) that the π electron layer of benzene flows from one side of the plane of the benzene ring to the other,

in phase with the γ wagging motion of the hydrogens. See Fig. 6.14b. This flow of electrons is due to rehybridisation at the carbon atom from SP^2 to SP^3 which is brought about by C-H bond approaching a tetrahedral orientation with respect to the neighbouring C-C bonds of the benzene ring at the limits of C-H wag. The solvent molecule may be thought of as riding the π electron layer as it vibrates and energy is transferred to the solvent molecule which is taken up as translational kinetic energy. Molecular speeds follow a Gaussian distribution (71) and kinetic energy is equal to $(\frac{1}{2} \times \text{mass of molecule} \times \text{speed}^2)$ which means that the distribution of translational energy is of an exponential form. It is thought that the quantity of energy transferred to the solvent molecule is determined by the translational kinetic energy the solvent molecule had before being trapped. The quantity of energy transferred thus follows an exponential decay function and this leads naturally to an exponential convolution of the original unbroadened band.

Earlier in this chapter it was seen that the amount that the three measured out-of-plane bands broadened out appeared to increase linearly with frequency. The above model for the complexing is consistent with this. If the solvent molecule is "complexed" for a certain time, then during this time

the numbers of vibrations which take place for the three vibrations will be in the ratio of 1960 : 1816 : 680 (for methyl iodide). If transfer of energy takes place with each vibration then more energy is likely to be transferred in the higher frequency vibrations, leading to greater broadening. It should be noted that increased broadening with frequency is not consistent with the possibility of this broadening being due to an uncertainty broadening, resulting from breaking and forming of a complex at a similar rate to the rate of vibration.

Now consider the shift in frequency of the band. The electrostatic interaction between the π electron layer and the solvent molecule would hinder the flow of the π electron layer during the wagging of the hydrogens. This hindering would be proportional to the dipole moment of the solvent molecule and manifest itself as a shift to higher frequency. This idea is seen to be far removed from La Lau's model.

These ideas do not explain the small amount of broadening produced when CS_2 and CCl_4 are used as solvents. Nevertheless, as one of the solvent molecules translates slowly past a benzene molecule there is still time for transfer of some energy. Also, repulsion between the sulphur or chlorine and the π electron layer would still lead to a hindering of the flow of electrons during the vibration, and still give a shift to higher frequency.

It is thought that 1,4 dioxane arranges itself in a boat conformation (see Fig. 6.15a) above the benzene ring and is held there through electrostatic interaction as a stronger "complex" than the previous cases. The dioxane stays "complexed" for a longer time and the broadening is thus larger.

The same ideas can be applied to liquid benzene, where different molecules may associate above each other for a short time whilst vibrating in phase with each other.

For the ν_{11} band of benzene, the rotations observed are about the x and y axes. The rotation about these axes may be expected to be hindered by the weak interactions above and below the ring. This would lead to an increased fourth moment which would yield a larger mean squared torque compared with the case for cyclohexane. The fourth moment results are seen to be consistent with this.

Lack of time prevented any variable temperature work being carried out and it is suggested that this is carried out to obtain a further understanding of these systems.

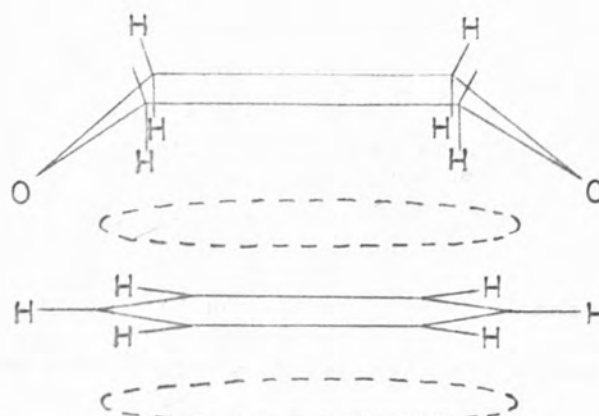


Fig.6.15a shows the possible orientation of 1,4 dioxane above the benzene ring. There would be a strong electrostatic interaction between the two oxygen atoms of the dioxane and the "end" hydrogens of the benzene, and also between the four hydrogens beneath the dioxane and the π electron layer.

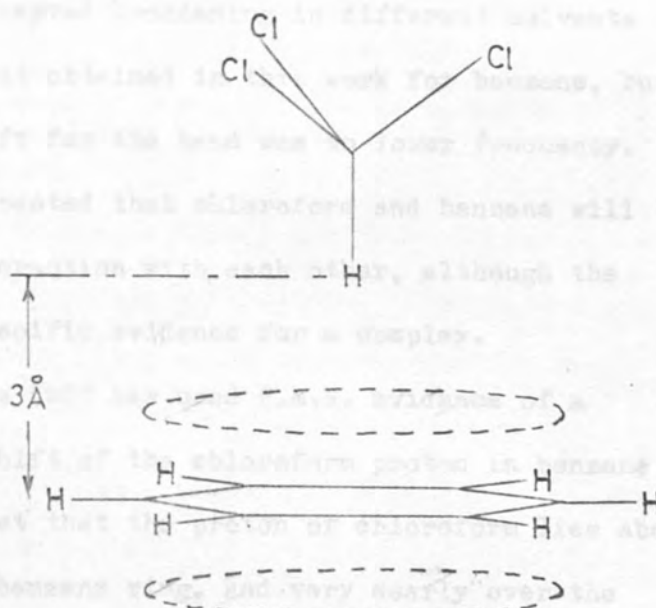


Fig.6.15b shows the suggested preferred orientation for chloroform above a benzene ring (62).

Section 6.9

Evidence for the Formation of Weak
Complexes between

- a) Benzene/Chloroform, and,
- b) Benzene/Hexafluorobenzene.

a) Winstein & Lucas (61) postulated in 1939 that an aromatic nucleus was an electron donor and, therefore, a Lewis base. They measured the heat of mixing for benzene and chloroform and determined that association between benzene and chloroform molecules occurred in the ratio of 1 : 1.

It was found that Whiffen (77) had observed broadening in the C-Cl stretching vibration of chloroform in various polar and non-polar solvents which included benzene. The observed broadening in different solvents was similar to that obtained in this work for benzene, but the frequency shift for the band was to lower frequency. Thus it may be expected that chloroform and benzene will have a strong interaction with each other, although the work showed no specific evidence for a complex.

Huntress (62) has used P.M.R. evidence of a large anomolous shift of the chloroform proton in benzene solution to suggest that the proton of chloroform lies above the plane of the benzene ring, and very nearly over the centre of the ring. The distance of the chloroform proton from the plane of the benzene ring is $3\overset{\circ}{\text{A}}$, calculated from this chemical shift, indicating that the most probable

structure for the complex is one in which the chloroform symmetry axis is perpendicular to the plane of the benzene ring as shown in Fig. 6.15b.

The evidence is thus for a weak complex which exists for a finite time in a definite configuration, but which is not visible using P.M.R. and thus has a shorter lifetime than the P.M.R. timescale. Rothschild (63) has looked at chloroform and benzene in a 1 : 1 mixture using infra-red and has compared the autocorrelation functions of bands of chloroform with those obtained from a chloroform and carbon disulphide solution. Because the short time behaviors of the two sets of autocorrelation functions did not change, Rothschild concluded that a concrete complex did not exist, or the ability for the chloroform to rotate about its x and y axes would be suppressed.

There is thus no evidence for true complex formation between chloroform and benzene. There is a paper as recent as 1973 (80) which disputes whether there is a complex at all.

b) There is much evidence in the literature in favour of the formation of a 1 : 1 complex between benzene and hexafluorobenzene (H.F.B.). Patrick and Prosser (64) have shown that H.F.B. forms 1 : 1 molecular complexes with several aromatic compounds in the solid state. They suggested that the complexes were of a charge transfer type with the aromatic hydrocarbon acting as the donor and H.F.B. as the acceptor. Additional evidence for a complex has been obtained from measurements of heats of mixing (65), vapour pressure in the gas (66) and liquid (67) states, and refractive indices (68). Gaw and Swinton (67) suggested that there was a purely electrostatic interaction, the most probable being a dipole - quadrupole interaction, the C-F bond dipoles of H.F.B. interacting with the π electron quadrupole of the aromatic hydrocarbon. Such an interaction would produce a maximum attractive force when the planes of the two molecules are parallel.

Barrett (69) has observed the 215 cm^{-1} band of H.F.B. in benzene and observed it to be broadened compared with when H.F.B. is dissolved in inert solvents. He explained this broadening as being due to the complex rapidly breaking and forming and that vibrational energy was transferred in every dissociative act. Assuming that there was no vibrational relaxation in the system with an inert solvent, this vibrational relaxation manifested

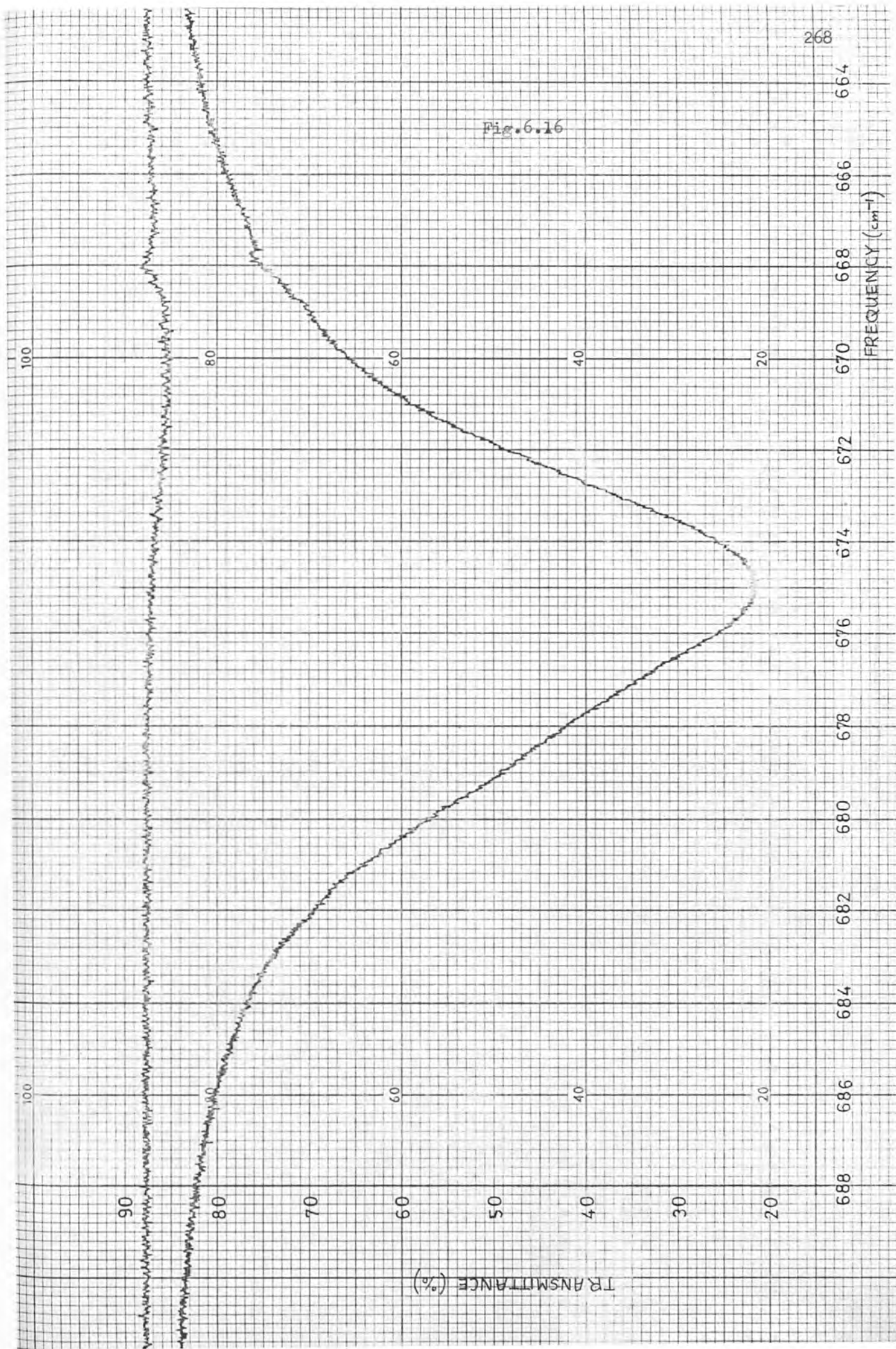
itself in the autocorrelation function as multiplication by an exponential, $\exp(-\beta_V)$, where β_V is associated with the vibrational relaxation. It has been suggested (70) that the vibrational relaxation is exponential and the total autocorrelation function, $C_T(t)$, is the product of the vibrational relaxation, $C_V(t)$ and the reorientational relaxation $C_R(t)$, so that we have at long time :-

$$C_T(t) = \exp(-\beta_R(t)) \exp(-\beta_V(t))$$

where $\beta_R(t)$ refers to the orientational relaxation of H.F.B. in an inert solvent. Barrett obtained the vibrational relaxation using the above equation and showed that $\beta_V(t)$ was roughly linearly dependent on the concentration of benzene relative to H.F.B. indicating the presence of a complex.

Section 6.10Infra-red Proof of the Existence of
the Benzene/Chloroform Complex and
Benzene/Hexafluorobenzene Complex

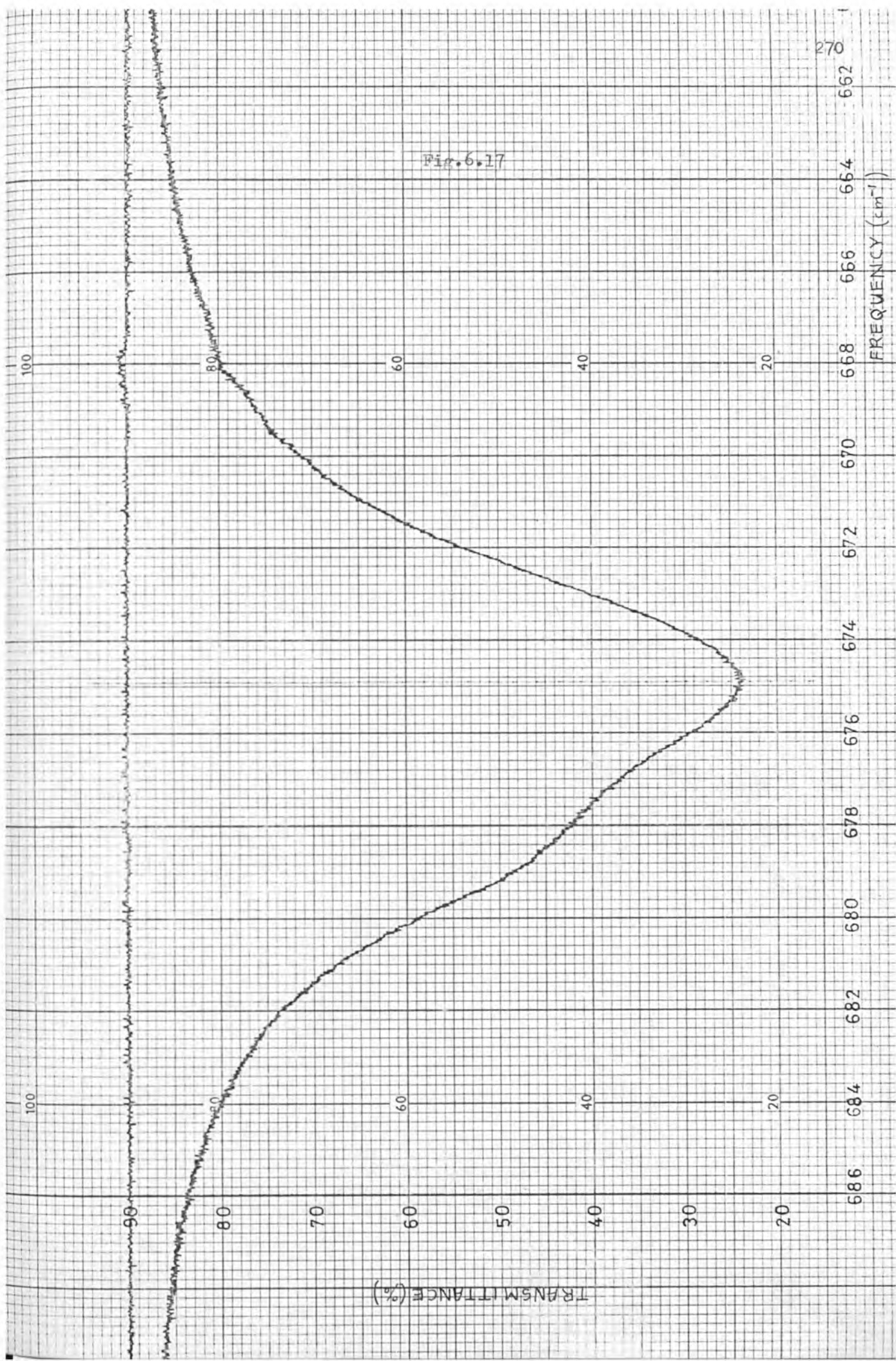
The ν_{11} band of benzene dissolved in chloroform has already been shown to be different in its properties from solutions in other polar solvents. There appeared to be an asymmetry in the high frequency side of the ν_{11} band of benzene dissolved in chloroform. This could not be proved for certain because chloroform has a medium strength band at 667 cm^{-1} which allowed only 7% transmittance in a 0.0028 cm path length cell. It was suspected that this asymmetry could be due to the complex. To explore this possibility cyclohexane was used in making up a new solution with volumes of benzene, chloroform and cyclohexane in the ratio of 1 : 5 : 45 respectively. The 667 cm^{-1} band of the chloroform was thus extremely weak in a 0.0028 cm cell now. The cyclohexane had the effect of narrowing the ν_{11} band and shifting it to lower frequency. In doing so the suspected asymmetry was resolved and it is definitely a new band arising from benzene. The spectrum is to be seen in Fig. 6.16. The main band is centered on 675 cm^{-1} and the new band on 678 cm^{-1} . Further dilution by cyclohexane lead to the disappearance of this new band.



This process was repeated for solutions in H.F.B. The ν_{11} band of benzene was first measured in H.F.B. The band was seen to be very broad, with a half height bandwidth of 8.5 cm^{-1} and with a band centre at 682.3 cm^{-1} . The band looked asymmetric, but the asymmetry was so close to the band centre that it was difficult to say. The band was then remeasured in a three component solution of benzene, H.F.B. and cyclohexane in the ratio of 1 : 10 : 50 by volume. The result is to be seen in Fig. 6.17. The second band is resolved much more clearly than for the chloroform/benzene case. The new band is again centered around 678 cm^{-1} although it was centered around 682 cm^{-1} before adding cyclohexane. The new band again disappeared on further dilution by cyclohexane.

Tamres and Yarwood (82) have stated that π -donor complexes can be expected to lead to a change in frequency on complexation and the observation of a new band due to the charge transfer complex. Person (83) adds that strong electrostatic interactions may lead to a similar frequency shift to that for the complex, resulting in weak charge transfer bands being masked by the electrostatic band.

Fig. 6.17



These facts are in keeping with the observations made on the ν_{11} band of benzene in chloroform and H.F.B. systems. It is thus thought that this work shows concrete evidence for the above mentioned complexes. The lifetimes of these complexes must be of the order of 10^{-12} seconds and longer. The P.M.R. timescale is of the order of 10^{-6} seconds and does not show concrete evidence of a complex, so the lifetime of the complex may be expected to be between these two limits.

Lack of time has again precluded further investigation of these systems. Vibrational force constant analysis on benzene should lead to a predicted frequency for the perturbed ν_{11} band during charge transfer. It is also expected that the relative intensities of the "complexed" ν_{11} band to the original ν_{11} band, in three component solutions with cyclohexane, may lead to an equilibrium constant for the complexing.

CHAPTER SEVEN Additional Work

Section 7.1 Vibrational Relaxation

During the course of this work several papers have been published concerning vibrational relaxation, which consider that it contributes a lot towards infra-red and Raman band contours, although Gordon considered it to be negligible. Morawitz and Eisenthal (70) proposed that infra-red bandshapes resulted not only from re-orientational relaxation but also from vibrational relaxation. This vibrational relaxation was said to result from hard collisions which involved energy transfer and de-excitation, whereas re-orientational relaxation results from soft collisions with no de-excitation. These two relaxation mechanisms are assumed to be independent of one another.

Clark and Miller (78) have proposed a method of separating the vibrational relaxation from the re-orientational relaxation for a Raman band. The depolarisation ratio, ρ , of a Raman band is given, for linearly polarised incident radiation, by the expression :-

$$\rho = 3 \beta'^2(\bar{\nu}) / (45 \bar{\alpha}'^2(\bar{\nu}) + 4 \beta'^2(\bar{\nu}))$$

where $\bar{\alpha}'(\bar{\nu})$ and $\beta'(\bar{\nu})$ are the mean isotropic and anisotropic invariants of the derived molecular polarisability tensor with respect to the molecular vibration (51).

The depolarisation ratio is also equal to the ratio of intensity of radiation scattered with its electric vector perpendicular to that of the incident plane polarised radiation ($I_{\perp}(\bar{\nu})$), to the intensity of that scattered with its electric vector parallel to the incident radiation ($I_{\parallel}(\bar{\nu})$). $I_{\perp}(\bar{\nu})$ is said to be the depolarised component and $I_{\parallel}(\bar{\nu})$ the polarised component of the Raman scattering. We thus have :-

$$\rho = I_{\perp}(\bar{\nu}) / I_{\parallel}(\bar{\nu})$$

We also have :-

$$\begin{aligned} I_{\perp}(\bar{\nu}) &= C_3 \beta^2(\bar{\nu}) (\bar{\nu}_L - \bar{\nu})^4 \\ I_{\parallel}(\bar{\nu}) &= C (45 \bar{\alpha}^2(\bar{\nu}) + 4 \beta^2(\bar{\nu})) \\ &\quad \cdot (\bar{\nu}_L - \bar{\nu})^4 \end{aligned}$$

where C is a constant, $\bar{\nu}_L$ is the frequency of the laser line and $\bar{\nu}$ refers to the Raman spectrum. From the above we get :-

$$\beta^2(\bar{\nu}) = I_{\perp}(\bar{\nu}) / (3 C (\bar{\nu}_L - \bar{\nu})^4) \quad (7.1)$$

$$\bar{\alpha}^2(\bar{\nu}) = \frac{I_{\parallel}(\bar{\nu}) - 4 I_{\perp}(\bar{\nu}) / 3}{45 C (\bar{\nu}_L - \bar{\nu})^4} \quad (7.2)$$

The constant C will be neglected because we are dealing with band shapes. The isotropic and anisotropic band shapes may thus be determined. Bartoli and Litovitz (84) have shown that the isotropic band shape is determined by the

vibrational relaxation and that the anisotropic band shape is determined by the product of the vibrational relaxation and the re-orientational relaxation. The anisotropic band shape is thus a convolution of the vibrational band shape and the re-orientational band shape. Therefore, the vibrational band shape is the same as the isotropic band shape. The re-orientational band shape may be obtained by deconvoluting the anisotropic band shape using the vibrational band shape. However, our concern is with the vibrational band shape. Various workers (84, 85 and 86) have shown that the vibrational band width of condensed phase bands is much larger than was previously thought, using Raman spectroscopy. An example is the ν_3 band of liquid methyl iodide which has a vibrational bandwidth of 4.4 cm^{-1} (86). The vibrational band shape should be the same in the infra-red (84) when a band is both Raman and infra-red active. The infra-red band shape is thus a convolution of the vibrational band shape and the infra-red re-orientational band shape. (In the Raman, rotation-vibration transitions are such that the rotational quantum number changes by 0 or ± 2). The papers looked at all assumed that the vibrational relaxation decay curve was a pure exponential. This is in agreement with experimental spectra which are normally Lorentzian in contour. However, if the vibration relaxation mechanism is through hard collisions, what happens at very short times of less than 0.2 psec ?

Presumably the relaxation curve follows a different path in the same way as for re-orientational relaxation. No mention has been made of this.

The vibrational band shape of the ν_3 band of liquid methyl iodide (86) was assumed to be a Lorentzian function and was used to separate the vibrational relaxation from the re-orientational relaxation for the infra-red band measured in this work. The success of the separation was viewed in terms of the second moment of the frequency spectrum. Examination of the Fourier transform of a Lorentzian function and the properties of convolution shows that the convolution of a Lorentzian function by another Lorentzian function yields another Lorentzian function which has a half height bandwidth equal to the sum of the original functions. The ν_3 band of liquid methyl iodide had a half height bandwidth of $6.4 \pm 0.2 \text{ cm}^{-1}$ (after correcting for the hot band). The half height bandwidth of the vibrational component of the band was $4.4 \pm 0.2 \text{ cm}^{-1}$. The half height bandwidth of the re-orientational component of the band should, therefore, be $2.0 \pm 0.4 \text{ cm}^{-1}$. The second moment of the experimental band was calculated to be 552 cm^{-2} at 119.6 cm^{-1} from the band centre. The second moment of the vibrational component was calculated to be 165 cm^{-2} over this frequency range (calculated using equation in Appendix I).

From Chapter Five we know that the second moment of the convolution of two functions is equal to the sum of the second moments of the original functions. Thus, the second moment of the re-orientational component of the band was calculated to be 387 cm^{-2} at 119 cm^{-1} from the band centre. This value is still much larger than the theoretical second moment of 220 cm^{-2} .

A computer programme was used to perform the above deconvolution using division of the Fourier transform of the experimental band by that of the vibrational component (DECON 2). The result was the same as the above calculations and also the exponential character of the wings was seen to be destroyed as can be seen in Fig. 7.1. It is not known for certain that a Lorentzian function fits the vibrational component at large frequencies relative to the band centre. It is possible that the vibrational component is an exponential function at large frequency. More accurate Raman data should throw some light of this problem.

The second moment of a Lorentzian function with a half height bandwidth of 6.4 cm^{-1} was calculated to be 238 cm^{-2} at 119.6 cm^{-1} from the band centre.

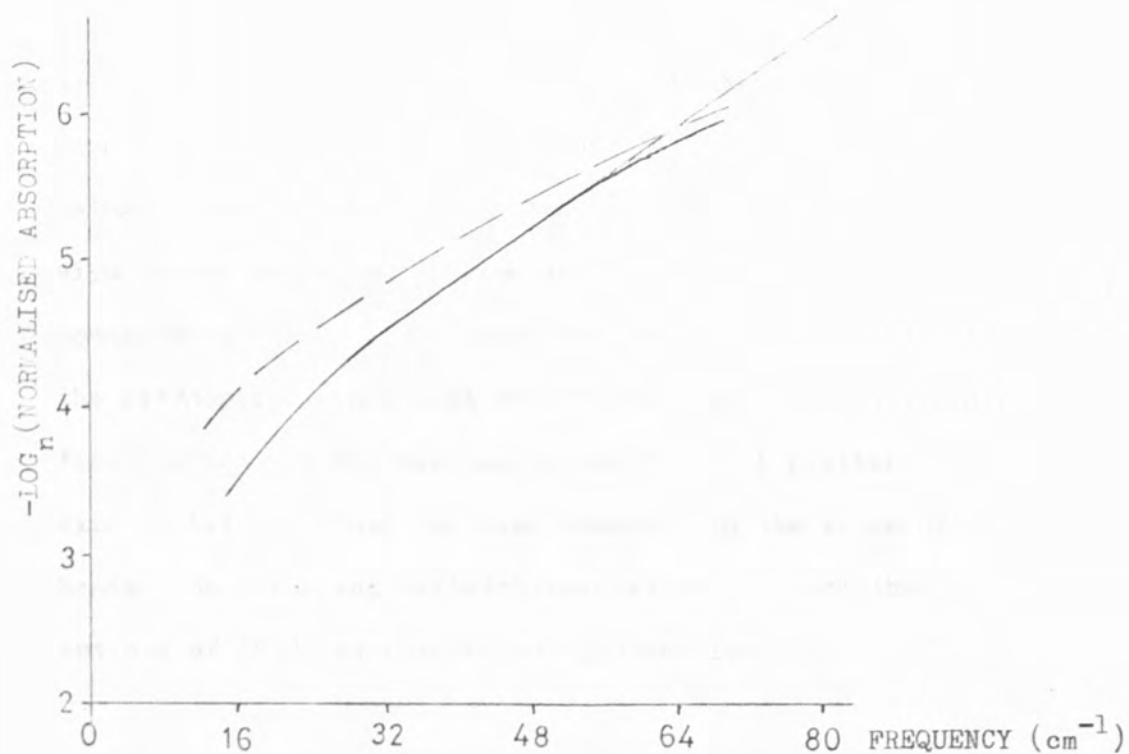


Fig.7.1 The solid line is for the wing of the ν_3 band of liquid methyl iodide, before deconvoluting. The broken line is after deconvoluting.

Although this is not a particularly good example to show, it can be seen that an increased curvature is apparent on the plot after deconvolution. This will always be the case unless an exponential function is used for the deconvolution, or a function which has exponential behavior in the wings.

This yielded a second moment of 314 cm^{-2} for the re-orientational component of the ν_3 bands of liquid methyl iodide. Thus, the high second moment of the experimental band cannot be accounted for by deconvolution using a simple Lorentzian. The author believes that the exponential wings of the experimental band may be connected with the vibrational relaxation. Alternatively, the exponential wings must result from some other broadening factor which has not been accounted for. A similar exponential behaviour has been observed in the wings of bands from Raman and Rayleigh scattering (84) and the authors of (84) are working on this problem.

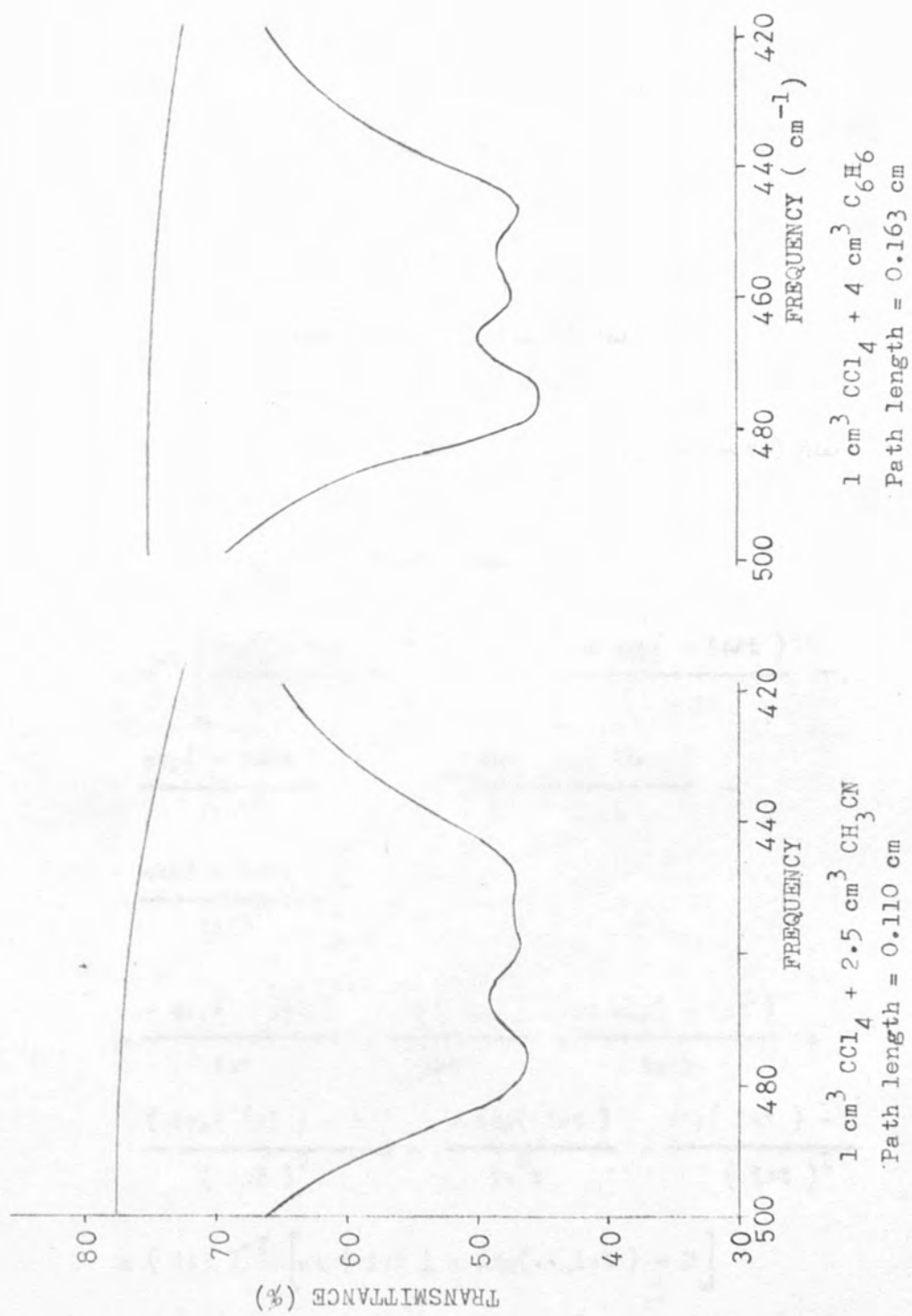
Section 7.2

Use of Carbon Tetrachloride as a Solvent

When measuring the ν_3 band of methyl iodide dissolved in carbon tetrachloride, it was noticed that an absorption was present at around 460 cm^{-1} which was not visible in liquid carbon tetrachloride. This absorption was weak and masked by two overlapping bands at 448 cm^{-1} and 476 cm^{-1} . This weak band was considered of interest because the fully symmetric stretching mode of carbon tetrachloride is at 460 cm^{-1} in the Raman and is not infra-red active (5). The spectra of liquid carbon tetrachloride and solutions of it in cyclohexane, benzene, methyl iodide, and acetonitrile were all measured between 500 cm^{-1} and 420 cm^{-1} . The results are compared in Fig.7.2 and Fig.7.3. The band system is broader for pure carbon tetrachloride, so there may be some absorption at 460 cm^{-1} which cannot be seen in the pure liquid, but is resolved when a solvent narrows the band system. It is to be seen that acetonitrile has had the greatest effect and cyclohexane the least over this frequency range. Acetonitrile is notably the most polar of these solvents. Therefore it would appear that there is a weak interaction between carbon tetrachloride and these solvents. This interaction may last long enough for the vibration at 460 cm^{-1} not to be fully symmetric and so enable it to be observed in the infra-red. This system may be of interest for someone to follow up. Only a superficial observation was made in the course of this work.



Fig. 7.3



APPENDIX I

A mathematical Appendix outlining the integration of
a) Fourier transform integrals and b) second moment integrals
of selected functions encountered in this work.

1. The equation of a triangle of base length $2s$ rad sec^{-1} .
For simplicity ω will be measured relative to the apex
of the triangle.

a) The Fourier transform, $A(t)$:-

$$\begin{aligned}
 A(t) &= s^{-1} \int_{-s}^s (1 - |\omega|/s) \exp(-i\omega t) d\omega \\
 &= s^{-1} \int_{-s}^s \exp(-i\omega t) d\omega - s^{-2} \int_0^s \exp(-i\omega t) d\omega \\
 &\quad + s^{-2} \int_{-s}^0 \omega \exp(-i\omega t) d\omega \\
 &= s^{-1} \left[\frac{\exp(-i\omega t)}{-it} \right]_{-s}^s - s^{-2} \left[\frac{\omega \exp(-i\omega t)}{-it} - \right. \\
 &\quad \left. \frac{\exp(-i\omega t)}{(it)^2} \right]_0^s + s^{-2} \left[\frac{\omega \exp(-i\omega t)}{-it} - \right. \\
 &\quad \left. \frac{\exp(-i\omega t)}{(it)^2} \right]_0^{-s} \\
 &= \frac{-\exp(-ist)}{ist} + \frac{\exp(ist)}{ist} + \frac{s \exp(-ist)}{is^2 t} + \\
 &\quad \frac{(\exp(ist) - 1)}{(ist)^2} - \frac{s \exp(ist)}{is^2 t} + \frac{\exp(ist) - 1}{(ist)^2} \\
 &= (ist)^{-2} \left[\exp(ist) + \exp(-ist) - 2 \right]
 \end{aligned}$$

$$= \left[\frac{\exp(ist/2) - \exp(-ist/2)}{ist} \right]^2$$

$$A(t) = \left[\frac{\sin(st/2)}{(st/2)} \right]^2$$

2. An exponential decay function expressed in wavenumbers relative to the centre of the function, $f(\bar{\nu}) = \exp(-s|\bar{\nu}|)$.

a) The Fourier-transform, $F(t)$:-

$$F(t) = \int_{-\infty}^{+\infty} \exp(-s|\bar{\nu}|) \exp(-i2\pi c \bar{\nu} t) d\bar{\nu}$$

$$= 2 \int_0^{+\infty} \exp(-s\bar{\nu}) \exp(-i2\pi c \bar{\nu} t) d\bar{\nu}$$

$$= 2 \operatorname{Re} \int_0^{+\infty} \exp - [(s + i2\pi ct) \bar{\nu}] d\bar{\nu}$$

$$= 2 \operatorname{Re} \left[\frac{-\exp - [(s + i2\pi ct) \bar{\nu}]}{s + i2\pi ct} \right]_0^{\infty}$$

$$= 2 \operatorname{Re} (1/(s + i2\pi ct))$$

$$= 2 \left[1/(s + i2\pi ct) \times 1/(s - i2\pi ct) \right]$$

$$F(t) = \frac{2/s^2}{1 + (4\pi^2 c^2/s^2) t^2}$$

$F(t)$ is therefore a Lorentzian function.

b) The second moment, $M(2)$, of the above exponential function is defined by :-

$$\begin{aligned}
 M(2) &= \frac{\int_{-\infty}^{+\infty} \bar{\nu}^2 \exp(-s|\bar{\nu}|) d\bar{\nu}}{\int_{-\infty}^{+\infty} \exp(-s|\bar{\nu}|) d\bar{\nu}} \\
 &= \frac{\int_0^{+\infty} \bar{\nu}^2 \exp(-s\bar{\nu}) d\bar{\nu}}{\int_0^{+\infty} \exp(-s\bar{\nu}) d\bar{\nu}}
 \end{aligned}$$

Firstly consider the numerator :-

$$\begin{aligned}
 \int_0^{+\infty} \bar{\nu}^2 \exp(-s\bar{\nu}) d\bar{\nu} &= \left[-(\bar{\nu}^2/s) \exp(-s\bar{\nu}) \right]_0^{+\infty} + \\
 &\quad \int_0^{+\infty} (2\bar{\nu}/s) \exp(-s\bar{\nu}) d\bar{\nu}
 \end{aligned}$$

$$\text{and } \int_0^{+\infty} (2\bar{\nu}/s) \exp(-s\bar{\nu}) d\bar{\nu} = \left[-(2/s^2) \exp(-s\bar{\nu}) \right]_0^{+\infty} + \\
 \int_0^{+\infty} (2/s^2) \exp(-s\bar{\nu}) d\bar{\nu}$$

$$\text{and } \int_0^{+\infty} (2/s^2) \exp(-s\bar{\nu}) d\bar{\nu} = \left[-(2/s^3) \exp(-s\bar{\nu}) \right]_0^{+\infty}$$

$$\Rightarrow \int_0^{+\infty} \bar{\nu}^2 \exp(-s\bar{\nu}) d\bar{\nu} = 0 + 0 + 2/s^3$$

Now consider the denominator :-

$$\begin{aligned}
 \int_0^{+\infty} \exp(-s\bar{\nu}) d\bar{\nu} &= \left[-\exp(-s\bar{\nu})/s \right]_0^{+\infty} \\
 &= 1/s
 \end{aligned}$$

$$M(2) = \frac{2/s^3}{1/s} = 2/s^2 \text{ cm}^{-2}$$

3. A Gaussian function expressed in wavenumbers relative to the centre of the function, $f(\bar{\nu}) = \exp(-s\bar{\nu}^2)$

a) The Fourier transform $F(t)$:-

$$\begin{aligned} F(t) &= \int_{-\infty}^{+\infty} \exp(-s\bar{\nu}^2) \exp(-i2\pi c\bar{\nu}t) d\bar{\nu} \\ &= 2 \int_{-\infty}^{+\infty} \exp(-s\bar{\nu}^2) \cos(2\pi c\bar{\nu}t) d\bar{\nu} \end{aligned}$$

This integral is of the form $\int \exp(-c^2x^2) \cos(bx) dx$

the solution of which is $(\pi^{1/2}/2c) \exp(-b^2/4c^2)$.

$$\Rightarrow F(t) = (\pi/s)^{1/2} \exp(-\pi^2 c^2 t^2 / s)$$

$F(t)$ is therefore a Gaussian function also.

b) The second moment of the above Gaussian function is defined by :-

$$M(2) = \frac{\int_{-\infty}^{+\infty} \bar{\nu}^2 \exp(-s\bar{\nu}^2) d\bar{\nu}}{\int_{-\infty}^{+\infty} \exp(-s\bar{\nu}^2) d\bar{\nu}}$$

Firstly consider the numerator :-

The numerator is of the form $\int x^{2n} \exp(-ax^2) dx$, which

has the solution of $(\pi/a)^{1/2} 1 \cdot 3 \cdot 5 \dots (2n-1) / (2^{n+1}$

$a^n)$. Therefore we have the solution $(\pi/s)^{1/2} / (4s)$

Now consider the denominator :-

The denominator is of the form $\exp(-a^2 x^2) dx$, which has the solution of $\pi^{1/2}/2a$. Therefore we have the solution $\pi^{1/2}/(2s^2)$.

$$\Rightarrow M(2) = (2s)^{-1} \text{ cm}^{-2}$$

4. A Lorentzian function expressed in wavenumbers relative to the centre of the function, $f(\bar{\nu}) = x_1/(1 + x_3 \bar{\nu}^2)$.

a) The Fourier transform, $F(t)$.

$$\begin{aligned} F(t) &= \int_{-\infty}^{+\infty} (x_1/(1 + x_3 \bar{\nu}^2)) \exp(-i2\pi c \bar{\nu} t) d\bar{\nu} \\ &= 2 \int_0^{+\infty} x_1/(1 + x_3 \bar{\nu}^2) \cos(2\pi c \bar{\nu} t) d\bar{\nu} \end{aligned}$$

This integral is of the form $\int \frac{\cos(mx)}{a^2 + x^2} dx$ which has the solution $(\pi/(2a)) \exp(-|m|a)$.

$$\Rightarrow F(t) = 4\pi x_1 x_3^{-1/2} \exp(-|2\pi ct| x_3^{1/2})$$

$F(t)$ is therefore an exponential function.

The function of the programme is made at the beginning

b) The second moment of the above Lorentzian function is defined by :-

$$M(2) = \frac{\int_0^{+\infty} \bar{\nu}^2 (x_1/(1 + x_3 \bar{\nu}^2)) d\bar{\nu}}{\int_0^{+\infty} x_1/(1 + x_3 \bar{\nu}^2) d\bar{\nu}}$$

The denominator is of the form $\int 1/(a + bx^2) dx$ which has the solution $(ab)^{-1/2} \tan^{-1}(x(ab)^{1/2}/a)$, for $ab > 0$

The numerator is of the form $\int x^2/(a + bx^2) dx$ which has the solution $(x/b) - (a/b) \int 1/(a + bx^2) dx$.

$$\Rightarrow M(2) = \frac{(x_1 \bar{\nu}/x_3) - (1/x_3) \left[(x_3/x_1^2)^{-\frac{1}{2}} \tan^{-1} \left[(x_3/x_1^2)^{\frac{1}{2}} x_1 \right] \right]}{(x_3/x_1^2) \tan^{-1} \left[(x_3/x_1^2)^{\frac{1}{2}} x_1 \right]}$$

If $\bar{\nu}$ is taken out to ∞ , then $M(2)$ can be seen to be ∞ also.

APPENDIX II

Appendix II is an alphabetical list of the programmes used in this work. A brief statement of the function of the programme is made at the beginning of each.

1 CONTINUE

2 ***** INTEGRATION BY TRAPEZIUM RULE

3 SUMF=0.0

4 DO 5 J=1,N

5 SUMF=SUMF+(Y(J)-Y(J-1))*X(J)-X(J-1)/2

6 CONTINUE

7 ***** FINDING FACTOR TO FIT DATA TO GRAPH

8 I=0.0

9 DO 10 J=1,N

10 IF (X(J).GT.E1) F1=X(J)

11 F2=X(J)

12 DO 13 K=1,N

BAKSHV corrects an experimental liquid phase band contour
for the local field effect.

```

PROGRAM BAKSHV(INPUT,OUTPUT)
DIMENSION D(600),D2(600),G(600),XN(600)
REAL IO(600),I(600),KA(600),NU(600),LINE(101),NEWI(600)
DIMENSION FACTOR(10),NL(10)
COMPLEX CN2,CTHE,CN2SO
DATA BLANK,STAR,ZERO,PLUS,DOT/1H ,1H*,1H0,1H+,1H./
C*****FOR WIDE PATH LENGTHS PATH IS KEPT CONSTANT AND 'FACTOR'
READ 106,NN
READ 107,RAD,BN
DO 10 KK=1,NN
READ 101,N
READ 107,FACTOR(KK)
READ 100,CONC,W0,XNE,SLIT,PATH,FIRST,DNU
READ 200,(IO(J),J=NQ,N)
READ 200,(I(J),J=NQ,N)
PRINT 301
PRINT 700,W0,PATH,SLIT,XNE,FIRST
NU(NQ)=FIRST
DO 1 J=NQ,N
K=J+1
1 NU(K)=NU(J)-DNU
DO 7 J=NQ,N
B=IO(J)/I(J)
E=ALOG(B)
7 D(J)=E/(NU(J)*FACTOR(KK))
NL(KK)=N
10 NQ=N+1
PI=3.14159 & AS=1./(4.*PI*PATH)
PISQ=PI**2 & WSO=W0**2
SXNF=XNE**2
DO 55 J=1,N
55 KA(J)=D(J)*AS
DO 2 J=1,N
DO 3 JB=1,N
X=NU(J)**2-NU(JB)**2
IF(X)71,20,71
71 G(JB)=KA(JB)*NU(JB)/X
GO TO 3
20 G(JB)=0.0
3 CONTINUE
C*****INTEGRATION BY TRAPEZIUM RULE
SUMF=0.0 & N2=N-1
DO 6 JC=2,N2
6 SUMF=SUMF+G(JC)
SUMG=(G(1)+2.*SUMF+G(N))*DNU/2.
XN(J)=XNE-2./PI*SUMG
2 CONTINUE
C*****FIND REDUCING FACTOR TO FIT DATA TO GRAPH
E1=0.0
DO 25 J=1,N
25 IF(XN(J).GT.E1) E1=XN(J)
E1=E1+0.1
E2=2.0
DO 26 J=1,N

```

IS USED

```

26 IF(XN(J).LT.E2) E2=XN(J)
E2=E2-0.1
E3=E1-E2
E4=100./E3
C****PLOT GRAPH OF RF AND I .V.NU
PRINT 300
PRINT 601
NA=1
DO 30 IJ=1,101
70 LINE(IJ)=BLANK
L2=IFIX((XN(E2)*E4)
DO 31 J=1,N
LINE(L2)=DOT
M=IFIX(I(J)+0.5)
L=IFIX((XN(J)-E2)*E4)
LINE(M)=STAR
LINE(L)=PLUS
IF(NA.NE.1) GO TO 33
IF(NU(J)-W0-0.5) 32,32,33
72 DO 35 IJ=1,100
75 LINE(IJ)=ZERO
PRINT 600,NU(J),LINE,XN(J),KA(J),I(J)
DO 36 IJ=1,101
76 LINE(IJ)=BLANK
NA=2
GO TO 31
77 PRINT 600,NU(J),LINE,XN(J),KA(J),I(J)
LINE(L)=BLANK
LINE(M)=BLANK
71 CONTINUE
LINE(L2)=BLANK
C****CALCULATE THE CORRECTED EINSTEIN ABSORPTION COEFFICIENT
C****FIELD EFFECT---DUE TO BAKHSHIEV LOCAL
C****RAD IS RADIUS ASSUMING CLOSE PACKING OF SPHERES
C****RN IS THE NUMBER OF MOLECULES OF THE LIQUID PER UNIT VOLUME
PRINT 950,RAD
PRINT 504
A=2.*PI*RN*RAD**3
DO 41 J=1,N
CN2=CMPLX(XN(J),KA(J))
CN2SQ=CN2**2
CTHE=(2.*CN2SQ+1.)/(3.*A*CN2SQ+(CN2SQ-1.）**2)
THE=CABS(CTHE)
THETA=XN(J)*A**2*THE**2
D2(J)=D(J)*THETA
41 CONTINUE
C****GRAPH TO COMPARE NEW AND OLD INTENSITIES
PRINT 300
PRINT 502
PRINT 972
E7=0.0
DO 45 J=1,N
IF(D(J).GT.E7) E7=D(J)
45 IF(D2(J).GT.E7) E7=D2(J)
E7=100./E7
DO 46 J=1,N
THETA=D2(J)/D(J)
L=(D(J)*E7)+1.5
M=(D2(J)*E7)+1.5
LINE(L)=STAR
LINE(M)=PLUS
PRINT 951,NU(J),LINE,THETA
LINE(L)=BLANK
46 LINE(M)=BLANK

```

```

PRINT 700
NQ=1
DO 11 KK=1,NN
LIM=NL(KK)
PRINT 104
DO 12 J=NQ,LIM
E=D2(J)*NU(J)*FACTOR(KK)
NEWI(J)=IO(J)*EXP(-E)
L=NFWI(J)
M=I(J)
IF(L.EQ.M) GO TO 13
LINE(L)=STAR
LINE(M)=PLUS
GO TO 14
13 LINE(L)=ZERO
14 PRINT 103,NU(J),LINE,I(J),NEWI(J)
LINE(L)=BLANK
12 LINE(M)=BLANK
11 NQ=NL(KK)+1
DO 84 J=1,N
84 D(J)=D2(J)
C****RECALCULATE W0 FOR NEW BAND
AA=0.0
DO 96 J=1,N
IF(D(J).LT.AA) GO TO 96
AA=D(J)
JNO=J
96 CONTINUE
W0=NU(JNO)
PRINT 971,W0
STOP
100 FORMAT(7F10.0)
101 FORMAT(I10)
102 FORMAT(E10.0,E10.0)
103 FORMAT(1X,F7.2,1H.,101A1,2X,F6.2,4X,F6.2)
104 FORMAT(113X,' I NEWI'/113X,' - ----')
106 FORMAT(I10)
107 FORMAT(F10.0)
200 FORMAT(16F5.0)
300 FORMAT(1H1)
301 FORMAT(////)
502 FORMAT(30X,'EINSTEIN COEFFICIENT SPECTRUM COMPARED WITH OLD
7UM'/30X,'-----')
7)
503 FORMAT(30X,'EINSTEIN COEFFICIENT SPECTRUM BAND SHAPE COMPARED
7 OLD SPECTRUM'/30X,'-----')
7)
504 FORMAT(///27X,'D D2 THETA
7)
7)
600 FORMAT(1H ,F6.1,2X,1H.,101A1,F6.4,2X,F6.4,2X,F5.2)
601 FORMAT(112X,'XN KA I '/112X,'-- -- -')
700 FORMAT(10X,'W0=',F6.1/10X,'PATH=',F9.7/10X,'SLIT=',F6.4/10X,'
Z,F4.2/10X,'FIRST=',F6.1)
900 FORMAT(1H1,20X,'ONSAGER-ROTTCHER RADIUS OF MOLECULE =',E14.6,
7//)
901 FORMAT(1H ,F6.1,2X,1H.,101A1,F6.4)
970 FORMAT(20X,E16.8,5X,E16.8,5X,F6.4,5X,F8.2)
971 FORMAT(////40X,'NEW W0 =',F7.1,' CM-1')
972 FORMAT(113X,'THETA'/113X,'-----')
END

```

SPECTR

WITH

NU

XNE=

CM'

COMCON convolutes an experimental band contour and plots the result out using a CALCOMP graph plotting routine.

```

PROGRAM COMCON(INPUT,OUTPUT)
DIMENSION D(187),A(187),CHART(101)
DIMENSION TEXT(8),D2XDT2(200),CORIO(200),CORI(200)
REAL KCON(189),NU(189),I(187),IO(187)
DATA C1,C2,C3,C4,C5/0.0,1.0,0.0,0.0,0.0/
DATA STAR,BLANK,PLUS,ZERO/1H*,1H ,1H+,1H0/
NO=1
READ 100,N,FIRST,DELNU,W0,CONC,PATH,SLIT
READ 200,(IO(J),J=NO,N)
READ 200,(I(J),J=NO,N)
READ 300,TEXT
PRINT 400
PRINT 301,TEXT
PRINT 101,N,FIRST,DELNU,W0,CONC,PATH,SLIT
DO 13 J=NO,N
  NU(J)=FIRST
13 FIRST=FIRST+DELNU
  DO 3 J=NO,N
    CORIO(J)=C1+C2*IO(J)+C3*(IO(J)**2)+C4*(IO(J)**3)+C5*(IO(J)**4)
 3 CORI(J)=C1+C2*I(J)+C3*(I(J)**2)+C4*(I(J)**3)+C5*(I(J)**4)
  PRINT 400
  PRINT 601
  DO 4 J=NO,N
4 D2XDT2(J)=0.0
  M=N-6
  DO 5 J=NO,M
5 D2XDT2(J+3)=(CORI(J+6)-CORI(J+4)-CORI(J+2)+CORI(J))/(8.*DELNU
  ZS1=SLIT**2/12.
  DO 7 J=NO,N
  XIO=IO(J)
  XI=I(J)
  CZS1=ZS1*D2XDT2(J)
  I(J)=CORI(J)-CZS1
  IO(J)=CORIO(J)
A7 PRINT 600,NU(J),XIO,XI,CORIO(J),CORI(J),D2XDT2(J),CZS1,I(J)
  DO 1 J=1,N
  B=IO(J)/I(J)
  E=ALOG(B)
 1 D(J)=E/(NU(J)*CONC*PATH)
  DO 16 J=1,N
  DO 17 JK=1,N
  XNL=NU(JK)-NU(J)
17 A(JK)=D(JK)*EXP(-ABS(XNU)*0.13)
  F=0.0 & M=N-1
  DO 18 JM=2,M
18 F=F+A(JM)
16 KCON(J)=(A(1)+2.*F+A(N))*ABS(DELNU)/2.
  X=0.0
  DO 14 J=1,N
14 IF(KCON(J).GT.X) X=KCON(J)
  DO 15 J=1,N
15 KCON(J)=KCON(J)/X
C****PLOT GRAPH
PRINT 400
DO 22 IJ=1,101

```

292

```

22  CHART(IJ)=BLANK
    DO 21 J=1,N
    L=KCON(J)*100.+1.0
    CHART(L)=STAR
    PRINT 500,NU(J),CHART,KCON(J)
21  CHART(L)=BLANK
    NU(188)=1900.0 & NU(189)=10.0
    KCON(188)=0.0 & KCON(189)=1.0/7.0
    CALL START
    CALL PLOT(1.0,1.0,-3)
    CALL AXIS(0.0,0.0,10,HABSORBANCE,-10,7.0,0.0,KCON(188),KCON
    CALL AXIS(0.0,0.0,7,HNU CM-1,7,9.35,90.0,NU(188),NU(189))
    CALL LINE(KCON,NU,187,1,0,1)
    CALL ENPLOT(9.0)
    STOP
100  FORMAT(I10,6F10.0)
101  FORMAT(20X,'N=',I5/20X,'FIRST=',F8.2,' CM-1'/20X,'DELNU=',
    ZM-1'/20X,'WO=',F8.2,' CM-1'/20X,'CONC=',E16.8,' MOLES/LITRE'
    ZPATH=',F10.6/20X,'SLIT=',F8.2,' CM-1')
200  FORMAT(16F5.0)
300  FORMAT(8A10)
301  FORMAT(/20X,8A10)
400  FORMAT(1H1)
500  FORMAT(1H ,F8.2,1X,101A1,2X,E12.5)
600  FORMAT(10X,F8.2,5X,F8.2,5X,F8.2,5X,F8.2,5X,F8.2,5X,F10.5,3X
    Z5X,F8.2)
601  FORMAT(15X,'NU',11X,'IO',11X,'I',10X,'CORIO',8X,'CORI',9X,'
    Z,5X,'2ND ORDER COR',4X,'NEWI')
    END

```

CORSILT simulates a typical condensed phase infra-red transmitted intensity curve. This curve is then convoluted using a triangular slit function, and then deconvoluted using the second derivative method.

```

PROGRAM CORSILT(INPUT,OUTPUT)
DIMENSION D2XDT2(1000),DMXDTM(1000),Y(1000)
REAL K(1000),NU(1000),LINE(101),ICON(1000),INEW(1000),IRAN
REAL ILOR(1000),IRNEW(1000)
DATA STAR,BLANK,PLUS,ZERO/1H*,1H ,1H+,1H0/
DO 30 KK=1,3
READ 104,N,X1,X3,DELNU,S,W0
VHALF=SQRT(4./X3)
PRINT 105,N,X1,X3,DELNU,S,W0,VHALF
N4=(2.*S)/DELNU+1 & N5=S/DELNU
N6=N5+1
N7=N-N5
NU(1)=0.0
DO 1 J=2,N
1  NU(J)=NU(J-1)+DELNU
DO 2 J=1,N
2  K(J)=X1/(1.0+X3*(NU(J)-W0)**2)

```

```

C*****MAKE K INTO A LINEAR PLOT BETWEEN 90 AND 20
      N3=N/2+1
      Z1=K(N3) & Z2=K(1)
      C=ALOG(4.5)/(Z1-Z2)
      DO 4 J=1,N
      DUMMY=ALOG(90.0)-C*K(J)
      4  ILOR(J)=EXP(DUMMY)
C*****CONVOLUTE ILCR
      DO 11 J=N6,N7
      J2=J-N5
      DO 12 IJ=1,N4
      XABS=ABS(NU(J2)-NU(J))
      XI=ILOR(J2)
      Y(IJ)=XI*(1.-(XABS/S))/S
      12  J2=J2+1
      F=0.0
      DO 13 IJ=1,N4
      13  F=F+Y(IJ)
      11  ICON(J)=(2.*F-Y(1)-Y(N4))*DELNU/2.
      IP=N
      DO 22 IJ=1,N5
      ICON(IJ)=ILOR(IJ)
      ICON(IP)=ILOR(IP)
      22  IP=IP-1
C*****USE A RANDOM GENERATOR TO PRODUCE NOISE BETWEEN -0.05 AND
      DO 18 J=1,N
      Y=RANF(0.0)
      Y2=(Y-0.5)/10.
      18  IPAN(J)=ICON(J)+Y2
C*****PLOT SPECTRUM---ILOR V ICON
      PRINT 200
      PRINT 500
      DO 21 IJ=1,101
      21  LINE(IJ)=BLANK
      DO 23 J=1,N,8
      L=ILOR(J)
      M=ICON(J)
      IF(L.EQ.M) GO TO 24
      LINE(L)=STAR
      LINE(M)=PLUS
      GO TO 25
      24  LINE(L)=ZERO
      25  PRINT 501,NU(J),LINE,ILOR(J),ICON(J)
      LINE(L)=BLANK
      23  LINE(M)=BLANK

```

```

C*****PERFORM SLIT CORRECTION
DO 15 J=1,N
15 D2XDT2(J)=0.0
M=N-6
DO 16 J=1,M
16 D2XDT2(J+3)=(ICON(J+6)-ICON(J+4)-ICON(J+2)+ICON(J))/(8.*DEL
ZS1=S**2/12. NU**2)
DO 17 J=1,N
CZS1=ZS1*D2XDT2(J)
17 INFW(J)=ICON(J)-CZS1
C*****PLOT SECCND DERIVATIVE
PRINT 200
PRINT 101
X=0.0 & Y=0.0
DO 9 J=1,N
IF (D2XDT2(J).LT.Y) Y=D2XDT2(J)
9 IF (D2XDT2(J).GT.X) X=D2XDT2(J)
Z=X-Y
X=100./Z
DO 10 J=1,N,8
L=((D2XDT2(J)-Y)*X)+1.5
LINE(L)=STAR
PRINT 102,NU(J),LINE,D2XDT2(J)
10 LINE(L)=BLANK
C*****PLOT CONTOURS
PRINT 200
PRINT 300
DO 20 J=1,N,8
L=ILOR(J)
M=INEW(J)
IF (L.EQ.M) GO TO 3
LINE(L)=STAR
LINE(M)=PLUS
GO TO 5
3 LINE(L)=ZERO
5 PRINT 103,NU(J),LINE,ILOR(J),INEW(J)
LINE(L)=BLANK
20 LINE(M)=BLANK
30 CONTINUE
STOP
100 FORMAT(5X,F7.2,1H.,101A1,2X,F6.3)
101 FORMAT(114X,'D2XDT2'/114X,'-----')
102 FORMAT(5X,F7.2,101A1,1X,F8.3)
103 FORMAT(5X,F7.2,1H.,101A1,1X,F6.3,1X,F6.3)
104 FORMAT(110,5F10.0)
105 FORMAT(40X,'N=',15/40X,'X1=',F6.2/40X,'X3=',F6.2/40X,'DELNU
Z/40X,'S=',F6.2/40X,'W0=',F8.2/40X,'VHALF=',F6.2) =' , F6.4
200 FORMAT(1H1)
300 FORMAT(116X,'ILOR INEW'/116X,'-----')
501 FORMAT(5X,F7.2,1H.,101A1,1X,F6.3,1X,F6.3)
500 FORMAT(116X,'ILOR ICON'/116X,'-----')
END

```

DECON2 is used to deconvolute an experimental band contour by the Fourier transform method. The second moment is also calculated.

```

PROGRAM DECON2(INPUT,OUTPUT)
DIMENSION D(500),PATH(10),NL(10),CT(500)
DIMENSION TEXT(8),CONC(10)
DIMENSION CTLOR(500),S(500)
REAL KLOR(500),NU2(500),M2(500)
REAL K(500),K2(500),NU(500),LINF(101)
REAL IO(500),I(500),I2(500)
COMPLEX SP,SM,EP,EM
INTEGER R
DATA STAR,BLANK,PLUS,ZERO/1H*,1H ,1H+,1H0/
READ 106,NN
READ 107,NT,XT
C*****NN IS NUMBER OF SETS OF DATA TO BE FED IN
PRINT 600
PRINT 110,NT,XT
PRINT 112,NN
NQ=1
KX=2
DO 30 KK=1,NN
READ 100,N,FIRST,DELNU,W0,CONC(KK),PATH(KK),SLIT
READ 200,(IO(J),J=NQ,N)
READ 200,(I(J),J=NQ,N)
READ 300,TEXT
PRINT 301,TEXT
PRINT 101,N,FIRST,DELNU,W0,CONC(KK),PATH(KK),SLIT
NL(KK)=N
DO 13 J=NQ,N
NU(J)=FIRST
13 FIRST=FIRST+DELNU
DO 1 J=NQ,N
B=IO(J)/I(J)
E=ALOG(B)
1 D(J)=E/(NU(J)*CONC(KK)*PATH(KK))
IF(KX.NE.1) GO TO 33
KY=2 & M=N-1
DO 35 J=3,M,2
I(KY)=I(J)
IO(KY)=IO(J)
D(KY)=D(J)
NU(KY)=NU(J)
35 KY=KY+1
N=N/2
NL(1)=N
33 NQ=N+1
KX=KX+1
30 CONTINUE
DO 60 J=1,N
60 K(J)=D(J)
N=300 & FIRST=582.0 & Y4=0.02764 & Y5=0.00484228
DO 84 J=NQ,N
NU(J)=FIRST
IO(J)=0.0 & I(J)=0.0
K(J)=Y5*EXP(-Y4*ABS(NU(J)-W0))
84 FIRST=FIRST+DELNU
PRINT 600
PRINT 400,(K(J),J=1,N)
C*****CALCULATE GAMMA OF EXPERIMENTAL BAND

```



```

M=N-1 E F=0.0
DO 46 IZ=2,M
46 F=F+K(IZ)
GAMMA=(K(1)+2.*F+K(N))*ABS(DELNU)/2.
C*****CALCULATE SECOND MOMENT
DO 47 J=1,N
47 S(J)=K(J)*(NU(J)-W0)**2
F=0.0 F M=N-1
DO 48 J=2,M
48 F=F+S(J)
SUM=(S(1)+2.*F+S(N))*ABS(DELNU)/2.
XM2=SUM/GAMMA
PRINT 702,XM2
C*****PERFORM FOURIER TRANSFORM
TIME=0.0 E XN=N
XT=1.0/(3.0*10.**10*XN*ABS(DELNU))*2.0
XT=XT/3.
FACTOR=2.*3.14159*3.0*10.**10
K(1)=K(1)/2. E K(N)=K(N)/2.
DO 12 R=1,N
CONST=FACTOR*TIME
SP=(0.0,0.0)
XD=ABS(DELNU)*CONST
EP=CMPLX(COS(XD),-SIN(XD))
DO 23 J=1,N
II=N-J+1
23 SP=K(II)+SP*EP
CT(R)=REAL(SP*ABS(DELNU))
12 TIME=TIME+XT
C*****CALCULATE THE LORENTZIAN
DO 81 J=1,N
81 KLOR(J)=1.0/(1.0+0.207*(NU(J)-W0)**2)
C*****CALCULATE SECOND MOMENT OF LORENTZIAN
M=N-1 E F=0.0
DO 90 IZ=2,M
90 F=F+KLOR(IZ)
GAM2=(KLOR(1)+2.*F+KLOR(N))*ABS(DELNU)/2.
DO 91 J=1,N
91 S(J)=KLOR(J)*(NU(J)-W0)**2
F=0.0 E M=N-1
DO 92 J=2,M
92 F=F+S(J)
SUM=(S(1)+2.*F+S(N))*ABS(DELNU)/2.
YM2=SUM/GAM2
PRINT 703,YM2
C*****PERFORM F.T.
TIME=0.0 E XN=N
KLOR(1)=KLOR(1)/2. E KLOR(N)=KLOR(N)/2.
DO 82 R=1,N
CONST=FACTOR*TIME
SP=(0.0,0.0)
XD=ABS(DELNU)*CONST
EP=CMPLX(COS(XD),-SIN(XD))
DO 83 J=1,N
II=N-J+1
83 SP=KLOR(II)+SP*EP
CTLOR(R)=REAL(SP*ABS(DELNU))

```



```

82  TIME=TIME+XT
    ZZ=CTLOR(1)
    DO 85 R=1,N
85  CTLOR(R)=CTLOR(R)/ZZ
C*****DEVIDE F.T. OF SPECTRUM BY F.T. OF LORENTZIAN
    DO 80 R=2,N
80  CT(R)=CT(R)/CTLOR(R)
C*****PLOT F.T.
    DO 21 IJ=1,101
21  LINE(IJ)=BLANK
    CC=10.**12
    ZT=XT*10.**12
    TIME=0.0
    PRINT 600
    PRINT 700
    PRINT 701
    Y=CT(1)
    Y=100./Y
    DO 41 R=1,N
    L=(CT(R)*Y)+1.5
    LINE(L)=STAR
    PRINT 501,TIME,LINE,CT(R),CTLOR(R)
    TIME=TIME+ZT
41  LINE(L)=BLANK
C*****NOW DO INVERSE FOURIER TRANSFORM
    CT(1)=CT(1)/2. & CT(N)=CT(N)/2.
    XT2=XT*3.*10.**10*4.
    DO 55 J=1,N
    CONST2=FACTOR*(NU(J)-W0)
    SM=(0.0,0.0)
    XD=XT*CONST2
    FM=CMPLX(COS(XD),SIN(XD))
    DO 56 R=1,N
    II=N-R+1
56  SM=CT(II)+SM*EM
55  K2(J)=PEAL(SM*XT2)
C*****COMPARE THE CONTOURS BEFORE AND AFTER F.T.
    K(1)=K(1)*2.
    KLOR(1)=KLOR(1)*2.
    PRINT 600
    PRINT 102
    Y=K2(1)
    Y=100./Y
    Y2=K(1)
    Y2=100./Y2
    DO 61 J=1,N
    L=(K(J)*Y2)+1.5
    L2=(KLOR(J)*100.)+1.5
    M=(K2(J)*Y)+1.5
    LINE(L)=STAR
    LINE(L2)=ZERO
    LINE(M)=PLUS
    PRINT 103,NU(J),LINE,K(J),K2(J)
    LINE(L)=BLANK
    LINE(L2)=BLANK
61  LINE(M)=BLANK
C*****CALCULATE GAMMA

```

```

M=N-1
F=0.0
DO 7 IZ=2,M
7 F=F+K2(IZ)
  GAMMA=(K2(1)+2.*F+K2(N))*ABS(DELNU)/2.
C*****CALCULATE THE SECOND MOMENT
DO 8 J=1,N
8 S(J)=K2(J)*(NU(J)-W0)**2
  NU2(1)=NU(1)
  N2=1 & N3=N/2
  DO 42 IZ=1,N3
  F=0.0 & N2=N2+2
  M=N2-1
  DO 43 J=2,M
43 F=F+S(J)
  M2(IZ)=(S(1)+2.*F+S(N2))*ABS(DELNU)/2.
  M2(IZ)=M2(IZ)/GAMMA
42 NU2(IZ)=NU(N2)
C*****PLOT GRAPH
PRINT 600
PRINT 500
X=0.0
DO 44 IZ=1,N3
44 IF(M2(IZ).GT.X) X=M2(IZ)
  X=X+0.2*X
  X=100./X
  DO 45 IZ=1,N3
  L=(M2(IZ)*X)+1.5
  LINE(L)=STAR
  PRINT 502,NU2(IZ),LINE,M2(IZ)
45 LINE(L)=BLANK
  STOP
100 FORMAT(I10,6F10.0)
101 FORMAT(20X,'N=',I5/20X,'FIRST=',F8.2,' CM-1'/20X,'DELNU=',
ZM-1'/20X,'W0=',F8.2,' CM-1'/20X,'CONC=',E16.8,' MOLES/LITRE',
ZPATH=',F10.6/20X,'SLIT=',F8.2,' CM-1')
102 FORMAT(116X,' K K2 '/116X,'-----')
103 FORMAT(1X,F7.2,1H.,101A1,2X,E11.5,1X,E11.5)
106 FORMAT(I10)
107 FORMAT(I10,E10.0)
110 FORMAT(///40X,'NT=',I5/40X,'XT=',E11.5)
112 FORMAT(///40X,'NN=',I3)
200 FORMAT(16F5.0)
300 FORMAT(8A10)
301 FORMAT(//20X,8A10)
400 FORMAT(10E12.5)
500 FORMAT(//40X,'GRAPH OF CONTRIBUTION TO SECOND MOMENT V FREQU
Z40X,'-----')
501 FORMAT(1X,F7.4,1H.,101A1,1X,E11.5,1X,E11.5)
502 FORMAT(5X,F8.2,1H.,101A1,E16.8)
600 FORMAT(1H1)
700 FORMAT(//40X,'CORRELATION FUNCTION V TIME'/40X,'-----')
Z-----')
701 FORMAT(111X,'CORPELATION'/1X,'PICOSEC',104X,'FUNCTION'/1X,'-
Z',104X,'-----')
702 FORMAT(//40X,'EXPERIMENTAL SECOND MOMENT=',E12.5,' CM-2')
703 FORMAT(//40X,'SECOND MOMENT OF LORENTZIAN=',E12.5,' CM-2')
END

```

√ F5.2, ' C

ENCY' /

EXTRAP calculates the integrated intensity, second moment and autocorrelation function of an experimental band contour.

```

PROGRAM EXTRAP(INPUT,OUTPUT)
DIMENSION TEXT(8),S(500),D(500)
DIMENSION CT(500),G(500),TIME(500)
REAL NU(500),NU2(500),M2(500),LINE(101)
REAL LNCT(500)
REAL IO(500),I(500)
COMPLEX SP,EP
INTEGER R
DATA STAR,BLANK,PLUS,ZERO/1H*,1H ,1H+,1H0/
READ 106,NN
READ 107,NT,XT
C*****NN IS THE NUMBER OF SETS OF DATA TO BE FED IN
PRINT 400
PRINT 110,NT,XT
PRINT 112,NN
NQ=1
DO 30 KK=1,NN
READ 100,N,FIRST,DELNU,W0,CONC,PATH,SLIT
READ 200,(IO(J),J=NQ,N)
READ 200,(I(J),J=NQ,N)
READ 300,TEXT
PRINT 301,TEXT
PRINT 101,N,FIRST,DELNU,W0,CONC,PATH,SLIT
DO 13 J=NQ,N
NU(J)=FIRST
13 FIRST=FIRST+DELNU
DO 1 J=NQ,N
B=IO(J)/I(J)
E=ALOG(B)
1 D(J)=E/(NU(J)*CONC*PATH)
NQ=N+1
30 CONTINUE
PRINT 400
PRINT 103
DO 34 J=1,N
34 PRINT 102,NU(J),IO(J),I(J),D(J)
C*****MAKE SURE N IS ODD
IN=(N+1)/2
N=(IN*2)-1
C*****CALCULATE GAMMA
C*****INTEGRATION BY TRAPEZIUM RULE
K=N/2
N2=1
DO 7 IZ=1,K
F=0.0
N2=N2+2
M=N2-1
DO 14 J=2,M
14 F=F+D(J)
G(IZ)=(D(1)+2.*F+D(N2))*ABS(DELNU)/2.
7 NU2(IZ)=NU(N2)
GAMMA=G(K)
PRINT 901,GAMMA
C*****PLOT CONTRIBUTION TO GAMMA V FREQUENCY
DO 10 IJ=1,101

```

```

10  LINE(IJ)=BLANK
    PRINT 400
    PRINT 600
    X=0.0
    DO 16 IZ=1,K
16  IF(G(IZ).GT.X)    X=G(IZ)
    X=100./X
    DO 17 IZ=1,K
    L=(G(IZ)*X)+1.5
    LINE(L)=STAR
    PRINT 601,NU2(IZ),LINE,G(IZ)
17  LINE(L)=BLANK
C****CALCULATE THE SECOND MOMENT
    DO 4 J=1,N
    4  S(J)=D(J)*(NU(J)-WO)**2
C****INTEGRATION BY SIMPSONS RULE
    N2=1
    DO 9 IZ=1,K
    F=0.0
    T=0.0
    N2=N2+2
    M=N2-1
    DO 5 J=2,M,2
    5  F=F+S(J)
    DO 6 J=3,N2,2
    6  T=T+S(J)
    M2(IZ)=(S(1)+4.*F+2.*T-S(N2))*ABS(DELFNU)/3.
    9  M2(IZ)=M2(IZ)/GAMMA
C****PLOT GRAPH
    PRINT 400
    PRINT 500
    X=0.0
    DO 11 IZ=1,K
11  IF(M2(IZ).GT.X)    X=M2(IZ)
    X=X+0.2*X
    X=100./X
    DO 12 IZ=1,K
    L=(M2(IZ)*X)+1.5
    LINE(L)=STAR
    PRINT 501,NU2(IZ),LINE,M2(IZ)
12  LINE(L)=BLANK
C****CALCULATE CORRELATION FUNCTION
    TIME(1)=0.0
    DO 75 R=2,NT
    75  TIME(R)=TIME(R-1)+XT
    FACTOR=2.*3.14159*2.99776*10.**10
    D(1)=D(1)/2. & D(N)=D(N)/2.
    DO 22 R=1,NT
    CONST=FACTOR*TIME(R)
    SP=(0.0,0.0)
    XD=ABS(DELFNU)*CONST
    EP=CMPLX(COS(XD),-SIN(XD))
    DO 23 J=1,N
    II=N-J+1
    23  SP=D(II)+SP*EP

```

```

        DUMMY=ABS(DELNU)
        SUM=REAL(SP*DUMMY)
22      CT(R)=SUM/GAMMA
        PRINT 902
C****PLOT CORRELATION FUNCTION
        A=1.0
        XTIME=0.0
        YT=XT*10.**12
        PRINT 400
        PRINT 700
        PRINT 701
        Y=CT(1)
        Y=100./Y
        NT2=NT/5
        DO 25 R=1,NT2
        L=(CT(R)*Y)+0.5
        IF(L.LT.1) GO TO 26
        LINE(L)=STAR
        PRINT 703,XTIME,LINE,CT(R)
        XTIME=XTIME+YT
25      LINE(L)=BLANK
26      CONTINUE
C****PLOT OF LOG OF CORRELATION FUNCTION
        DO 27 R=1,NT
        Z=CT(R)
        IF(Z.LT.0.00001) GO TO 50
27      LNCT(R)=ALOG(Z)
50      CONTINUE
        Y=0.0
        DO 28 R=1,NT2
28      IF(LNCT(R).LT.Y) Y=LNCT(R)
        Y=100./Y
        PRINT 400
        PRINT 800
        PRINT 701
        XTIME=0.0
        DO 29 R=1,NT2
        L=(LNCT(R)*Y)+1.5
        L=10?-L
        LINE(L)=STAR
        PRINT 702,XTIME,LINE,LNCT(R)
        XTIME=XTIME+YT
29      LINE(L)=BLANK
        ZT=YT*5.0 & Y=0.0
        DO 60 R=1,NT,5
60      IF(LNCT(R).LT.Y) Y=LNCT(R)
        Y=100./Y
        PRINT 400
        PRINT 800
        PRINT 701
        XTIME=0.0
        DO 61 R=1,NT,5
        L=(LNCT(R)*Y)+1.5
        L=10?-L
        LINE(L)=STAR

```



```

PRINT 702,XTIME,LINE,LNCT(R)
XTIME=XTIME+ZT
61 LINE(L)=BLANK
STOP
100 FORMAT(I10,6F10.0)
101 FORMAT(20X,'N=',I5/20X,'FIRST=',F8.2,' CM-1'/20X,'DELNU=',
ZM-1'/20X,'W0=',F8.2,' CM-1'/20X,'CUNC=',E16.8,' MOLES/LITRE
ZPATH=',F10.6/20X,'SLIT=',F8.2,' CM-1')
102 FORMAT(20X,F8.2,5X,F6.2,5X,F6.2,5X,E16.8)
103 FORMAT(24X,'NU',10X,'IO',9X,'I',16X,'D')
106 FORMAT(I10)
107 FORMAT(I10,E10.0)
110 FORMAT(///40X,'NT=',I5/40X,'XT=',E11.5)
112 FORMAT(///40X,'NN=',I3)
200 FORMAT(16F5.0)
300 FORMAT(8A10)
701 FORMAT(//20X,8A10)
400 FORMAT(1H1)
500 FORMAT(//40X,'GRAPH OF CONTRIBUTION TO SECOND MOMENT V FREQU
Z40X,'-----')
501 FORMAT(5X,F8.2,1H.,101A1,E16.8)
600 FORMAT(//40X,'GRAPH OF CONTRIBUTION TO GAMMA V FREQUENCY'/40X
Z-----')
601 FORMAT(5X,F8.2,1H.,101A1,E16.8)
700 FORMAT(//40X,'CORRELATION FUNCTION V TIME'/40X,'-----
Z-----')
701 FORMAT(111X,'CORRELATION'/1X,'PICOSEC',104X,'FUNCTION'/1X,'--
Z',104X,'-----')
702 FORMAT(2X,F5.2,1X,1H.,101A1,2X,E11.5)
703 FORMAT(2X,F5.2,1X,1H.,101A1,2X,E11.5)
800 FORMAT(//40X,'LOG OF CORRELATION FUNCTION V TIME'/40X,'-----
Z-----')
901 FORMAT(///40X,'GAMMA=',F10.5///)
902 FORMAT(///)
END

```

FTSLIT performs a double Fourier transform on a simulated Lorentzian curve to see if the original function is accurately reproduced, and so tell how accurate the Fourier transform routine is. The print out here uses the traditional method of evaluating the integrals.


```

PROGRAM FTSLIT(INPUT,OUTPUT)
DIMENSION CT(2000)
REAL K(2000),NU(2000),ILOR(2000),KCOR(2000),NEWI(2000),
INTEGER R
DATA STAR,BLANK,PLUS,ZERO/1H*,1H ,1H+,1H0/
READ 100,N,W0,FIRST,DELNU,X1,X3
PRINT 301,N,W0,FIRST,DELNU,X1,X3
DO 1 J=1,N
NU(J)=FIRST
K(J)=X1/(1.0+X3*(NU(J)-W0)**2)
1 FIRST=FIRST+DELNU
C*****MAKE K INTO A LINEAR PLOT BETWEEN 90 AND 20
Z1=K(1) & Z2=K(N)
C=ALOG(4.5)/(Z1-Z2)
DO 4 J=1,N
DUMMY=ALOG(90.0)-C*K(J)
4 ILOR(J)=EXP(DUMMY)
C*****DO FOURIER TRANSFORM ON LINEAR CURVE
TIME=0.0 & XN=N
XT=1.0/(3.0*10.**10*XN*DELNU*2.0)
FACTOR=2.*3.14159*3.0*10.**10
DO 12 R=1,N
CONST=FACTOR*TIME
DO 13 J=1,N
X=(NU(J)-W0)*CONST
X2=COS(X)
XI=90.0-ILOR(J)
13 KCOR(J)=XI*X2
C*****INTEGRATION BY TRAPEZIUM RULE
F=0.0
M=N-1
DO 14 J=2,M
14 F=F+KCOR(J)
CT(R)=(KCOR(1)+2.*F+KCOR(N))*DELNU/2.
12 TIME=TIME+XT
C*****NOW DO INVERSE FOURIER TRANSFORM
TIME=0.0
DO 55 J=1,N
CONST2=FACTOR*(NU(J)-W0)
DO 56 R=1,N
ZX=TIME*CONST2
ZX2=COS(ZX)
KCOR(R)=CT(R)*ZX2
56 TIME=TIME+XT
C*****INTEGRATION BY TRAPEZIUM RULE
F=0.0
M=N-1
DO 57 R=2,M
57 F=F+KCOR(R)
XI2=(KCOR(1)+2.*F+KCOR(N))*2.*3.*10.**10*XT
C*****ALTERNATE XI2 ARE -VE SO USE ABS()
55 NEWI(J)=90.0-ABS(XI2)
C*****COMPARE THE CONTOURS BEFORE AND AFTER F.T.
PRINT 200
PRINT 102
DO 21 IJ=1,101
21 LINE(IJ)=BLANK
DO 20 J=1,200

```

```

L=ILOR(J)
M=NEWI(J)
IF(L.EQ.M) GO TO 3
LINE(L)=STAR
LINE(M)=PLUS
GO TO 5
3 LINE(L)=ZERO
5 PRINT 103,NU(J),LINE,ILOR(J),NEWI(J)
LINE(L)=BLANK
20 LINE(M)=BLANK
STOP
100 FORMAT(I10,5F10.0)
102 FORMAT(116X,'ILOR NEWI'/116X,'-----')
103 FORMAT(5X,F7.2,1H.,101A1,1X,F6.3,1X,F6.3)
200 FORMAT(1H1)
301 FORMAT(40X,'N=',I5/40X,'WO=',F8.2,'CM-1'/40X,'FIRST=',F8.2,
740X,'DELNU=',F5.3,'CM-1'/40X,'X1=',F6.4/40X,'X3=',F6.4)
END

```

HOTBND is used to remove hot bands and low abundance isotopic bands from an experimental condensed phase band.

```

PROGRAM HOTBND(INPUT,OUTPUT)
DIMENSION TEXT(8),D2XDT2(500),D(500),DHOT(500)
REAL NU(500)
REAL I(500),INEW(500),IO(500),LINE(101)
DATA STAR,BLANK,PLUS,ZERO/1H*,1H ,1H+,1H0/
READ 103,N2,CONC2,PATH2,N3,CONC3,PATH3
NQ=1
READ 100,N,FIRST,DELNU,W0,CONC,PATH,SLIT
READ 200,(IO(J),J=NQ,N)
READ 200,(I(J),J=NQ,N)
PRINT 101,N,FIRST,DELNU,W0,CONC,PATH,SLIT
DO 13 J=NQ,N
NU(J)=FIRST
13 FIRST=FIRST+DELNU
DO 14 J=NQ,N
14 D2XDT2(J)=0.0
M=N-6
DO 15 J=NQ,M
15 D2XDT2(J+3)=(I(J+6)-I(J+4)-I(J+2)+I(J))/(8.*DELNU**2)
ZS1=SLIT**2/12.
DO 17 J=NQ,N
CZS1=ZS1*D2XDT2(J)
17 I(J)=I(J)-CZS1
DO 1 J=NQ,N
B=IO(J)/I(J)
E=ALOG(B)
1 D(J)=E/(NU(J)*CONC*PATH)
DO 2 J=1,N
2 DHOT(J)=0.0
M=N-21
DO 3 J=1,M
3 DHOT(J)=0.00277*D(J+21)
DO 4 J=1,N2
D(J)=D(J)-DHOT(J)
E=D(J)*NU(J)*CONC2*PATH2
B=EXP(E)
4 INEW(J)=IO(J)/B

```

```

C*****PLOT GRAPH
PRINT 400
DO 6 IJ=1,101
6 LINE(IJ)=BLANK
DO 7 J=1,N2
L=I(J)
M=INEW(J)
IF(L.EQ.M) GO TO 8
LINE(L)=STAR
LINE(M)=PLUS
GO TO 9
8 LINE(L)=ZERO
9 PRINT 102,NU(J),LINE,I(J),INEW(J)
LINE(L)=BLANK
LINE(M)=BLANK
7 CONTINUE
STOP
100 FORMAT(I10,6F10.0)
101 FORMAT(20X,'N=',I5/20X,'FIRST=',F8.2,' CM-1'/20X,'DELNU='
ZM-1'/20X,'W0=',F8.2,' CM-1'/20X,'CONC=',E16.8,' MOLES/LITRE
ZPATH=',F10.6/20X,'SLIT=',F8.2,' CM-1')

```

```

102 FORMAT(2X,F8.2,2X,101A1,2X,F5.2,2X,F5.2)
103 FORMAT(I10,2F10.0,I10,2F10.0)
200 FORMAT(16F5.0)
400 FORMAT(1H1)
END

```

LORGAP is used to compare the profiles of experimental condensed phase bands with simulated functions. A Lorentzian function is simulated in this print out.

```

PROGRAM LORGAP(INPUT,OUTPUT,TAPE1=INPUT,TAPE3=OUTPUT)
DATA STAR,BLANK,PLUS,ZERO/1H*,1H ,1H+,1H0/
DIMENSION D(500)
REAL IO(500),I(500),NU(500),K(500),LINE(100),KA(500)
READ(1,106) INP
READ (1,105) X1,X3
WRITE (3,103) X1,X3
NQ=1
DO 30 KK=1,INP
READ (1,101) N,FIRST,W0,DELNU,VHALF,PATH,CONC
READ (1,100) (IO(J),J=NQ,N)
READ(1,100) (I(J),J=NQ,N)
WRITE(3,200)
WRITE(3,102) N,FIRST,W0,DELNU,VHALF,PATH,CONC
DO 1 J=NQ,N
NU(J)=FIRST
FIRST=FIRST+DELNU
B=IO(J)/I(J)
E=ALOG(B)
D(J)=E/NU(J)
1 KA(J)=D(J)/(4.*3.14159*PATH*CONC)
NQ=N+1
30 CONTINUE
DO 21 J=1,N
21 K(J)=X1/(1.+X3*(NU(J)-W0)**2)
WRITE(3,200)
WRITE(3,700)
DO 12 J=1,N
12 WRITE(3,800) NU(J),IO(J),I(J),KA(J),K(J)
X=0.0
DO 3 J=1,N
IF(KA(J).GT.X) X=KA(J)
3 CONTINUE
DO 11 J=1,N
11 IF(K(J).GT.X) X=K(J)
X=100./X
WRITE(3,200)
DO 4 J=1,N
DIF=KA(J)-K(J)
DO 5 IJ=1,100
5 LINE(IJ)=BLANK
L=(KA(J)*X)+0.5
M=(K(J)*X)+0.5
IF(L.EQ.M) GO TO 50
LINE(L)=STAR
LINE(M)=PLUS
GO TO 51
50 LINE(L)=ZERO
51 WRITE(3,400) NU(J),LINE,DIF
4 CONTINUE
STOP
100 FORMAT(16F5.0)
101 FORMAT(I10,6F10.0)
102 FORMAT(/40X,6HN =,I7/40X,6HFIRST=,F7.1/40X,6HW0 =,F7.1
ZHDELNU=,F7.1/40X,6HVHALF=,F7.1/40X,6HPATH =,F7.5/40X,5HCONC=
Z)
103 FORMAT(/40X,3HX1=,E12.5/40X,3HX3=,E12.5)
105 FORMAT(2F10.0)

```

| |
|--------------------|
| /40X,6 |
| =,F7.1 |
| =,F7.5/40X,5HCONC= |
| ,E12.5 |

```

106  FORMAT(I5)
200  FORMAT(1H1)
400  FORMAT(2X,F7.2,1X,1H.,100A1,2X,E12.5)
500  FORMAT(30X,3H A=,F10.5,4X,9HB**2   =,F10.5/   ,2H--,9
700  FORMAT(28X,2HNU,9X,2HI0,8X,1HI,12X,2HKA,14X,1HK/28X,2H--,9X
ZX,1H-,12X,2H--,14X,1H-)
800  FORMAT(25X,F7.1,5X,F5.1,5X,F5.1,5X,E11.5,5X,E11.5)
      END

```

PLBAND is used to plot out an experimental condensed phase band contour using the CALCOMP graph plotting routine. All plots are normalised to the same height and are also the same height as those obtained from COMCON, for the purposes of comparison.

```

PROGRAM PLBAND(INPUT,OUTPUT)
DIMENSION TEXT(8),D2XDT2(500),CORIO(500),CORI(500)
DIMENSION D(203),CHART(101)
REAL NU(203),I(201),IO(201)
DATA C1,C2,C3,C4,C5/0.0,1.0,0.0,0.0,0.0/
DATA STAR,BLANK,PLUS,ZERO/1H*,1H ,1H+,1H0/
NQ=1
READ 100,N,FIRST,DELNU,W0,CONC,PATH,SLIT
READ 200,(IO(J),J=NQ,N)
READ 200,(I(J),J=NQ,N)
READ 300,TEXT
PRINT 400
PRINT 701,TEXT
PRINT 101,N,FIRST,DELNU,W0,CONC,PATH,SLIT
DO 13 J=NQ,N
  NU(J)=FIRST
13 FIRST=FIRST+DELNU
  DO 2 J=NQ,N
    CORIO(J)=C1+C2*IO(J)+C3*(IO(J)**2)+C4*(IO(J)**3)+C5*(IO(J)**4)
  3 CORI(J)=C1+C2*I(J)+C3*(I(J)**2)+C4*(I(J)**3)+C5*(I(J)**4)
  PRINT 400
  PRINT 601
  DO 4 J=NQ,N
4 D2XDT2(J)=0.0
  M=N-6
  DO 5 J=NQ,M
5 D2XDT2(J+3)=(CORI(J+6)-CORI(J+4)-CORI(J+2)+CORI(J))/(8.*DELNU)**2)
  ZS1=SLIT**2/12.
  DO 7 J=NQ,N
  XIO=IO(J)
  XI=I(J)
  CZS1=ZS1*D2XDT2(J)
  I(J)=CORI(J)-CZS1
  IO(J)=CORIO(J)
7 PRINT 600,NU(J),XIO,XI,CORIO(J),CORI(J),D2XDT2(J),CZS1,I(J)
  DO 1 J=1,N
  B=IO(J)/I(J)
  E=ALOG(B)

```



```

1  D(J)=E/(NU(J)*CONC*PATH)
   X=0.0
   DO 14 J=1,N
14  IF(D(J).GT.X) X=D(J)
   DO 15 J=1,N
15  D(J)=D(J)/X
C****PLOT GRAPH
   PRINT 400
   DO 22 IJ=1,101
22  CHART(IJ)=BLANK
   DO 21 J=1,N
   L=D(J)*100.+1.0
   CHART(L)=STAR
   PRINT 500,NU(J),CHART,D(J)
21  CHART(L)=BLANK
   NU(202)=1760.0 & NU(203)=10.0
   D(202)=0.0 & D(203)=1.0/7.0

   CALL START
   CALL PLOT(1.0,1.0,-3)
   CALL AXIS(0.0,0.0,10*ABSORBANCE,-10,7.0,0.0,D(202),D(203))
   CALL AXIS(0.0,0.0,7*HNU CM-1,7,10.05,90.0,NU(202),NU(203))
   CALL LINE(D,NU,201,1,0,1)
   CALL ENPLOT(9.0)
   STOP
100 FORMAT(I10,6F10.0)
101 FORMAT(20X,'N=',I5/20X,'FIRST=',F8.2,' CM-1'/20X,'DELNU=',
ZM-1'/20X,'WO=',F8.2,' CM-1'/20X,'CONC=',E16.8,' MOLES/LITRE
ZPATH=',F10.6/20X,'SLIT=',F8.2,' CM-1')
200 FORMAT(16F5.0)
300 FORMAT(8A10)
301 FORMAT(/20X,8A10)
400 FORMAT(1H1)
500 FORMAT(1H ,F7.2,1X,101A1,2X,E12.5)
600 FORMAT(10X,F8.2,5X,F8.2,5X,F8.2,5X,F8.2,5X,F8.2,5X,F10.5,3X
Z5X,F8.2)
601 FORMAT(15X,'NU',11X,'IO',11X,'I',10X,'CORIO',8X,'CORI',9X,
Z,5X,'2ND ORDER COR',4X,'NEWI')
END

```

F5.2, 'C
'/20X, '

, F10.5,

'01X0T2'

PLESPC simulates a degenerate gas phase band of a symmetric top molecule and plots it out using the CALCOMP graph plotting routine.


```

PROGRAM PLESPC(INPUT,OUTPUT)
DIMENSION A(1500),A2(1502),XNU(1502),CHART(100)
REAL INTP,INTR,INTQ,NUR,NUP,NUC,J,K2
REAL NUPPK,NUPMK,NURPK,NURMK,NLQPK,NUQMK
DATA STAR,BLANK/1H*,1H /
X=0.479606E-2
C-----X=F*C/(K*T)
READ 300,W0,ETA,BO,BI,A0,AI,DELNU,JMAX
READ 400,WSPEC
PRINT 100
PRINT 301,W0,ETA,BO,BI,A0,AI,DELNU,JMAX,WSPEC
BDIF=BI-BO & BSUM=BI+BO & AB=AO-BO & AIDBI=AI-BI & ABDAB=(
ZA0=BO) AI-BI)-(
DO 1 I=1,1500
1 A(I)=0.0
C-----CALCULATE P, Q, R BRANCHES FOR K=0
DO 2 I=1,JMAX
J=I
C-----P BRANCH
NUP=W0-BSUM*(J+1.)+BDIF*(J+1.)**2+AIDBI-2.*AI*ETA
P=NUP-WSPEC
NP=(P/DELNU)+0.5
DUMMY=BO*(J+1.)*(J+2.)*X
Z=EXP(-DUMMY)
INTP=Z*J
A(NP)=A(NP)+INTP
C-----R BRANCH
NUR=W0+2.*BI+(3.*BI-BO)*(J-1.)+BDIF*(J-1.)**2+AIDBI-2.*AI*ETA
RR=NUR-WSPEC
NR=(RR/DELNU)+0.5
DUMMY=BO*J*(J-1.)*X
Z2=EXP(-DUMMY)
INTP=Z2*(J+1.)
A(NR)=A(NR)+INTR
C-----CALCULATE Q BRANCH
NUC=W0+BDIF*J*(J+1.)+AIDBI-2.*AI*ETA
Q=NUC-WSPEC
NQ=(Q/DELNU)+0.5
DUMMY=BO*J*(J+1.)*X
Z3=EXP(-DUMMY)
INTQ=Z3*(2.*J+1.)
A(NQ)=A(NQ)+INTQ
2 CONTINUE
C-----CALCULATE THE REST OF THE SPECTRUM WHERE K.NE.0
DO 3 K=1,JMAX
K2=K**2
AK=K
DO 4 I=K,JMAX
J=I
PLUSK=AIDBI+AIDBI*2.*AK+ABDAB*AK**2-2.*AI*ETA*(AK+1.)
AMINK=AIDBI-AIDBI*2.*AK+ABDAB*AK**2+2.*AI*ETA*(AK-1.)
C-----P BRANCH FOR DELTA(K)=1
NUP=W0-BSUM*(J+2.)+BDIF*(J+2.)**2
NUPPK=NUP+PLUSK
P=NUPPK-WSPEC

```

```

NP=(P/DELNU)+0.5
Z4=W0*(J+2.)*(J+3.)+(A0-R0)*K2
ZPK=Z4*X
V1=EXP(-ZPK)
GPPK=(J-AK+2.)*(J-AK+1.)/(J+2.)
INTP=V1*GPPK
A(NP)=A(NP)+INTP
C-----P BRANCH FOR DELTA(K)=-1
WUP=W0-BSUM*J+BDIF*J**2
NUPMK=NUP+AMINK
P=NUPMK-WSPEC
NP=(P/DELNU)+0.5
Z5=W0*J*(J+1.)+(A0-B0)*K2
ZMK=Z5*X
V2=EXP(-ZMK)
GPMK=(J+AK)*(J+AK-1.)/J
INTP=V2*GPMK
A(NP)=A(NP)+INTP
C-----R BRANCH FOR DELTA(K)=+1
NUR=W0+2.*BI+(3.*BI-B0)*J+BDIF*J**2
NURPK=NUR+PLUSK
RR=NURPK-WSPEC
NR=(RR/DELNU)+0.5
GRPK=(J+AK+1.)*(J+AK+2.)/(J+1.)
INTR=V2*GRPK
A(NR)=A(NR)+INTR
C-----R BRANCH FOR DELTA(K)=-1
NURMK=NUR+AMINK
RR=NURMK-WSPEC
NR=(RR/DELNU)+0.5
GRMK=(J-AK+1.)*(J-AK+2.)/(J+1.)
INTR=V2*GRMK
A(NR)=A(NR)+INTR
C-----G BRANCH FOR DELTA(K)=+1
NUG=W0+BDIF*(J+1.)*(J+2.)
NUGPK=NUG+PLUSK
G=NUGPK-WSPEC
NQ=(G/DELNU)+0.5
GQPK=(2.*J+3.)*(J-K+1.)*(J+K+2.)/(J+1.)/(J+2.)
Z6=W0*(J+1.)*(J+2.)+(A0-R0)*K2
ZMK=Z6*X
V4=EXP(-ZMK)
INTQ=V4*GQPK
A(NQ)=A(NQ)+INTQ
C-----Q BRANCH FOR DELTA(K)=-1
NUG=W0+BDIF*J*(J+1.)
NUGMK=NUG+AMINK
Q=NUGMK-WSPEC
NQ=(Q/DELNU)+0.5
GQMK=(2.*J+1.)*(J+K)*(J-K+1.)/J/(J+1.)
A(NQ)=A(NQ)+INTQ
4 CONTINUE
3 CONTINUE
C*****FINI) MAX A(I)
E=0.0
DO 30 I = 1,1500

```

```

20 IF(A(I).GT.E) E=A(I)
   CONST=E/ALOG(90.0/20.0)
   I2=1500
   DO 31 I=1,1500
     DUMMY=A(I2)/CONST
     A2(I)=90.0*EXP(-DUMMY)
31 I2=I2-1
C****PLOT GRAPH
   PRINT 100
   DO 6 N=1,100
     6 CHART(N)=BLANK
     DO 7 I=1,1500,5
       L=A2(I)+0.5
       CHART(L)=STAR
     PRINT 200,CHART
     7 CHART(L)=BLANK
       I2=1500 & WVN=WSPEC
       DO 32 I=1,1500
         XNU(I2)=WVN
         I2=I2-1
32 WVN=WVN+DELNU
   XNU(1501)=1160.0 & XNU(1502)=-25.4
   A2(1501)=0.0 & A2(1502)=12.7
   CALL START
   CALL PLOT(1.0,1.0,-3)
   CALL AXIS(0.0,0.0,7HNU CM-1,-7,23.62,0.0,XNU(1501),XNU(1502))
   CALL AXIS(0.0,0.0,13HTRANSMITTANCE,13,7.87,90.0,A2(1501),A2
   CALL LINE(XNU,A2,1500,1,0,1)
   CALL ENPLOT(28.0)
   STOP
100 FORMAT(1H1)
200 FORMAT(1H ,100A1)
300 FORMAT(7F10.0,I10)
301 FORMAT(20X,'W0=',F8.2,4X,'ETA=',F8.5/20X,'B0=',F7.5,4X,'BI=
220X,'A0=',F7.5,4X,'AI=',F7.5/20X,'DELNU=',F4.2/20X,'JMAX=',
Z'WSPEC=',F7.2)
400 FORMAT(F10.0)
   END

```

PLSPEC simulates a non degenerate gas phase band of a symmetric top molecule and plots it out using the CALCOMP graph plotting routine.

```

PROGRAM PLSPEC(INPUT,OUTPUT)
DIMENSION A(1500),A2(1502),XNU(1502)
REAL INTP,INTR,INTQ,NUP,NUR,NUC,J,K2
DIMENSION CHART(100)
DATA STAR,BLANK/1H*,1H /
JMAX=150
X=0.479606E-2
READ 300,W0,B0,BI,A0,WSPEC,DELNU
C-----X=F*C/(K*T)
BDIF=BI-B0 & BSUM=BI+B0
AB=A0-B0
DO 1 I=1,1500
  1 A(I)=0.0
C-----CALCULATE P AND R BRANCHES FOR K=0
DO 2 I=1,JMAX
  J=I
C-----P BRANCH
  NUP=W0-BSUM*J+BDIF*J**2
  P=NUP-WSPEC
  NP=(P/DELNU)+0.5
  IF(NP.LT.1) GO TO 20
  DUMMY=(B0*J*(J+1.))*X
  Z=EXP(-DUMMY)
  INTP=J*Z
  A(NP)=A(NP)+INTP
  20 CONTINUE
C-----R BRANCH
  NUR=W0+2.*BI+(3.*BI-B0)*(J-1.)+BDIF*(J-1.)**2
  RR=NUR-WSPEC
  NR=(RR/DELNU)+0.5
  IF(NR.GT.1500) GO TO 2
  DUMMY=B0*J*(J-1.)*X
  Z2=EXP(-DUMMY)
  INTR=J*Z2
  A(NR)=A(NR)+INTR
  2 CONTINUE
C-----CALCULATE REST OF SPECTRUM WHERE K.NE.0
DO 3 K=1,JMAX
  K2=K**2
  DO 4 I=K,JMAX
    J=I
C-----P BRANCH
    NUP=W0-BSUM*(J+1.)+BDIF*(J+1.)**2
    P=NUP-WSPEC
    NP=(P/DELNU)+0.5
    IF(NP.LT.1) GO TO 21
    Z3=(B0*(J+1.)*(J+2.)+(A0-B0)*K2)*X
    V3=EXP(-Z3)
    G=2.*(J**2-K2+2.*J+1.)/(J+1.)
    INTP=G*V3
    A(NP)=A(NP)+INTP
    21 CONTINUE
C-----R BRANCH
    NUR=W0+2.*BI+(3.*BI-B0)*J+BDIF*J**2
    RR=NUR-WSPEC

```



```

NR=(RR/DELNU)+0.5
IF(NR.GT.1500) GO TO 22
Z4=(B0*J*(J+1.)+(A0-B0)*K2)*X
V4=EXP(-Z4)
INTR=G*V4
A(NR)=A(NR)+INTR
22 CONTINUE
C-----G BRANCH
NUG=W0+J*(J+1.)*BDIF
G=NUG-WSPEC
NQ=(Q/DELNU)+0.5
G2=2.*(2.*J+1.)*K2/(J*(J+1.))
INT0=G2*V4
A(NQ)=A(NQ)+INT0
4 CONTINUE
2 CONTINUE
C*****FIND MAX A(I)
E=0.0
DO 20 I=1,1500
20 IF(A(I).GT.E) E=A(I)
CONST=E/ALOG(90.0/20.0)
I2=1500
DO 31 I=1,1500
DUMMY=A(I2)/CONST
A2(I)=90.0*EXP(-DUMMY)
31 I2=I2-1
C*****PLOT GRAPH
PRINT 100
DO 6 N=1,100
6 CHART(N)=BLANK
DO 7 I=1,1500,5
L=A2(I)+0.5
CHART(L)=STAR
PRINT 200,CHART
7 CHART(L)=BLANK
I2=1500 & WVN=WSPEC
DO 32 I=1,1500
XNU(I2)=WVN
I2=I2-1
32 WVN=WVN+DELNU
XNU(1501)=1320.0 & XNU(1502)=-6.35
A2(1501)=0.0 & A2(1502)=12.7
CALL START
CALL PLOT(1.0,1.0,-3)
CALL AXIS(0.0,0.0,7HNU CM-1,-7,23.62,0.0,XNU(1501),XNU(1502))
CALL AXIS(0.0,0.0,13HTRANSMITTANCE,13,7.87,90.0,A2(1501),A2
CALL LINE(XNU,A2,1500,1,0,1)
CALL ENPLOT(28.0)
STOP
100 FORMAT(1H1)
200 FORMAT(1H ,100A1)
300 FORMAT(6F10.0)
END

```

(1502)

SECDIV was used to test different methods of calculating the second derivatives of experimental transmitted intensity curves.

```

PROGRAM SEC DIV (INPUT, OUTPUT)
DIMENSION LXDT(500), D2XDT2(500), DLXDTL(500), DMXDTM(500)
REAL K(500), NU(500), LINE(101)
DATA STAR, BLANK, PLUS, ZERO/1H*, 1H ,1H+, 1H0/
X1=1.0 & X3=0.04
DELNU=0.25 & N=400
NU(1)=0.0
DO 1 J=2,N
1 NU(J)=NU(J-1)+DELNU
W0=50.0
DO 2 J=1,N
2 K(J)=X1/(1.0+X3*(NU(J)-W0)**2)
DO 3 J=1,N
D2XDT2(J)=0.0
DLXDTL(J)=0.0
3 DMXDTM(J)=0.0
Z1=8.*X1*X3**2
Z2=2.*X1*X3
N2=N-6
DO 5 J=1,N2
Z3=1.+X3*(NU(J)-W0)**2
D2XDT2(J)=Z1*(NU(J)-W0)**2/Z3**3-Z2/Z3**2
DLXDTL(J+3)=(K(J+6)-K(J+4)-K(J+2)+K(J))/(8.*DELNU**2)
5 DMXDTM(J+1)=(K(J+2)-2.*K(J+1)+K(J))/DELNU**2
C*****MAKE K INTO A LINEAR PLOT BETWEEN 90 AND 20
N3=N/2+1
Z1=K(N3) & Z2=K(1)
C=ALOG(4.5)/(Z1-Z2)
DO 4 J=1,N
DUMMY=ALOG(90.0)-C*K(J)
4 K(J)=EXP(DUMMY)
C*****PLOT CONTOUR
PRINT 200
DO 7 IJ=1,101
7 LINE(IJ)=BLANK
DO 8 J=1,N+2
L=(K(J)+1.5
L2=K(J)+1.5
LINE(L)=STAR
PRINT 100, NU(J), LINE, K(J)
8 LINE(L)=BLANK
PRINT 200
PRINT 101
D2XDT2(1)=0.0
Y=0.0
X=0.0
DO 9 J=1,N
IF (D2XDT2(J).LT.Y) Y=D2XDT2(J)
IF (DLXDTL(J).LT.Y) Y=DLXDTL(J)
IF (DMXDTM(J).LT.Y) Y=DMXDTM(J)
IF (D2XDT2(J).GT.X) X=D2XDT2(J)
IF (DLXDTL(J).GT.X) X=DLXDTL(J)
9 IF (DMXDTM(J).GT.X) X=DMXDTM(J)
Z=X-Y
X=100./Z
DO 10 J=1,N,2
L=((D2XDT2(J)-Y)*X)+1.5
M=((DLXDTL(J)-Y)*X)+1.5
I=((DMXDTM(J)-Y)*X)+1.5
LINE(L)=STAR
LINE(M)=PLUS
LINE(I)=ZERO

```



```

PRINT 102, NU(J), LINE, D2XDT2(J), DLXDTL(J), DMXDTM(J)
LINE(L)=BLANK
LINE(M)=BLANK
10 LINE(I)=BLANK
STOP
100 FORMAT(5X,F7.1,1H.,101A1,2X,F6.3)
101 FORMAT(112X,'D2XDT2 DLXDTL DMXDTM'/112X,'-----')
102 FORMAT(1H.,F7.1,2X,1H.,101A1,1X,F6.3,1X,F6.3,1X,F6.3)
200 FORMAT(1H1)
END

```

THFILM corrects an experimental transmitted intensity curve
for reflection loss at the sample/cell window interfaces.

```

PROGRAM THFILM(INPUT,OUTPUT)
DIMENSION CORI(500),D(500),G(500),XN(500)
REAL IO(500),I(500),KA(500),NU(500),LINE(101),NEWI(500)
COMPLEX CN1,CN2,CT1,CT2,CTI,CR1,CR2,CB,CB2,CEX1,CEX2,CDEN,CD
DATA BLANK,STAR,ZERO,PLUS,DOT/1H.,1H*,1H0,1H+,1H./ IV,CI
CN1=(1.526,0.0)
C*****1.526 IS THE REFRACTIVE INDEX OF K BR
READ 101,N
READ 100,CONC,W0,XNE,SLIT,PATH,FIRST,DNU
READ 200,(IO(J),J=1,N)
READ 200,(I(J),J=1,N)
READ 200,(CORI(J),J=1,N)
PRINT 300
PRINT 700,W0,PATH,SLIT,XNE,FIRST
PI=3.14159 & AS=1./(4.*PI*PATH)
PISO=PI**2 & WSQ=W0**2
SXNE=XNE**2
NU(1)=FIRST
DO 1 J=1,N
K=J+1
1 NU(K)=NU(J)-DNU
DO 88 IY=1,4
DO 7 J=1,N
B=IO(J)/CORI(J)
E=ALOG(B)
7 D(J)=E/NU(J)
DO 55 J=1,N
55 KA(J)=D(J)*AS
DO 2 J=1,N
DO 3 JB=1,N
X=NU(J)**2-NU(JB)**2
IF(X)71,20,71
71 G(JB)=KA(JB)*NU(JB)/X
GO TO 3
20 G(JB)=0.0
3 CONTINUE
C*****INTEGRATION BY TRAPEZIUM RULE
SUMF=0.0 & N2=N-1
DO 6 JC=2,N2
6 SUMF=SUMF+G(JC)
SUMG=(G(1)+2.*SUMF+G(N))*DNU/2.
XN(J)=XNE-2./PI*SUMG
2 CONTINUE

```

```
C*****FIND REDUCING FACTOR TO FIT DATA TO GRAPH
```

```

E1=0.0
DO 25 J=1,N
25 IF(XN(J).GT.E1) E1=XN(J)
   E1=E1+0.1
   E2=2.0
   DO 26 J=1,N
26 IF(XN(J).LT.E2) E2=XN(J)
   E2=E2-0.1
   E3=E1-E2
   E4=100./E3

```

```
C*****PLOT GRAPH OF RF AND I .V.NU
```

```

PRINT 300
PRINT 601
NA=1
DO 30 IJ=1,101
30 LINE(IJ)=BLANK
   LP=IFIX((XN-E2)*E4)
   DO 31 J=1,N
   LINE(LP)=DOT
   M=IFIX(CORI(J)+0.5)
   L=IFIX((XN(J)-E2)*E4)
   LINE(M)=STAR
   LINE(L)=PLUS
   IF(NA.NE.1) GO TO 33
   IF(NU(J)-W0-0.5) 32,32,33
32 DO 35 IJ=1,100
35 LINE(IJ)=ZERO
   PRINT 600,NU(J),LINE,XN(J),KA(J),CORI(J)
   DO 36 IJ=1,101
36 LINE(IJ)=BLANK
   NA=2
   GO TO 31
33 PRINT 600,NU(J),LINE,XN(J),KA(J),CORI(J)
   LINE(L)=BLANK
   LINE(M)=BLANK
31 CONTINUE
   DO 4 J=1,N
   CN2=CMPLX(XN(J),KA(J))
   CB=2.*PI*NU(J)*CN2*PATH
   CR1=(CN1-CN2)/(CN1+CN2)
   CR2=(CN2-CN1)/(CN2+CN1)
   CT1=2.*CN1/(CN1+CN2)
   CT2=2.*CN2/(CN2+CN1)
   CI=CMPLX(0.0,1.0)
   CB2=CB*CI
   CEX1=CEXP(CB2)
   CEX2=CEXP(2.*CB2)
   CDEM=1.+CR1*CR2*CEX2
   CDIV=CT1*CT2*CEX1
   CTT=CDIV/CDEM
   TRAN=CAHS(CTT)
   TRSQ=TRAN**2
   NEWI(J)=TRSQ*IO(J)
4 CONTINUE
C*****PLOT A GRAPH TO COMPARE NEW AND OLD I
PRINT 300
PRINT 501
DO 5 IJ=1,101
5 LINE(IJ)=BLANK

```

```

DO 9 J=1,N
DIF=I(J)-NEWI(J)
L=NEWI(J)+0.5
M=I(J)+0.5
IF(L.EQ.M) GO TO 10
LINE(L)=STAR
LINE(M)=PLUS

GO TO 11
10 LINE(L)=ZERO
11 PRINT 500,NU(J),LINE,I(J),NEWI(J),DIF
LINE(L)=BLANK
LINE(M)=BLANK
9 CONTINUE
DO 97 J=1,N
DIF2=CORI(J)-NEWI(J)
97 CORI(J)=I(J)+DIF2
98 CONTINUE
C**** PLOT GRAPH TO COMPARE CORRECTED AND APPARANT INTENSITIES
PRINT 300
PRINT 502
DO 99 IJ=1,101
99 LINE(IJ)=BLANK
DO 90 J=1,N
DIF=I(J)-CORI(J)
L=CORI(J)+0.5
M=I(J)+0.5
IF(L.EQ.M) GO TO 91
LINE(L)=STAR
LINE(M)=PLUS
GO TO 92
91 LINE(L)=ZERO
92 PRINT 500,NU(J),LINE,I(J),CORI(J),DIF
LINE(L)=BLANK
93 LINE(M)=BLANK
STOP
100 FORMAT(7F10.0)
101 FORMAT(I10)
200 FORMAT(16F5.0)
300 FORMAT(IH1)
500 FORMAT(1H ,F6.1,2X,1H.,101A1,F5.2,4X,F5.2,4X,F6.2)
501 FORMAT(40X,'REFLECTION CORRECTION',52X,'I',6X,'NEWI',5X,'DIF',
/1-----',52X,'-',6X,'-----',5X,'-----')
502 FORMAT(40X,'REFLECTION CORRECTION',52X,'I',6X,'CORI',5X,'DIF',
/1-----',52X,'-',6X,'-----',5X,'-----')
600 FORMAT(1H ,F6.1,2X,1H.,101A1,F6.4,2X,F6.4,2X,F5.2)
601 FORMAT(112X,'XN KA CORI'/112X,'-----')
700 FORMAT(10X,'W0=',F6.1/10X,'PATH=',F9.7/10X,'SLIT=',F6.4/10X,
7,F4.2/10X,'FIRST=',F6.1)
END

```

REFERENCES

1. R.Bracewell, The Fourier Transform and its Applications, McGraw-Hill, 1965.
2. S.G.Rautian, Sov.Phys.Uspekhi, 1958, 66 , 245.
3. S.Brodersen and A.Langseth, Mat.Fys.Skr.Dan.Vid.Selsk., 1956, 1 , no.1 .
4. A.C.Hardy and F.M.Young, J.Opt.Soc.Amer., 1949, 39 , 265.
5. G.Herzberg, Molecular Spectra and Molecular Structure II, D.Van Nostrand, 1945.
6. J.W.Strutt, Phil.Mag., 1871, XLII , 441.
7. C.Runge, Z.Math., 1897, 42 , 205.
8. J.T.Houghton and S.D.Smith, Infrared Physics, Oxford University Press, 1966.
9. H.A.Lorenz, The Theory of Electrons, G.E.Stechert, New York, 1923.
10. Stoicheff, Can.J.Phys., 1954, 32 , 339.
11. E.Born and E.Wolf, Principle of Optics, Pergamon, New York, 1964.
12. R.P.Young and R.N.Jones, Chem.Rev., 1971, 71 , 219.
13. N.G.Bakhshiev and O.P.Girin, Usp.Fiz.Nauk., 1963, 79 , 235.
14. N.G.Bakhshiev, O.P.Girin and V.S.Libov, Opt.Spectry.(U.S.S.R.), 1963, 14 , 255.
15. N.G.Bakhshiev, O.P.Girin and V.S.Libov, ibid, 1963, 14 , 336.
16. N.G.Bakhshiev, O.P.Girin and V.S.Libov, ibid, 1963, 14 , 395.
17. N.G.Bakhshiev, O.P.Girin and V.S.Libov, ibid, 1964, 16 , 549.
18. H.Frohlich, Theory of Dielectrics, Clarendon, Oxford, 1949.
19. C.Bottcher, Theory of Electric Polarisation, Elsevier, Amsterdam, 1952.

39. A.Cabana, C.Bardoux and A.Chamberland, *Can.J.Chem.*,
1969, 47, 2915.
40. J.G.Rothschild, *J.Chem.Phys.*, 1970, 53, 990.
41. C.E.Favelukes, A.A.Clifford and B.Crawford, jnr., *J.Phys.*
Chem., 1968, 72, 962.
42. S.Abramowitz and R.F.Bauman, *J.Chem.Phys.*, 1963, 39, 2757.
43. H.A.Lorenz, *Fininkl.Ned.Akad.Wetenschap.Proc.*, 1906, 8, 591.
44. K.S.Seshadri and R.N.Jones, *Spec.Acta*, 1963, 19, 1013.
45. J.H.Van Vleck and V.F.Weisskopf, *Rev.Mod.Phys.*, 1945, 17, 227.
46. J.Pitha and R.N.Jones, *Can.Spec.*, 1966, 11, 14.
47. J.Pitha and R.N.Jones, *Can.J.Chem.*, 1966, 44, 3031.
48. W.Voight, *Munch.Ber.*, 1912, 603.
49. R.Kubo and K.Tomita, *J.Phys.Soc.(Japan)*, 1954, 9, 888.
50. R.G.Gordon, *J.Chem.Phys.*, 1965, 43, 1307.
51. D.Steele, *Theory of Vibrational Spectroscopy*, W.B.Saunders,
London, 1971.
52. W.A.Steele, *J.Chem.Phys.*, 1963, 38, 2411.
53. L.Favro, *Phys.Rev.*, 1960, 119, 53.
54. W.G.Rothschild, *J.Chem.Phys.*, 1970, 53, 3265.
55. W.G.Schneider, *J.Phys.Chem.*, 1962, 66, 2653.
56. T.Hedaaal, *Tetrahedron Letters*, 1968, 1683.
57. T.L.Brown and K.Stark, *J.Phys.Chem.*, 1965, 69, 2679.
58. J.Ronayne and D.H.Williams, *Chem.Comm.*, 1966, 712.
59. R.S.Armstrong, R.J.W. Le Fevre, et al, *J.Chem.Soc.(Perkin*
II), 1973, 1272.
60. J.Homer and M.Cooke, *J.Chem.Soc. A*, 1969, 777.
Molecular Complexes (chapter 3), edited by J.Tarwood,
Plenum, London, 1973.

61. S.Winstein and H.J.Lucas, *J.Amer.Chem.Soc.*, 1939, 60 ,836
62. W.T.Huntress, *J.Phys.Chem.*, 1969, 73 , 103.
63. V.G.Rothschild, *J.Chem.Phys.*, 1971, 55 , 1402.
64. C.R.Patrick and G.S.Prosser, *Nature*, 1960, 187 , 1021.
65. D.V.Fenby and R.L.Scott, *J.Phys.Chem.*, 1967, 71 , 4103.
66. E.M.Dantzler and C.M.Knobler, *J.Phys.Chem.*, 1969, 73 ,1602.
67. J.J.Gaw and F.L.Swinton, *Trans.Far.Soc.*, 1968, 64 , 2023.
68. M.E.Baur et al, *J.Phys.Chem.*, 1969, 73 , 641.
69. R.M.Barret, Ph.D. thesis, University of London, 1973.
70. H.Morawitz and K.B.Eisenthal, *J.Chem.Phys.*, 1971, 55 , 887.
71. E.A.Moelwyn-Hughes, *Physical Chemistry*, Pergamon, 1964.
72. A.R.H.Cole and A.J.Michell, *Spec.Acta*, 1964, 20 , 739.
73. A.R.H.Cole and A.J.Michell, *ibid*, 1964, 20 , 747.
74. L.Onsager, *J.Amer.Chem.Soc.*, 1936, 58 , 1486.
75. Lange, *Handbook of Chemistry*, McGraw-Hill, New York, 1967.
76. C.La Lau, *Proceedings of the Conference on Molecular Spectroscopy - February 1958*, edited by E.Thornton and H.W.Thompson, Pergamon.
77. D.H.Whiffen, *Trans.Far.Soc.*, 1953, 49 , 878.
78. J.H.R.Clarke and S.Miller, *Chem.Phys.Letters*, 1972, 13 , 97.
79. P.Borval, J.Lauransan, J.Peron and P.Saumagne, *J.Mol.Stuct.*, 1968, 2 , 73.
80. D.L.VanderHart, *J.Chem.Phys.*, 1974, 60 , 1858.
81. H.Spedding and D.H.Whiffen, *Proc.Roy.Soc.(London)*, 1956, A238, 245.
82. M.Tamres and J.Yarwood, *Spectroscopy and Structure of Molecular Complexes*,(chapter 3), edited by J.Yarwood, Plenum, London, 1973.

- 83.. W.B.Person, *ibid*, (chapter 1).
- 84.. F.J.Bartoli and T.A.Litovitz, *J.Chem.Phys.*, 1972, 56 , 404.
85. M.Constant and R.Fauquemberque, *J.Chem.Phys.*, 1973, 58 , 4030.
86. H.S.Goldberg and P.S.Pershan, *J.Chem.Phys.*, 1973, 58 , 3816.
87. W.T.King, I.M.Mills and B.Crawford, jnr., *J.Chem.Phys.*, 1957, 27 , 455.

transmission of a sample of material by a spectrometer will differ in a lesser extent from the true transmission for a variety of reasons. Correcting the observed data requires a knowledge of the appearance of true incident radiation after passage through the system. This depends on so-called instrument functions. If the true and observed intensities of frequencies are given by $I(\nu)$ and $I'(\nu)$ respectively, then

$$I'(\nu) = \int_{-\infty}^{+\infty} I(\nu') G(\nu - \nu') d\nu' \quad (1)$$

where $G(\nu - \nu')$ defines the fraction of the energy of frequency ν' which is transmitted through the system to the recorder when the instrument is set to record at a frequency ν . Provided that the spectralf $I(\nu')$ and the apparatus function $G(\nu - \nu')$ are known, the true spectrum can be obtained by Fourier transform methods. In practice this is very time consuming and impractical for routine measurements. If the form of $G(\nu - \nu')$ can be given then it is possible to derive relations in which $I(\nu)$ is a function of $I'(\nu)$, of the spectral slit width Δ , and of the derivatives of $I'(\nu)$ with respect to frequency. This approach has been applied to a number of cases, as the recording of spectra on photographic emulsions²⁸ and the use of spectral lines using the Fabry Perot etalon.²⁹

It was the aim to consider how to make an approximate correction for the distortion due to finite slit width. This analysis was based on a simple Taylor expansion of the observable as a function of the instrument setting and led to the conclusion that a first order correction to the true observable, $I(\nu)$, is given by

$$I(\nu) \approx I'(\nu) + \frac{\Delta^2}{2} \frac{d^2 I'(\nu)}{d\nu^2} \quad (2)$$

where Δ is the spectral slit width. The analysis was subsequently extended by Rings³⁰ who derived some higher order correction terms. In the opinion of the authors, the theory does not appear to have had any effect at least on infrared spectroscopy. The above is probably an historical case.

Rayleigh (Strutt) Method of Making an Approximate Correction to Spectra for Finite Slit Widths

BY IAN R. HILL AND DEREK STEELE *

Dept. of Chemistry, Royal Holloway College, University of London,
Egham Hill, Egham, Surrey TW20 0EX

Received 9th November, 1973

An expression is derived for the distortion of spectral band contours resulting from use of finite slit widths. The leading term is in agreement with a correction proposed by Rayleigh in 1871 and derived from curvature arguments. It is shown that this correction, which is proportional to the second derivative of the observed spectrum, $d^2f/d\nu^2$, allows the true band contour to be recovered to a good approximation provided that the slit width is not greater than the half band width. Loss of resolution due to finite slit widths may also be recovered. Higher power correction terms are also given, but due to the sensitivity of the higher power gradients, $d^n f/d\nu^n$, to noise, n even and greater than two, the terms appear to be of little practical importance at the present time.

The transmittance of a sample as measured by a spectrometer will differ to a greater or lesser extent from the true transmittance for a variety of reasons. Correction of the observed data requires a knowledge of the appearance of truly monochromatic radiation after passage through the system. This defines the so-called "apparatus function".¹ Thus if the true and the apparent intensities of frequencies ν and ν' are given by $\phi(\nu)$ and $f(\nu')$ respectively, then

$$f(\nu') = \int_{-\infty}^{+\infty} a(\nu' - \nu)\phi(\nu) d\nu. \quad (1)$$

In the above $a(\nu' - \nu)$ defines the fraction of the energy of frequency ν which is transmitted through the system to the recorder when the instrument is set to record at a frequency ν' . Provided that the spectrum $f(\nu')$ and the apparatus function are known then the true spectrum can be obtained by Fourier transform methods.¹ In practice this method is very time consuming and impractical for routine measurements. If an analytic form of $a(\nu)$ can be given then it is possible to derive relations in which $\phi(\nu)$ is expressed as a function of $f(\nu')$, of the spectral slit width s , and of the derivatives of $f(\nu')$ with respect to frequency.¹ This approach has been applied to a number of situations, such as the recording of spectra on photographic emulsions^{2a} and the investigation of spectral lines using the Fabry Perot etalon.^{2b}

Strutt was the first to consider how to make an approximate correction for the spectral distortion due to finite slits.³ His analysis was based on a simple Taylor series expansion of the observable as a function of the instrument setting and led to the conclusion that a first order correction to the true observable, ϕ , is given by

$$\phi(\nu) - f(\nu) = -\frac{h^2}{6} \frac{d^2 f}{d\nu^2} \quad (2)$$

where $\sqrt{2h}$ is the spectral pass, or slit width. The analysis was subsequently extended by Runge⁴ who derived some higher order correction terms.

Despite the eminence of the authors, the theory does not appear to have had any impact, at least on infra-red spectroscopy. The reason is probably an historical one.

In early infra-red spectrometers resolution was so low that the slit widths were generally much greater even than the true widths of the spectral bands. In these circumstances convergence of the Taylor series is very slow. Furthermore, due to the various sources of spectral noise, derivatives higher than those of second order in frequency are very difficult to obtain with reasonable precision. In recent years there has been a resurgence of interest in the problem of intensity corrections due to finite slits. The major reasons are as follows.

(i) With modern grating spectrometers the resolution is usually signal limited, and consequently the finite spectral slit width is the major source of signal distortion. Corrections for the non-linearity of the detection system are easily made. The spectral slit widths are generally an order of magnitude larger than the wavelengths of the radiation,* so eliminating diffraction at the slits as a significant contributing factor to the distortion.

(ii) Spectral intensity measurements are potentially of great value to the analyst.^{5, 6} While the potential has been realized in part there has been a sad history of failure to reproduce intensities and absorption coefficients between different laboratories which has impeded the transferability of data. It is accepted that this is largely due to slit width limitations.

(iii) Band shapes are known to be a valuable source of information on molecular dynamics.⁷

Ramsey, amongst other things, determined the extent to which the absorption maxima and integrated absorption intensities of Cauchy (Lorentzian) type bands were altered by triangular slit functions. It seems to the authors that much less interest has been shown in these aspects than they deserve, though his experimental procedures in measuring bands in the condensed phases are widely adopted. We shall refer to his results in the context of our own results later.

In the recent literature, effort has been focussed on the method of Burger and van Cittert as a means of making approximate and readily computable corrections to observed absorption bands.^{10, 11} This iterative "pseudo-deconvolution" method is well documented and needs no further discussion. Its weakness lies in an instability of the solution in the iterative procedure.¹² Nevertheless it has been shown that the first cycle yields a deconvoluted curve which is a very good approximation to the true curve. Other methods based on Fourier relations have been devised but they suffer from the fact that errors in the measured transmittances in the wings may lead to large errors in the corrections, and besides they are cumbersome to apply.^{12, 13} These techniques permit, at least in principle, the true bands contours to be evaluated even when the bands are of indeterminate contour and, as implied by that statement, are overlapping. The tabulations of Ramsey do not lend themselves to these problems.

In this communication our aim is to show the following.

(a) Rayleigh's method is extremely simple to apply and yet gives quite good corrections to observed spectra, provided that band widths are not less than the slit widths. Thus significant improvements may be achieved in the accuracy of absorption coefficients and integrated intensities even where bands do not conform to Lorentzian band contours. This will be of particular value in two situations namely (i) for analytical data on instruments of medium to low resolving power, (ii) in situations where Fourier transformation of data is difficult due to the absorption being non-zero at the limits of the recorded spectrum.

* With the Perkin Elmer 325 the mechanical slit width is $350 \mu\text{m}$ at a wavelength of $12 \mu\text{m}$ for a resolution of 1 cm^{-1} .

(b) Where low noise spectra with precise values of apparent absorption coefficients are attainable (as for example, in digital recording system combined with repetitive scanning) an extension of the Taylor series expansion (2) permits an excellent recovery of the true spectrum even when the band width is close to the slit width;

(c) A significant increase in resolution is attainable in principle by the Rayleigh correction for a spectrometer system in which resolution is limited by the finite slit widths.

EXAMINATION OF RAYLEIGH'S EQUATION IN ITS EXTENDED FORM

It is shown in an Appendix that the relation between the true spectrum, $\phi(v)$, and the observed spectrum, $f(v)$, is given by

$$\phi(v) = f(v) - \frac{s^2}{12} \frac{d^2 f(v)}{dv^2} + \frac{s^4}{240} \frac{d^4 f(v)}{dv^4} - \dots \quad (3)$$

provided that the series is rapidly convergent. The coefficients differ from those given by Runge⁴ (see Appendix). s is the spectral slit width in frequency units.

If eqn (3) is to be of any practical use it is necessary that the contributions of the derivatives higher than the second should be small. To test this, Lorentzian curves of various half band widths were convoluted with a triangular slit function.

$$a(v) = \begin{cases} \frac{1}{s} [1 - |v|/s] & \text{for } |v| \leq s \\ 0 & \text{for } |v| > s \end{cases}$$

The resulting band was then deconvoluted using (3) including terms up to the 6th derivative, and the percentage recovery noted. A typical set of results are shown in table 1. The correction to the maximum absorption coefficient is broken into the contributions of the various derivatives. The most noteworthy point is that the relative importance of the second derivative increases sharply with an increasing ratio of half bandwidth to slit width. Even for a half band width equal to the slit width the second order derivative term leads to nearly 60% recovery.

TABLE 1.—SHOWING THE RELATIVE IMPORTANCE OF THE n TH DERIVATIVES IN EQN (3) AS A FUNCTION OF SLIT WIDTH FOR A HALF WIDTH OF 2 cm^{-1} AND A TRUE MINIMUM TRANSMITTANCE OF 18.5% AND TRUE MAXIMUM TRANSMITTANCE OF 90%

| slit width/ cm^{-1} | total % change in minimum transmittances | % correction in min. trans due to n th derivative, | | | correction as % of total change due to | |
|---------------------------------|--|---|-----|------|---|---------------|
| | | $n = 2$ | 4 | 6 | $n = 2$ | $n = 2, 4, 6$ |
| 2.0 | 13.3 | 7.8 | 2.4 | 0.18 | 59 | 84 |
| 1.0 | 4.4 | 3.7 | 0.5 | 0.1 | 84 | 99 |
| 0.5 | 1.2 | 1.2 | 0.0 | 0.0 | 100 | 100 |

The percentage changes in minimum transmittance as recorded in table 1 are in excellent agreement with values derived from tables I and II of ref. 8. Thus for a slit width of 1 cm^{-1} and a true half band width of 2 cm^{-1} we deduce from table II of Ramsey that $\Delta v_{\frac{1}{2}}^a / \Delta v_{\frac{1}{2}}^t \approx 1.17$. $\Delta v_{\frac{1}{2}}^a$ is the apparent half band width and $\Delta v_{\frac{1}{2}}^t$ is the true half band width. From Table 1 this gives the ratio of the true to the apparent absorption coefficients as 1.16. This is equal to $\ln(90.0/18.5) / \ln(90.0/(18.5+4.4))$ within the accuracy of numbers retained.

It is fortunate that the second derivative in (3) gives such a high proportion of the correction for $s/\Delta\nu_{\frac{1}{2}} < 0.5$. Computer simulation of a noise level of $\pm 0.05\%$ produces changes in the $d^4f(\nu)/d\nu^4$ of several times their actual magnitude. Clearly it is only in situations where repetitive scanning with digital recording is feasible and worthwhile that these higher derivatives are going to be of any practical use. On the basis of this further studies employed only the second derivatives.

It is of interest to examine how successful eqn (1) is when the contours are non-Lorentzian and when there is band overlapping. Indeed when bands overlap the Lorentzian character is automatically lost. Two overlapping bands of varying half band widths and varying intensities were convoluted with a triangular slit function. The success of (1) in correcting absorption coefficients throughout the band and in allowing corrections of integrated intensities in such cases was examined.

For $s/\Delta\nu_{\frac{1}{2}} > 1.0$ the contribution of the higher derivatives in (3) becomes much more significant. Despite that, for $s/\Delta\nu_{\frac{1}{2}} = 0.67$, the integrated intensity error is only 8.9% dropping to 5.8% after correction. These figures are comforting and indicate that with modern spectrometers capable of better than 1 cm^{-1} resolution severe errors will only occur when the band or line widths are significantly less than 1 cm^{-1} . Such indications are in good accord with the experimental results shown in fig. 3 of ref. (5). This figure shows the effect of $s/\Delta\nu_{\frac{1}{2}}$ on the integrated intensity and the ϵ_{max} of the $\nu_{\text{C=O}}$ band of butyl n-butyrate. At the same time it was possible to explore the possibility of resolving bands which had become merged as a result of finite slit widths.

Table 2 contains a sample of the results showing the effects of the second derivative correction on the errors in the intensities and in the maximum absorption coefficients for pairs of bands of varying separation. The following points are worth noting.

TABLE 2.—THE EFFECTS OF SLIT WIDTHS OF 0.75 cm^{-1} ON THE MEASURED INTENSITIES (Γ) AND ON THE MAXIMUM ABSORPTION COEFFICIENTS (ϵ_{max}) OF PAIRS OF BANDS. THE HALF WIDTHS OF THE BANDS ARE TAKEN AS THE SAME AND EQUAL TO $\Delta\nu_{\frac{1}{2}}$. THE SEPARATION OF THE BANDS IS $\nu_2 - \nu_1$. THE PERCENTAGE ERRORS IN Γ AND ϵ_{max} AFTER APPLICATION OF THE SECOND DERIVATIVE CORRECTION IS SHOWN IN THE "AFTER" COLUMNS.

| $(\nu_2 - \nu_1)/\text{cm}^{-1}$ | $\Delta\nu_{\frac{1}{2}}/\text{cm}^{-1}$ | $\ln(I_0/I_1)_{\text{max}}$ | $\ln(I_0/I_2)_{\text{max}}$ | % error in Γ | | % error in ϵ_{max} | |
|----------------------------------|--|-----------------------------|-----------------------------|---------------------|-------|------------------------------------|-------|
| | | | | before | after | before | after |
| 1.5 | 2.0 | 1.0 | 1.0 | 1.01 | 0.16 | 2.7 | 0.3 |
| 2.0 | 2.0 | 1.0 | 1.0 | 0.93 | 0.18 | 5.7 | 1.1 |
| 2.0 | 2.0 | 1.0 | 0.1 | 1.01 | 0.19 | 7.9 | 1.0 |
| 2.0 | 3.0 | 1.0 | 1.0 | 0.65 | 0.17 | 1.2 | 0.06 |
| 2.0 | 1.0 | 1.0 | 1.0 | 2.92 | 0.90 | 27.6 | 9.2 |
| 2.0 | 0.5 | 1.0 | 1.0 | 8.92 | 5.80 | 55.0 | 40.2 |

(a) The errors in the integrated intensities are much less than those in the absorption maxima. This fact is already well known.

(b) The errors in the integrated intensities are little affected by the separation or the relative intensities of the two bands. This is in marked contrast to the behaviour of the absorption coefficients. As the band separation decreases so do the second derivatives near to the band maxima, and consequently the maximum extinction coefficients becoming more accurate. This clearly shows the danger in applying Ramsey's correction without checking first that the band contour is close to a Lorentzian.

(c) Even when $s/\Delta\nu_{\frac{1}{2}} \rightarrow 1.0$ the error in the integrated intensity is only 3-4%. With the second derivative correction this can be reduced to 1%.

DISCUSSION

The computer experiments described in this communication clearly demonstrate the usefulness of the Rayleigh formula (eqn (2)). In the case of bands well separated from neighbouring bands it is probably best to correct the observed maximum extinction coefficients using the tabulations of Ramsey. Where overall band contours are of interest the present treatment is advocated in that it is simple to apply and yet for $\nu/\Delta\nu_{1/2} \leq 1$ gives good corrections. The nature of the correction leads to an interesting possibility. It is a simple electronic problem to generate the second derivative of a signal. By suitable attenuation and feedback the signal to the recorder can be "corrected" for slit width distortion. Unfortunately one can never gain something for nothing. The noise in the second derivative signal will increase the overall noise level. It follows that it may be necessary to reduce the signal amplification, in order to keep the noise within acceptable limits, and perhaps to increase the slit widths. It then becomes a question of whether the gain in resolution is greater than the loss.

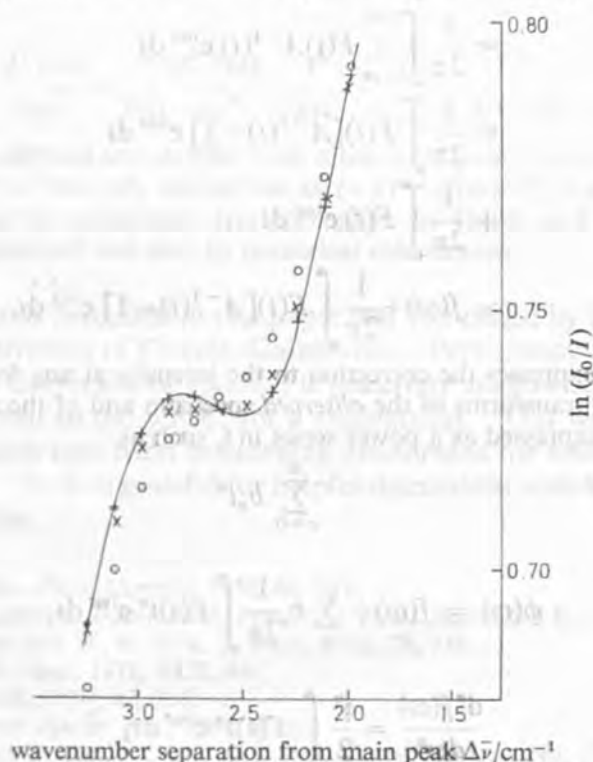


FIG. 1.—The resolution enhancement resulting from the second derivative correction. The graph is for two Lorentzian bands of half band widths 2 cm^{-1} , frequency separation 3 cm^{-1} , relative intensities 1 : 5 and for a slit width of 0.75 cm^{-1} . Only that part of the graph in the region of the weaker component is shown. +, (joined by solid line), true spectrum; O, "observed" spectrum, that is convoluted with triangular slit function; x, after second derivative correction has been applied.

It seems certain that the full potential of the technique is going to be realized with data collection systems and repetitive scanning techniques. Our own experience has been limited to single scan runs and no problems in applying the second derivative correction have yet been experienced.

Since eqn (2) is so successful in drastically reducing the errors due to slit width distortion, it follows that where resolution of bands has been lost due to finite slit widths the correction should permit a recovery of the band resolution. This is well exemplified by the calculations for 2 bands with intensities in the ratio 5 : 1 and

$s : \Delta v_{\frac{1}{2}} : v_2 - v_1$ of 0.75 : 2 : 3. That part of the overall band contour which is relevant to the demonstration of band resolution is shown in fig. 1. The resolution of the two bands on applying the correction is clearly demonstrated.

APPENDIX I

For convenience we shall express eqn (1) in radial frequency $\omega = 2\pi\nu$. Thus

$$f(\omega) = \int_{-\infty}^{+\infty} \phi(\omega') a(\omega - \omega') d\omega'$$

By the convolution theorem

$$F(t) = \Phi(t)A(t)$$

where $F(t)$, $\phi(t)$ and $A(t)$ are the fourier transforms of $f(\omega)$, $\phi(\omega)$ and $a(\omega)$ respectively. Thus

$$\begin{aligned} \phi(\omega) &= \frac{1}{2\pi} \int_{-\infty}^{+\infty} \Phi(t) e^{i\omega t} dt \\ &= \frac{1}{2\pi} \int_{-\infty}^{+\infty} F(t) A^{-1}(t) e^{i\omega t} dt \\ &= \frac{1}{2\pi} \int F(t) [A^{-1}(t) - 1] e^{i\omega t} dt \\ &\quad + \frac{1}{2\pi} \int F(t) e^{i\omega t} dt \\ &= f(\omega) + \frac{1}{2\pi} \int F(t) [A^{-1}(t) - 1] e^{i\omega t} dt. \end{aligned}$$

This exact equation expresses the correction to the intensity at any frequency as a function involving the fourier transforms of the *observed* spectrum and of the apparatus function.

If $A^{-1}(t)$ can be expressed as a power series in t , such as

$$\sum_{n=0}^{\infty} b_n t^n$$

then

$$\phi(\omega) = f(\omega) + \sum_n b_n \frac{1}{2\pi} \int F(t) t^n e^{i\omega t} dt,$$

but

$$\frac{d^n f(\omega)}{d\omega^n} = \frac{i^n}{2} \int F(t) t^n e^{i\omega t} dt,$$

hence

$$\phi(\omega) = f(\omega) + \sum_n \frac{b_n}{i^n} \frac{d^n f(\omega)}{d\omega^n}. \quad (\text{A1})$$

Thus if we can identify the coefficients b_n , the true spectrum can be deduced from the observed spectrum by taking differentials.

For systems in which the electrical and optical aberrations are small the apparatus function can be approximated by a slit function. In the case of a spectrometer which has mirror symmetry about the dispersive element and equal entrance and exit slits the appropriate slit function is a triangular function

$$\begin{aligned} a(\omega) &= \frac{1}{2s} \left[1 - \frac{|\omega|}{s} \right] \quad \text{for } |\omega| \leq s \\ &= 0 \quad \text{for } |\omega| > s, \end{aligned} \quad (\text{A2})$$

Note that $a(\omega)$ is normalized so that $\int a(\omega) = 1$, and also that ω and s must be expressed in the same units for the function to be meaningful. We see then that s is expressed in radial frequency as the product of linear dispersion at the exit slit multiplied by the physical slit width.

The fourier transform of (A2) is

$$A(t) = \left[\frac{\sin\left(\frac{st}{2}\right)}{\frac{st}{2}} \right]^2 \quad (\text{A3})$$

Expanding (A3) as a power series in st we obtain

$$A^{-1}(t) - 1 = \frac{(st)^2}{12} + \frac{(st)^4}{240} + \dots$$

and hence

$$\phi(\omega) = f(\omega) - \frac{s^2}{12} \frac{d^2 f(\omega)}{d\omega^2} + \frac{s^4}{240} \frac{d^4 f(\omega)}{d\omega^4} - \frac{s^6}{6048} \frac{d^6 f(\omega)}{d\omega^6} + \frac{s^8}{604800} \frac{d^8 f(\omega)}{d\omega^8} \dots \quad (\text{A4})$$

The coefficients as derived above differ from those for $N \geq 4$ given by Runge. The latter gives the coefficients of the n th derivatives as $(-1)^{n/2} 2[(n/2)!]^2 / (n+2)!$. An alternative method of computing the corrections has been given by Hardy and Young.¹³ We have verified (A4) by this method and also by numerical calculations.

Part of the research described in this paper was completed by D. S. while on leave of absence at the University of Florida, Gainesville. Partial support from the Department of Chemistry, University of Florida, is gratefully acknowledged.

I. R. H. is indebted to the S.R.C. for a studentship. This work forms part of a programme of research into band broadening phenomena for which a grant has been given by the S.R.C. D. S. is grateful for helpful discussions with W. B. Person during his stay in Gainesville.

¹ S. G. Rautian, *Sov. Phys. Uspekhi*, 1958, **66**, 245.

² (a) M. M. Sushchinskii, *Dissertation* (Phys. Inst. Acad. Sci. U.S.S.R., Moscow, 1957);

(b) L. C. Ornstein and W. R. Wyk, *Z. Phys.*, 1932, **78**, 734.

³ J. W. Strutt, *Phil. Mag.*, 1871, **XLII**, 441.

⁴ C. Runge, *Z. Math.*, 1897, **42**, 205.

⁵ A. S. Wexler, *Appl. Spectr. Rev.*, 1967, **1**, 29.

⁶ W. B. Person and D. Steele, *Chem. Soc. Spec. Periodical Rep.*, No. 29, vol. 2, editors R. F. Barrow, D. A. Long and D. J. Miller (Chem. Soc., London, 1974).

⁷ For reviews of this subject see for example,

(a) R. G. Gordon, *Adv. Magnetic Resonance*, 1968, **3**, 1.

(b) K. D. Möller and W. G. Rothschild, *Far Infrared Spectroscopy* (Wiley Interscience, New York, 1971), p. 273.

⁸ D. A. Ramsey, *J. Amer. Chem. Soc.*, 1952, **74**, 72.

⁹ H. C. Berger and P. H. Van Cittert, *Z. Phys.*, 1932, **79**, 722; 1933, **81**, 428.

¹⁰ W. F. Herget, W. E. Deeds, N. M. Gailar, R. J. Lovell and A. H. Nielsen, *J. Opt. Soc. Amer.*, 1962, **52**, 1113.

¹¹ R. N. Jones, R. Venkataraghavan and J. W. Hopkins, *Spectrochim. Acta*, 1967, **23A**, 925.

¹² J. S. Rollett and L. A. Higgs, *Proc. Phys. Soc.*, 1962, **79**, 87.

¹³ A. C. Hardy and F. M. Young, *J. Opt. Soc. Amer.*, 1949, **39**, 265.

Vibrational Band Contours

Part 1.—The Hexafluorobenzene-Benzene System

By R. M. BARRETT, F. P. GILL AND DAVID STILES

Department of Chemistry, Royal Holloway College, (University of London), Egham, Surrey TW20 0EX

Received 10th March 1974

Interactions between benzene and hexafluorobenzene lead to a frequency shift and a broadening of the band arising from the out-of-phase C-H stretching vibration. It is demonstrated that the intramolecular interactions are short lived, stochastic, are not simple polar interactions and that the resulting forces are directed perpendicular to the ring plane. This is based on symmetry considerations and on the concentration of the absorption intensity in the C-H stretching region.

VIBRATIONAL BAND CONTOURS

PART 1.—THE HEXAFLUOROBENZENE-BENZENE SYSTEM

G.H.R.

LIBRARY

Any absorption band is characterized by three parameters, its frequency, its intensity and its band contour. For vibrational absorption bands in the liquid or solution state, the latter parameter was neglected as a source of molecular information until the late 1960s. At that time, the case of the Scherer-Long and Long-Scherer systems of stationary energy states showed from this study, the main non-frequency and intensity of a band are both well defined molecular parameters, but the band contour is determined by entirely separate considerations, such as Doppler broadening and collisional interactions. Transition of the problem into the Herzberg formalism shows that the Fourier transform of intensity with respect to the frequency shift from the band centre leads to the autocorrelation function of the transition moment. If the transition moment at a time t is written as $m(t)$, where m is the magnitude and ω is a unit vector defining the direction of the moment, then

$$m(t) = \sum_i m_i(t) \exp(i\omega_i t) \quad (1)$$

the correlation function is

$$C(t) = \langle m(t) \cdot m(0) \rangle = \langle \sum_i m_i(t) \exp(i\omega_i t) \cdot \sum_j m_j(0) \rangle \quad (2)$$

where $\langle \dots \rangle$ is the ensemble average. The correlation function $C(t)$ is a function of time and is independent of the direction of the band centre. The frequency of the band centre, $\bar{\omega}$, is the frequency of the band centre; ω_i is the frequency of the i th transition and $m_i(t)$ is the transition moment over the entire band and $m_i(0) = m_i(t)$ at $t=0$. The correlation function $C(t)$ is independent of time and if the motions of different molecules are uncorrelated, then the Fourier transform of the absorption intensity simplifies to the

Vibrational Band Contours

Part 1.—The Hexafluorobenzene–Benzene System

BY R. M. BARRETT,† E. B. GILL AND DEREK STEELE*

Department of Chemistry, Royal Holloway College (University of London),
Egham, Surrey TW20 OEX

Received 18th March, 1974

Interactions between benzene and hexafluorobenzene lead to a frequency shift and a broadening of the band arising from the out-of-plane CF bending vibration (a_{2u} species). It is deduced that the intermolecular interactions are short lived, stochastic, are not simple polar interactions and that the resulting forces are directed perpendicular to the ring plane. This is based on symmetry considerations and on the concentration dependence and magnitudes of the frequency shifts and of the Fourier transforms of the absorption band contours. Assuming that vibrational relaxation occurs through dissociation of the complex with 100% efficiency, leads to lower limits for the rate constants for complex formation and dissociation. There are still a number of outstanding problems of interpretation.

Any absorption band is characterised by three parameters, its frequency, its intensity and its band contour. For vibrational absorption bands in the liquid or solution state, the latter parameter was neglected as a source of molecular information until ten years ago. A probable cause of this neglect was the use of the Schrödinger picture of stationary energy states. Viewed from this angle, the transition frequency and intensity of a band are both well defined molecular parameters, but the band contour is determined by entirely separate considerations, such as Doppler broadening and collisional interactions. Translation of the problem into the Heisenberg formulation shows that the Fourier transform of intensity with respect to the frequency shift from the band centre leads to the autocorrelation function of the transition moment.^{1, 2} If the transition moment at a time t is written as $m(t)\mathbf{u}(t)$ where $m(t)$ is the magnitude and $\mathbf{u}(t)$ is a unit vector defining the direction of the moment, then

$$\frac{\langle m(t)\mathbf{u}(t) \cdot m(0)\mathbf{u}(0) \rangle}{m(0)^2} = \frac{\int \Gamma(\nu) \exp[i2\pi(\nu - \nu_0)t] d\nu}{\int \Gamma(\nu) d\nu} = G_1(t). \quad (1)$$

ν_0 is the frequency of the band centre; $\Gamma(\nu)$ is $\ln(I_0/I)_\nu$ where $(I_0/I)_\nu$ is the fractional transmission at a frequency ν ; the integrations are over the entire band and $m(t)\mathbf{u}(t) = \langle \psi' | \mu | \psi'' \rangle$.

If $m(t)$ is independent of time and if the motions of different molecules are uncorrelated, then the Fourier transform of the absorption intensity simplifies to the

† present address: Dearborn Chemicals Limited, Water Treatment Division, Foundry Lane, Ditton, Widnes, Lancs.

autocorrelation function of the unit vector defining the direction of the transition moment :

$$\langle \mathbf{u}_i(0) \cdot \mathbf{u}_i(t) \rangle = \frac{\int \Gamma(\nu) \exp[i2\pi(\nu - \nu_0)t] d\nu}{\int \Gamma(\nu) d\nu} = G_{1R}(t).$$

Until recently it has been assumed that $G_1(t)$ is governed solely by the reorientation of the transition dipole with time. However, it is now clear (see below) that vibrational relaxation, vibrational frequency shifts and vibrational rotation interaction all frequently contribute to a significant degree. We shall show in a future publication that vibration rotation interaction produces predictable changes in the expansion of correlation functions in terms of time.³ For our present purposes this may be neglected. In a low viscosity fluid, it appears that separation of the total autocorrelation function into rotational and vibrational parts leads to the identification of two quite different situations. If vibrational relaxation (or, more generally isotropic relaxation) and vibrational frequency shifts are independent of rotational relaxation, the $G_1(t)$ can be expressed as the simple product of the rotational and vibrational contributions.⁴ Thus :

$$G_1(t) = G_V(t) \cdot G_{1R}(t).$$

The stochastic behaviour of the intermolecular interactions in this case leads to the result that at times, which are long compared with the average time between collisions, both $G_V(t)$ and $G_{1R}(t)$ show an exponential decay with time. This is shown to be the situation for the a_{2u} band of hexafluorobenzene in the solvent system benzene + cyclohexane.

If on the other hand there is significant coupling between translation and vibrations, a non exponential decay of $G(t)$ results. An example of this behaviour is probably shown by the out-of-plane CH bending modes of benzene in polar solvents.⁵ The increase in rate of decay of $G_1(t)$ for these vibrations over the corresponding values in cyclohexane is a Lorentzian function in t . Also, broadening is proportional to the dipole moment of the solute.

When hexafluorobenzene (HFB) and benzene are mixed in equimolar quantities, the system has a melting point 20°C higher than that of either component.⁶ It was inferred that HFB and benzene complex, and a considerable number of experimental studies have now been made on the system. The observed effects of the interactions have been disappointingly weak. The dipole moment for the postulated complex was shown to be less than 0.1 debye.⁷ No charge transfer bands have been identified and as recently as 1970 it could reasonably be stated that "spectroscopic evidence for complexing has been conspicuous by its absence".⁸ Thermodynamic properties of the mixtures clearly show interactions do exist in the liquid state, but the interaction forces seem to be quite weak [see ref. (8) and earlier references therein]. It has been suggested that the interaction is purely electrostatic and is probably of a dipole-quadrupole type.⁹ Powell, Swinton and Young applied the statistical theory of Rowlinson and Sutton to measurements of gas-liquid critical temperatures and deduced that there is an angle dependent force, but were of the opinion that the interaction is short lived and could probably be explained without invoking specific covalent bonding forces.¹⁰

In the following it is shown that subtle changes in the spectrum of HFB resulting from interactions with benzene give new insight into the molecular dynamics and forces obtaining in the system.

EXPERIMENTAL

Hexafluorobenzene was a spectroscopically pure sample from Bristol Organics Ltd. Acetonitrile and cyclohexane were of spectroscopic quality from B.D.A. Spectra in the region of the a_{2u} mode of hexafluorobenzene were recorded both on an RIIC FS 720 interferometer and on a Perkin Elmer 325 double beam spectrometer at resolutions of about 2.0 cm^{-1} . The transmission linearity of the PE 325 was verified as being within 0.5 % by the use of calibrated choppers. Good agreement was obtained from the different runs on frequencies and band widths. The interferometric studies suggested that the a_{2u} band increased in intensity by about 30 % in going from cyclohexane solution to benzene solution. However, the PE 325 measurements showed that no increase occurred on addition of benzene to cyclohexane up to at least a 1 : 1 mixture. A small increase of 10 % occurred in going to HFB in pure benzene. All these measurements were made at an HFB concentration of about 0.08 mol dm^{-3} and in a caesium iodide or polythene cell with a 2 mm path length. The discrepancies in intensities arose because of difficulties in locating the background on the interferometer trace. It would appear that the extended but shallow wings of the band in cyclohexane were not noted in the spectral noise. The error decreased in the much broader band in benzene. The interferometer results were previously reported to lead to an equilibrium constant for the HFB-benzene association of $1.0 \text{ dm}^3 \text{ mol}^{-1}$ and a broadening proportional to the complex concentration.¹¹ These results were in error and serve to show the difficulties which can occur when seeking to derive equilibrium constants from bands which change in contour.

Data were processed on a CDC 6600 using programs developed in our laboratories. All data were corrected for slit width distortion using the formula :

$$I(\nu) = T(\nu) - \frac{s^2}{12} \frac{\partial^2 T}{\partial \nu^2}$$

where $I(\nu)$ and $T(\nu)$ are the true and apparent transmitted intensities and s is the spectral slit width.¹² This method has an advantage over full spectral deconvolution in that it can be applied even when the absorption does not decrease to zero at the spectral limits and also in that it is simple and rapid to apply. Corrections due to refractive index and field distortions were so low as to be negligible.

RESULTS AND DISCUSSION

The most significant observation is that no e_{1u} band is affected in any way by change of solvent whereas the a_{2u} umbrella mode suffers both an increase in wave-number of 5 cm^{-1} in going from cyclohexane or CS_2 to benzene solution and a drastic change in band contour (see fig. 1). This suggests that benzene and HFB are interacting on collision in such a way as to perturb those orbitals which are symmetric with respect to the C_6 axis. Such an interaction would arise from π - π complexing. The lack of any significant intensity change in the a_{2u} mode does not exclude the possibility of long lived complexing of the π - π type but suggests that it is not very probable. The bands are reasonably symmetric in all solutions. Since the band centre moves by about one half band width this excludes the possibility that such broadening arises from overlapping of bands due to molecules in different long lived states of aggregation. By long lived in this context, we mean existing for longer than the reciprocal of the radial frequency separation between the bands in the two pure solvents ($\sim 1 \times 10^{-12} \text{ s}$).

On this basis we can expect the changes in the Fourier transforms of the bands in the solutions to give information on the relaxation mechanisms for the vibration in its various environments. The lack of any second isotope of fluorine simplifies the procedure. We have made no effort to account for the shift of band centre resulting from the natural ^{13}C content on the grounds that the effect will be small and that it

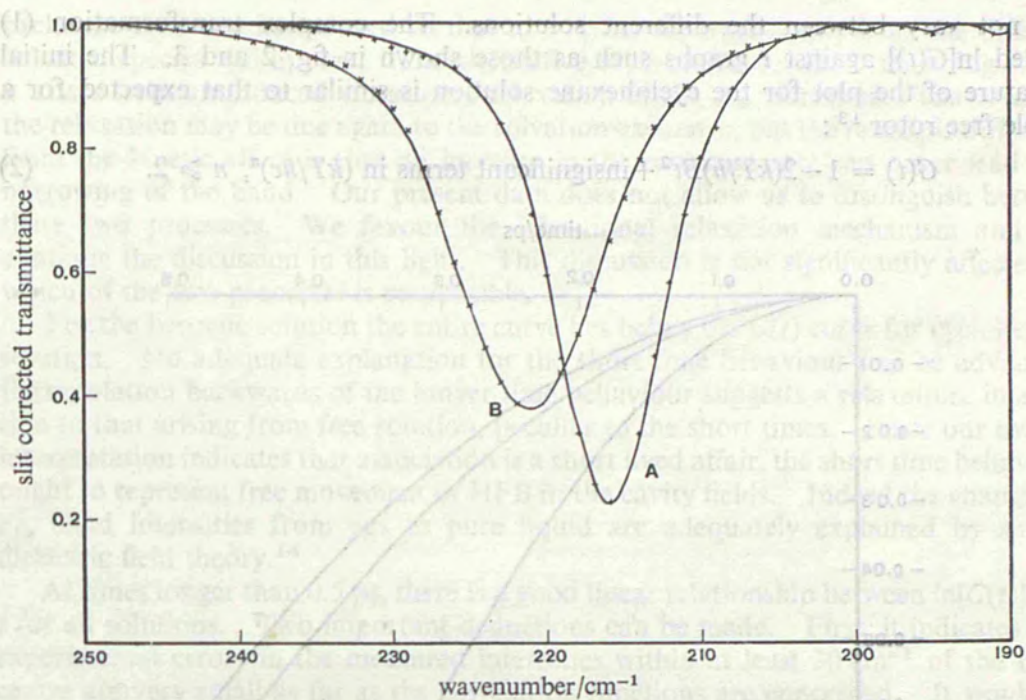


FIG. 1.—The a_{2u} absorption band of hexafluorobenzene (A) in cyclohexane solution and (B) in benzene solution (2 cm path length and 0.08 mol dm^{-3}).

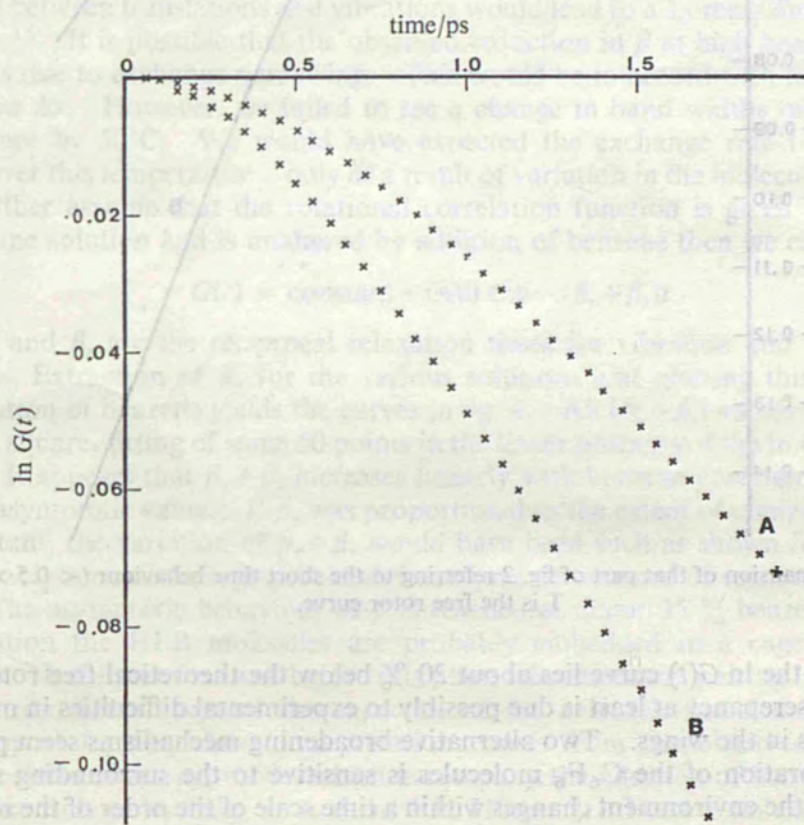


FIG. 2.—The $\ln[G(t)]$ against time plot for the a_{2u} vibration of hexafluorobenzene in benzene solution (B) and in cyclohexane solution (A).

will not vary between the different solutions. The complex transformation (1) yielded $\ln[G(t)]$ against t graphs such as those shown in fig. 2 and 3. The initial curvature of the plot for the cyclohexane solution is similar to that expected for a simple free rotor¹³:

$$G(t) = 1 - 2(kT/h)Bt^2 + \text{insignificant terms in } (kT/hc)^n, n \geq 2. \quad (2)$$

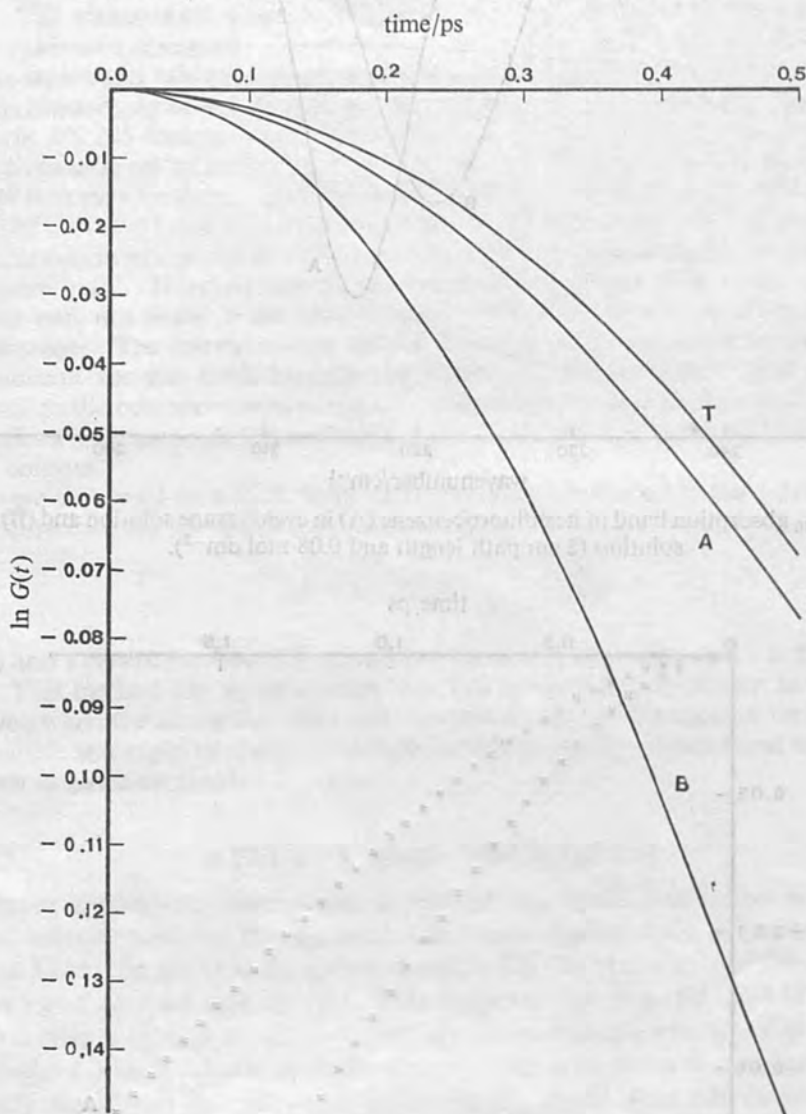


FIG. 3.—An expansion of that part of fig. 2 referring to the short time behaviour ($< 0.5 \times 10^{-12}$ s). T is the free rotor curve.

Up to 0.5 ps the $\ln G(t)$ curve lies about 20 % below the theoretical free rotor curve. The initial discrepancy at least is due possibly to experimental difficulties in measuring the intensities in the wings. Two alternative broadening mechanisms seem plausible. If the a_{2u} vibration of the C_6F_6 molecules is sensitive to the surrounding solvation sheath and if the environment changes within a time scale of the order of the reciprocal of the radial frequency difference between the transition frequencies in the two environments ($\tau_e \approx 1/\Delta\omega$), then exchange broadening will occur. In the event of very fast exchange ($\tau_e \ll 1/\Delta\omega$) then coalescence to a single sharp band will occur, whereas if the

exchange time can be reduced so that $\tau_e \gg 1/\Delta\omega$ separate bands from the different solvated species will appear. The alternative explanation for the broadening is that it arises from an induced vibrational relaxation of the a_{2u} vibration. The origin of the relaxation may be due again to the solvation exchange, but the principle difference from the kinetic effect is that an increase in the exchange rate can never lead to a narrowing of the band. Our present data does not allow us to distinguish between these two processes. We favour the vibrational relaxation mechanism and will continue the discussion in this light. This discussion is not significantly affected by which of the two processes is responsible.

For the benzene solution the entire curve lies below the $G(t)$ curve for cyclohexane solution. No adequate explanation for the short time behaviour can be advanced. Extrapolation backwards of the longer time behaviour suggests a relaxation, in addition to that arising from free rotation, peculiar to the short times. Since our overall interpretation indicates that association is a short lived affair, the short time behaviour ought to represent free movement of HFB in the cavity fields. Indeed the changes in e_{1u} band intensities from gas to pure liquid are adequately explained by simple dielectric field theory.¹⁴

At times longer than 0.5 ps, there is a good linear relationship between $\ln[G(t)]$ and t for all solutions. Two important deductions can be made. First, it indicates that experimental errors in the measured intensities within at least 30 cm^{-1} of the band centre are very small as far as the correlation functions are concerned. It would be more than fortuitous if errors converted a non-linear relationship into a linear one. Secondly we see that all the relaxation processes involved at these times are random. Coupling between translations and vibrations would lead to a Lorentzian contribution to $G(t)$.^{5, 15} It is possible that the observed reduction in β at high benzene concentrations is due to exchange narrowing. This would be in accord with the continuing increase in $\Delta\nu$. However, we failed to see a change in band widths on varying the temperature by 50°C . We would have expected the exchange rate to vary significantly over this temperature if only as a result of variation in the molecular velocities. If we further assume that the rotational correlation function is given by β for the cyclohexane solution and is unaltered by addition of benzene then we can write:

$$G(t) = \text{constant} + G(0) \exp -(\beta_v + \beta_r)t$$

where β_v and β_r are the reciprocal relaxation times for vibration and rotation respectively. Extraction of β_v for the various solutions and plotting this against the concentration of benzene yields the curves in fig. 4. All $(\beta_v + \beta_r)$ values were derived by a least squares fitting of some 50 points in the linear portions of the $\ln G(t)$ against t graphs. It appears that $\beta_v + \beta_r$ increases linearly with benzene concentration almost up to its asymptotic value. If β_v was proportional to the extent of complexing and β_r was constant, the variation of $\beta_v + \beta_r$ would have been such as shown for curve (B). It is probably unrealistic to expect such behaviour on account of solvent cage effects alone. The asymptotic behaviour of β is reached at about 35% benzene. At this concentration the HFB molecules are probably embedded in a cage of benzene molecules. It follows that well before this point relaxation and pairing is going to be enhanced above and beyond the expectations for a simple bimolecular reaction. Some support for the above interpretation comes from the observed vibrational frequency shifts of the a_{2u} mode, which accompany the addition of benzene. These shifts are considerable, being up to 5 cm^{-1} in 210 cm^{-1} . There is an excellent linear relationship between the shift and β up to the maximum value of the relaxation constant. Thereafter, while β changes only very slightly, the frequency shift continues to increase at its previous rate.

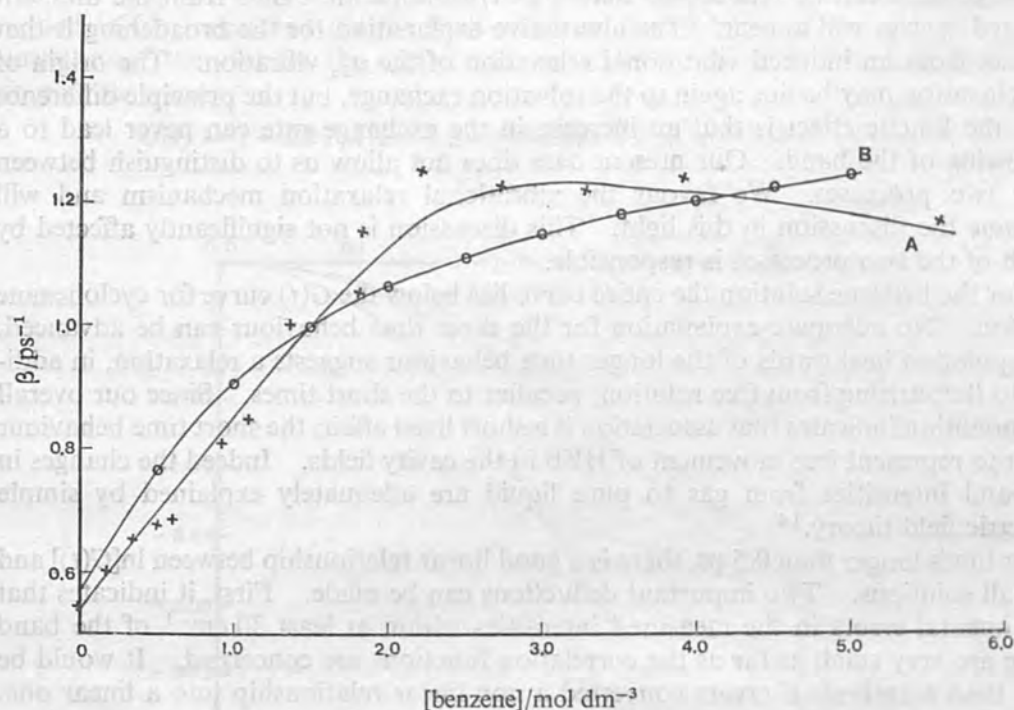
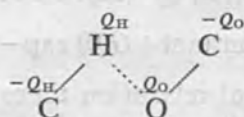


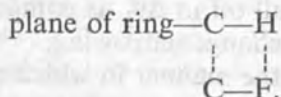
FIG. 4.—A plot of the reciprocal relaxation time ($\beta = \beta_v + \beta_r$) against concentration of benzene. The concentration of hexafluorobenzene is 0.8 mol dm^{-3} in cyclohexane + benzene mixtures [curve (A)]. Curve B is as expected for a property arising from a HFB + benzene complex with an equilibrium constant of $0.625 \text{ dm}^3 \text{ mol}^{-1}$ and assumes $\beta(0) = 0.545 \text{ s}^{-1}$ and $\beta(\text{max}) = 1.445 \text{ s}^{-1}$.

The out-of-plane γ_{H} vibrations of aromatic systems increase in frequency on addition of polar solvents, and the bands are broadened. LaLau proposed¹⁶ that these effects were due to polar interactions of the type



where O represents a terminal atom of any polar bond. If r is the distance between the polar group terminal atom and the hydrogen nucleus then the increment to the force constant for movement of the hydrogen towards the C—O axis is $Q_{\text{H}}Q_{\text{O}}/4\pi\epsilon_0r^3$. Substitution of accepted values for these parameters gives excellent agreement between calculated and observed shifts for systems such as acetone + benzene and acetonitrile + benzene. There are difficulties with the model which are discussed below. However, the predicted magnitude of the shift for the benzene + HFB case is far too small to account for the observations. Taking the CH and CF bond dipoles as 0.3 D and 0.6 D (1×10^{-30} and $2 \times 10^{-30} \text{ C m}$)^{17, 18} and taking the average distance of approach, r , as about 2.3 \AA then the extra dipolar restoring force is $0.0010 \text{ m dyn \AA}^{-1}$ (0.10 N m^{-1}) which is to be compared with the actual force constant for movement of the fluorine out of the plane of $0.2 \text{ m dyn \AA}^{-1}$ (20 N m^{-1}). This would explain only a 0.5 cm^{-1} shift. In fact there are other difficulties with the model. If we accept a model in which the interacting bonds are collinear, it is difficult to see why only the out-of-plane CH vibrations are affected. It might be expected that the in-plane β_{H} modes are affected equally. No shifts or band broadening are observed for the in-

plane modes. A more favourable configuration than that suggested above might be one in which the two dipoles were opposed in the manner



In this configuration only the γ modes would be affected, but now the modification to the restoring forces through electrostatic interactions must be much reduced since during the γ distortion one pair of interacting poles will approach while the other recedes. It appears then that, at least for the case being investigated, electrostatic interactions are an inadequate explanation of the observed phenomena. We postulate that the observed frequency shifts arise from π - π interactions which modify the restoring forces. This seems reasonable, but the relation between the frequency shift and the reciprocal relaxation time shown in fig. 5 must be rationalised. It should be noted that the observed sharp change in gradient in the β against $\Delta\nu$ curve occurs at a very high benzene concentration (35 %). This indicates that at an attainable concentration all excited molecules have achieved their maximum relaxation rate, but that the HFB molecules have not yet been surrounded by the maximum density of benzene molecules. A continued increase in the number of benzene molecules in the HFB environment leads to further increases in the restoring force.

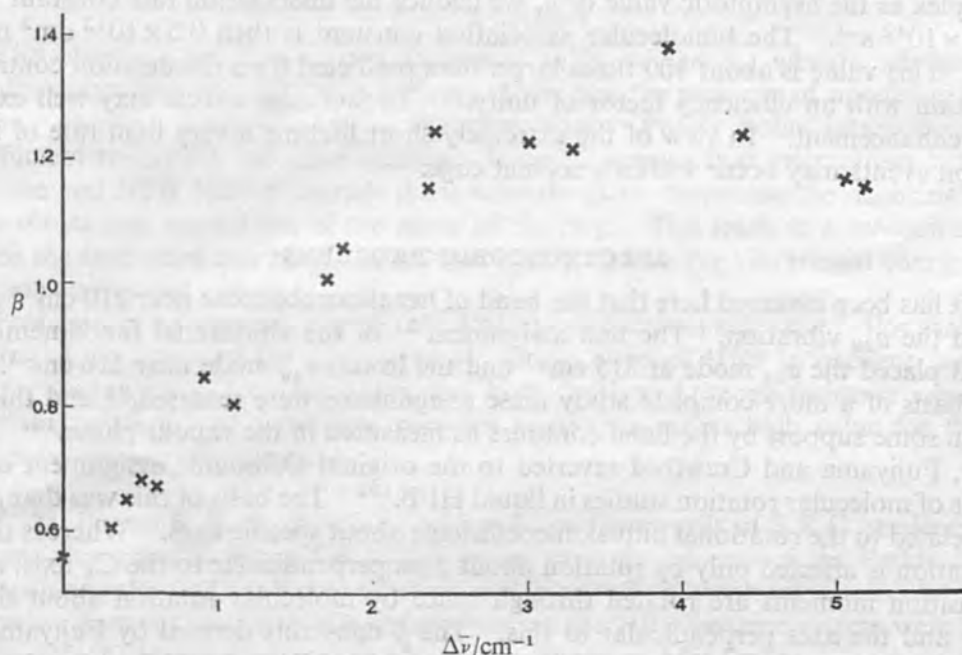


FIG. 5.—A plot of reciprocal relaxation time against frequency shift for the HFB + benzene + cyclohexane system.

Indeed the continued increase in $\Delta\nu$ up to 100 % benzene solvent is in accord with the thermodynamic evidence that the association energy between HFB and benzene is very small. Some studies of the temperature dependence have been made. Experimental difficulties have resulted in the results being of low accuracy, but any temperature effects on bands widths over a 50°C temperature range are clearly very small. Small frequency shifts of $0.03 \text{ cm}^{-1} \text{ } ^\circ\text{C}^{-1}$ were observable. If the kinetic exchange, rather than the vibrational relaxation, mechanism is responsible for the band width

effects we would have expected to have seen some sign of further band narrowing in the benzene + C₆F₆ solution on increasing the temperature. This is based on the assumption that the observed fall off in $\Delta\nu_{\frac{1}{2}}$ as compared with the frequency shift, is due in this interpretation, to exchange narrowing.

While it is easy to visualise the manner in which interactions (charge transfer for example) can lead to an increase in the γ restoring force, the mechanism of vibrational relaxation is less obvious. In the time intervals involved, vibrational energy transfer seems most unlikely. It may be significant however that the vibrational quantum is very close to kT (~ 210 cm⁻¹). Differences between the effective bond dipoles as derived from intensity measurements of in-plane and out-of-plane fundamentals of benzene and HFB¹⁷⁻¹⁹ have been interpreted as showing that there is an electronic rehybridisation moment resulting from movement of the H or F atoms out of the plane of the ring. It follows that any π - π interactions will be modified to some extent by γ type motions. It could well be then that in a dissociation process the vibrational quantum has a significant probability of being degraded into thermal energy. This process will be rendered much more likely by the similarity in magnitude of kT and $h\nu$. The implications of such a process will now be explored. If every dissociation of a molecular pair involving a vibrationally excited HFB molecule led to vibrational relaxation, then from the data in fig. 4 we can deduce that the equilibrium constant for complex formation is about 0.8 mol dm⁻³. Taking the reciprocal lifetime of the complex as the asymptotic value of β_v we deduce the dissociation rate constant to be 0.70×10^{12} s⁻¹. The bimolecular association constant is then 0.5×10^{12} dm³ mol⁻¹ s⁻¹. This value is about 100 times larger than predicted for a dissociation controlled reaction with an efficiency factor of unity.²⁰ In fact cage effects may well explain this enhancement. In view of the extremely short lifetime a very high rate of interaction events may occur within a solvent cage.

SPECTROSCOPIC PROBLEMS

It has been assumed here that the band of hexafluorobenzene near 210 cm⁻¹ arises from the a_{2u} vibration. The first assignment²¹ of the vibrational fundamentals of HFB placed the a_{2u} mode at 315 cm⁻¹ and the lowest e_{1u} mode near 210 cm⁻¹. On the basis of a more complete study these assignments were reversed,²² and this was given some support by the band contours as measured in the vapour phase.¹⁸ However, Fujiyama and Crawford reverted to the original Delbouille assignment on the basis of molecular rotation studies in liquid HFB.^{14b} The basis of this was that β_r can be related to the rotational diffusion coefficients about specific axes. Whereas the a_{2u} vibration is affected only by rotation about axes perpendicular to the C₆ axis, all e_{1u} transition moments are rotated through space by molecular rotation about the C₆ axis and the axes perpendicular to this. The β constants derived by Fujiyama and Crawford (actually $\beta_v + \beta_r$ for pure liquid) were 0.83, 0.84 and 0.44 ps⁻¹ for the 1534, 1010 and 315 cm⁻¹ bands respectively. Since the low frequency value was so much smaller it was proposed that it arises from a different species to the two high frequency bands. These deductions are valid only in the absence of important vibration rotation interactions. All e_{1u} modes must exhibit first order Coriolis coupling between the degenerate components. While molecular rotation undergoes frequent interruptions in the condensed state, the coupling must still exist during rotation. The necessary theory has not yet been developed to account for the dependence of the long time behaviour of $G(t)$ on the Coriolis coupling constants. We note however that the $\beta_v + \beta_r$ value for the 210 cm⁻¹ band in cyclohexane is 0.55 ps⁻¹, which is only slightly higher than that for the 315 cm⁻¹ band. A comprehensive study of the out-of-plane

and in-plane vibrations and force fields of all substituted benzenes has yielded confirmation of the assignments used in the present work.^{23, 24}

Baur, Horsma, Knobler and Perez⁷ have shown how atomic polarisabilities can be deduced from polarisation and refraction data for systems containing two weakly interacting compounds. Applying their method to benzene and HFB they found a non linear dependence of the atomic polarisation on the fractional composition of the benzene + hexafluorobenzene mixtures. The deviation from linearity is up to 20 %. Now atomic polarisation P_a is related²⁵ to infra-red band intensities through

$$P_a = \frac{Nc}{3\pi^2} \sum_i \frac{\Gamma_i}{\nu_i}$$

The above result implies that intensities of either the benzene bands or the HFB bands should change in a non linear fashion on mixing. We have measured the intensities of two lowest e_{1u} bands of HFB in benzene and cyclohexane and found no significant changes. Because of band overlapping between the 1500 cm^{-1} bands of benzene and of HFB, we were unable to carry out such studies for these bands. At the present time we can only say that the intensity changes implied by the atomic polarisation data are surprising and that we have not observed them in the vibrational absorption bands studied.

CONCLUSIONS

The observed broadening and frequency shifts of the a_{2u} vibrational band of hexafluorobenzene on addition of benzene shows that the presence of significant interactions directed perpendicular to the ring plane. Purely polar interactions are insufficient to explain the observations. It would appear that interactions between benzene and HFB directly perturb those orbitals which determine the restoring force on a substituent moved out of the plane of the ring. This leads to a mechanism by which the frequency can be perturbed and also by which the vibrational energy may degrade to thermal energy.

Problems in interpretation of details of the available data still exist. For example, the initial curvature of the $G(t)$ curve of the a_{2u} band of HFB in benzene is much greater than expected for a free rotor, and identification of the relaxation process with the "dissociation" of a collision complex leads to a rather high value for the bimolecular association constant.

R. M. B. and E. B. G. gratefully acknowledge the awards of S.R.C. studentships. We are also grateful to the S.R.C. for grants towards the cost of the Perkin Elmer 325 spectrometer and for technical assistance in a study of weak intermolecular interactions. Some of the earliest measurements on the HFB benzene system were made by Dr. W. Wheatley, now at B.P. Chemicals, Sunbury, Middlesex.

¹ R. Kubo, *Lectures in Theoretical Physics* (Interscience, New York, 1961), vol. 1, p. 120.

² R. G. Gordon, *Adv. Magnetic Resonance*, 1968, **3**, 1.

³ I. R. Hill and D. Steele, *J. C. S. Faraday II*, 1975, **71**, 555.

⁴ (a) H. Morawitz and K. B. Eisenthal, *J. Chem. Phys.*, 1971, **55**, 887; (b) H. S. Goldberg and P. S. Pershan, *J. Chem. Phys.*, 1973, **58**, 3816.

⁵ I. R. Hill and D. Steele, to be published.

⁶ C. R. Patrick and G. S. Prosser, *Nature*, 1960, **187**, 1021.

⁷ M. E. Baur, D. A. Horsma, C. M. Knobler and P. Perez, *J. Phys. Chem.*, 1969, **73**, 641.

⁸ R. J. Powell and F. L. Swinton, *J. Chem. Thermodynamics*, 1970, **2**, 87.

⁹ M. W. Hanna, footnote on page 4108 of D. V. Fenby and R. L. Scott, *J. Phys. Chem.*, 1967, **71**, 4103.

- ¹⁰ R. J. Powell, F. L. Swinton and C. L. Young, *J. Chem. Thermodynamics*, 1970, **2**, 105.
¹¹ D. Steele, *Theory of Vibration Spectroscopy* (Saunders, Philadelphia, 1971), p. 203.
¹² I. R. Hill and D. Steele, *J.C.S. Faraday II*, 1974, **70**, 1233.
¹³ R. G. Gordon, *J. Chem. Phys.*, 1963, **39**, 2788.
¹⁴ (a) W. Wheatley, *Ph. D. Thesis* (University of London, 1968); (b) T. Fujiyama and B. Crawford Jr., *J. Phys. Chem.*, 1968, **72**, 2174.
¹⁵ D. A. Chisholm and H. L. Welsh, *Canad. J. Phys.* 1954, **32**, 291.
¹⁶ C. La Lau, *Proc. Conf. Molecular Spectroscopy*, 1958, ed. E. Thornton and H. W. Thompson (Pergamon, 1959), p. 205.
¹⁷ H. Spedding and D. H. Whiffen, *Proc. Roy. Soc. A*, 1956, **238**, 245.
¹⁸ D. Steele and W. Wheatley, *J. Mol. Spectr.*, 1969, **32**, 265.
¹⁹ (a) G. Jalsovszky and W. J. Orville Thomas, *Trans. Faraday Soc.*, 1971, **67**, 1894; (b) R. E. Bruns and W. B. Person *J. Chem. Phys.*, 1972, **57**, 324.
²⁰ see for example, D. N. Hague, *Fast Reactions* (Wiley-Interscience, New York, 1971), p. 12.
²¹ L. Delbouille, *J. Chem. Phys.*, 1956, **25**, 182.
²² D. Steele and D. H. Whiffen, *Trans. Faraday Soc.*, 1959, **55**, 369.
²³ R. A. R. Pearce, D. Steele and K. Radcliffe, *J. Mol. Structure*, 1973, **15**, 409.
²⁴ V. J. Eaton and D. Steele, *J. Mol. Spectr.*, 1973, **48**, 446.
²⁵ D. H. Whiffen, *Trans. Faraday Soc.*, 1958, **54**, 327.

Vibrational Band Contours

Part 2.—The Second Moments of the Intensity Distribution in Bands of Symmetric Top Molecules

BY IAN R. HILL AND DEREK STEELE*

Department of Chemistry, Royal Holloway College,
Egham, Surrey TW20 0EX

Received 8th July, 1974

Expressions are derived for the second intensity moments of vibrational bands of symmetric top molecules in the limit of rotational broadening. An expression for the moments for parallel bands agrees, apart from one minor term, with that given by Gordon. First order Coriolis effects are included for perpendicular bands, for which the second moment is given by

$$M(2) = B'^2[2kT/Bhc + 1/3 + B/3A] + A'^2 [2(1 - \zeta)^2 kT/hc] - \frac{B^2/3A^2 + (1 - 2\zeta)^2}{(1 - 2\zeta)^2} + 2B'A'(1 - 2\zeta).$$

The potential and the problems in the use of the formulae are discussed.

A great deal of information about molecular motion is contained within the band contour of a vibrational absorption or scattering band. The interpretation of the intensity at any specific frequency is a very complex function of the history of motion of the ensemble of molecules and is not amenable to interpretation.¹ There are two principal techniques used to deduce information from the contours about the average molecular motions and about the forces to which the molecules are subjected. The first involves the Fourier transformation of the band intensity with respect to the frequency shift from the band centre.² Thus for an absorption band in a liquid (molecular motions not strongly correlated), this transform is equal to the autocorrelation function of the transition dipole, μ ,

$$\langle \mu(0) \cdot \mu(t) \rangle = \text{constant} \times \int_{\text{band}} \frac{\ln(I_0/I)_v}{v} e^{i2\pi\Delta\nu t} d\nu.$$

In the derivation of this equation² from Gordon's equation (Hii) it is assumed either that hot bands cause no significant band shape distortion, or that their effects have been eliminated by appropriate mathematical techniques. This eliminates the need for the terms, $[1 - \exp(-h\nu/kT)]$, in the denominator of Gordon's equation. Provided that rotational motions dominate the changes in $\langle \mu(0) \cdot \mu(t) \rangle$ then the scalar of the transition dipole vector can be extracted and by normalising the band area to unity the autocorrelation function reduces to $\langle \cos \theta_t \rangle$ where θ_t is the angle between the dipole (molecular orientation) at a time t and at the arbitrarily chosen time 0.

It was shown by Gordon² that the normalised autocorrelation function of the molecular orientation can be expressed as a power series in time and that the coefficients at short times are analytic functions of the inertial constants and of the intermolecular torques. In a number of studies of symmetric top molecules³ the experimental orientation correlation function has been compared with that of a free rotor with the appropriate inertial constants. Agreement up to a certain time has

been taken as evidence that the molecules rotate on an average over that period of time before intermolecular collisions reorient the transition dipoles.

A second and in principle rather more powerful method arises from the identification of the time coefficients in the autocorrelation function expansion as the intensity moments of the band about the band centre. Thus if $G(t)$ is the autocorrelation function normalised so that $G(0) = 1.0$, then

$$G(t) = \sum_{n=0}^{\infty} \frac{(-2\pi i)^n}{n!} M(n)$$

where

$$M(n) = \int (v - v_0)^n \frac{\ln(I_0/I)_v}{v} dv.$$

If we can measure these moments, then, provided still that molecular reorientation dominates the decay of the autocorrelation function and that we can express moments as functions of the inertial constants and forces, it is possible to derive a great deal about the molecular dynamics. None of the conditions mentioned in the preceding sentence are trivial and this is one of a series of papers in which we are examining these questions. Here our concern is with the effects of first order Coriolis forces on the band contours and the second moments of symmetric top molecules. It is well known that the Coriolis forces produce dramatic changes in the band contours of perpendicular transitions [see for example ref. (4)]. It follows that the effects on the moments must be considerable.

Gordon computed expressions for the moments¹ by considering the commutators $[\mathcal{H}, \mu]$ where \mathcal{H} is the Hamiltonian and μ is the dipole operator. In our investigation we use the somewhat simpler, but rather less powerful method, of using the known expressions for the transition frequencies and transition probabilities of symmetric top molecules. This has the sole disadvantage of not allowing the effects of intermolecular forces on the moments to be deduced. These, however, have already been computed by Gordon.¹

The second moments have been recomputed for parallel transitions and agree well with the expression given by Gordon.

THEORY

The transition probabilities for parallel and perpendicular transitions of symmetric top molecules have been derived by Hönl and London⁵ and by Reiche and Radermaker.⁶ They are proportional to $A_{J,K} \exp(-F_{J,K}hc/kT)$ where $F_{J,K}$ is the rotational term number of the ground state and $A_{J,K}$ is a term dependent on the rotational quantum numbers J and K and takes the values shown below for the indicated transitions:

| parallel transitions | value of $A_{J,K}$ |
|-------------------------------------|--|
| $J, K \rightarrow J+1, K$ | $(2 - \delta_{K,0})(J+K+1)(J-K+1)/(J+1)$ |
| $J, K \rightarrow J, K$ | $(2 - \delta_{K,0})(2J+1)K^2/J(J+1)$ |
| $J, K \rightarrow J-1, K$ | $(2 - \delta_{K,0})(J^2 - K^2)/J$ |
| perpendicular transitions | |
| $J, K \rightarrow J+1, K \pm 1$ | $(J \pm K + 1)(J \pm K + 2)/(J+1)$ |
| $J, K \rightarrow J, K \pm 1$ | $(2J+1)(J \mp K)(J \pm K + 1)/J(J+1)$ |
| $J, K \rightarrow J-1, K \pm 1$ | $(J \mp K)(J \mp K - 1)/J.$ |

(1)

Substitution of (1) and of known term values into (2),

$$M(2) = \frac{\int (v - v_0)^2 \Gamma(v) dv}{\int \Gamma(v) dv} \quad (2)$$

where $\Gamma(v)$ is the intensity at a frequency v , $[= \ln(I_0/I)_v/v]$, leads to the following for the parallel case

$$\begin{aligned} M(2) \left[\sum_{J,K} A_{J,K} \exp(-F_{J,K} hc/kT) \right] = & \sum_{J,K} \left[\{ [B'(J+1)(J+2) - BJ(J+1) + z]^2 (J^2 - K^2 + 2J + 1) / (J+1) \} + \right. \\ & \left. [(B' - B)J(J+1) + z]^2 (2J+1)K^2 / J(J+1) + \right. \\ & \left. [B'J(J-1) - BJ(J+1) + z]^2 (J^2 - K^2) / J \right] \exp(-F_{J,K} hc/kT) \\ \equiv M(2)S(1) = & 4 \{ S[J(J+1)] + S(1) - S(K^2) \} B'^2 + \\ & S[J^2(J+1)^2] (\Delta B)^2 + S(K^4) [\Delta(A-B)]^2 + \\ & 4S[J(J+1)] \Delta BB' + 2S[J(J+1)K^2] \Delta B \Delta(A-B) + 4S(K^2) B' \Delta(A-B). \quad (3) \end{aligned}$$

Primed constants refer to upper vibrational states and unprimed refer to the ground state. $\Delta(x)$ defines the difference between the parameter x in the upper and lower vibrational states thus:

$$\Delta(A-B) = (A' - B') - (A - B)$$

$z = \Delta(A-B)K^2$ and $S(f)$ is as defined by Kassel.⁷ Thus:

$$S(f) = \sum_{J=0}^{\infty} \sum_{K=-J}^{\infty} (2J+1) f \exp(-F_{J,K} hc/kT).$$

Kassel computed expressions for the $S(f)$ required above by suitable differentiation of the rotational partition function expression $S(1)$. $S(1)$ itself was computed by Viney⁸ and corrected by Kassel.⁷ Translating into modern symbolism and reproducing only the dominant terms for each leads to

$$\begin{aligned} S(1) &= X \left[1 + \frac{Bx}{12} - \frac{B^2x}{12A} + \frac{7x^2}{480} \left(B^2 - \frac{2B^3}{A} + \frac{B^4}{A^2} \right) + \dots \right] \\ S(K^2) &= \frac{X}{2Ax} \left[1 + \frac{Bx}{12} - \frac{B^2x}{4A} + \dots \right] \\ S[J(J+1)] &= \frac{X}{Bx} \left[1 + \frac{B}{2A} - \frac{Bx}{4} + \frac{B^2x}{8A} - \frac{B^3x}{8A^2} + \dots \right] \\ S[J^2(J+1)^2] &= \frac{X}{4B^2x^2} \left[8 + \frac{4B}{A} + \frac{3B^2}{A^2} - 2Bx - \frac{B^2x}{A} + \frac{5B^3x}{4A^2} + \frac{21B^4x}{4A^3} + \dots \right] \\ S(K^4) &= \frac{X}{4A^2x^2} \left[3 + \frac{Bx}{4} - \frac{5B^2x}{4A} + \dots \right] \\ S[J(J+1)K^2] &= \frac{X}{4ABx^2} \left[2 + \frac{3B}{A} - \frac{Bx}{2} + \frac{3B^2x}{4A} - \frac{5B^3x}{4A^2} + \dots \right] \quad (4) \end{aligned}$$

where $X = (\pi/AB^2x^3)^{\frac{1}{2}} \exp(Bx/4)$ and $x = hc/kT$. Retaining only the terms of lowest order in the rotational constants for each $S(f)$ and substitution in (3) gives

$$\begin{aligned} M(2) = & \left(\frac{4}{Bx} + \frac{8}{3} + \frac{2B}{3A} \right) B'^2 + \left(8 + \frac{4B}{A} + \frac{3B^2}{A^2} \right) \frac{(\Delta B)^2}{4B^2x^2} + \frac{3}{4A^2x^2} [\Delta(A-B)]^2 + \\ & \left(\frac{4}{B} + \frac{2}{A} \right) \frac{\Delta BB'}{x} + \left(\frac{1}{AB} + \frac{3}{2A^2} \right) \frac{\Delta B}{x^2} \Delta(A-B) + \frac{2}{Ax} B' \Delta(A-B). \quad (5) \end{aligned}$$

Expression (5) agrees well with that derived from eqn (40) of ref. (1). The only difference is in 1 minor term. Thus we deduce from Gordon's equation that $\{8/3 + 2B/3A\}B'^2$ should be $4B'^2$. Extension of (5) to include terms of higher order may be readily accomplished if necessary using the next order terms of the $S(f)$.

The same procedure applied to a doubly degenerate band yields:

$$4M(2)S(1) = B'^2\{2S[J(J+1)] - 2S(K^2) + S(1)\} + \bar{A}^2 4S(K^2) + \bar{A}^2 S(1) + 2\bar{A}B'S(1) + (B' + \bar{A})\Delta(A-B)2S(K^2) + [\Delta(A-B)]^2 S(K^4) + (\Delta B)^2 S[J^2(J+1)^2] + (B' + \bar{A})\Delta B 2S[J(J+1)] \quad (6)$$

$\bar{A} = A(1-\zeta)$ and $\bar{A} = A(1-2\zeta)$ where ζ is the first order Coriolis constant. Use of (4) and retaining up to second order terms for B'^2 and A'^2 leads to:

$$M(2) = B'^2 \left\{ \frac{2}{Bx} + \frac{1}{3} + \frac{B}{3A} \right\} + \bar{A}^2 + 2\bar{A}B' + [\Delta(A-B)]^2 \frac{3}{4A^2 x^2} + \frac{(\Delta B)^2}{x^2} \left\{ \frac{2}{B^2} + \frac{1}{AB} + \frac{3}{4A^2} \right\} + \frac{\Delta B}{x} (B' + \bar{A}) \left\{ \frac{2}{B} + \frac{1}{A} \right\} + \Delta(A-B)(B' + \bar{A}) \frac{1}{Ax} + \bar{A}^2 \left\{ \frac{2}{Ax} - \frac{B^2}{3A^2} \right\}.$$

DISCUSSION

Eqn (3) and (6) allow the determination, to any required degree of accuracy, of the theoretical second moments of a symmetric top in the absence of collisional or vibrational relaxation broadening. To a very good approximation the $M(2)$ of perpendicular bands can be obtained from Gordon's equations¹ by substitution of $A'(1-\zeta)$ for A' . It follows that the higher even moments may be adequately obtained by the same approximation. This establishes the necessary equations from which intermolecular torques may be deduced from $M(2)$ and $M(4)$.

We contend that there are still severe problems to be solved before any reliance can be placed on such values. The intensity distribution in the wings of the bands is critical in determining the ratio $M(4)/M(2)$. We have examined a wide range of perpendicular transitions of symmetric top systems (e.g. C_6F_6 , C_6H_6 , CH_3I , CF_3Br) in the hope of establishing some general features in the contours of the wings. In all cases examined the wings show very considerable interference from overlapping bands and we do not feel that we are yet in a position to make any clear observations on this matter.

The degenerate ν_6 band of CH_3I in the liquid phase at 883 cm^{-1} is overlapped on the high frequency side, but appears clear on the low frequency side of the band. Assuming that the band is symmetrical the second moment was measured in the pure liquid phase to be $1800 \pm 100\text{ cm}^{-2}$. The Coriolis constant (ζ) for this degenerate mode is 0.206 which leads to a calculated second moment of 1450 cm^{-2} , which is to be compared with the $\zeta = 0$ value of 2250 cm^{-2} . As the rotational kinetic energy is not reduced by liquefaction this result suggests the existence of other broadening mechanisms. This conclusion is supported by Raman studies of band widths for CH_3I arising from isotropic relaxation processes. Bartoli and Litovitz⁹ found half band widths for the $\bar{\alpha}'$ component of 2.6 cm^{-1} for both the A_1 bands at 1251 and 527 cm^{-1} . Goldberg and Pershan¹⁰ obtained values of 2.4 to 2.2 cm^{-1} for all three A_1 fundamentals in the pure liquid state. For a 1% solution in CS_2 these widths decreased by 0.4 to 0.8 cm^{-1} . Obviously these isotropic processes are going to increase the band

moments. Unfortunately, as $\bar{\alpha}'$ is zero for a non-totally symmetric band, it is not feasible to measure the widths and to make an appropriate correction by the Raman tensor method. It may be possible to estimate the correction by use of the methods of Rakov.¹¹ These are based on the assumption that the intrinsic (non-orientational) band width is not dependent on temperature. There are obvious dangers in this assumption and cases where the assumption appears to be invalid are reviewed by Bartoli and Litovitz.

It has been suggested that the wings of the bands in liquids follow the smoothed contours of the gaseous system.¹² If this could be established then it would permit the difficulties arising from band overlapping to be resolved in many situations. At present the usual procedure is to assume that rotational relaxation process and the background can be floated so that the observed $M(2)$ is equal to the theoretical value. In some instances it may be that this procedure is valid. However, we have been investigating a number of cases in which band broadening accompanies concentration variations of the absorber in specific solvents. In several cases (mainly dipolar molecules with aromatic systems) we have established the existence of translation rotational coupling¹³ and in one case (hexafluorobenzene-benzene) vibrational relaxation¹⁴ is indicated. For chlorine and bromine dissolved in benzene, Raman studies have established that the halogen band is in fact two sets of overlapping isotope bands, one due to the uncomplexed halogen and the other set arising from benzene-halogen interaction species. In view of these observations we suggest that considerable caution be exercised in floating the background.

In the case of a degenerate band the Coriolis constant may not be known, and therefore the theoretical $M(2)$ could be unknown. A measurement of $M(2)$ itself then, even if overlapping bands can be eliminated, may not allow the establishment of the dominance of rotational relaxation. A possible method of overcoming this problem is to compare the first and second order orientational correlation functions, $\langle \mathbf{U}(0) \cdot \mathbf{U}(t) \rangle$ and $\langle P_2[\mathbf{U}(0) \cdot \mathbf{U}(t)] \rangle$, as derived from the corresponding infra-red and Raman band contours respectively. $P_2[x]$ represents the second Legendre polynomial of x . It was proposed by Berne, Pechukas and Harp¹⁶ that $\langle P_2[\mathbf{U}(0) \cdot \mathbf{U}(t)] \rangle$ could be derived from $\langle \mathbf{U}(0) \cdot \mathbf{U}(t) \rangle$ by maximising the information entropy of the distribution. In practice this means that if $\langle \mathbf{U}(0) \cdot \mathbf{U}(t) \rangle = -1/\beta(t) + \coth\beta(t)$ then $\langle P_2[\mathbf{U}(0) \cdot \mathbf{U}(t)] \rangle = 1 - [3/\beta(t)]\langle \mathbf{U}(0) \cdot \mathbf{U}(t) \rangle$. $\beta(t)$ is a Lagrangian multiplier. This appeared to be well satisfied by computer simulated spectra¹⁶ and a band of CH_3I ¹⁷ to which the theory was applied. Isotropic relaxation processes should affect the first and second order correlation functions to identical extents and therefore invalidate the above relation.¹⁸

One interesting possibility is suggested by the strong dependence of $M(2)$ on the Coriolis constant, ζ . If $M(2)$ can be measured it should be possible to establish ζ from liquid phase studies. Once again it is essential to ensure that other relaxation processes are insignificant.

One of us (I. R. H.) gratefully acknowledges the tenure of an S.R.C. studentship. We also thank the S.R.C. for a grant.

¹ R. G. Gordon, *J. Chem. Phys.*, 1963, **39**, 2788.

² R. G. Gordon, *J. Chem. Phys.*, 1965, **43**, 1307.

³ for example W. G. Rothschild, *J. Chem. Phys.*, 1971, **55**, 1402; P. van Konynenburg and W. A. Steele, *J. Chem. Phys.*, 1972, **56**, 4776.

⁴ W. F. Edgell and R. E. Moynihan, *J. Chem. Phys.*, 1966, **45**, 1205.

⁵ H. Hönl and F. London, *Z. Phys.*, 1925, **33**, 803; *Ann. Phys.*, 1926, **79**, 273.

⁶ F. Reiche and H. Rademaker, *Z. Phys.*, 1926, **39**, 444; 1927, **41**, 453.

- ⁷ L. S. Kassel, *J. Chem. Phys.*, 1933, **1**, 576.
⁸ Miss Viney, *Proc. Cambridge Phil. Soc.*, 1933, **29**, 142.
⁹ F. J. Bartoli and T. A. Litovitz, *J. Chem. Phys.*, 1972, **56**, 404.
¹⁰ H. S. Goldberg and P. S. Pershan, *J. Chem. Phys.*, 1973, **58**, 3816.
¹¹ A. V. Rakov, *Tr. Fiz. Inst. Akad. Nauk S.S.S.R.*, 1964, **27**, 111; *Optics and Spectr.*, 1959, **7**, 128.
¹² W. B. Person and A. Théorêt, unpublished results.
¹³ I. R. Hill, R. J. W. Pulham and D. Steele, to be published.
¹⁴ R. M. Barrett, E. B. Gill and D. Steele, *J.C.S. Faraday II*, 1975, **71**, 532.
¹⁵ E. B. Gill, T. C. Jao, D. Steele and W. B. Person, to be published.
¹⁶ B. J. Berne, P. Pechukas and G. D. Harp, *J. Chem. Phys.*, 1968, **49**, 3125.
¹⁷ M. Constant and R. Fauquembergue, *J. Chem. Phys.*, 1973, **58**, 4031.
¹⁸ L. A. Nafie and W. L. Peticolas, *J. Chem. Phys.*, 1972, **57**, 3145; S. Sykora, Report, U. S. Clearinghouse Fed. Sci. Tech. Inf. No. 724330, 1971, p. 20.

LIBRARY

